Functional characterization of Pol5 in the maturation of both ribosomal subunits

DISSERTATION

ZUR ERLANGUNG DES
DOKTORGRADES DER NATURWISSENSCHAFTEN (DR. RER. NAT.)
DER FAKULTÄT FÜR BIOLOGIE UND VORKLINISCHE MEDIZIN
DER UNIVERSITÄT REGENSBURG

vorgelegt von

Christina Braun, geb. Schmidt

aus Regensburg

im April 2020

Das Promotionsgesuch wurde eingereicht am:
15. April 2020

Die Arbeit wurde angeleitet von:
PD Dr. Jorge Pérez-Fernández

Das Promotionskolloquium wurde abgehalten am:
15. Oktober 2020

Die vorliegende Arbeit wurde mit „**summa cum laude**“ benotet.

Regensburg, 16. Oktober 2020

Christina Braun

So, don't worry about tomorrow
Take it today

AC/DC – Have a Drink on Me

Für meine Familie

Contents

Abstract

Ribosome biogenesis is a complex process. In the yeast *Saccharomyces cerevisiae*, it requires the concerted action of 79 ribosomal proteins (RPs), more than 150 assembly factors (AFs), four ribosomal RNAs (rRNAs), and several snoRNAs. During the past 50 years, most studies focused on the pathway how ribosomes are synthesized and how this process is regulated. Using multidisciplinary approaches, we know most of the factors involved in the synthesis of ribosomes, the steps in which they participate, and the structure of several ribosomal intermediates. In addition, for several AFs their specific catalytic activities and putative functions have been proposed. Nevertheless, there are many AFs whose function is far from being understood or even weakly related to ribosome synthesis.

Among the not well characterized factors, the protein Pol5 was initially described as a B-type like DNA polymerase with a putative role in the assembly of the small ribosomal subunit and in rDNA transcription due to its physical association with proteins participating in these processes.

In this study, Pol5 was characterized and it was described as the fourth AF involved in the maturation of both ribosomal subunits. By performing a detailed phenotypic analysis of yeast cells in dependency of Pol5 expression, the role of Pol5 in the initial folding of the polypeptide exit tunnel within the large ribosomal subunit could be defined. In contrast to the published association of Pol5 with AFs involved in the assembly of the small subunit, the data presented in this thesis do not support a stable association of these early assembling proteins under optimal growth conditions. However, Pol5 might play a role in the recycling of several AFs of the small subunit, which is required to maintain an ongoing synthesis of ribosomes. Moreover, part of the N-terminal domain of the protein, and more specifically, a motif participating in the recruitment of the nuclear exosome, is suggested to be involved in the recycling process.

Thus, Pol5 might connect the recycling of AFs of the small subunit with the correct assembly of the large subunit. This theory, which is compatible with alternative regulatory pathways, contributes to a rational explanation for the balanced synthesis of both ribosomal subunits in eukaryotic organisms.

Zusammenfassung

Ribosomenbiogenese ist ein komplexer Prozess, der in der Hefe *Saccharomyces cerevisiae* auf der aufeinander abgestimmten Wirkungsweise 79 ribosomaler Proteine (RPs), von über 150 Assemblierungsfaktoren (AFs), vier ribosomaler RNAs (rRNAs) und verschiedener snoRNAs beruht. Während der vergangenen 50 Jahre lag der Fokus der wissenschaftlichen Arbeit darauf, wie Ribosomen synthetisiert werden und wie dieser Prozess reguliert ist. Dank multidisziplinärer Ansätze kennen wir inzwischen den Großteil der Faktoren, die in die Synthese von Ribosomen involviert sind, und können einordnen, an welchen Assemblierungsschritten diese Faktoren beteiligt sind. In diesem Zusammenhang konnten auch die Strukturen verschiedener ribosomaler Assemblierungsintermediate aufgeklärt werden. Von einigen AFs wird angenommen, dass sie katalytisch aktiv sind, während für andere nur über mögliche Funktionen spekuliert werden kann. Die Funktion vieler AFs ist bis dato nur wenig verstanden und steht häufig kaum in direktem Zusammenhang mit der Ribosomenbiogenese.
Zu den wenig charakterisierten Faktoren gehört auch Pol5. Dieses Protein wurde ursprünglich als B-Typ-ähnliche DNA-Polymerase mit einer möglichen Rolle in der Assemblierung der kleinen ribosomalen Untereinheit und in der Transkription der rDNA beschrieben. Diese Funktion von Pol5 wurde angenommen, da es mit Proteinen assoziiert gefunden wurde, die an beiden genannten Prozessen beteiligt sind.
In dieser Arbeit wird die funktionelle Charakterisierung von Pol5 vorgestellt, wobei dieses Protein als vierter AF beschrieben wird, der an der Reifung beider ribosomaler Untereinheiten mitwirkt. Mithilfe einer detaillierten Phänotyp-Analyse, in der Hefezellen verglichen wurden, die Pol5 exprimieren oder depletieren, konnte die Beteiligung von Pol5 an der Faltung des Polypeptid-Exit-Tunnels innerhalb der großen ribosomalen Untereinheit festgestellt werden. Trotz der früher beschriebenen Assemblierung von Pol5 an AFs der kleinen Untereinheit, deuten die Daten dieser Arbeit nicht auf eine stabile Assoziation von Pol5 mit den AFs der kleinen Untereinheit unter idealen Wachstumsbedingungen hin. Dennoch stützen meine Daten die Vermutung, dass Pol5 für das Recycling einiger AFs während der Reifung der kleinen Untereinheit benötigt werden könnte. Die Freisetzung der AFs ist unerlässlich, wenn die effiziente Synthese der Ribosomen aufrechterhalten werden soll. Außerdem deuten die Ergebnisse darauf hin, dass ein Teil der N-terminalen Domäne von Pol5, genauer gesagt ein Protein-Motiv, das das nukleäre Exosom rekrutieren kann, am Recycling der AFs beteiligt ist.
Das bedeutet, Pol5 könnte die Disassemblierung des Vorläufers der kleinen Untereinheit mit der korrekten Assemblierung der großen Untereinheit verknüpfen. Diese Theorie wird im Rahmen dieser Arbeit ausführlich diskutiert und stimmt mit alternativen Regulationsmechanismen überein. Außerdem würde sie eine Erklärung liefern, wie die stöchiometrische Produktion beider ribosomaler Untereinheiten in Eukaryoten möglich ist.

1. Introduction

1.1 Overview of the relevance of ribosomes and their biogenesis

Ribosomes are molecular machineries present in the cytoplasm and they are responsible for the translation of mRNAs into proteins. For this reason, ribosomes are essential elements for every living cell and highly conserved components among all known organisms (Woolford and Baserga, 2013).

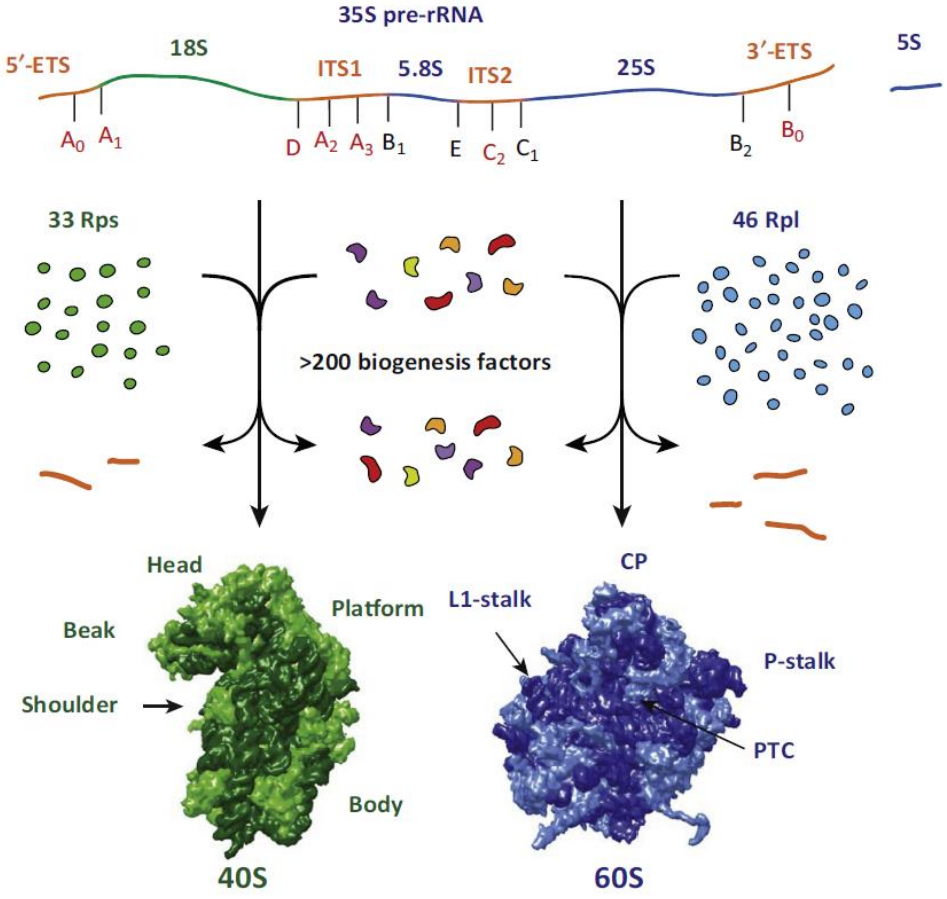

Figure 1: Schematic overview of ribosome biogenesis in *Saccharomyces cerevisiae* obtained from Kressler et al. (2017).
Ribosomal proteins (green and blue) and assembly factors (variegated) of the 40S (green) and the 60S (blue) subunits are synthesized in the cytoplasm from mRNAs produced by RNA polymerase II (RNA Pol II). 35S pre-rRNA and 5S rRNA (dark blue) are synthesized by RNA polymerase I (RNA Pol I) and RNA polymerase III (RNA Pol III), respectively. External and internal transcribed spacers (5'ETS, ITS1, ITS2, 3'ETS; orange) are removed from 35S pre-rRNA during ribosome biogenesis by endo- and exonucleolytic cleavages at processing sites indicated in red and black, respectively. Mature 40S subunits contain 33 ribosomal proteins (light green) and the 18S rRNA (dark green). Mature 60S subunits contain 46 ribosomal proteins (light blue) and the 5.8S, 25S, and 5S rRNAs (dark blue). Structural hallmarks of both mature subunits are indicated. CP is short for central protuberance, P-stalk for phospho-stalk, and PTC for peptidyl transferase center.

To decode the mRNA and join the single amino acids together to form a polypeptide chain, ribosomes use two main active sites, the decoding center and the **p**eptidyl **t**ransferase

center (PTC). The former is located within the **s**mall ribosomal **s**ub**u**nit (SSU) and the latter is part of the **l**arge ribosomal **s**ub**u**nit (LSU). Joining of both subunits builds a mature ribosome. Related to their sedimentation under high centrifuge forces, the small and the large subunits in eukaryotes are known as the 40S and 60S subunits, respectively, while the mature eukaryotic ribosome is known as 80S ribosome (Deley, 1964). Ribosomes are a paradigm for fundamental studies on **r**ibo**n**ucleo**p**rotein particles (RNPs) because they are a main component of every cell, composed of RNAs (**r**ibosomal RNA, rRNA) and proteins (**r**ibosomal **p**roteins, RPs). In the yeast *Saccharomyces cerevisiae*, the SSU contains 33 RPs and the 18S rRNA, whereas the LSU harbors 46 RPs and the 25S, 5.8S, and 5S rRNAs (Figure 1) (Klinge and Woolford, 2019; Kressler et al., 2017).
In eukaryotic cells, ribosome assembly is a challenging process involving the action of three RNA polymerases. RNA polymerases I (RNA Pol I) and III (RNA Pol III) transcribe the **r**ibosomal DNA (rDNA) in the nucleolus to produce the precursor transcripts of the mature rRNAs. RNA polymerases II (RNA Pol II) and III produce small nucleolar RNAs required for the synthesis of ribosomes. Furthermore, RNA Pol II synthesizes the mRNAs, which are translated in the cytoplasm to form the RPs. In addition, the synthesis of ribosomes takes place along different cellular compartments, starting in the nucleolus and ending in the cytoplasm, where the mature ribosomes are required. Synthesis of ribosomes requires processing and folding of the rRNA, the incorporation of the 80 RPs, and the transport of the ribosomal subunits to the cytoplasm. These processes need the action of about 200 **a**ssembly **f**actors (AFs) and 77 **s**mall **n**ucle**o**lar RNAs (snoRNAs) (Figure 1) (de la Cruz et al., 2015).
Since exponential growing yeast cells contain about 200,000 ribosomes and they divide every 90 minutes, each cell needs to produce about 1,000 ribosomes per minute. Thus, synthesis of ribosomes is a very dynamic process requiring 60% of total cellular transcription and with 50% of RNA Pol II activity dedicated to the production of enough RPs and AFs (Warner, 1999). Moreover, the choreography of the more than 200 AFs (including snoRNAs) participating in the synthesis of both ribosomal subunits needs to be fine-tuned to avoid an excessive formation of non-functional particles.

1.2 Functional and structural description of mature ribosomal subunits

1.2.1 The 40S or small subunit (SSU)

The mature 40S subunit adopts, compared to the mature 60S subunit, a relatively simple conformation consisting of five main parts named as head, beak, body, platform, and central pseudoknot (Figure 2). The mRNA tunnel crosses the SSU between the beak and body. The active site of the small subunit, the decoding center, lies in the middle of the small subunit close to the central pseudoknot (Klinge and Woolford, 2019).

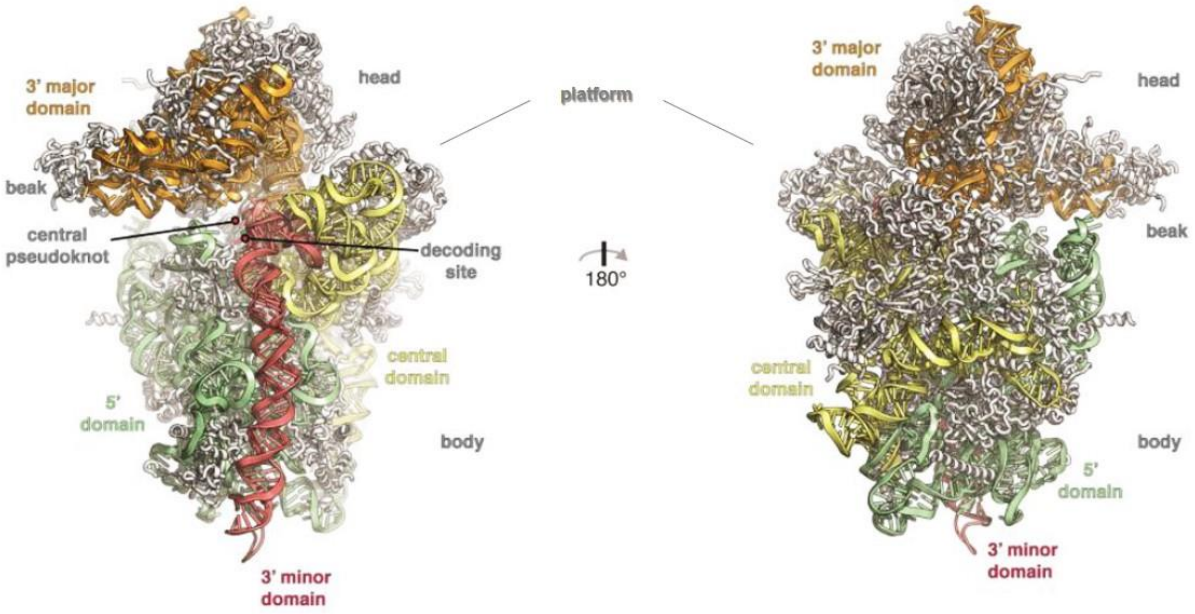

Figure 2: Tertiary structures of the mature small ribosomal subunit adapted from Klinge and Woolford (2019).
Cartoon representation of the subunit interface (left) and the solvent-exposed side (right) of the small ribosomal subunit. The subdomains of the 18S rRNA are colored and indicated. RPs are depicted in white. Positions of head, beak, body, platform, central pseudoknot, and decoding center are annotated.

The rRNA component of the SSU is the 18S rRNA, which harbors four structural domains: 5' domain, central domain, 3' major domain, and 3' minor domain. The 3' minor domain is oriented upright within the body along the subunit interface surrounded by the 5' domain and the central domain (on the left in Figure 2). The 3' major domain lies exclusively in the upper part of the SSU structure and constitutes head and beak. Thus, the central domain connects head and body. The central pseudoknot forms in the middle of the subunit at the interface of the other four domains and it is required for the function of the decoding center (on the left in Figure 2) (Ben-Shem et al., 2011; Klinge and Woolford, 2019).

1.2.2 The 60S or large subunit (LSU)

The mature 60S subunit harbors at least eight main sites with specific names and functions, which are described in detail in Figure 3. In the right part of the structure, the **p**hospho-stalk (P-stalk) is the binding site of translation factors and the **s**arcin **r**icin **l**oop (SRL) triggers GTP hydrolysis in translation factors with GTPases activity (Pérez-Fernández et al., 2005; Santos and Ballesta, 2005; Voorhees et al., 2010). The binding sites for tRNAs known as, A-, P-, and E-sites (Aminoacyl-, Peptidyl-, and Exit-) localize in the middle of the LSU. The nascent polypeptide chain runs along the LSU through the **p**olypeptide **e**xit **t**unnel (PET) (Konikkat and Woolford, 2017). On the top, the **c**entral **p**rotuberance (CP), composed of 5S rRNA and the RPs Rpl5 and Rpl11, enhances translational fidelity possibly by allowing the communication between the different functional centers (Dinman, 2005; Smith et al., 2001).

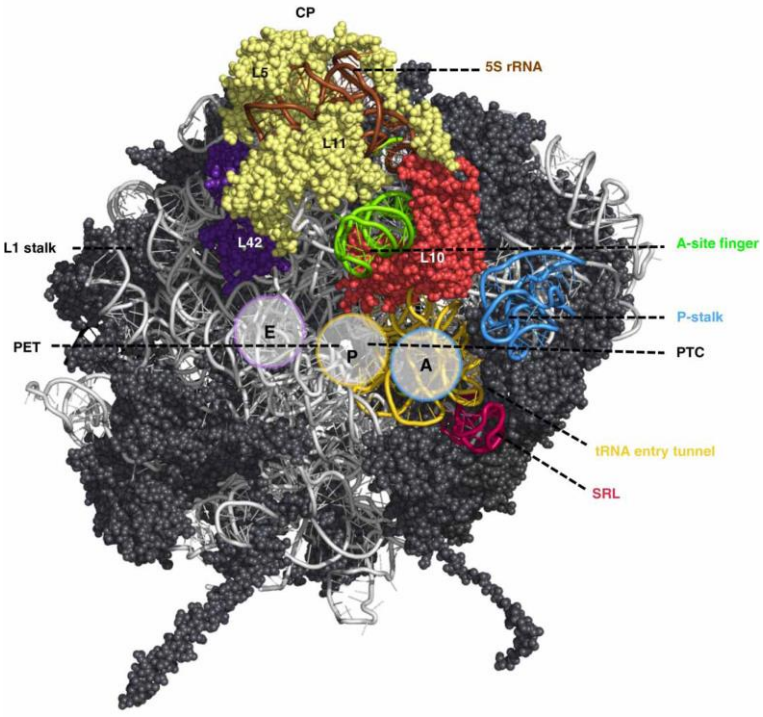

Figure 3: Functional centers of the mature large ribosomal subunit depicted in the quaternary structure obtained from Konikkat and Woolford (2017).
The 60S subunit is oriented to visualize the subunit interface, containing the peptidyl transferase center (PTC) and other active sites. Above, the central protuberance (CP) containing the 5S rRNA (brown) and the RPs Rpl5 and Rpl11 (pale yellow) is depicted. On the right, the RNA-binding site of the phospho-stalk (P-stalk) is shown in blue and the sarcin ricin loop (SRL) in red. In the center, the helices H89 and H91 (yellow) belong to the tRNA entry tunnel and mark the beginning of the tRNA accommodation corridor with A- and P-sites. The ending of the corridor at the E-site can be identified by Rpl42 colored in purple. In addition, the A-site finger is depicted in green and Rpl10 in red. In the center, the position of the polypeptide exit tunnel (PET) is indicated. It proceeds toward the solvent-exposed side (on the reverse side).

The LSU contains three mature rRNA components, named 25S, 5.8S, and 5S. The primary structure of 25S rRNA contains six conserved domains (I to VI from 5' to 3' end). Domains I, II, and the 5.8S rRNA lie at the solvent-exposed surface of the LSU (on the right in Figure 4). Domains IV and V build the PTC containing the A-, P-, and E-sites (on the left in Figure 4). Domains II, III, and V participate in formation of the PET and domain III surrounds the exit of the PET at the solvent-exposed side (on the right in Figure 4). Both domains III and VI bridge the subunit interface and the solvent-exposed side. Domains I and III trap the 5.8S rRNA (on the right in Figure 4), while domains II and V dock the 5S rRNA and form the PTC (on the left in Figure 4) (Ben-Shem et al., 2011; Klinge and Woolford, 2019).

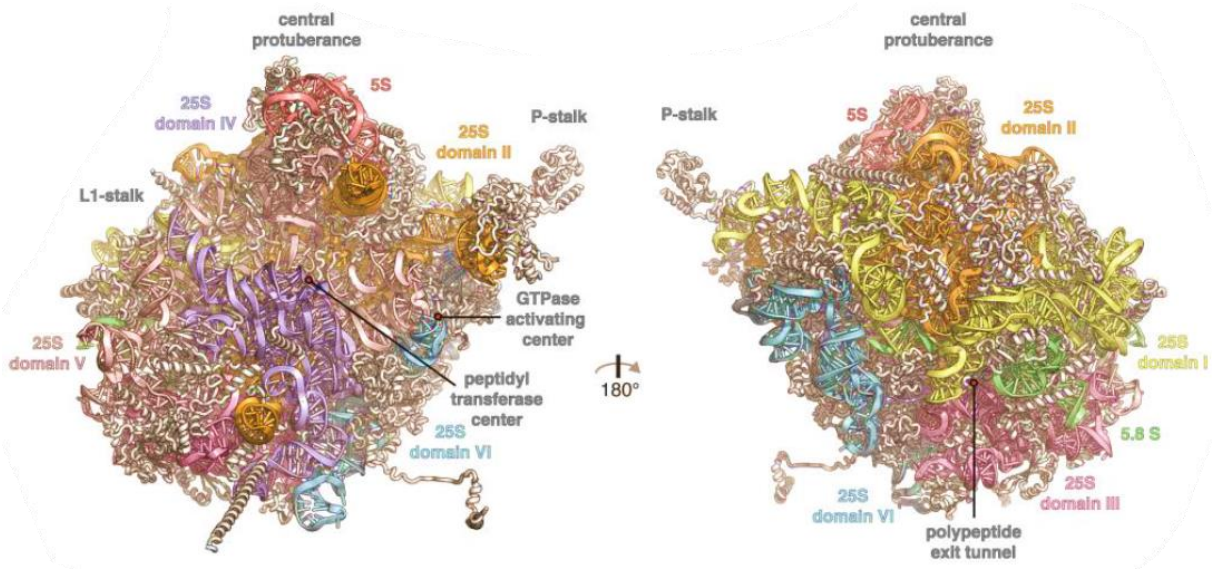

Figure 4: Tertiary structures of the mature large ribosomal subunit adapted from Klinge and Woolford (2019).
Cartoon representation of the subunit interface (left) and the solvent-exposed side (right) of the large ribosomal subunit. The subdomains of the 25S rRNA are colored and indicated, as well as 5.8S and 5S rRNAs. RPs are depicted in white. Positions of the central protuberance, L1-stalk, P-stalk, GTPase activating center (named SRL in Figure 3), peptidyl transferase center, and polypeptide exit tunnel are annotated.

1.2.3 The 80S ribosome

The 40S and 60S subunits assemble in 80S ribosomes during translation initiation. This process starts in eukaryotic cells with the scanning of the mRNA by the 43S preinitiation complex to identify the start codon. Therefore, the 40S subunit guides the mRNA coming from the mRNA entry tunnel (Figure 5) between beak and body through the ribosome (Ben-Shem et al., 2011).

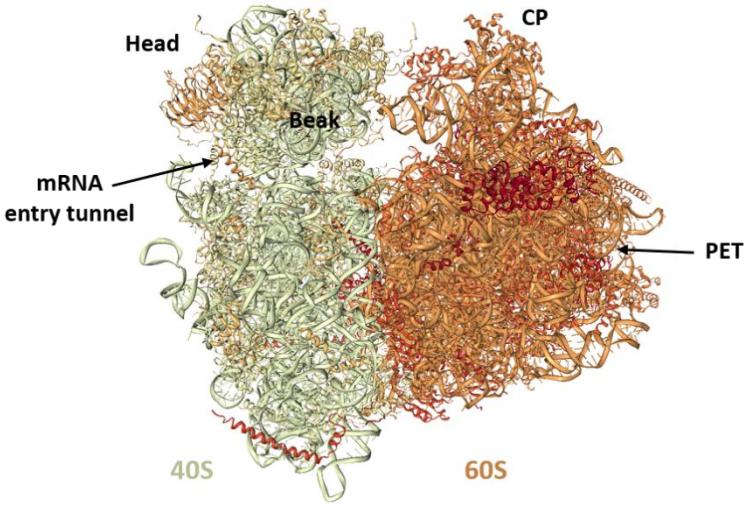

Figure 5: Structure of the mature 80S ribosome (PDB ID: 4V88).
Cartoon representation of the 80S ribosome consisting of 40S subunit (light green) and 60S subunit (orange). Positions of head, beak, and mRNA entry tunnel of the 40S subunit and central protuberance (CP) and polypeptide exit tunnel (PET) of the 60S subunit are annotated.

Once the start codon is identified by the 43S particle carrying the initiator-tRNA, the 60S subunit joins to form the 80S ribosome. The association of the 60S subunit is allowed by initiation factor eIF2 triggered GTP hydrolysis, which leads to the dissociation of initiation factors from the 43S particle, which precluded unspecific association with 60S subunits (Kimball, 1999). The formation of the 80S creates the A-, P-, and E-sites, which are occupied during elongation with tRNAs. Therefore, an amino-acylated tRNA enters the tRNA tunnel and binds to the A-site, while the tRNA connected to the polypeptide chain sits at the P-site. The peptide bond formation between the new amino acid and the polypeptide chain is carried out by the PTC. After the formation of the peptide bond, tRNAs are translocated. The tRNA at the P-site moves toward the E-site. The tRNA at A-site is now bound to the nascent polypeptide and moves toward the P-site releasing the A-site for the association of a new amino-acylated tRNA. Once the stop codon is reached, the release factors transfer a water molecule to the polypeptide chain and trigger GTP hydrolysis, terminate translation, disassemble the 80S ribosome, and release the completed polypeptide chain.

1.3 Transcription of the ribosomal DNA

In eukaryotic cells, the synthesis of ribosomes begins with the transcription of the rDNA in the nucleolus. In *S. cerevisiae*, each cell contains around 150 copies of the rDNA, which are organized as head-to-tail tandem repeats on chromosome XII (Figure 6) (Petes, 1979; Schweizer et al., 1969).

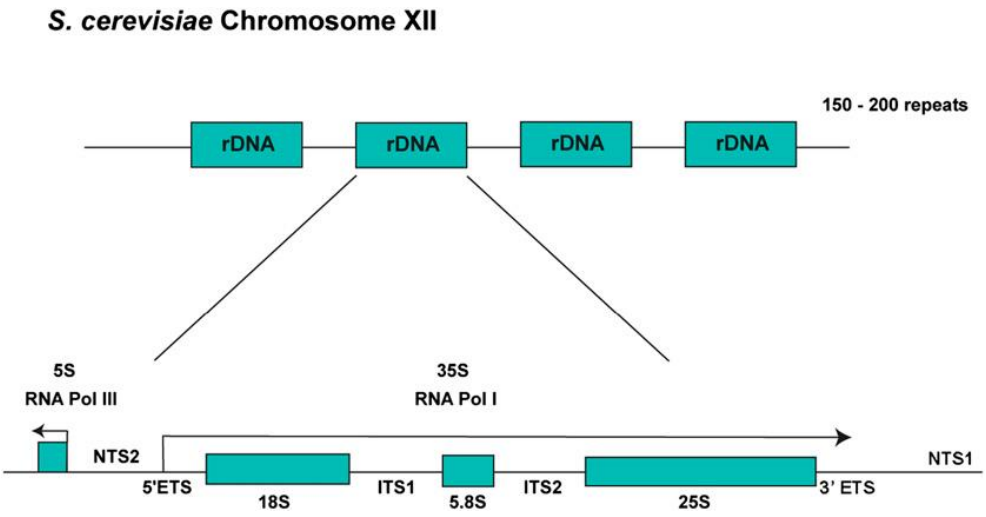

Figure 6: rDNA locus of *S. cerevisiae* obtained from Woolford and Baserga (2013).
Schematic representation of the rDNA locus on chromosome XII of the yeast *S. cerevisiae* encoding around 150 rDNA repeats. One repeat is depicted in more detail containing the sequences of 5S, 18S, 5.8S, and 25S rRNAs. As indicated, 5S rRNA is produced by RNA Pol III in the opposite direction and separated from the remaining rRNA sequences by NTS2 (non-transcribed spacer). RNA Pol I produces the 35S pre-rRNA transcript reaching from 5'ETS to 3'ETS (external transcribed spacer). NTS1 (non-transcribed spacer) separates the rDNA loci.

Each copy contains the sequence of the 35S gene encoding for three out of four rRNAs (18S, 5.8S, 25S) and the 5S rRNA gene, which are located on complementary strands and separated by **n**on-**t**ranscribed **s**pacers (NTS; Figure 6). RNA Pols I and III transcribe the 35S and 5S genes, respectively, in opposed senses. The 35S pre-rRNA contains the sequences of the 18S, the 5.8S, and the 25S rRNAs, which are separated by the **i**nternal **t**ranscribed **s**pacers ITS1 and ITS2 and flanked by the **e**xternal **t**ranscribed **s**pacers 5'ETS and 3'ETS (see Figure 1 and Figure 6) (Udem and Warner, 1972).
RNA Pol I is an outstanding RNA polymerase because it exclusively transcribes the 35S gene. In contrast, besides 5S rRNA synthesis, RNA Pol III produces tRNAs and several other RNAs, which include the RNA component of the signal recognition particle and snoRNAs (Dieci et al., 2007).
In *S. cerevisiae*, RNA Pol I consists of 14 subunits and it needs several transcription factors to be recruited to the promoter region of the 35S gene (Engel et al., 2018; Keener et al., 1997; Keys et al., 1994, 1996; Lalo et al., 1996; Siddiqi, 2001; Steffan et al., 1996; Yamamoto et al., 1996). Both transcription initiation and elongation by RNA Pol I are regulated steps in rRNA synthesis (French et al., 2003; Zhang et al., 2010). Moreover, the production of rRNAs can be primary regulated by the number of rDNA copies accessible for transcription (Sandmeier et al., 2002). Due to the high activity of RNA Pol I required to support the demand of ribosomes, actively transcribed rDNA can even be visualized by electron microscopy with the so-called "Miller spread"-technique, initially developed by Oscar Miller using amphibian oocytes (Miller and Beatty, 1969).

1.4 Processing of the ribosomal RNAs

35S pre-rRNA is processed by several endo- and exonucleolytic cleavages to produce the mature rRNAs. Processing of the pre-rRNA might occur as co- and post-transcriptional events.

1.4.1 Co-transcriptional processing

Co-transcriptional processing involves the cleavage events at sites A0, A1, and A2 (Figure 7). Co-transcriptional cleavage in A2 occurs in 50 to 70% of the nascent transcripts under optimal growth conditions (Kos and Tollervey, 2010; Osheim et al., 2004). However, it is not clear which are the molecular mechanisms behind the selection for co- or post-transcriptional processing. In any case, the efficient cleavage at these sites requires the formation of the first pre-ribosomal particle called SSU processome (Dragon et al., 2002). Based on the accumulation of the major SSU precursor (Figure 7), the order of cleavage events has been established by convention.
Therefore, processing at sites A0 and A1 within the 5'ETS region constitutes the primary cleavage events (Figure 7). Cleavage at the A1 site produces the mature 5' end of the 18S rRNA and it requires the evolutionarily conserved nucleotides upstream of the A1

sequence in the 5'ETS (Venema et al., 1995) and the stem-loop structure downstream of A1 within the sequence of the mature 18S rRNA (Sharma et al., 1999).
Cleavage at the A2 site splits the 35S transcript into the pre-rRNAs for the small and the large ribosomal subunit (20S and 27SA2 pre-rRNAs, Figure 7). As for the A1 cleavage, positioning of the cleavage site A2 is defined by a downstream stem-loop structure (Allmang et al., 1996). Although, cleavages at the A1 and A2 sites might involve the activity of Utp24 (Bleichert et al., 2006; Wells et al., 2016), some authors suggest Rcl1 as the putative endonuclease for at least the A2 site (Billy et al., 2000; Delprato et al., 2014; Horn et al., 2011). As an alternative, it is possible that the cleavage activity of Utp24 is supported by Rcl1 (Khoshnevis et al., 2019).

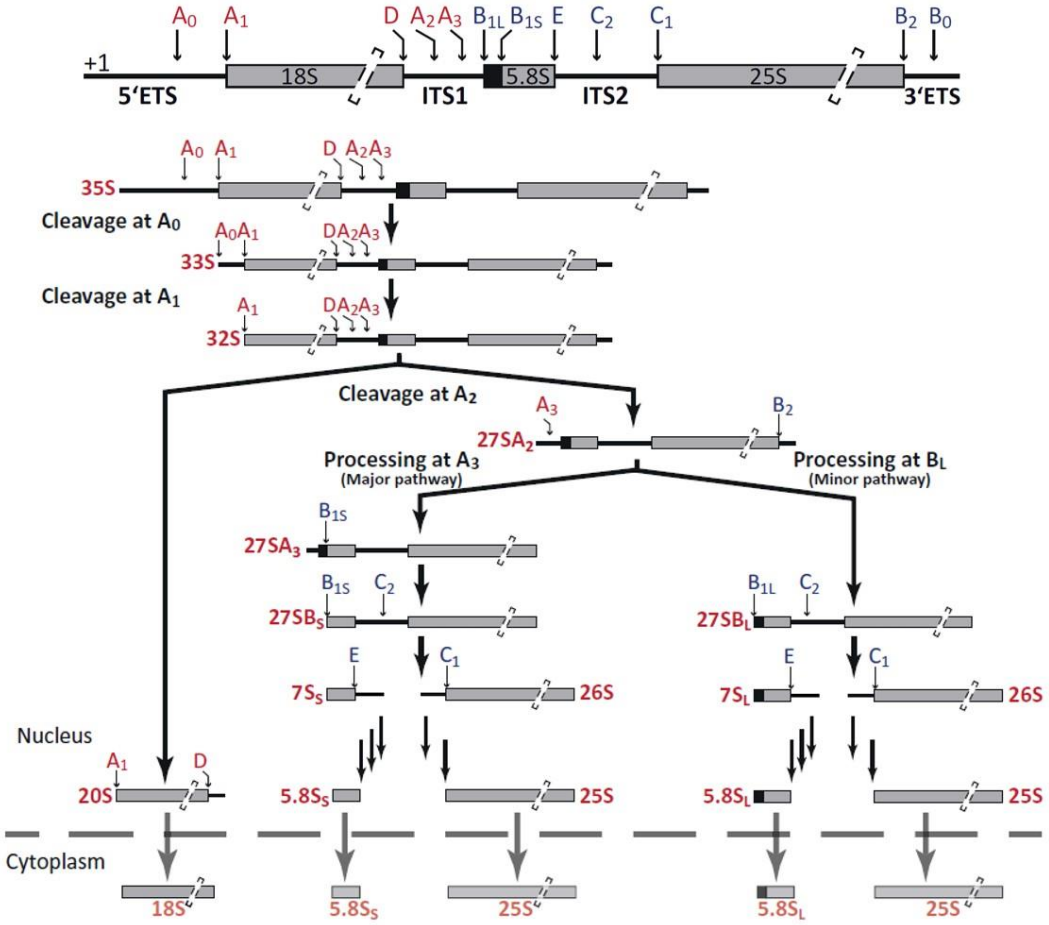

Figure 7: pre-rRNA processing in *S. cerevisiae* adapted from Braun et al. (2020).
Schematic representation of the pre-rRNA processing pathway(s) in yeast. Names of the precursors and mature rRNAs are indicated in red. Cleavage sites producing 18S rRNA are depicted in red. Processing sites for the maturation of 5.8S and 25S rRNAs are colored blue. The dashed line represents the nuclear envelope.

In contrast with this systematic cleavage pattern, some studies suggest the existence of alternative processing pathways, which are evident when yeast cells are cultivated under stress conditions (Kos-Braun et al., 2017). In fact, previous work of our group, using highly sensitive methods as affinity purifications, showed the presence of all possible precursors associated with AFs. These data suggest the stochastic cleavage at A0, A1, A2, and A3 sites

as a first-come/first-served model for the early steps of ribosome biogenesis (Boissier et al., 2017).

1.4.2 Post-transcriptional processing

At least the final maturation of SSU particles and the processing of LSU pre-rRNAs take place as post-transcriptional processing events. Moreover, at least 30% of transcripts are processed post-transcriptionally at the A0, A1, and A2 sites and this ratio increases when cells are cultivated in suboptimal growth conditions (exhausted nutrients, galactose containing medium, stationary growth phase, etc.) (Kos-Braun et al., 2017). It is supposed that the post-transcriptional cleavages at sites A0, A1, and A2 occur in the same order as in the co-transcriptional process, but as for co-transcriptional cleavage, also alternative processing pathways might be possible (Boissier et al., 2017). Afterward, the resulting 20S pre-rRNA is immediately exported from the nucleolus into the cytoplasm (Udem and Warner, 1973). In the cytoplasm, the endonuclease Nob1, which already associates with the pre-rRNA in the nucleolus, reaches the processing site D, cleaving and producing the mature 18S rRNA (see Figure 7) (Fatica et al., 2003; Lamanna and Karbstein, 2009; Pertschy et al., 2009).
The second product of the cleavage at the A2 site is the 27SA2 pre-rRNA, precursor of 5.8S and 25S rRNAs. 27SA2 is processed at the A3 site by the RNase MRP, which requires the correct formation of the 3'ETS by release of the nascent transcript via endonucleolytic cleavage of Rnt1 at site B0 (Allmang and Tollervey, 1998; Kufel et al., 1999). Therefore, processing events at the 5' and 3' ends of the 27SA2 pre-rRNA are connected, most likely by the interaction of Rpl3 with both ends of the 27SA2 pre-rRNA. Moreover, Rpl3 is required for the association of the early acting AFs, which participate in the initial formation of the pre-60S particle (Gamalinda et al., 2014; Hitchen et al., 1997; Kufel et al., 1999; Rosado et al., 2007a).
After A3 cleavage, the 5'-3' RNases Rat1, Xrn1, and Rrp17 process the 5' end of 27SA3 pre-rRNA to the $B1_S$ site present in the 5' of the 27SB pre-rRNA (El Hage et al., 2008; Henry et al., 1994; Oeffinger et al., 2009). As an alternative, an unknown endonuclease might process the 27SA2 pre-rRNA directly at $B1_L$ (see Figure 7) (Faber et al., 2006). These two pathways define the 5' end of the 5.8S, which is seven nucleotides longer in the $5.8S_L$ rRNA. However, the two processing pathways are asymmetrical and the of $5.8S_S$ rRNA accounts for up to 80% of the total 5.8S. Interestingly, inhibition of MRP leads to an exclusive synthesis of $5.8S_L$ rRNA (Chamberlain et al., 1998; Chu et al., 1994; Lygerou et al., 1996; Schmitt and Clayton, 1993), and accordingly, the absence of factors involved in the major pathway as Rrp5 and Dbp3 causes an imbalance in the production of $5.8S_S$ and $5.8S_L$ rRNAs (Eppens et al., 1999; Lebaron et al., 2013; Venema and Tollervey, 1996; Weaver et al., 1997).
In parallel to the processing of the mature 5' end of the 5.8S rRNA, an unknown 3'-5' exonuclease produces the mature 3' end of the 25S rRNA at the B2 site (see Figure 7) (Elela et al., 1996; Fernández-Pevida et al., 2015; Kufel et al., 1999).

Independently of the pathway producing the 5' end of the 27SB pre-rRNA, the next step includes the separation of 5.8S and 25S rRNA precursors by the endonucleolytic cleavage of the 27SB pre-rRNA at site C2 within the ITS2 region by Las1 (see Figure 7) (Gasse et al., 2015). Two secondary structures were initially predicted for the ITS2 called "ring" and "hairpin". Both structures are formed by alternative base-pairing within the ITS2 and the conformational change between both might trigger C2 cleavage (Côté et al., 2002; Joseph et al., 1999; Peculis and Greer, 1998; Yeh and Lee, 1990). Nevertheless, a third conformation showing a long helical organization is supposed to be the most accessible structure for the C2 endonuclease (Coleman, 2015; Pöll et al., 2017).
Cleavage at C2 produces the 7S and the 26S pre-rRNAs and the subsequent cleavage at site E leading to the mature 5.8S rRNA is a complex multi-step process (see Figure 7) (Mitchell et al., 1996). The first steps are carried out by the exosome (Lebreton et al., 2008a; Liu et al., 2006; Mitchell et al., 1997) and among several other factors, the helicase Mtr4 guides the exosome to the pre-rRNA (de la Cruz et al., 1998a; Fromm et al., 2017; Jackson et al., 2010). The obtained 6S pre-rRNA is finally matured to 5.8S rRNA in the cytoplasm, where the last steps are performed by a concerted action of the putative non-essential 3'-5' exonucleases Rex1, Rex2, and Rex3 and by the putative non-essential nuclease Ngl2 (Faber et al., 2002; van Hoof et al., 2000; Thomson and Tollervey, 2010).
The processing of 26S pre-rRNA at the C1 site by exonucleases Rat1, Rrp17, and Xrn1, as well as the AF Las1, forms the mature 5' end of the 25S rRNA (see Figure 7) (Gasse et al., 2015; Geerlings et al., 2000; Oeffinger et al., 2009; Schillewaert et al., 2012).

1.4.3 Regulation of co- and post-transcriptional processing at the A0, A1, and A2 sites

Growth of the yeast cells under stress or beyond exponential growth phase can lead to increased post-transcriptional pre-rRNA processing at the expense of co-transcriptional processing. Post-transcriptional processing takes place on the completely synthesized 35S pre-rRNA either after terminated transcription or after cleavage at site B0. As a result, higher amounts of 35S and 23S pre-rRNAs are detected.
The second cleavage step after cut at B0 might occur either at sites A0, A1 (producing 33S or 32S pre-rRNA, respectively), or at site A3 (producing the 23S pre-rRNA reaching from 5'ETS to A3) (Figure 8) (Allmang and Tollervey, 1998). The preferential use of the A3 pathway, producing 23S and 27SA3 pre-rRNAs, may directly depend on the nutrient availability and may be regulated by the TORC1 (Tor complex 1) pathway, which also controls the transcription activity of all three RNA polymerases. Tor1 kinase is constitutively active and inactivated in the absence of nutrients. Besides transcription, TORC1 activates the CK2 kinase, which leads to preferential cleavage at the A2 site (Kos-Braun et al., 2017). Contrary, when the CK2 kinase is not activated, the A3 pathway is predominantly used. Upon nutrient depletion, both 27SB (derived from 27SA3) and 23S pre-rRNAs might be non-fully productive intermediates, which are not further processed (Kos-Braun et al., 2017), most possibly due to the absence of RPs (Philippi et al., 2010).

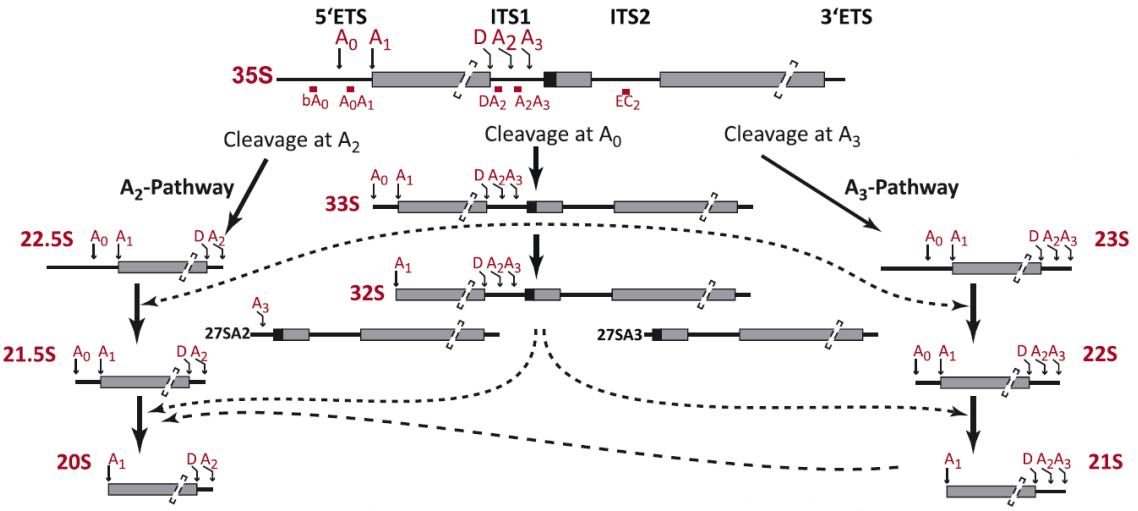

Figure 8: Alternative pre-rRNA processing adapted from Boissier et al. (2017).
Schematic representation of the alternative pre-rRNA processing pathways for removal of the 5'ETS sequence of the 35S pre-rRNA. Names of the pre-rRNAs and cleavage sites are depicted in red. Probes used for northern blot detection of the pre-rRNA intermediates are indicated in red below 35S precursor and named after their hybridization sites.

All intermediates depicted in Figure 8 can be observed when components of the exosome are mutated (Allmang et al., 2000). Non-productive pre-rRNA intermediates are polyadenylated by the TRAMP complex (LaCava et al., 2005). Poly(A) tail targets the exosome to aberrant intermediates, which are degraded (Allmang et al., 2000; Wery et al., 2009; Zanchin and Goldfarb, 1999). Nevertheless, the removal of aberrant intermediates by the exosome might require additional cleavage events at novel cleavage sites (Choque et al., 2018).
In contrast, affinity purification of AFs increases the sensitivity for the detection of alternative processed transcripts, which are visualized and might represent productive intermediates. It is possible that the reduced synthesis of RPs in suboptimal growth conditions slows down the processing of particles requiring the assembly of large sets of RPs and speeds up the processing of particles less dependent on RPs. This mechanism would explain an increase in the lifetime of early particles but a decrease in the lifetime of the late ones. In addition, the absence of the exosome might reduce the recycling of AFs and, therefore, increase the half-life of aberrant pre-rRNA intermediates (Figure 8), which are usually short-living intermediates due to the fast kinetics producing mature 18S rRNA.

1.4.4 Recycling events during pre-rRNA processing

As explained in the previous section, the exosome and the TRAMP complex are responsible for the degradation of dead-end products, which accumulate when pre-rRNA intermediates cannot be further processed (Dez et al., 2006; LaCava et al., 2005).
Moreover, the 3'-5' exonuclease activity of the exosome and 5'-3' exonucleases are directly involved in pre-rRNA processing for removal of the ETS and ITS regions. The 5'ETS-A0 fragment is degraded by the exosome, which is recruited by the helicase Mtr4 (Allmang et al., 2000; Bernstein et al., 2008; Suzuki et al., 2001). The second 5'ETS

fragment reaching from A0 to A1 is a substrate of the exosome and the nucleolar 5'-3' exoribonuclease Rat1 (Allmang et al., 2000; Johnson, 1997; Petfalski et al., 1998). The D-A2 fragment resulting from cleavages at A2 and D is degraded by the cytoplasmic 5'-3' exoribonuclease Xrn1 (Johnson, 1997; Stevens et al., 1991).
After A3 cleavage, Rat1, Xrn1, and Rrp17 also process the 27SA3 pre-rRNA to the B1S site present in the 5' of the 27SB pre-rRNA (El Hage et al., 2008; Henry et al., 1994; Oeffinger et al., 2009). It is assumed that the correct assembly of Rpl17 at this point is required to stop the degradation process toward the B1 site. This implies that aberrant pre-60S intermediates, which lack at least Rpl17, are directly degraded instead of being further processed (Henry et al., 1994; Sahasranaman et al., 2011). Within the ITS2 region, the E-C2 fragment is degraded first by the exosome in the nucleolus and by other 3'-5' exonucleases in the cytoplasm (see 1.4.2). Recruitment of exosome would occur most possibly by recruitment of Mtr4 through Nop53 (Cepeda et al., 2019; Falk et al., 2017; Thoms et al., 2015). The remaining ITS2 fragment reaching from C2 to C1 is degraded by the 5'-3' exonucleases Rat1, Rrp17, and Xrn1 and the B2-B0 fragment of the 3'ETS is degraded by an unknown 3'-5' exonuclease (see 1.4.2).
Altogether, the mentioned events are important to recover the excised nucleotides and to recycle AFs, which are associated with the spacer regions (5'ETS, ITS1, and ITS2) or accumulated in dead-end products (Houseley and Tollervey, 2009).

1.5 Assembly of the small subunit

During assembly of the small subunit, three defined particles are identified.
In the early steps of ribosome synthesis, the first pre-SSU particle or **s**mall **s**ub**u**nit processome (SSU processome) is formed in the nucleolus. However, post-transcriptional cleavage allows the formation of the 90S pre-ribosome, which contains the 35S pre-rRNA and for instance the SSU-processome factors but also early AFs of the large subunit. The third particle corresponds to the pre-40S particle, which is formed in the nucleus (after A0, A1, and A2 cleavages) and transported to the cytoplasm, where the last cleavage event takes place and the 40S or small subunit is produced.

1.5.1 Stepwise formation of the SSU processome

The formation of the SSU processome can be currently explained by two non-exclusive models. The hierarchical model defines a stepwise process, in which the assembly of some AFs and RPs is required for the further association of others (e. g. Dutca et al., 2011; Pérez-Fernández et al., 2007, 2011) . The second model only establishes a relevant role for rRNA domains on the consecutive recruitment of AFs (Hunziker et al., 2019). In both cases, the assembly of the SSU processome starts with the assembly of the 5'ETS particle. Subsequently, the different domains of the 18S rRNA are folded and gradually integrated into the precursor particle (Figure 9).

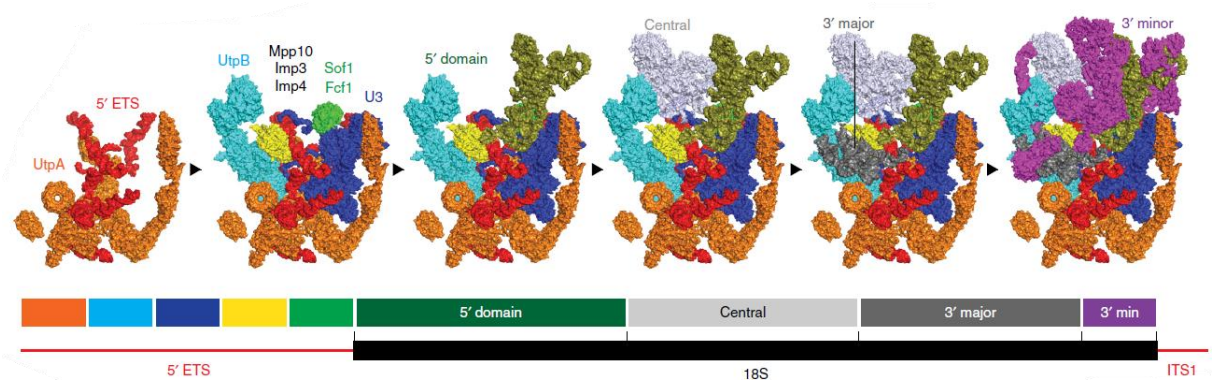

Figure 9: Schematic model for SSU-processome assembly adapted from Peña et al. (2017).
tUTP/UTP-A complex (orange) is bound first to the 5'ETS (red) and forms the base of the SSU processome. Binding of UTP-B complex (turquois), U3 snoRNP (blue), and some other AFs (yellow, green) completes the 5'ETS particle. 5' domain (moss green), as well as the central domain (light gray), 3' major domain (dark gray), and 3' minor (min) domain (purple) are transcribed, folded, and decorated with factors in a hierarchical manner.

The finally assembled SSU processome contains 36 AFs and 18 RPs out of the 33 RPs present in the mature 40S subunit. Within the available models of the SSU processome, the folding of the 5' and central domains resembles the folding state in the mature small subunit, whereas the 3' major and minor domains still require large structural reorganization to adopt the conformation of the mature subunit (Sun et al., 2017; Zhang et al., 2016b).

1.5.1.1 Assembly of the 5'ETS particle

The first step within the formation of the 5'ETS particle involves the association of the heptameric tUTP/UTP-A (derived from **U** three **p**rotein; Dragon et al., 2002) complex with the 5'ETS of the nascent transcript produced by RNA Pol I (Gallagher et al., 2004; Pérez-Fernández et al., 2007). The **t**UTP complex formed by the proteins Utp4, Utp5, Utp8, Utp9, Utp10, Utp15, and Utp17/Nan1, was identified as functional subcomplex of the SSU processome, which might also participate in the efficient **t**ranscription of the rDNA (Gallagher et al., 2004). With a protein composition similar to the tUTP complex, the UTP-A complex was identified containing Pol5 instead of Utp5 (Krogan et al., 2004). Since the nomenclature of tUTP and UTP-A complexes is not always clearly used in the literature, we will refer to them as two independent complexes containing either Utp5 or Pol5, respectively, or as tUTP/UTP-A complex when the protein composition is unclear. The association of the tUTP/UTP-A complex with the 5'ETS is required for the subsequent stable assembly of the hexameric complexes UTP-B (consisting of Utp1/Pwp2, Utp6, Utp12, Utp13, Utp18, Utp21) and U3 snoRNP (composed of C/D box U3 snoRNA, Nop1, Snu13, Nop56, Nop58, Rrp9) (Figure 10) (Boissier et al., 2017; Dosil and Bustelo, 2004; Pérez-Fernández et al., 2007; Watkins et al., 2000). In addition, both complexes are mutually required for their stable association onto the pre-rRNA (Pérez-Fernández et al., 2007). The final assembly of the 5'ETS particle is achieved by the association of the Mpp10 complex (consisting of Imp3, Imp4, Mpp10) (Pérez-Fernández et al., 2011; Sá-Moura et al., 2017) and some other AFs, like Utp3/Sas10, Sof1, Utp7, Utp11, and Bud21/Utp16 (see

Figure 10 and Figure 12) (Chaker-Margot et al., 2015). Finally, the proteins Fcf2, as well as the putative A1 and A2 endonuclease Fcf1/Utp24, are recruited to the 5'ETS (Zhang et al., 2016b).

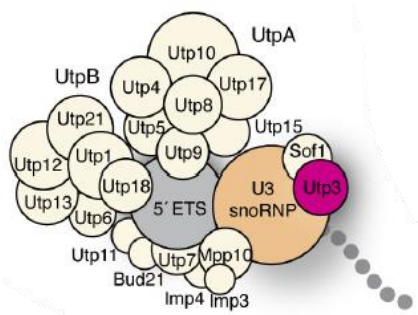

Figure 10: Protein components of the 5'ETS particle adapted from Chaker-Margot et al. (2015). Schematic representation of the protein and RNA composition of the 5'ETS particle defined by mass spectrometry. 5'ETS sequence of the pre-rRNA is depicted in gray, U3 snoRNP containing the U3 snoRNA is colored orange, AFs are showed in beige, and Utp3 as predicted exosome interactor is depicted in pink.

The tUTP/UTP-A complex associates with helices I to IV of the 5'ETS (Figure 11). While Utp8, Utp9, and Utp17 assemble at the most 5' end of the 5'ETS, the remaining four proteins Utp4, Utp5, Utp10, and Utp15 are incorporated downstream (Hunziker et al., 2016). Utp17, Utp4, and Utp15 might stabilize the first three helices, while Utp5 and Utp10 connect the tUTP/UTP-A complex to the UTP-B complex by interaction with the UTP-B components Utp21 and Utp18. The UTP-B component Utp18 is a central interactor within the 5'ETS particle by binding to the tUTP/UTP-A component Utp10, the UTP-B components Utp21 and Utp6, and the U3 snoRNP components Nop58 and Snu13 (Hunziker et al., 2016). Within the UTP-B complex the tWD domains of Utp1 and Utp21 interact together and their C-terminal domains associate with the C-terminal domains of Utp12 and Utp13 (Boissier et al., 2017; Zhang et al., 2016a). In addition, Utp21 bridges the association with Utp6 and Utp18 (Boissier et al., 2017; Hunziker et al., 2016; Pöll et al., 2014; Zhang et al., 2016a). We have proposed that the presence of Utp12 and Utp13 is not required for the assembly of the UTP-B core components Utp6, Utp18, Utp21, and Utp1, but the association with the 5'ETS particle requires the complete formation of the UTP-B complex (Boissier et al., 2017).

The U3 snoRNA base pairs the middle part of the 5'ETS through its 5' and 3' hinge regions (Figure 11) (Beltrame and Tollervey, 1992, 1995; Beltrame et al., 1994; Dutca et al., 2011; Marmier-Gourrier et al., 2011). This association might be stabilized by interactions with the tUTP/UTP-A and UTP-B complexes (Pérez-Fernández et al., 2007) and the U3 snoRNA may participate in folding of the helices V and VI and stabilization of pre-ribosomal particles. The initial interaction between U3 snoRNA and 5'ETS seems to be mediated by the 3' hinge, whereas the incorporation of additional AFs, like UTP-B components, U3 snoRNP factors, and Mpp10 complex might depend on the additional binding of the 5' hinge to the 5'ETS (Dutca et al., 2011; Marmier-Gourrier et al., 2011). Association of Imp3 and Imp4 might occur concomitantly with Mpp10 as a single protein complex (Pérez-Fernández et al., 2011), which has no influence on the stability of the 5'ETS particle itself,

but it is essential for later assembly steps of the SSU processome (Gérczei et al., 2009; Pérez-Fernández et al., 2011; Shah et al., 2013).

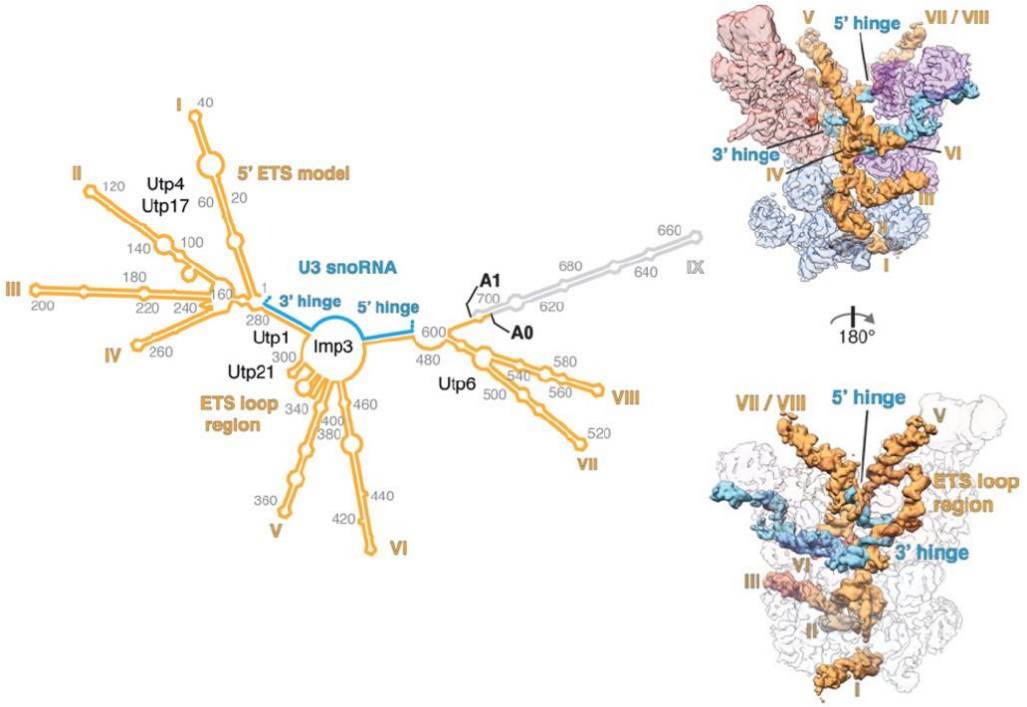

Figure 11: Secondary and tertiary structures of the 5'ETS particle adapted from Chaker-Margot et al. (2017).
On the left, the secondary structure model of the 5'ETS (orange) and the interaction with the U3 snoRNA (blue) are depicted. Helix IX is not observed in the EM density map and it is depicted in gray. Names of some of the associated proteins, the pre-rRNA domains, and the A0 and A1 processing sites are indicated. On the right, front (above) and back (below) view of the tertiary structure of the 5'ETS particle with RNA elements colored as on the left are shown. tUTP/UTP-A complex is colored in light blue, U3 snoRNP in light violet, and UTP-B complex in light red.

Distant regions of the 5'ETS are also connected by UTP-B, with helices VII and VIII bound by Utp6, the 5'ETS loop region between helices IV and V by Utp1 and Utp21, and helix V by Utp18 (Chaker-Margot et al., 2017), and therefore suggesting a chaperone activity for UTP-B (Chaker-Margot et al., 2017). In addition, Utp18 may play an additional role in recruiting the exosome, due to the presence of an **a**rch-**i**nteraction **m**otif (AIM) domain, which binds the "arch" domain in Mtr4 (Jackson et al., 2010; Thoms et al., 2015).
Altogether, the 5'ETS particle has a very dense structure, which is stabilized by many protein-protein interactions maintaining the folding of the RNAs and providing a base for the assembly of the remaining AFs in the SSU processome (Barandun et al., 2017; Chaker-Margot et al., 2017; Hunziker et al., 2016; Sun et al., 2017; Zhang et al., 2016b).

1.5.1.2 Assembly of the 5' domain, the central domain, and the 3' major domain

Domains of the 18S rRNA assemble after formation of the 5'ETS particle has taken place (see Figure 12) (Chaker-Margot et al., 2017; Sun et al., 2017; Zhang et al., 2016b).
The 5' domain of the 18S rRNA includes the first 18 helices. The RPs Rps9, Rps23, Rps24, and Rps30 associate with the helices 3, 4, and 15 to 18, while Rps4, Rps6, Rps8, and Rps11

associate with helices 5 to 14. Helix 6 contains the binding site of the C/D box snoRNA U14, which is required for 2'-O methylation of nucleotides 414 and 415 within the 5' domain (Chaker-Margot, 2018; Liang and Fournier, 1995; Zhang et al., 2016b). AFs like Enp2, Bfr2, and Lcp5 are stably bound between helices 14 and 15 and they recruit AFs like the helicase Dbp4/Hca4 (Soltanieh et al., 2014). Lcp5 contains an exosome interaction domain and it may assist Utp18 to bring the exosome in the proximity of the 5'ETS domain (Barandun et al., 2017; Chaker-Margot et al., 2015; Wiederkehr et al., 1998). Although the function of most of the AFs recruited to the 5' domain is not yet defined, assembly of the 5' domain is required for the subsequent incorporation of the other rRNA domains within the SSU processome (Chaker-Margot et al., 2015; Sun et al., 2017; Zhang et al., 2016b).

Next, the central domain formed by helices 19 to 27 is folded into the nascent SSU processome (see Figure 12). The helices 20, 22, 23, and 26 are bound by six RPs (Rps1, Rps7, Rps13, Rps14, Rps22, and Rps27) (Sun et al., 2017). In addition, the H/ACA box snoRNAs snR30 and snR10 base-pair within the central domain. Although both snoRNPs are required for small subunit biogenesis, their specific functions remain elusive and they need to be removed to achieve the mature conformation of the 18S rRNA (Atzorn et al., 2004; Bohnsack et al., 2008; Fayet-Lebaron et al., 2009; Kiss et al., 2010; Martin et al., 2014). During the formation of the central domain, among others, the large AF Rrp5 is recruited and it is required for the stable assembly of the UTP-C complex, formed by Utp22, Rrp7, and the four CKII subunits (Krogan et al., 2004; Pérez-Fernández et al., 2007; Torchet et al., 1998). Similar to the other UTP complexes, UTP-C promotes the folding and stabilization of the SSU precursor particle by interactions with RPs and rRNA sequences (Lin et al., 2013; Pérez-Fernández et al., 2007). Strikingly, Rrp5 interacts with the central domain and with other binding sites throughout the 35S pre-rRNA, being also relevant for the synthesis of the large subunit (Eppens et al., 1999; Lebaron et al., 2013; Zhang et al., 2016b). Finally, Utp13 and Sof1, which associate with the 5'ETS, contribute to the folding of the central domain onto the 5'ETS via interactions with Utp7 and the UTP-B complex and provide additional stabilization by connecting the central domain with the 5'ETS (Barandun et al., 2017; Chaker-Margot et al., 2017; Sun et al., 2017; Zhang et al., 2016b).

The 3' major domain of the 18S rRNA contains helices 28 to 43 (see Figure 12). However, helices 35 to 40 are not resolved in Cryo-EM structures, most likely because they are initially poorly folded and only a few proteins are associated during these early steps. The RPs Rps5, Rps16, and Rps28 associate with helices 28 to 30 and 41 to 43, while Rps12 and Rps31 bind to helices 32 to 34. Altogether, five AFs are recruited at this step. The AFs Nsr1, Mrd1, and Nop9 associate with helix 28 close to one of the 18S rRNA binding sites of the U3 snoRNA (Chaker-Margot et al., 2015; Sun et al., 2017; Zhang et al., 2016b). Since U3 snoRNA binding sites at the 18S rRNA might be later involved in the formation of the central pseudoknot, it is suggested that these three AFs contribute to chaperoning this RNA element (Zhang et al., 2016b). Similar to Utp13 and Sof1, the Mpp10 complex might stabilize the SSU-processome by connecting the first and the last helices (helix 28 and helix 43) of the 3' major domain with the 5'ETS (Barandun et al., 2017; Chaker-Margot, 2018; Sun et al., 2017; Zhang et al., 2016b).

1.5.1.3 Assembly of the 3' minor domain and finishing of the SSU processome

The final step of SSU processome formation is the folding of the 3' minor domain (Jakob et al., 2012). In contrast to the 3' major domain, a multitude of AFs are recruited at this step and many interactions, stabilizing the folding of the other domains and the structure of the complete SSU processome, are formed (Figure 12) (Chaker-Margot et al., 2017).

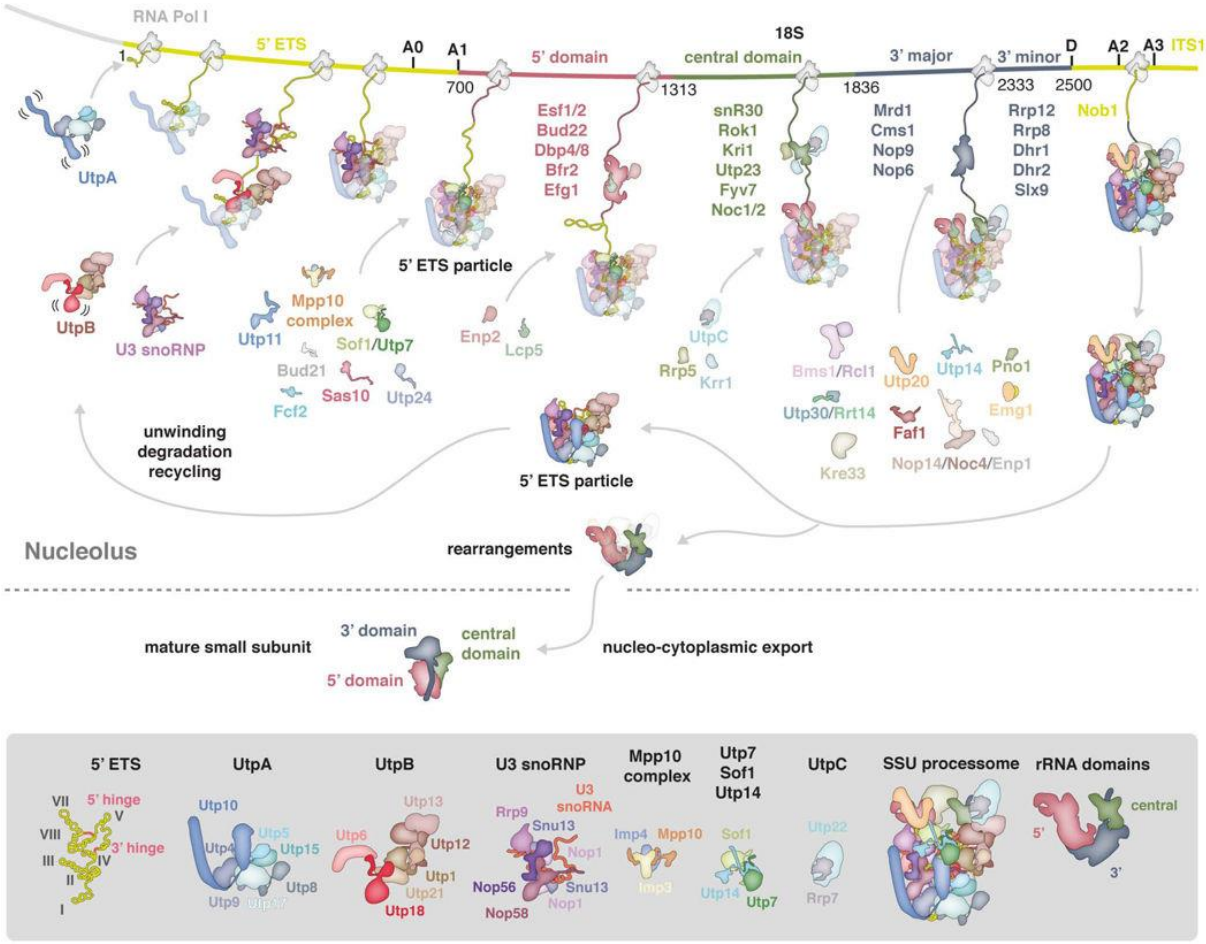

Figure 12: Schematic representation of the co-transcriptional assembly of the SSU processome obtained from Barandun et al. (2018).
Early events of small subunit assembly in the nucleolus and subsequent maturation resulting in the mature cytoplasmic small subunit are depicted. The relevant parts of the rDNA locus are depicted including 5'ETS and ITS1 (yellow), 5' domain (red), central domain (green), 3' major and minor domains (gray) of the 18S rRNA. Factors of the assembled SSU processome are shown as schematic outline. Transient components are listed and colored according to their associated rRNA domain. Below, the SSU processome and its major components are depicted in detail.

The 3' minor domain contains the helices 44 and 45. Helix 44 is the longest within the 18S rRNA and it contacts the UTP-C component Utp22 present at the central domain and the UTP-B components Utp12 and Utp13 at the 5'ETS (Hunziker et al., 2016; Sun et al., 2017). The AFs Utp30, Bms1, Rcl1, Kre33, Nop14, Noc4, Utp14, Utp20, Enp1, Pno1/Dim2, Rrp12, and Rrt14 and the helicases Dhr1 and Dhr2 were found to be assembled at this point (Chaker-Margot et al., 2015; Zhang et al., 2016b). In contrast during folding of the 3' minor

domain, helicases like Dbp4, which unwind the snoRNA-rRNA interaction might release 14 earlier AFs and the snoRNAs U14, snR30, and snR10 (Soltanieh et al., 2014).
The heterodimer Rcl1-Bms1 bridges the domains 3' major and 5' (Chaker-Margot et al., 2017). This position might allow the GTPase activity of Bms1 to exert mechanical force and facilitate the structural rearrangement of the SSU processome required for A2 cleavage (Delprato et al., 2014). In addition, Kre33 connects the 3' minor domain to 3' major and 5' domains and Utp20 the 3' minor domain to 5' domain and helices VII and VIII of the 5'ETS (Chaker-Margot et al., 2017). The heterodimer Nop14-Noc4 assembles once the head structure is formed and bridges the 5'ETS, the 5' domain, and the central domain by association with tUTP/UTP-A, Mpp10-Imp5, and Bms1-Rcl1 (Barandun et al., 2017; Jakob et al., 2012). The AF Utp14 might contribute to join together helix V of the 5'ETS and 3' domains by association with Utp6 and Utp7 to Sof1 (Barandun et al., 2017). Finally, the endonuclease of the D site, Nob1, is recruited into the SSU processome concomitantly with the folding of the ITS1 (Chaker-Margot et al., 2015).

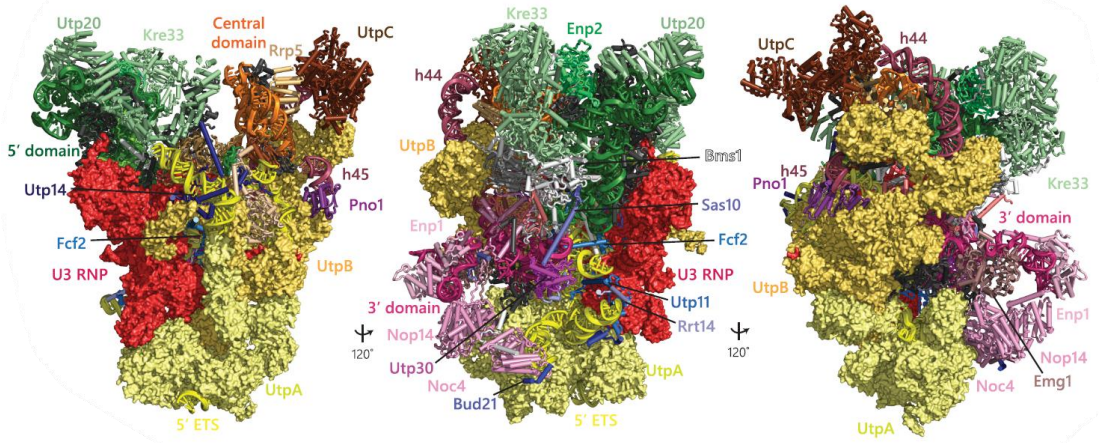

Figure 13: Structure of the SSU processome of *S. cerevisiae* adapted from Chaker-Margot (2018).
Each view of the structure is rotated by 120°. 5'ETS (yellow) is bound by tUTP/UTP-A complex (pale yellow), UTP-B complex (dark yellow), and U3 snoRNP (red). The domains of the 18S rRNA are depicted in green (5' domain), orange (central domain), bright pink (3' major domain), and dark pink (3' minor domain). The associated AFs are shown in similar colors, respectively.

A special feature of the mature SSU processome is the physical separation of the four domains of the 18S rRNA, which might facilitate their individual downstream maturation (Figure 13) (Barandun et al., 2017; Chaker-Margot et al., 2017). Interestingly, several AFs (Utp20, Rrp5, Enp1, Krr1, and Pno1/Dim2) might prevent the SSU processome from adopting a premature conformation, and apparently, the formation of the central pseudoknot is inhibited by the presence of Bms1, Nop14, Imp4, Faf1, and Mpp10. Bms1, Nop14, Imp4, and Faf1 might stabilize the base pairing between the U3 snoRNA and the 5' domain of the 18S rRNA, which needs to be destabilized to form the central pseudoknot. In addition, Mpp10 holds helix 44 of the 3' minor domain in a partially unfolded conformation (Barandun et al., 2017; Chaker-Margot, 2018; Sun et al., 2017; Zhang et al., 2016b; Chaker-Margot et al., 2015, 2017).

1.5.2 Transition to the cytoplasmic pre-40S particle

Subsequent maturation of the SSU processome in the cytoplasmic pre-40S particle requires several extensive structural rearrangements (Figure 14).
First, the cleavages at A1 and A2 sites must take place and 18S rRNA must adopt the central pseudoknot structure. Both events seem to be coordinated by the action of the helicase Dhr1, which unwinds at least one of the rRNA-U3 snoRNA duplexes and the resulting open structure would be the substrate for the endonuclease Utp24 (Bleichert et al., 2006; Sardana et al., 2015; Wells et al., 2016).
Second, the 5'ETS particle must be removed in order to recycle the AFs (see Figure 12), possibly achieved by the exosome (Allmang et al., 2000). As previously explained, either the UTP-B component Utp18, through its AIM domain, or the AFs Utp3 and Lcp5, because of their resemblance to the exosome cofactor Rrp47, might mobilize the exosome to the 5'ETS particle (Chaker-Margot, 2018; Costello et al., 2011; Klinge and Woolford, 2019).

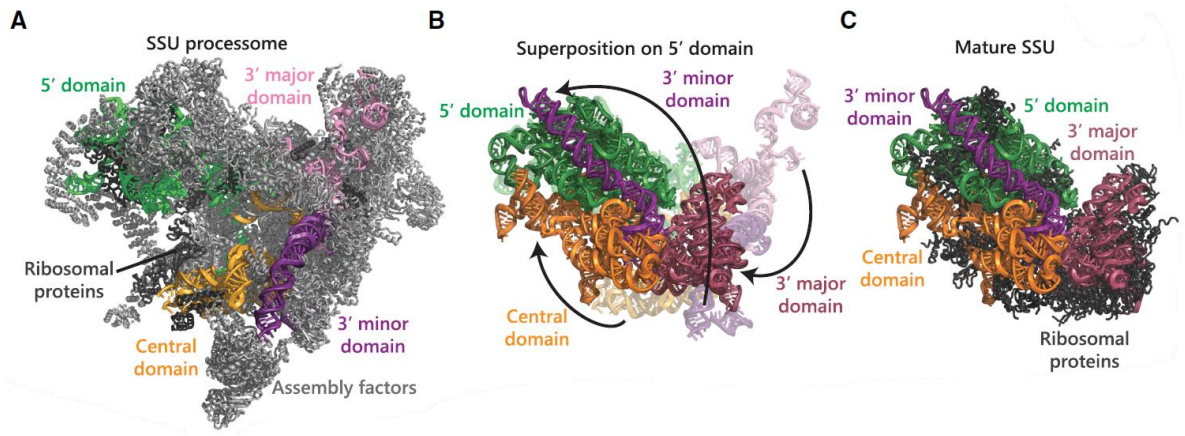

Figure 14: Structural rearrangement of the SSU processome to obtain the mature small ribosomal subunit adapted from Chaker-Margot (2018).
Comparative view of the 18S rRNA domains in the SSU processome (**A**) and the mature small ribosomal subunit (**C**). The required rotations of the domains to achieve the mature conformation are demonstrated in **B**, showing the domains in their SSU-processome conformation in pale colors. The rearrangements begin in the nucleus and are finished in the cytoplasm.

Third, most AFs, with the exception of Enp1, Pno1/Dim2, and Rrp12, must be removed, the AFs Rio2, Dim1, Tsr1, and Ltv1 must associate, and the RPs Rps15, Rps18, and Rps28 join the pre-rRNA to allow the export of pre-40S particles. Ltv1 interacts with Enp1 and replaces Nop14, while Tsr1, a catalytically inactive GTPase, substitutes Bms1 (Chaker-Margot, 2018; Ferreira-Cerca et al., 2005; Heuer et al., 2017; Klinge and Woolford, 2019; McCaughan et al., 2016; Scaiola et al., 2018; Schäfer et al., 2003). These assembly steps assure the export competence of pre-40S particles (Peña et al., 2017).

1.5.3 Final maturation of the small subunit

The pre-40S complex transported into the cytoplasm contains only a few AFs (Figure 15), which in general hold the complex in a premature conformation that is translationally

inactive (Scaiola et al., 2018). It is very likely that the stepwise release of the factors and the association of RPs directly lead to the final maturation of the small subunit (Heuer et al., 2017; Scaiola et al., 2018).
The factors Enp1 and Ltv1 lie between head and body on the solvent-exposed side and they maintain the pre-head structure by preventing the formation of one of the three-way-junctions required for the mature head structure (Collins et al., 2018; Strunk et al., 2011, 2012). The missing connection between helices 34, 35, and 38 requires the association of Rps3, Rps10, and Rps14, which is blocked by Enp1 and Ltv1 (Heuer et al., 2017; Scaiola et al., 2018).

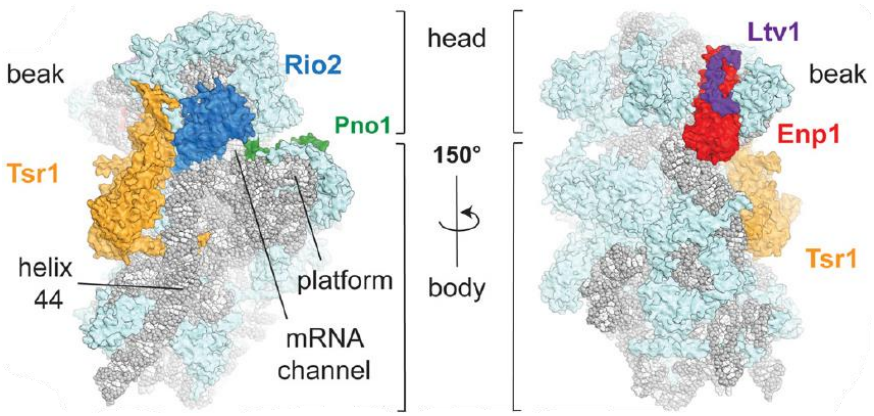

Figure 15: Structure of the cytoplasmic pre-40S subunit adapted from Scaiola et al. (2018).
Overview of the front and back of the pre-40S structure. 20S pre-rRNA is depicted in gray, RPs in light blue, Tsr1 in yellow, Rio1 in blue, Pno1 in green, Enp1 in red, and Ltv1 in purple. Structural hallmarks are annotated.

The core structure of A- and P-sites at the decoding center is composed of the central pseudoknot, already built by helices 1, 2, and 28 of the 5' domain and by helices 44 and 45 of the 3' minor domain. Factors Tsr1 and Rio2 are positioned at the subunit interface and they block the final formation of the decoding center by association with helices 28 and 44 (Heuer et al., 2017; Strunk et al., 2011). Dim1 (not depicted in Figure 15), Tsr1, and Rio2 prevent the premature association of initiation factors (Heuer et al., 2017; Scaiola et al., 2018; Strunk et al., 2011). In addition, the conformation of the premature head structure allows the association of Pno1, which protects the D site of the 20S pre-rRNA from premature cleavage (Scaiola et al., 2018).
Phosphorylation of Enp1 and Ltv1 by the kinase Hrr25 triggers their release and induces the gradual conformational change of the described particle toward the mature small subunit (Figure 16) (Schäfer et al., 2006). The conformational change allows the association of Rps3 (Mitterer et al., 2016) and the formation of the beak causes the rotation of the head and induces the ATPase activity of Rio2, which is required for its release (Ferreira-Cerca et al., 2012). Disassembly of Rio2 induces the subsequent release of Tsr1 and enables helix 44 to adopt its mature conformation in proximity to helix 28, allowing the association of Rps26. Incorporation of Rps26 changes the position of Pno1 and exposes the D site to the nuclease Nob1 (Heuer et al., 2017). This last step may represent a checkpoint, assuring that 20S pre-rRNA cleavage is not carried out until the

40S subunit is prepared to bind a 60S subunit (Fatica et al., 2003; Johnson et al., 2017; Pertschy et al., 2009; Turowski et al., 2014).

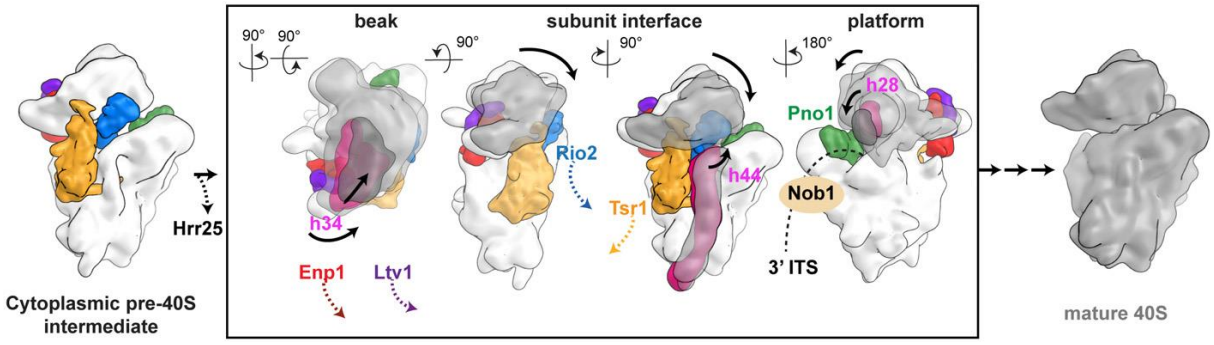

Figure 16: Model for cytoplasmic pre-40S maturation obtained from Scaiola et al. (2018).
The boxed region of the scheme represents a single species and highlights the conformational changes coupled to the release of individual AFs without implying a sequential order. The changing rRNA conformations between pre-40S (white, changing part in pink) and the mature 40S (gray, changed part in dark gray) are indicated with arrows. The reorientation of helices 34, 44, and 28 is interconnected leading to conformational changes in the beak, the subunit interface, and the platform, inducing the release of the depicted AFs from their binding sites.

Thus, the nearly complete formation of the mature 40S subunit prior to the cleavage at D site allows the pre-40S particle to be tested for its functionality by forming an 80S-like complex together with a mature 60S subunit (see 1.7.2) (Chaker-Margot, 2018; Ghalei et al., 2017; Hector et al., 2014; Lebaron et al., 2012; Strunk et al., 2012).

1.6 Assembly of the large subunit

The assembly of the large subunit occurs in three different compartments within the eukaryotic cell. The maturation process starts in the nucleolus, proceeds in the nucleoplasm, and concludes in the cytoplasm with the final maturation of the 60S or large ribosomal subunit.

1.6.1 Stepwise assembly of the nucleolar pre-60S particle

Formation of the nucleolar pre-60S particle is a hierarchical process that starts co-transcriptionally (see 1.5.1) (Gamalinda et al., 2014; Hierlmeier et al., 2013). However, most stages in 60S formation are post-transcriptional since A3 cleavage is concomitant with the removal of the 3'ETS (Allmang and Tollervey, 1998). It is assumed that the transcription termination is not required for the association of the factors itself but for their stable incorporation (Chaker-Margot and Klinge, 2019; Chen et al., 2017).

1.6.1.1 Assembly of the solvent-exposed side

Despite the co-transcriptional assembly of the early AFs, most of the knowledge about 60S formation has been obtained from post-transcriptional particles. Therefore, very early

assembly steps of the pre-60S complex have only been studied after A2 cleavage, when the pre-rRNAs for the small and large ribosomal subunits are well defined (see 1.4.2 and 1.5.2). The binding of AFs and RPs at this stage leads to the compaction of the particle and the structural rearrangements inducing the formation of a stable precursor RNP (de la Cruz et al., 2004; Rosado et al., 2007a, 2007b). These very early steps may precede the formation of the pre-ribosomal particles visualized by Cryo-EM (Kater et al., 2017; Sanghai et al., 2018; Zhou et al., 2019a).

The correct formation of the 3'ETS by cleavage at B0 is a prerequisite for the processing at A3 within the 27SA2 pre-rRNA and early pre-60S formation (Allmang and Tollervey, 1998; Hitchen et al., 1997; Kufel et al., 1999). Rpl3, the largest RP present in the large subunit, associates very early with domain VI of the 25S rRNA near the 3'ETS and close to the 5' end of the 5.8S rRNA. Due to its early assembly at both sides of the 27SA2, it is assumed that Rpl3 brings together both ends of the precursor to induce and support the subsequent assembly events and structural rearrangements (Gamalinda et al., 2014; Rosado et al., 2007a). It is also possible that Rpl3 might protect the 3' end of the 25S rRNA from degradation by RNases. Rpl3 interacts with the AFs Npa1, Npa2, Nop8, and Rsa3, which form a subcomplex together with the helicase Dbp6 (de la Cruz et al., 2004; Rosado et al., 2007b). Among these very early AFs, also other helicases (e. g. Dbp7 and Dbp9) associate with the pre-rRNA and their high potential to induce structural reorganizations contributes to the rearrangement of the very early 60S precursor particle (Klinge and Woolford, 2019; Woolford and Baserga, 2013).

Four other AFs, Nop4, Noc1/Mak21, Noc2, and Rrp5 may stabilize very early pre-60S particles by multiple interactions (Milkereit et al., 2001; Sun and Woolford, 1994). Rrp5 seems to play a predominant role in the biogenesis of both ribosomal subunits since its **N**- and **C**-**t**erminal **d**omains (NTD and CTD) are necessary for cleavages at A3 and A2 sites, respectively (Eppens et al., 1999; Hierlmeier et al., 2013; Khoshnevis et al., 2019; Lebaron et al., 2013; Torchet et al., 1998; Venema and Tollervey, 1996). The role of Rrp5 in the assembly of the small subunit is related to the association with the central domain of the 18S rRNA and it is important for SSU maturation (see 1.5.1.2). On the other hand, the role of Rrp5 in the assembly of the large subunit might be related to the association of the trimeric module formed by Rrp5, Noc1, and Noc2 at the ITS1 region (Hierlmeier et al., 2013; Lebaron et al., 2013).

The subsequent association of RPs and AFs is required for processing of the pre-rRNA at the A3 site and trimming of the 5' end to produce the 27SB pre-rRNA harboring the mature 5' end of the 5.8S rRNA (Fernández-Pevida et al., 2015). Moreover, the folding of 5.8S rRNA, ITS2, 25S rRNA domain I, and parts of domains II and VI initiates the "foot" structure and other parts of the solvent-exposed side (Figure 17). These rRNA folding states are visualized by Cryo-EM and the observed pre-ribosomal particles are grouped as states 1 (Sanghai et al., 2018) or A (Kater et al., 2017), respectively.

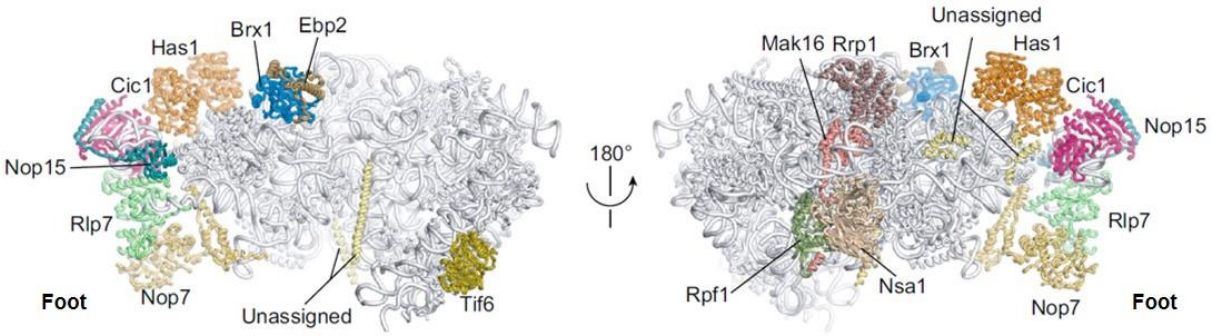

Figure 17: Cryo-EM structure of the pre-60S particle in state 2/B adapted from Zhou et al. (2019).
View from the subunit interface (left) and the solvent-exposed side (right) onto the AFs observed in Rpf1-TAP pre-60S particle. Assembled AFs belong to "A3 factors" and "Nsa1 module". rRNAs and RPs are colored gray, AFs are color-coded.

RPs associated with domain I of the 25S rRNA (Rpl4, Rpl8, Rpl13, Rpl15) are required for the stable incorporation of the RPs at domain II (Rpl6, Rpl7, Rpl14, Rpl16, Rpl18, Rpl20, Rpl32, Rpl33) (Gamalinda et al., 2014; Jakovljevic et al., 2012). These proteins are referred as "early" RPs of the pre-60S particle since they are required for the early processing steps at A2 and A3 sites (Gamalinda et al., 2014). The AFs involved include the twelve "A3 factors", Ebp2, Brx1, Pwp1, Nop12, Nop7, Ytm1, Erb1, Rlp7, Nop15, Cic1/Nsa3, Drs1, and Has1 (Dembowski et al., 2013a; Granneman et al., 2011; Sahasranaman et al., 2011; Talkish et al., 2014), as well as the proteins belonging to the "Nsa1 module" Nsa1, Rrp1, Rpf1, and Mak16 (Figure 17) (Kater et al., 2017; McCann et al., 2015). However, recruitment of these AFs depends on the previous association of the "early" RPs (Gamalinda et al., 2014; Jakovljevic et al., 2012). Despite the "A3 factors" assisting cleavage of the 5' end of the 5.8S rRNA, most of them associate with the 3' end of the 5.8S rRNA, the 5' end of the 25S rRNA, and the 5' end of the ITS2 (Babiano et al., 2013; Granneman et al., 2011).

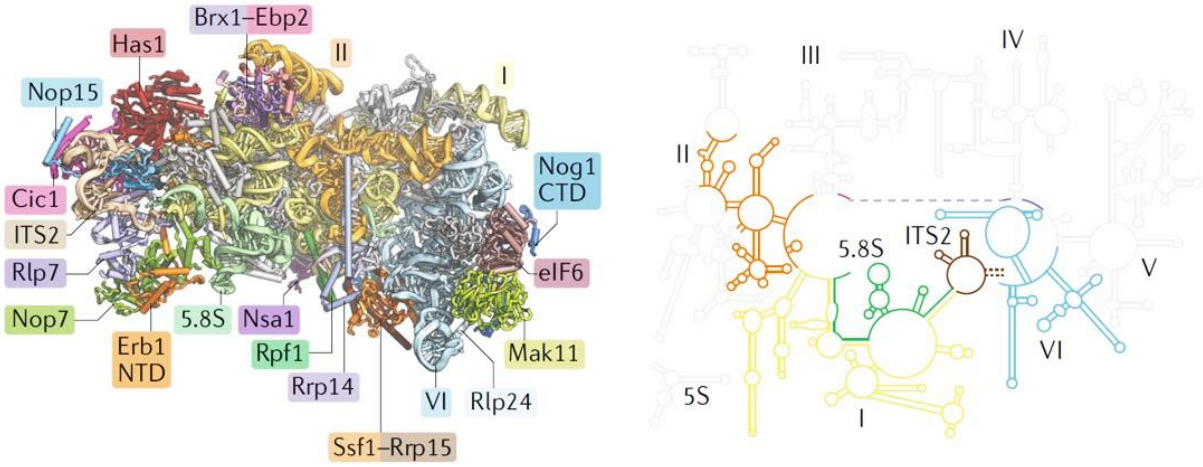

Figure 18: Cryo-EM structure and rRNA secondary fold of pre-60S particle in state 2/B adapted from Klinge and Woolford (2019).
View from the subunit interface onto the architecture of the pre-60S particle in state 2/B (left). AFs assigned to this state are specified. 5.8S rRNA, ITS2 region, and domains I, II, and VI of 25S rRNA are folded in the particle and color-coded as on the right. Disordered RNAs are indicated in light gray and largely ordered RNAs as dashed lines.

The “A3 factors” Cic1/Nsa3, Nop7, Nop15, Rlp7, and the NTD of Erb1 together with the RPs Rpl8 and Rpl15 associate at the ITS2 region to form the “foot” structure (Figure 17 and Figure 18) (Ben-Shem et al., 2011; Jakovljevic et al., 2012; Kater et al., 2017). The “Nsa1 module” initiates formation of the solvent-exposed side by clamping domains I and II between ES7A and Rpf1. At this stage, Rpf1 might determine the location of the PET by positioning its N-terminal helix as “place holder” (Kater et al., 2017; Zhou et al., 2019a).
The association of the “A3 factors” and the processing at the A3 site allow the stable incorporation of the “middle” RPs Rpl17, Rpl26, Rpl35, and Rpl37, and the association of some “B factors” (Gamalinda et al., 2013, 2014). Removal of the ITS1 leads to the stabilization of the base-pairing between domains I and II and the 5.8S rRNA (Dembowski et al., 2013a; Jakovljevic et al., 2012; Sahasranaman et al., 2011). This structural rearrangement is required for the recruitment of these four “middle” RPs to the ITS2/“foot” and the subsequent processing at the C2 site. It is assumed that the binding of the RPs serves as a checkpoint for correct A3 processing, because the exonuclease trimming the ITS1 region, Rat1, does not stop at B site and degrades the pre-rRNA in the absence of Rpl17 (Sahasranaman et al., 2011). Comparing at this step the solvent-exposed side of the formed pre-60S particle with the mature 60S subunit, nearly all required RPs already define the mature structures (Figure 19) (Gamalinda et al., 2014; Zhou et al., 2019a).

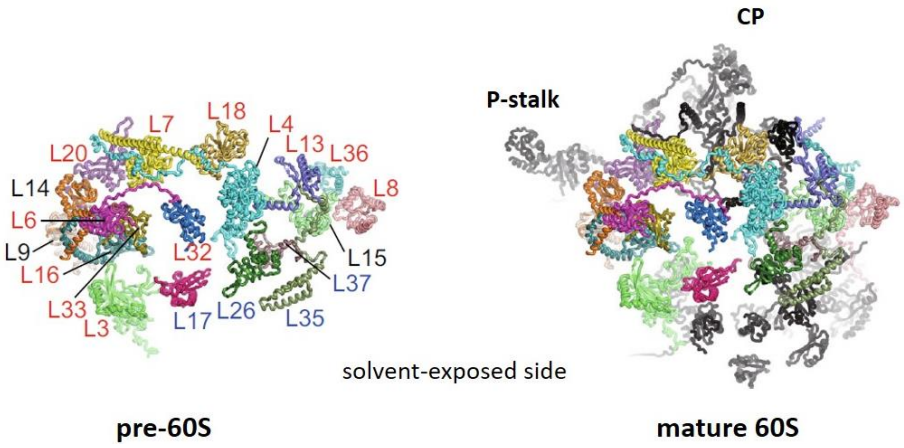

Figure 19: RP coverage of solvent-exposed sides of pre-60S and mature 60S particles adapted from Zhou et al. (2019).
View from the solvent-exposed side onto the RPs in Rpf1-TAP pre-60S (left) and mature 60S (right). “Early” RPs are labeled in red, “middle” RPs in blue, and unclassified RPs in black. RPs present in pre-60S are color-coded and those missing in pre-60S are depicted in black.

After assembly of all “A3 factors” and four of the “middle” RPs, eight out of twelve “B factors” (Nop2, Nip7, Rpf2, Rrs1, Mak11, Rlp24, Nog1, and Tif6) assemble into the pre-60S particle in a hierarchical and interdependent manner. All “B factors” are required for cleavage at the C2 site (Lebreton et al., 2008b; Saveanu et al., 2003; Talkish et al., 2012).
Two Cryo-EM structures corresponding to states 2 (Sanghai et al., 2018) and B (Kater et al., 2017) are supposed to resemble this assembly state, where two components of the “Nsa1 module” (Nsa1 and Rpf1) together with Rrp14, Ssf1-Rrp15, and Brx1-Ebp2 bridge domains I, II, and VI by forming a stabilizing ring around the center of the particle (Figure 18) (Sanghai et al., 2018). Interestingly, the “B factors” Rpf2 and Rrs1 bring Rpl5, Rpl11,

and the 5S rRNA, to form the central protuberance (CP) in the pre-60S particle. However, the CP cannot be observed in the Cryo-EM structures most possibly due to its unstable association (Asano et al., 2015; Kharde et al., 2015; Zhang et al., 2007).

1.6.1.2 Assembly of the polypeptide exit tunnel

During folding and incorporation of domain III and parts of domains IV and V, nine RPs, the "B factors" Spb4, Dbp10, and Nsa2, and the AFs Noc3 and Spb1 join the pre-60S particle. The recruitment of Nsa2 requires the presence of the "B-factors" Nop2, Nip7, Rlp24, Nog1, and Dbp10 (Kater et al., 2017; Lebreton et al., 2006; Saveanu et al., 2001; Talkish et al., 2012).
Comparison of pre-ribosomal particles identified in earlier states B/2 and C (Kater et al., 2017; Sanghai et al., 2018) with the ones at states D and E (Kater et al., 2017) or the intermediate state described by Sanghai et al. (2018) indicates the structural rearrangement of pre-60S particles from an arch-like morphology to a globular shape more similar to the mature 60S subunit (Figure 20).

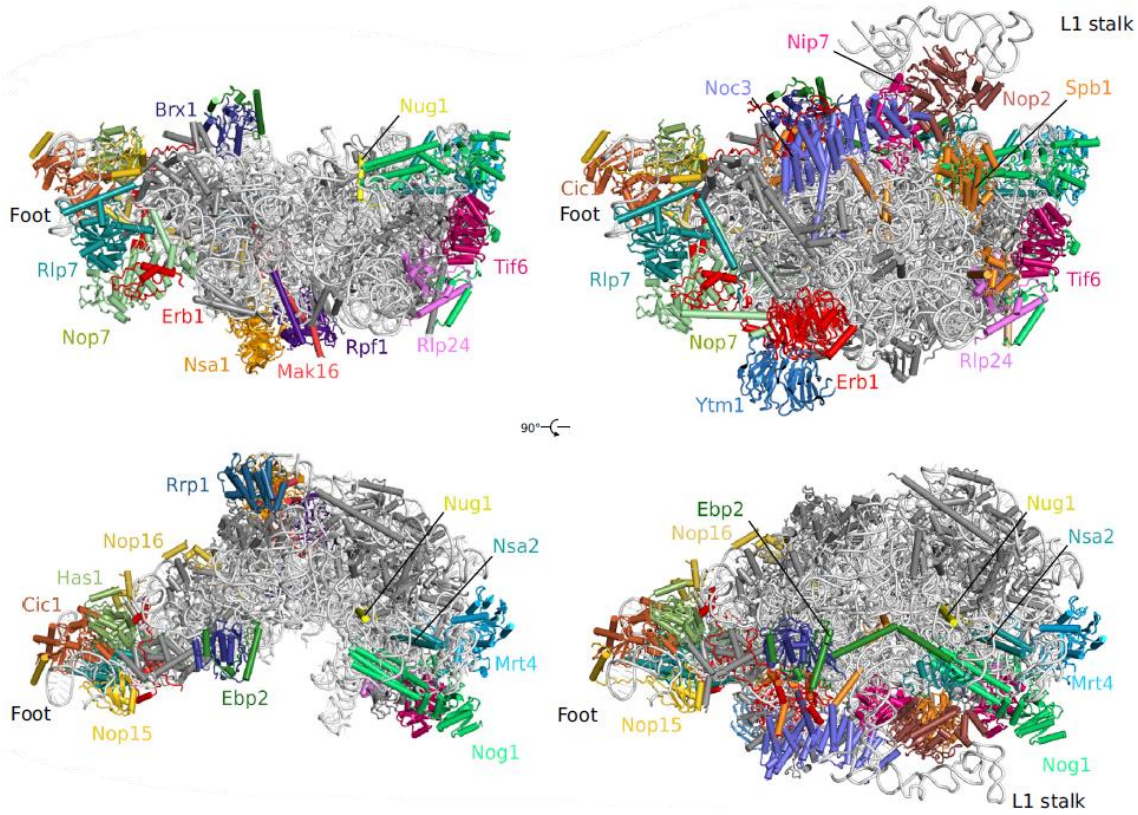

Figure 20: Cryo-EM structures of two nucleolar pre-60S assembly intermediates adapted from Kater et al. (2017).
Front (above) and top (below) views of states C (left) and E (right) of the pre-60S particles. rRNA and RPs are colored in light and dark gray, respectively. AFs are highlighted in colors with names indicated. Structural hallmarks "foot" and L1-stalk are named.

The "Nsa1 module", including the "place holder" Rpf1 is released by the AAA-ATPase Rix7 from the PET, during the transition to state E (Gadal et al., 2001; Kressler et al., 2008).

Consequently, the inner side of the PET is not occupied anymore in the state E. The final assembly of the PET might involve the release of Ssf1-Rrp15 and Rrp14, which probably allows the association of Rpl19, Rpl25, and Rpl31 and the formation of the rim surrounding the PET exit (Biedka et al., 2018; Klinge and Woolford, 2019).
In state E, also the interactions of Erb1 within the particle can be observed. Erb1 and Ytm1 belong to the "A3 factors" and are rather early assembled into the pre-60S particle. Erb1 occupies half of the pre-60S particle and establishes extensive contacts with domains I, III, and IV, with the RPs Rpl27, Rpl36, Rpl38, and with nine AFs, Ytm1, Nop7, Rlp7, Spb1, Noc3, Ebp2, Brx1, Nop16, and Has1 (Figure 20) (Kater et al., 2017; Klinge and Woolford, 2019; Sanghai et al., 2018).

1.6.1.3 Assembly of structural hallmarks

Nsa2 together with AFs Nip7, Nop2, Noc3, and Ebp2 might keep the L1-stalk in a premature rotated conformation as suggested by the position of helices 76 and 79 observed in states D and E (see Figure 20) (Kater et al., 2017). The remodeling of the "foot" is a prerequisite for the L1-stalk to adopt its mature conformation. This event is triggered by the AAA-ATPase Rea1/Mdn1, which binds to Ytm1 and releases the Ytm1-Erb1 subcomplex from the pre-60S subunit (Bassler et al., 2010). Therefore AFs Has1, Brx1, Ebp2, and Nop16, previously associated with Erb1, leave the pre-ribosomal particle (Biedka et al., 2018). This step allows two major structural changes at the "foot": Rlp7 rotates toward the "foot" and the AF Nop53 binds the ITS2 because its binding site, previously occupied by the NTD of Erb1, becomes accessible. Release of Ebp2 might increase the flexibility of the L1-stalk, which can reach its mature position since it is not blocked anymore by Rlp7 (Figure 21) (Bassler et al., 2010; Kater et al., 2017; Sanghai et al., 2018).

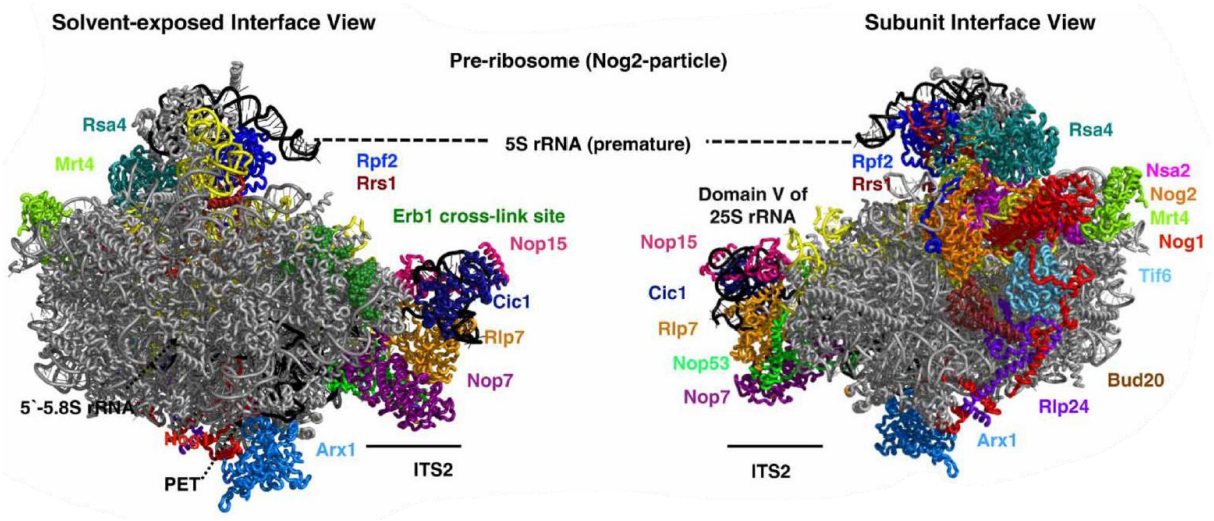

Figure 21: Cryo-EM structure of the Nog2-particle adapted from Konikkat and Woolford (2017).
In the Nog2-particle the ITS2 spacer has not yet been removed and the 5S rRNP/CP is still in a premature conformation, as indicated. AFs associated to the Nog2-particle are color-coded. Nog1 with its insertion in the PET is depicted in red. The 25S rRNA domain V containing the PTC is colored in yellow. Some of the structural hallmarks are indicated.

The AFs Nip7, Nop2, Noc3, Spb4, and Spb1 interfere with the mature conformation of domains II and V and block formation of the mature PET (Klinge and Woolford, 2019). Release of these AFs and the subsequent recruitment of Nog2 and Rsa4 to domain V by the remaining "B factors" allow the required structural rearrangements to promote maturation of the PET (Biedka et al., 2018; Saveanu et al., 2001). In addition, Nog1 places its NTD to the entrance of the PET and it inserts its elongated CTD inside the PET (Figure 21) (Wu et al., 2016), which was unoccupied since the removal of the "Nsa1 module" (Fuentes et al., 2007; Wu et al., 2016). Finally, the RPs forming the rim of the PET associate together with the nuclear export factor Arx1. It is assumed that the binding of Arx1 controls the correct formation of the PET, which indicates competence to exit the nucleus (Bradatsch et al., 2012; Kater et al., 2017).
When the fourth structural hallmark, the 5S rRNP or central protuberance (CP) is stably incorporated into the pre-60S particle, it becomes visible in the Cryo-EM structures referred as state F and Nog2-particle (Figure 21) (Kater et al., 2017; Wu et al., 2016). The 5S rRNP is brought to the pre-60S particle by the AFs Rpf2 and Rrs1. Both AFs belong to the group of "B factors" and they associate during previous assembly stages as explained above (Talkish et al., 2012; Zhang et al., 2007). Thus, the 5S rRNP joins the pre-ribosome rather early, but might be kept in a flexible state until this stage and it is therefore not observed in "earlier" Cryo-EM particles. It is likely that release of Nip7 and Nop2 stabilizes the 5S rRNP since their binding sites are subsequently occupied by Rpf2 and Rrs1 within the Nog2-particle. However, the CP does not yet adopt its mature conformation but is kept in a 180°-rotated premature state by its accompanying AFs Rpf2 and Rrs1 (Klinge and Woolford, 2019).

1.6.2 Development of the nucleoplasmic pre-60S particle

Several assembly steps take place during the transition from the nucleolus to nucleoplasm to prepare the pre-60S particle for its nuclear export. Therefore, a large portion of the ITS2 is removed, the CP is restructured, and domain V, representing the main part of the PTC, is folded (Konikkat and Woolford, 2017).
Removal of the ITS2 region including the "foot" structure is carried out by the exosome (see 1.4.2), which is most possibly recruited by the interaction of Mtr4 with the AIM domain of Nop53 (Cepeda et al., 2019; Falk et al., 2017; Thoms et al., 2015) (as described for Utp18, see 1.5.2). In addition, the exonucleases Rat1, Rrp17, and Xrn1, as well as the Grc3/Las1 processing complex are required (see 1.4.2). Finally, the AFs Nop15, Cic1, Rlp7, Nop53, and Nop7 are removed before the degradation of the ITS2 (Konikkat and Woolford, 2017).
For the final maturation of the CP/5S rRNP, the AF Sda1 associates with pre-60S particles to enable the subsequent binding of the Rix1-Rea1 subcomplex. Association of these factors disrupts the contact between the 5S rRNP, Rsa4, Rpf2, and Rrs1. Thus, Rpf2 and Rrs1 are displaced from the particle and the CP is stabilized in its mature conformation by the Rix1-Rea1 complex. To do this, the Rix1-Rea1 complex establishes contacts with L1-stalk and Rsa4 and promotes the rotation of helix 38 toward the subunit interface. The

subsequent ATP hydrolysis by Rea1 activates the GTPase Nog2, which triggers its own release and also the release of Sda1, Rix1, Rea1, and Rsa4 (Figure 22) (Asano et al., 2015; Barrio-Garcia et al., 2016; Biedka et al., 2017; Kharde et al., 2015).

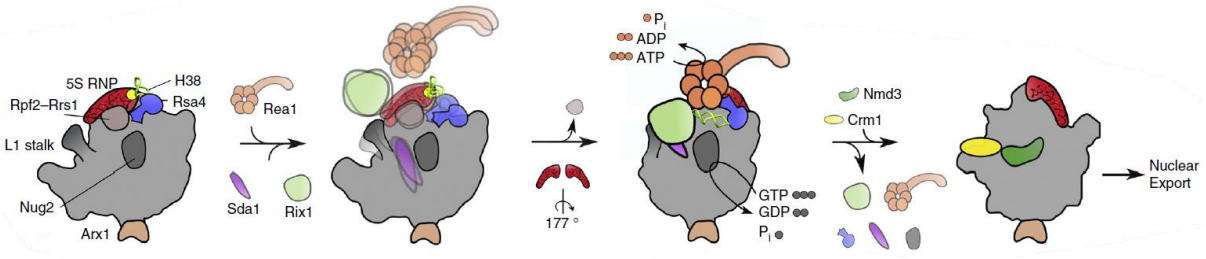

Figure 22: Model for CP rotation induced by Rix1-Rea1 obtained from Barrio-Garcia et al. (2016). Nog2-particle (Nug2=Nog2) is decorated with Rix1-Rea1 in the nucleoplasm and forms the Rix1-Rea1-particle. After the release of Rpf2-Rrs1, the CP (5S rRNP) is rotated by 177°C and Rix1, Rea1, and other factors leave the particle. The obtained pre-60S subunit is ready for nuclear export.

After the release of Nog2, the PTC already acquired a mature-like conformation, which enables the binding of the export factor Nmd3, which exhibits large contacts with the subunit interface interacting with L1-stalk, E-site, P-site, and SRL (Gartmann et al., 2010; Ma et al., 2017; Sengupta et al., 2010). In contrast to the solvent-exposed side, the subunit interface lacks still many RPs and several AFs like Bud20, Arx1, Nog1, Nug1, Nsa2, Rlp24, Tif6, and Mrt4 remain bound to this part shielding the negative charges of the rRNA during the export of pre-60S subunits through the nuclear pore complex (Konikkat and Woolford, 2017).

1.6.3 Final maturation of the large subunit

After arrival in the cytoplasm, the pre-60S subunit is subjected to the final maturation steps including the complete trimming of the 3' end of 5.8S rRNA, the removal of the remaining AFs, the assembly of still missing RPs, and the proofreading of the functional centers (Klinge and Woolford, 2019; Konikkat and Woolford, 2017).
The AAA-ATPase Drg1 releases Rlp24 and Nog1 from cytoplasmic pre-60S particles. While the AF Rlp24 is substituted by the RP Rpl24, the release of Nog1 opens the binding site of Rei1 within the PET (remember that the CTD of Nog1 was previously inserted into the PET) (Kappel et al., 2012). Rei1 inserts its CTD into the PET in a similar way as Nog1 and Rei1-CTD is stabilized by interactions with Rpl4 and Rpl27. Alb1 and Arx1 bind at the tunnel exit and they also interact with Rei1. In addition, Alb1 mediates the contact between Arx1 and the pre-60S subunit (Greber et al., 2016).
Formation of the phospho-stalk might require the protein phosphatase Yvh1 to release the P0-homolog Mrt4 from the premature stalk region formed by helices H42 and H43 within domain II of the 25S rRNA (Zhou et al., 2019b). The release of Mrt4 is supposed to expose the binding site of P0, allowing also the recruitment of the adjacent Rpl10 (Kemmler et al., 2009; Lo et al., 2009). Interestingly, in an alternative model the assembly of P0 occurs in the absence of the non-essential protein Mrt4 (Rodríguez-Mateos et al., 2009a). Instead of Mrt4, the RPs Rpl12 and P0 assemble in the nucleus and they promote

together with the P-stalk proteins P1 and P2 the export of pre-60S subunits into the cytoplasm (Francisco-Velilla et al., 2013; Rodríguez-Mateos et al., 2009a, 2009b).
The AFs Reh1, Ssa1, Ssa2, and Jjj1 release Rei1 and Alb1-Arx1 from the PET. Reh1 occupies the tunnel as previously done by Nog1 and Rei1. In parallel, Lsg1 is recruited and it interacts with Nmd3 to occupy the space between PTC and the tRNA exit site at the subunit interface likely to avoid undesired interactions with a 40S subunit (Figure 23) (Ma et al., 2017).
The binding of Rpl10 helps the P-stalk to reach its mature conformation and the mature P-stalk triggers the recruitment of the GTPase Efl1 by the Efl1 co-factor Sdo1 (Luviano et al., 2019). Sdo1 binds to the P-site, formed by Rpl10, and interacts by its NTD with the PTC (Gijsbers et al., 2013; Patchett et al., 2017). Thus, the formation of PTC and P-stalk is controlled by Rpl10, Efl1, and Sdo1. Together with the SRL, Rpl10 and Sdo1 activate Efl1, which triggers the release of Nmd3 and the "A3 factor" Tif6 (Bussiere et al., 2012; Klinge et al., 2011; Konikkat and Woolford, 2017; Zhou et al., 2019b). An alternative model suggests that Rpl10 directly releases Nmd3 and Lsg1 allowing the association of Sdo1 and Efl1 to induce the release of Tif6 (Figure 23) (Ma et al., 2017; Malyutin et al., 2017).

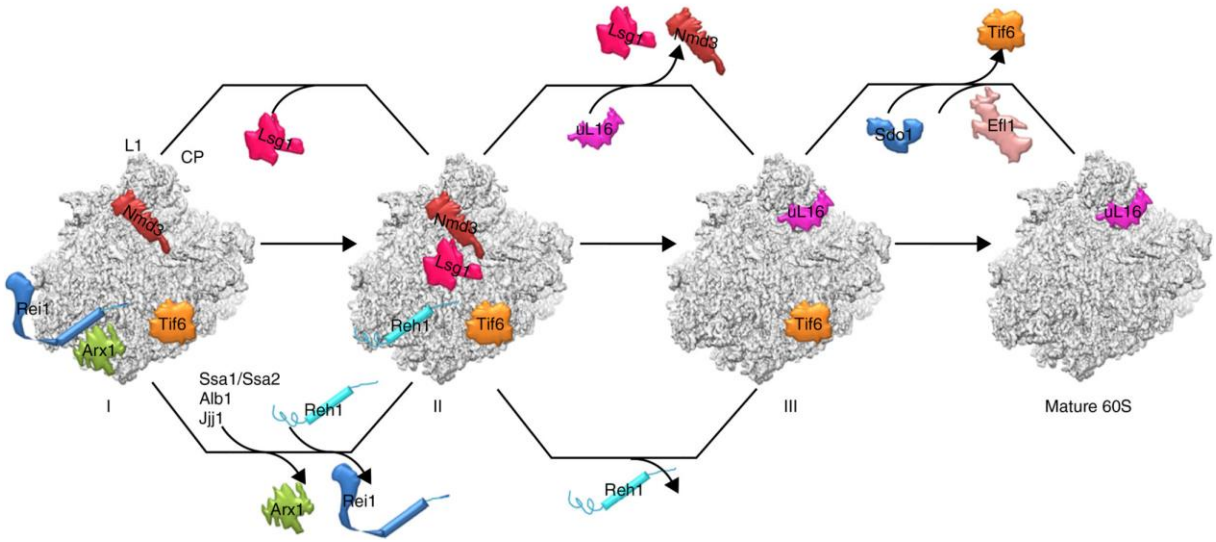

Figure 23: Model for final steps of cytoplasmic pre-60S maturation obtained from Ma et al. (2017). The two functional centers of the 60S subunit, the PTC-CP region (above), and the PET exit region (below), are matured in two parallel pathways. Three states prior to the mature 60S subunit are depicted with participating factors indicated. The last assembled RP is Rpl10 (uL16).

The successful finalization of these last maturation steps releases the last AFs from the active sites, which in turn allows the association of missing RPs to complete the maturation of the large ribosomal subunit.

1.7 Quality control mechanisms during ribosome biogenesis

As described in the previous chapters, ribosome assembly is a very complicated process aiming at the production of translation competent ribosomes. Since accurate protein

synthesis is essential for life, the construction of functional ribosomes must be well controlled and organized. Thus, efficient quality control mechanisms at different assembly stages might be evolved to allow cell life.

1.7.1 Avoiding premature ribosomes to be engaged in translation

From an economic point of view, pre-ribosomal particles that are engaged in non-productive translation processes might also consume cell resources, including energy, translation factors, mRNAs, and tRNAs. Thus, the economy of cellular processes demands that ribosome maturation must be carefully supervised, especially in the cytoplasm, where the pre-ribosomal particles strongly resemble mature ribosomes.
On one hand, masking the binding site of essential RPs with AFs makes the premature ribosomes incompetent for translation. This function might be played in pre-40S subunits by Enp1 and Ltv1, which prevent the binding of Rps10, or by Pno1 blocking the association of Rps26 (Parker et al., 2019; Strunk et al., 2011). Regarding pre-60S subunits, Mrt4 impairs the association of P0 with the phospho-stalk, and the AFs Rlp7 and Rlp24 were previously thought to inhibit the association of Rpl7 and Rpl24 to the subunit interface (Gadal et al., 2002; Rodríguez-Mateos et al., 2009a, 2009b; Saveanu et al., 2003). Further studies disproved the "placeholder" role of Rlp7 by showing the simultaneous presence of Rlp7 and Rpl7 in pre-60S particles (Babiano et al., 2013).
On the other hand, AFs can preclude the activity of functional sites. In pre-40S subunits, several AFs might block every step of the translation pathway by avoiding the association of translation factors, initiator tRNAs, mRNAs, and mature 60S subunits. Dim1 and Tsr1 cover the subunit interface and thereby, they might block subunit joining (Karbstein, 2013; Strunk et al., 2011). In pre-60S subunits, the export factor Nmd3 and the translation factor Tif6 may prevent their association with 40S subunits (Gartmann et al., 2010; Sengupta et al., 2010).

1.7.2 Inspecting pre-ribosomes to be functional

The correct activity of functional centers at the mature subunits seems to be carefully surveyed before conclusion of the maturation process (Karbstein, 2013; Lebaron et al., 2012).

1.7.2.1 Probing the structure

Linking the proofreading with nuclear export is one possibility to assure that only subunits having the correct structure reach the cytoplasm (Karbstein, 2013; Klinge and Woolford, 2019).
In pre-40S subunits, this control might be achieved by the association of late RPs, which are required to allow the export of pre-ribosomal particles through the nuclear pore (Ferreira-Cerca et al., 2005; Léger-Silvestre et al., 2004).
In pre-60S subunits, the correct assembly of the active sites is controlled ahead of nuclear export. The first criterion allowing export is the correct positioning of the CP. The

combined action of Rea1-ATPase and Nog2-GTPase triggers the rotation of the CP by 180° from the premature to the mature conformation leading to a structural reorganization of the PTC (Barrio-Garcia et al., 2016). Second, the association of the export factor Nmd3 only takes place when the L1-stalk has its correct position, which depends on the previous removal of the "foot"/ITS2 (Bassler et al., 2010). Moreover, the Nmd3 association also allows controlling the conformation of the SRL, the E-site, and the P-site (Gartmann et al., 2010; Sengupta et al., 2010). Third, the export factor Arx1 together with Nog1 inspect the correct assembly of the PET before pre-60S subunits leave the nucleus (Bradatsch et al., 2012; Kater et al., 2017; Wu et al., 2016).

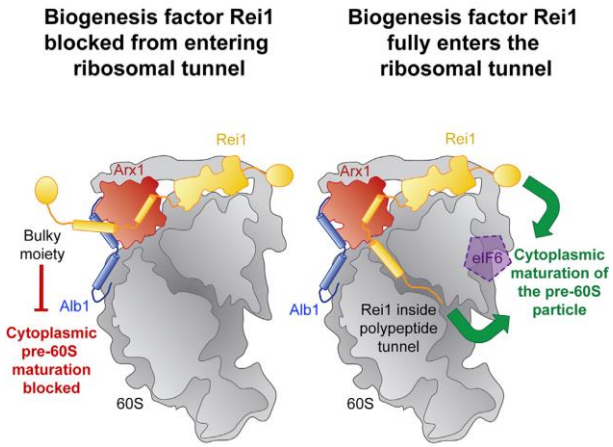

Figure 24: Model for the cytoplasmic control of PET formation by Rei1 adapted from Greber et al. (2016).
The fusion of a bulky moiety at the CTD of Rei1 does not allow its insertion into the PET and blocks cytoplasmic pre-60S maturation (on the left). If the insertion of the CTD into the PET is possible, Rei1 can approach the subunit interface from two sides (on the right). The positions of the AFs Arx1, Alb1, and Tif6 (eIF6) are indicated.

Rei1 and Arx1 continue the inspection of PET formation in the cytoplasm. The CTD of Rei1 is inserted into the tunnel probably mimicking the way of a nascent polypeptide chain placed in the PET. If the PET is not accessible and Rei1 cannot introduce its CTD into the tunnel, the release of Arx1 is blocked and, likewise the downstream maturation of the pre-60S subunit (Figure 24) (Greber et al., 2016).

1.7.2.2 Inspecting the composition

Testing the functionality of ribosomal subunits in a translation-like process might inspect the functional centers. It has been proposed that pre-40S subunits associate with 60S subunits to form a translation competent 80S-like ribosome (Figure 25) (Lebaron et al., 2012; Strunk et al., 2012). The formed 80S-like particles do not constitute translation intermediates as AFs associated with the pre-40S ribosomes inhibit the binding of mRNA, tRNA, and initiation factors (Figure 25). Formation of 80S-like ribosomes is promoted by the translation factor eIF5B and the ATPase Rio1, while the AF Fap7 and the termination factors Rli1 and Dom34 trigger the dissociation of eIF5B and Rio1 by a pseudo-translocation step. Moreover, the endonuclease activity of Nob1, responsible for the

processing at site D in 20S pre-rRNA, may be triggered within the 80S-like particles (Ghalei et al., 2017; Lebaron et al., 2012; Strunk et al., 2012). This model suggests that the formation of the mature 3' end of the 18S rRNA is only possible in 40S subunits checked for translation competence (Karbstein, 2013). Nevertheless, the presence of non-processed 20S pre-rRNAs in polysome fractions might challenge this hypothesis (Belhabich-Baumas et al., 2017; Soudet et al., 2010).

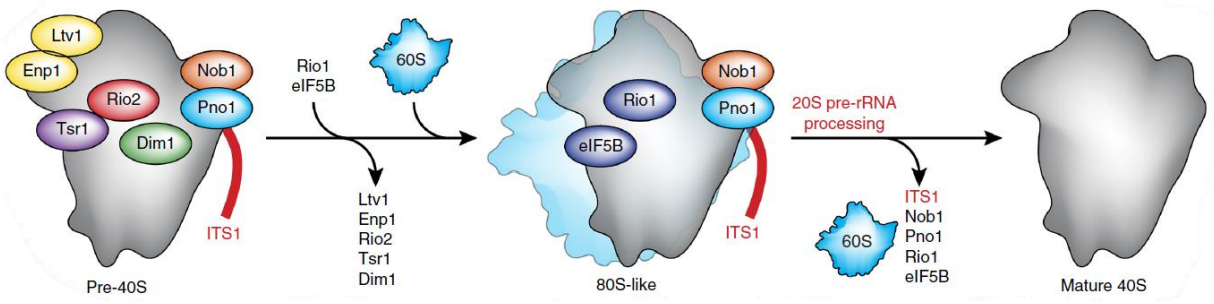

Figure 25: Model for cytoplasmic quality control of pre-40S subunits adapted from Peña et al. (2017).
Before cleavage at D site, the translation ability of pre-40S subunits is checked together with mature 60S subunits in a translation-like cycle. Only AFs with known binding sites are indicated. eIF5B is also known as Fun12.

Even though there is no evidence about a similar test for pre-mature 60S subunits until now, at least the translocation activity might be monitored by Efl1 (Bussiere et al., 2012). The activation of the GTPase Efl1 requires the correct formation of the PTC and the P-stalk. Therefore, the release of Tif6 from pre-60S subunits by Efl1 might resemble the translocation of tRNAs during translation (Bussiere et al., 2012; Klinge et al., 2011; Konikkat and Woolford, 2017).

1.7.3 Degrading non-functional ribosomes stalled in translation

Despite the described quality control mechanisms, pre-ribosomal particles may enter translation. Either premature or defective ribosomes or defective mRNAs can cause stalling of the translational process. In each case, the degradation of both mRNAs and ribosomes is induced (Karbstein, 2013).
The absence of Rio1 or Nob1 causes the entry of pre-40S subunits in translation (Soudet et al., 2010). Pre-60S subunits containing the "foot" can join 40S subunits and participate in translation, since the "foot" is at the solvent-exposed site (Sarkar et al., 2017). In any case, stalled ribosomes are ubiquitinated by Hel2 at Rps3 and Rps20 (Matsuo et al., 2017) and thus, the no go decay (NGD) pathway and the ribosome quality-control complex (RQC) are triggered (Yan and Zaher, 2019). The NGD pathway degrades mRNAs caught in stalled ribosomes (Doma and Parker, 2006). Therefore, the factors Dom34 and Hbs1 lead to dissociation of the ribosomal subunits with the peptidyl-tRNA associated with the 60S subunit (Shoemaker et al., 2010). The mRNA still associated with the 40S subunit is cleaved by the endonuclease Cue2 (D'Orazio et al., 2019), which promotes the cleavage reaction upon the binding of Rps3 within the ribosome mRNA channel (Simms et al.,

2018). Since the previous ubiquitination does not target the released 40S subunit for degradation, its fate is still unknown (Matsuo et al., 2017). The RQC comprises the E3 ubiquitin ligase Ltn1, the ATPase Cdc48, and the factors Rqc1 and Rqc2. After subunit dissociation, the RQC associates with the 60S subunit carrying still the peptidyl-tRNA with the nascent polypeptide chain (Zurita Rendón et al., 2018). Ltn1 and Rqc1 are required for the ubiquitination of the nascent polypeptide chain, which is extracted from the 60S subunit and degraded by the proteasome (Brandman and Hegde, 2016; Brandman et al., 2012; Shao et al., 2015). Ltn1 and Rqc2 induce the release of the peptidyl-tRNA by the so-called CAT tailing (Kostova et al., 2017). The clearance of the PET by removal of the peptidyl-tRNA and the nascent polypeptide chain leads to the exposure of previously hidden lysine residues at the tunnel wall, which can be efficiently ubiquitinated for proteasomal degradation (Zurita Rendón et al., 2018). Moreover, the Ski7-exosome and the exonuclease Xrn1 are engaged in the degradation of the rRNAs and also the stalled mRNA (Lafontaine, 2010).

1.7.4 Sensing the balanced production of both ribosomal subunits

Although the synthesis of both ribosomal subunits is well controlled at several steps, both subunits are required for translation and they should be produced in stoichiometric amounts. The unbalanced production of ribosomal subunits might be responsible for altered translation patterns (Cheng et al., 2019). Thus, the unbalanced production of ribosomal subunits emerges as a possible etiology for some human diseases known as ribosomopathies (Khajuria et al., 2018; Lodish, 1974; Ludwig et al., 2014). How this balanced production is sensed is still unknown, but there are existing ideas about how this control could be achieved.

Specific AFs engaged in the maturation of both subunits could play a role in the balanced synthesis of the subunits. Indeed, three of all known AFs are participating in the synthesis of the small and the large ribosomal subunits.

The RNA helicase Has1 is required for the release of the U14 snoRNP from pre-40S particles during SSU assembly (Liang and Fournier, 2006). In LSU assembly, Has1 belongs to the group of "A3 factors" and it participates in the reorganization of domains I and II in the 25S rRNA and in the recruitment of the RPs Rpl17, Rpl26, Rpl35, and Rpl37 to pre-60S particles (Dembowski et al., 2013a).

A second AF required for synthesis of both ribosomal subunits is the RNA helicase Prp43. In pre-40S particles, Prp43 is supposed to participate with other factors in the exposure of the D site to facilitate cleavage by the nuclease Nob1 (Pertschy et al., 2009). In LSU biogenesis, Prp43 is likely involved in the dissociation of snoRNAs from 25S rRNA precursors, since UV crosslinking revealed several contact sites of Prp43 within the 25S rRNA and with different snoRNAs (Bohnsack et al., 2009).

Both factors play independent roles in the synthesis of both ribosomal subunits and it is difficult to find how they can coordinate these processes.

Interestingly, a third AF called Rrp5 is required for pre-rRNA processing at sites A0, A1, A2, and A3 and the absence of Rrp5 causes the reduced production of 18S and 5.8S rRNAs

(Venema and Tollervey, 1996). During the co-transcriptional cleavage of pre-rRNA, Rrp5 might block the A2 cleavage site until domain I of the 25S rRNA is synthesized (Kos and Tollervey, 2010; Osheim et al., 2004). Rrp5 contains two independent functional domains, which participate in the synthesis of the small or the large subunit. While the NTD is involved in the processing of 5.8S$_S$ rRNA, the CTD is engaged in 18S rRNA production. The independent expression of both protein domains produces a fully functional Rrp5 (Eppens et al., 1999). The CTD of Rrp5 contacts nearby the A2 cleavage site within the pre-rRNA and the snoRNAs U3, U14, snR30, and snR10, which are required for cleavages at A0, A1, and A2. The NTD displays contacts close to the A3 cleavage site of the pre-rRNA and associates with Nme1, the RNA component of the A3 site nuclease MRP (Lebaron et al., 2013). The ATP hydrolysis by Rok1 releases Rrp5 from pre-40S particles and it might be a prerequisite for the function of Rrp5 in LSU maturation (Khoshnevis et al., 2016), where the NTD of Rrp5 associates with Noc1 and Noc2 (Hierlmeier et al., 2013). It might be interesting to test if Rok1 activity is also important for the association of Rrp5 with Noc1-Noc2 at this step. However, the changed binding of Rrp5 to the rRNA renders the A2 site accessible and it can be cleaved (Khoshnevis et al., 2019). This dual role of Rrp5 in ribosome assembly may sense the crosstalk between the biogenesis of the two subunits.

1.8 Classification of Pol5 in the context of ribosome assembly

Pol5 is a putative AF, whose role in ribosome synthesis remains uncharacterized. It is an essential protein in *S. cerevisiae*, initially identified as a B-type DNA polymerase. However, this activity is not an essential function of Pol5 *in vivo* (Shimizu et al., 2002). In contrast, the nucleolar localization of Pol5 and its binding close to the rDNA enhancer within the NTS1 region has suggested a regulatory role of Pol5 in rRNA synthesis and the rDNA copy number in *S. cerevisiae* (Shimizu et al., 2002; Yang et al., 2003).

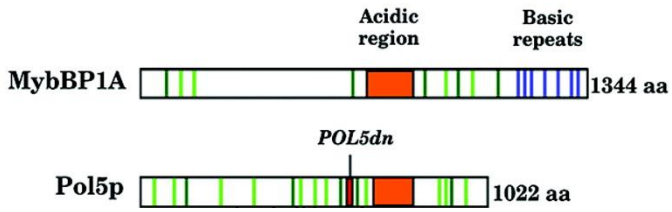

Figure 26: Scheme of protein domains found in human MybBP1A and in yeast Pol5 adapted from Shimizu et al. (2002).
Both, acidic regions (orange) and leucine-charged domains (light and dark green) are found in MybBP1A and Pol5. Pol5 is lacking the basic repeats located at the C-terminus of MybBP1A. The B-type DNA polymerase-like domain of Pol5 is depicted in red. "*POL5dn*" indicates the two point-mutations of this domain proving that it has no essential function *in vivo*.

MybBP1A, the human ortholog of Pol5 (Figure 26), was initially characterized by two independent groups in 2012 (Hochstatter et al., 2012; Tan et al., 2012). MybBP1A is required for the efficient repression of rDNA gene transcription by interaction with the RNA Pol I-machinery. Moreover, its overexpression led to the accumulation of 18S

precursors indicating a role of MybBP1A in pre-rRNA processing (Hochstatter et al., 2012).
Pol5 has been identified as a protein component of the UTP-A complex together with other tUtps, suggesting a role of Pol5 during the very early steps of ribosome assembly (Krogan et al., 2004). As defined for the tUtps, Pol5 might play a role during rDNA transcription. However, Pol5 is supposed to be only present in sub-stoichiometric amounts in the SSU processome or to be part of very early and transient complexes (Gallagher, 2019; Gallagher et al., 2004). In contrast, the group of Lafontaine identified the association of Pol5 during transcription of the 25S containing region and not earlier (Wery et al., 2009). Therefore, several discrepancies exist in the literature, which indicates that the tUTP and UTP-A complexes are two different entities (Gallagher et al., 2004; Pérez-Fernández et al., 2007; Pöll et al., 2014; Wery et al., 2009). On the other hand, a recent work suggests that Pol5 is an accessory factor of the UTP-A complex at the beginning of RNA Pol I transcription (Gallagher, 2019). Within this model, the release of Pol5 might allow the formation of the Utp5-containing tUTP complex, which would be stably assembled into the SSU processome.

1.9 Objectives of this thesis

In this thesis, we aimed to characterize the function of Pol5 during ribosome synthesis trying to better understand the early steps of ribosome synthesis. To this end, we attempted to answer the following questions:

- Is Pol5 a component of the tUTP/UTP-A complex?
- Which pre-ribosomal particles associate with Pol5?
- Which steps of ribosome synthesis are affected in the absence of Pol5?
- How does Pol5 influence rDNA transcription?
- How many functional domains are present in Pol5 and which functions do they have?

To answer these questions, we applied a multidisciplinary concept based on yeast genetics, molecular biology, and biochemical approaches to purify and characterize protein complexes. To answer the first question, we aimed to purify soluble complexes containing Pol5. Second, we investigated the pre-rRNAs, which are predominantly associated with Pol5 by affinity purifications. To tackle the third question, we investigated the effects of Pol5 depletion on ribosome biogenesis in general but also specifically during the assembly of the small and large subunits. To narrow the scope of Pol5, we intended to analyze the influence of Pol5 depletion on rRNA production, pre-rRNA processing, and protein composition of different pre-ribosomal particles. Fourth, we aimed to elucidate whether Pol5 is directly associated with rDNA or may rather influence rDNA transcription via protein-protein interactions. The fifth question was initially answered by mutant analysis *in vivo* and it might be completed by *in vitro* approaches.

2. Results

2.1 Pol5 interactions within pre-ribosomes

2.1.1 Characterization of the UTP-A complex

To gain knowledge about the interaction partners of the tUTP/UTP-A complex, we affinity purified Pol5 and several tUtps using a similar workflow as described by Krogan et al. (2004) (see 4.2.2.13 and 4.2.2.16) (Figure 27).

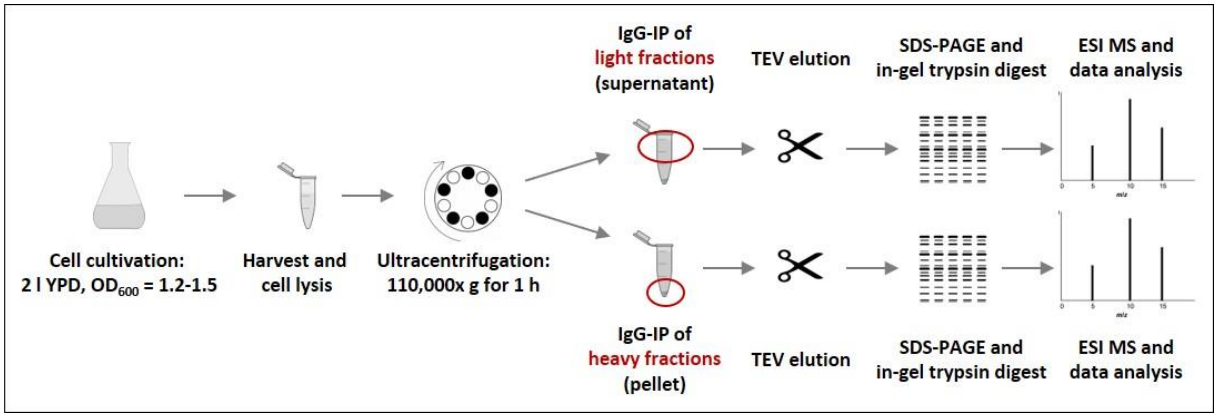

Figure 27: Workflow for tUtp purifications adapted from Krogan et al. (2004).

According to the workflow presented in Figure 27, the non-tagged control strain and strains expressing the TAP-tagged proteins Utp4, Pol5, and Utp17 were cultivated in rich medium containing glucose (YPD). The obtained cell pellets were processed for affinity purification with IgG-coupled beads. Since the TAP tag consists of two elements for affinity purification, two protein A domains and the calmodulin binding peptide (CBP), separated by a cleavage site for the TEV protease, the elution of affinity purified protein complexes was performed by TEV cleavage and the eluted samples were analyzed by SDS-PAGE followed by either western blotting (see 4.2.5.4) (Figure 28A) or Coomassie staining (see 4.2.5.3) (Figure 28B).
Western blot analysis and detection with anti-CBP antibody showed the enrichment of the bait proteins Utp4, Pol5, and Utp17 in the eluates of the heavy fractions after ultracentrifugation. In lanes corresponding to the eluates of the light fractions, we could not detect any signal, probably due to the presence of bait proteins below the detection limit for the antibody against CBP. In agreement, Coomassie staining revealed a similar enrichment of proteins in the eluted samples from the heavy fractions, whereas only few prominent bands were visible in the eluted samples from the light fractions. This result would suggest the existence of low amounts of ribosome biogenesis factors not associated with pre-ribosomal particles under optimal growth conditions.
Gel lanes containing the tagged proteins were excised, digested with trypsin in gel, and analyzed by HPLC-coupled electron spray ionization mass spectrometry (HPLC-ESI-MS),

as indicated in section 4.2.2.16, by Dr. Astrid Bruckmann and Eduard Hochmuth (department of Biochemistry I). The obtained ESI-MS datasets for purifications obtained from light and heavy fractions were filtered by the peptide coverage, arbitrarily sorted from the highest to the lowest peptide coverage in Utp4, and only proteins related to the synthesis of ribosomes were plotted (Figure 29A and 29B). For light fractions, a peptide coverage higher than 30% was chosen, whereas the limit for heavy fractions was set to 50% peptide coverage both corresponding to the top 50 proteins identified by ESI-MS. The graph of the light fraction exclusively filtered for the peptide coverage is illustrated in supplemental Figure 57.

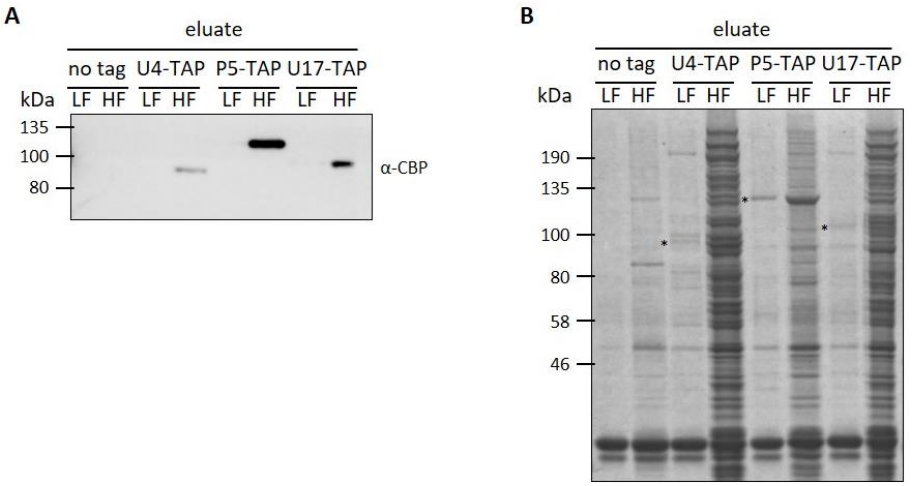

Figure 28: Analysis by western blotting and Coomassie staining of eluates from control and TAP-tagged strains Utp4, Pol5, and Utp17 obtained using the protocol adapted from Krogan et al. (2004). Affinity purification using cell extracts from non-tagged control (no tag) and the TAP-tagged strains Utp4 (U4), Pol5 (P5), and Utp17 (U17) was performed as described in Figure 27. Elution of purified proteins was performed by digestion with the TEV protease. (**A**) 10% of the eluates from light fractions (LF) and heavy fractions (HF) were resolved in 8% SDS-PAGE followed by western blotting. Bait proteins were detected with an antibody against CBP still present in the TAP tag. (**B**) 30% of the eluates from light (LF) and heavy fractions (HF) were resolved in NuPAGE 4-12% Bis-Tris gradient gel system and stained with commercially available Coomassie staining solution (SimplyBlue SafeStain from Invitrogen). Lanes corresponding to purifications of Utp4, Pol5, and Utp17 (U4, P5, and U17, respectively) were excised, in-gel digested with trypsin, and analyzed by HPLC-coupled electron spray ionization mass spectrometry (HPLC-ESI-MS). Respective identified bait proteins in supernatant lanes were labeled with *.

In the light fractions, proteins engaged in ribosome synthesis were only purified with Utp4 and Utp17 but not with Pol5. Interestingly, Pol5 was not found in the Utp4 and Utp17 affinity purifications. As expected, Utp4 and Utp17 showed association with a very similar set of proteins, which mainly belonged to the tUTP complex and other components of the SSU processome. This result suggests that most of the proteins purified from the light fractions might correspond to disassembly complexes, to the unspecific degradation of pre-rRNA during the affinity purification, or small precursors of the SSU processome. The proteins detected in all three samples were predominantly comprised of heat shock proteins, cell cycle proteins, ATPases, and kinases, unless we filtered by ribosome AFs (see Figure 57). These very abundant proteins are frequently co-purified from yeast cells as background contaminants and their enrichment in all purifications was most likely unrelated to a direct interaction with the bait proteins.

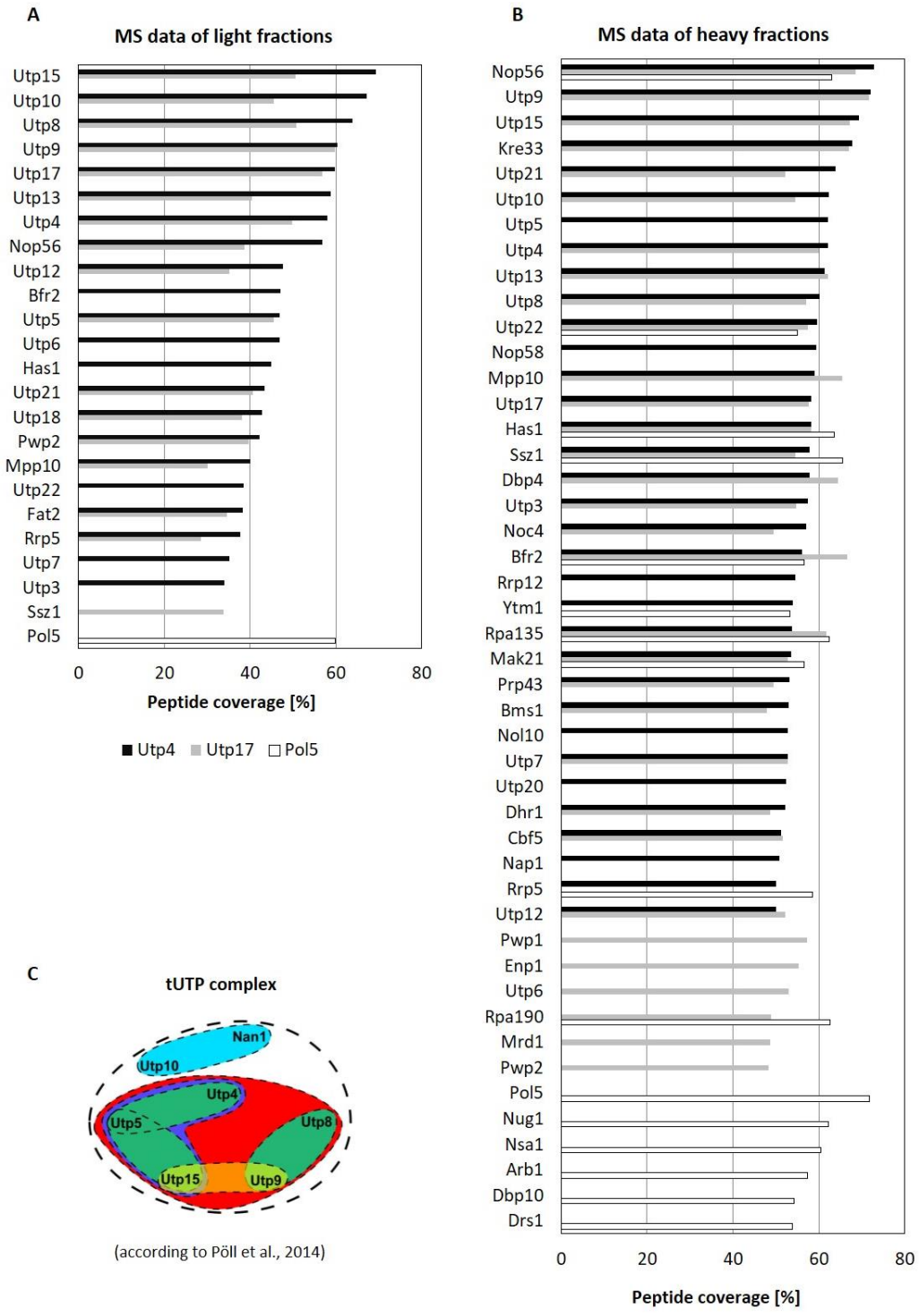

Figure 29: HPLC-ESI-MS datasets of light and heavy fractions obtained from TAP-tagged and affinity purified Utp4, Utp17, and Pol5.
Light and heavy fractions obtained after ultracentrifugation were used for affinity purification with the indicated TAP-tagged proteins. After TEV elution, samples were resolved in Bis-Tris gradient gel system (see Figure 28B), digested with trypsin in gel, and analyzed by HPLC-ESI-MS. (**A**) MS datasets were obtained from the eluates of the affinity purified light fractions of TAP-tagged Utp4 (black), Utp17 (gray), and Pol5 (white). All proteins found with a peptide coverage higher than 30% and related to the synthesis of ribosomes were plotted. (**B**) MS datasets were obtained from the eluates of the affinity purified heavy fractions of TAP-tagged Utp4 (black), Utp17 (gray), and Pol5 (white). All proteins found with a peptide coverage higher than 50% and related to the synthesis of ribosomes were plotted. (**C**) Cartoon depiction of the *in vitro*-architecture of the tUTP complex as published by Pöll et al. in 2014. Nan1 is the alternative name of Utp17.

In the case of the heavy fractions, Utp4 and Utp17 shared a high number of common interaction partners, as expected from proteins belonging to the same protein complex (Figure 29C). In contrast, Pol5 co-purified with only few SSU-processome related proteins like Utp22, Nop56, and Bfr2 with a similar peptide coverage as in Utp4 or Utp17 purifications (Krogan et al., 2004; Lafontaine and Tollervey, 2000; Pérez-Fernández et al., 2007; Soltanieh et al., 2014). Moreover, neither Pol5 was identified in the affinity purifications of tUtps nor the tUtps were identified in Pol5 purified samples. Interestingly, several proteins corresponding to RNA Pol I subunits (Rpa190 and Rpa135) and AFs involved in the synthesis of both ribosomal subunits (Rrp5, Has1, and Prp43) were found in all purified samples (Bohnsack et al., 2009; Dembowski et al., 2013a; Liang and Fournier, 2006; Venema and Tollervey, 1996). In contrast, some LSU AFs, like Nug1, Nsa1, or Drs1, were only enriched with Pol5 (Baßler et al., 2001; Harnpicharnchai et al., 2001; Ripmaster et al., 1992).

Since we could not exclude that the obtained data differed from published results (Krogan et al., 2004) due to the use of different bait proteins in both affinity purifications (Utp4 and Utp17 instead of Utp8, Utp9, and Utp10), we repeated the experiment using TAP-tagged Utp10 and Pol5 as bait proteins.

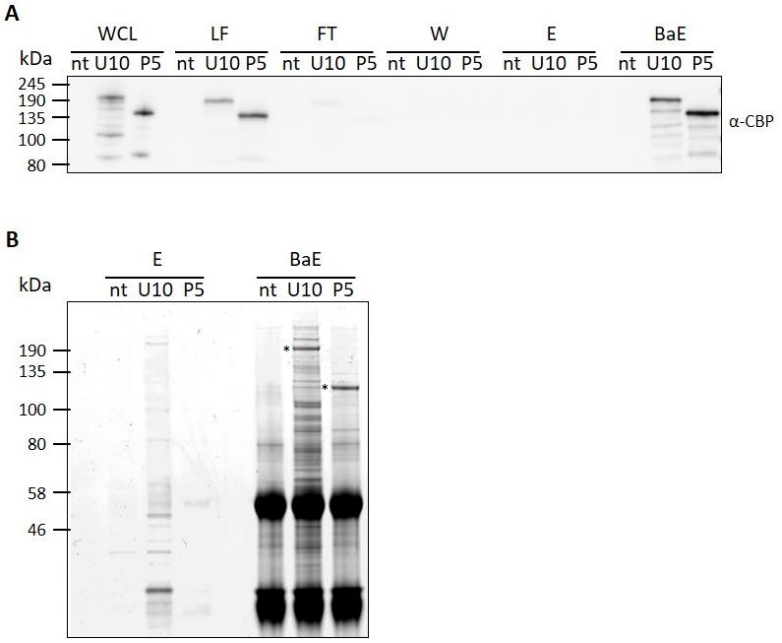

Figure 30: Analysis by western blotting and Coomassie staining of eluates from control and TAP-tagged strains Utp10 and Pol5 obtained using the protocol adapted from Krogan et al. (2004).
Affinity purification using cell extracts from non-tagged control (nt) and the TAP-tagged strains Utp10 (U10) and Pol5 (P5) was performed as described in Figure 27. Elution of purified proteins was performed by digestion with the TEV protease. (**A**) We resolved in 8% SDS-PAGE, 0.05% of the whole cell lysate (WCL), 0.2% of the light fraction obtained after ultracentrifugation (LF), 0.2% of the fraction not bound to the beads (flow-through, FT), 4.5% of the last washing step (W), 5.5% of the eluate (E), and 7% of the beads obtained after elution (BaE). After western blotting bait proteins were detected using an antibody against CBP still present in the TAP tag. (**B**) 17% of eluates (E) and 14% of beads obtained after elution (BaE) were resolved in NuPAGE 4-12% Bis-Tris gradient gel system and stained with commercially available Coomassie staining solution (SimplyBlue SafeStain from Invitrogen). Lanes corresponding to the beads after elution fractions (BaE) obtained from non-tagged control, Utp10, and Pol5 purifications were excised, in-gel digested with trypsin, and analyzed by HPLC-coupled ESI-MS. Respective identified bait proteins in supernatant lanes were labeled with *.

Cell growth and affinity purification were again performed with the workflow described in Figure 27 and the TEV eluates were analyzed by western blotting (Figure 30A) and Coomassie straining (Figure 30B).

In western blot analysis, we analyzed all steps of the affinity purification performed from the light fractions. Bands for Utp10 and Pol5 were detected in whole cell lysates before and after ultracentrifugation as well as in the beads obtained after the elution. A significant part of the bait proteins present in the light fraction was effectively and strongly bound to the beads (5 to 10% of the total). Since the TEV protease could not release the purified proteins from the beads, elution was achieved by heat denaturation of proteins. In agreement, Coomassie staining only showed a few bands in the TEV-eluted fractions, and many bands were detected in the heat-eluted fraction. As observed for the tUTP components Utp4 and Utp17, the protein patterns from the Pol5-TAP and Utp10-TAP lanes differed completely. Despite the high stringency of the second elution step, we did not observe any clear enrichment of proteins in the sample corresponding to the control strain. Therefore, we decided to analyze the lanes corresponding to the heat-eluted fractions by in gel digestion with trypsin and HPLC-ESI-MS analysis.

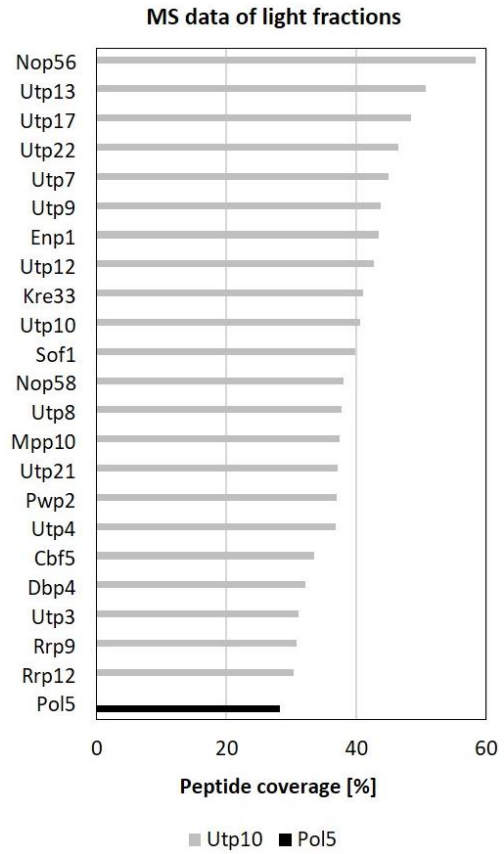

Figure 31: HPLC-ESI-MS datasets of light fractions obtained from TAP-tagged and affinity purified Utp10 and Pol5.

Light fractions obtained after ultracentrifugation were used for affinity purification with the indicated TAP-tagged proteins. After TEV elution, samples were resolved in Bis-Tris gradient gel system (see Figure 30B), digested with trypsin in gel, and analyzed by HPLC-ESI-MS. MS datasets were obtained from the bead fractions of the affinity purified light fractions of TAP-tagged Utp10 (gray) and Pol5 (black). All proteins found with a peptide coverage higher than 30% and related to the synthesis of ribosomes were plotted.

The obtained MS datasets of supernatants from Utp10 and Pol5 purifications were filtered, sorted, and plotted as described previously (30% of peptide coverage for proteins involved in ribosome biogenesis; Figure 31). Many of the proteins co-purified with Utp10, most notably Utps, were also identified in the previous affinity purifications of Utp4 and Utp17 (see Figure 29A). In contrast, Pol5 was neither identified in the Utp10 affinity purification nor vice versa. Neither tUTP- nor SSU-processome components were found in the lane corresponding to the Pol5 purification. In addition, several proteins found with Utp10 and Pol5 were also detected to be co-purified in the non-tagged strain. These proteins are very abundant in the yeast cells and are therefore often co-purified as background contaminants (see Figure 58).

2.1.2 Analysis of pre-ribosomal particles containing tUTP or UTP-A components

Using the workflow adapted from Krogan et al. including an ultracentrifugation step, we did not identify Pol5 in the purified soluble tUTP complexes (see 2.1.1).

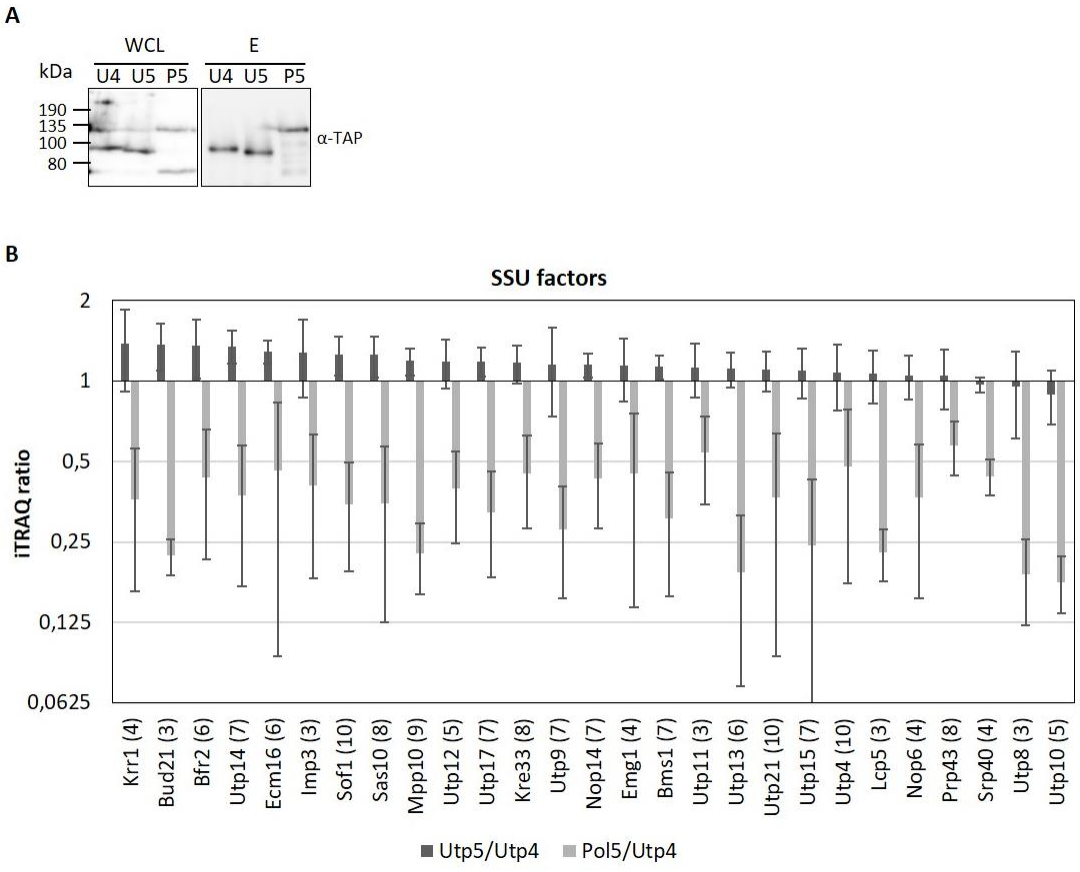

Figure 32: Analysis by western blotting and mass spectrometry of eluates from TAP-tagged Utp4 (U4), Utp5 (U5), and Pol5 (P5) obtained by affinity purification.
(**A**) 0.01% of whole cell lysate (WCL) and 10% of eluate (E) were resolved in 8% SDS-PAGE, proteins were transferred to PVDF membrane, and detected using an antibody against protein A present in the TAP tag. (**B**) Comparative proteomic analysis of Utp5 and Pol5 affinity purifications, each compared to Utp4 affinity purification. For SSU factors identified with at least three peptides (number of peptides is given in brackets), quotients of average iTRAQ ratios (115/114 = Utp5/Utp4 in dark gray; 117/114 = Pol5/Utp4 in light gray) were calculated and depicted in log2 scale. Identified proteins were sorted according to their calculated Utp5/Utp4-quotient. Error bars represent iTRAQ standard deviation.

In order to analyze, whether Pol5 is a stable part of assembled pre-ribosomal particles, we skipped the ultracentrifugation step and we analyzed particles affinity purified with Utp4, Utp5, and Pol5. To have a more comprehensive overview of the co-purified proteins, we used semi-quantitative mass spectrometry by iTRAQ® labeling (**i**sobaric **T**ag for **R**elative and **A**bsolute **Q**uantitation) as method of choice.
Strains containing TAP-tagged Utp4, Utp5, or Pol5 were cultivated in rich medium containing glucose (YPD), and cell pellets were processed for affinity purification with IgG-coupled magnetic beads (see 4.2.2.13 and 4.2.2.15). Elution was performed in the presence of ammonium hydroxide (basic elution) and eluted fractions were analyzed by western blotting and MALDI TOF mass spectrometry after iTRAQ® labeling (see 4.2.6).
The obtained whole cell lysates and eluates were analyzed by western blotting using an antibody against protein A present in the TAP tag (Figure 32A). The results showed expression and purification of all bait proteins.
SSU-processome factors identified via semi-quantitative mass spectrometry in Utp5 or Pol5 affinity purifications were compared to Utp4 affinity purification (Figure 32B). Similar purification level of AFs with Utp5 and Utp4 was reflected by their values close to 1. This result is consistent with our previous observations and it is also expected since Utp4 and Utp5 belong to the same protein complex. In contrast, comparison of affinity purifications with Pol5 and Utp4 showed ratios between 0.25 and 0.5, indicating a lower amount of SSU factors detected in Pol5 purified samples. Therefore, we cannot conclude that proteins Pol5 and Utp4 are part of the same complex.
Altogether, the results presented in the previous paragraphs suggest that Pol5 does not belong to the same protein complex as Utp4, Utp5, Utp10, and Utp17, which are all components of the tUTP complex.

2.2 Functional characterization of Pol5 (published in Braun et al., 2020)

2.2.1 Association of Pol5 with pre-rRNA

2.2.1.1 Analysis of pre-rRNA species predominantly associated with Pol5

Since Pol5 has been identified to be associated with LSU biogenesis factors (see 2.1), we first tried to characterize the pre-ribosomal particles containing Pol5. To do so, we compared affinity purifications of Pol5, three exemplary AFs, and a non-tagged control (see 4.2.2.13 and 4.2.2.14). Obtained samples were analyzed by western and northern blotting (see 4.2.4) (Figure 33). We chose Utp10, one of the earliest SSU factors assembling on the 5'ETS region (Pérez-Fernández et al., 2007), and the early AFs of the large ribosomal subunit Noc2 and Rlp7 (Dunbar et al., 2000; Gadal et al., 2002; Milkereit et al., 2001).
As reported, Utp10 co-purified especially RNAs of the small subunit, like U3 snoRNA, 35S, 23S, and 20S pre-rRNAs (Dragon et al., 2002; Gallagher et al., 2004). In contrast, Noc2 predominantly co-purified 27SA2 pre-rRNA and Rlp7 was mainly associated with 27SB

pre-rRNA (Babiano et al., 2013; Hierlmeier et al., 2013). Moreover, our results confirmed that Rlp7 remained bound to 7S containing pre-ribosomal particles, whereas Noc2 had already been released at this point (Figure 33B and 33C) (Babiano et al., 2013; Hierlmeier et al., 2013).

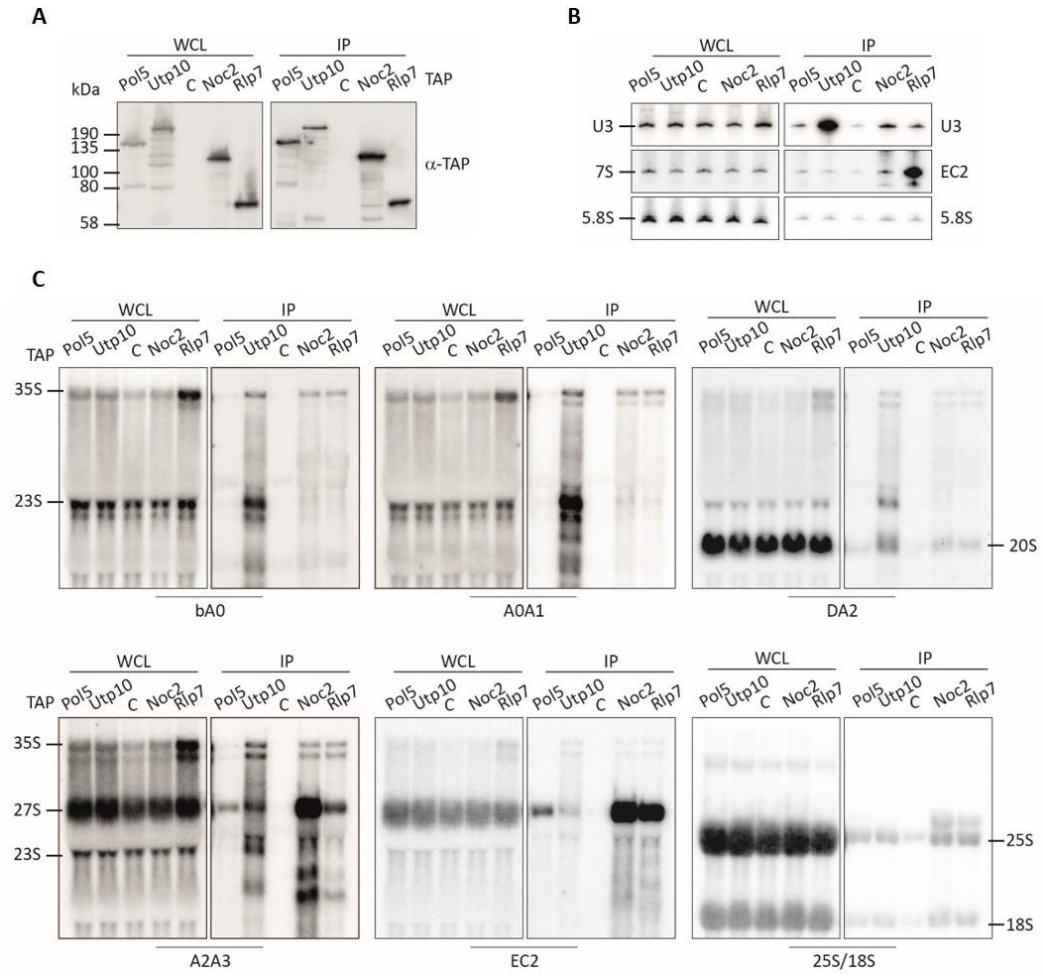

Figure 33: Timing of Pol5 association to pre-ribosomes in comparison to known AFs.
(**A**) Non-tagged BY4741 strain as control C and strains containing the TAP tag fused to Pol5, Utp10, Noc2, or Rlp7 were used for IgG-affinity purification. 0.12% of whole cell lysates (WCL) and 8% of eluates (IP) were resolved in 8% SDS-PAGE followed by western blotting. Detection was performed with an antibody against protein A present in the TAP tag. (**B, C**) Northern blot analyses of RNA samples obtained from whole cell lysates (WCL) and eluates (IP) were resolved on denaturing acrylamide (B) or agarose (C) gels and detected with radioactively labeled probes specified on the right side (B) or below (C). Identified RNA species are indicated on the left and on the right sides, respectively.

In comparison, although Pol5 was associated with 27SA2 and 27SB pre-rRNAs compared to the non-tagged control, similar amounts of 27SA2 were also obtained with Utp10-TAP. In addition, 35S and 32S pre-rRNAs were slightly enriched with Pol5 in comparison to the control strain, indicating a very mild association (Figure 33C).
These results indicate that Pol5 is preferentially associated with pre-ribosomal particles containing the 27SB pre-rRNA.

2.2.1.2 CRAC of pre-rRNA species contacting Pol5

In order to find the putative binding or contact sites of Pol5 on pre-rRNA, we devised crosslinking and analysis of cDNA (CRAC) on Pol5 as ideal method for this purpose. Thus, we established a collaboration with the group of Prof. Dr. Markus Bohnsack from the University of Göttingen. Our collaborators performed CRAC analysis on HTP-tagged Pol5 (**H**IS-**T**EV protease cleavage site-**p**rotein A) and on non-tagged wildtype strain as background control (Figure 34A).
Details about experimental setup, data acquisition, and data analysis are explained in Braun et al. (2020).

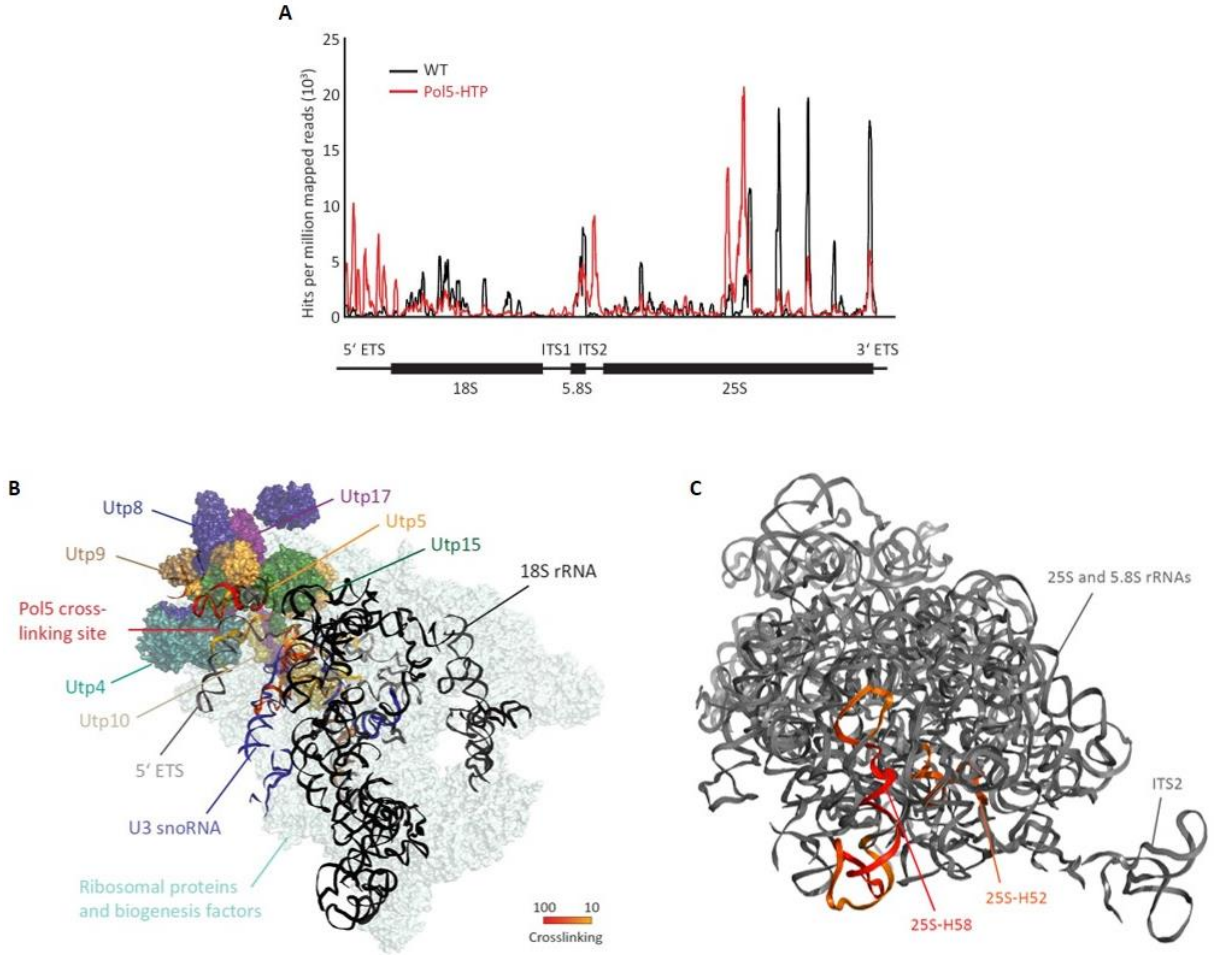

Figure 34: Crosslinks of Pol5-HTP mapped on 35S pre-rRNA sequence and on Cryo-EM structures of SSU processome and pre-60S particle.
(**A**) Graph showing normalized numbers of reads of HTP-tagged Pol5 (Pol5-HTP; red) and non-tagged wildtype control (WT; black) mapped to 35S pre-rRNA encoded on RDN37 locus. Below, a respective scheme of 35S pre-rRNA is depicted. (**B**) The number of sequencing reads in the Pol5-HTP dataset mapping to each nucleotide of the 5'ETS sequence was mapped onto the tertiary structure of the SSU processome purified via Utp1 and Kre33 (PDB: 5TZS). The tUTP proteins are highlighted in different colors and labeled. The rRNA sequences and the U3 snoRNA are shown as ribbon in gray and blue, respectively, and overlay the RPs and AFs depicted in pale cyan. (**C**) The number of sequencing reads in the Pol5-HTP dataset mapping to each nucleotide of the 25S rRNA sequence was mapped onto the tertiary structure of the pre-60S particle purified via Ytm1 (PDB: 6ELZ). A color-code was used in which the maximum number of reads is shown in red and lower numbers of reads are shown in yellow (B, C).

Two distinct crosslinking sites of Pol5 to the 35S pre-rRNA were detected within domain III of the 25S rRNA sequence in helices H58 and H52 (Figure 34C). Moreover, Pol5 contacted also the ITS2 region, where the C2 processing site is located. In addition, a broad crosslinking zone of Pol5 was detected at the 5'ETS region clustering the binding sites of the tUTP components (Figure 34B) proposing a potential role of Pol5 in the synthesis of the SSU.
Altogether, these data imply Pol5 to be very transiently associated with pre-ribosomal particles, especially regarding the 5'ETS region, since no clear accumulation of the 35S pre-rRNA could be detected by northern blotting (see Figure 33C).

2.2.2 Depletion studies of Pol5

2.2.2.1 Setup of a Pol5 depletion system and growth analysis

Since *POL5* is an essential gene, we needed to setup a depletion system to figure out the role of Pol5 in ribosome biogenesis. This system was used as basis for all functional studies presented in this thesis (Figure 35).

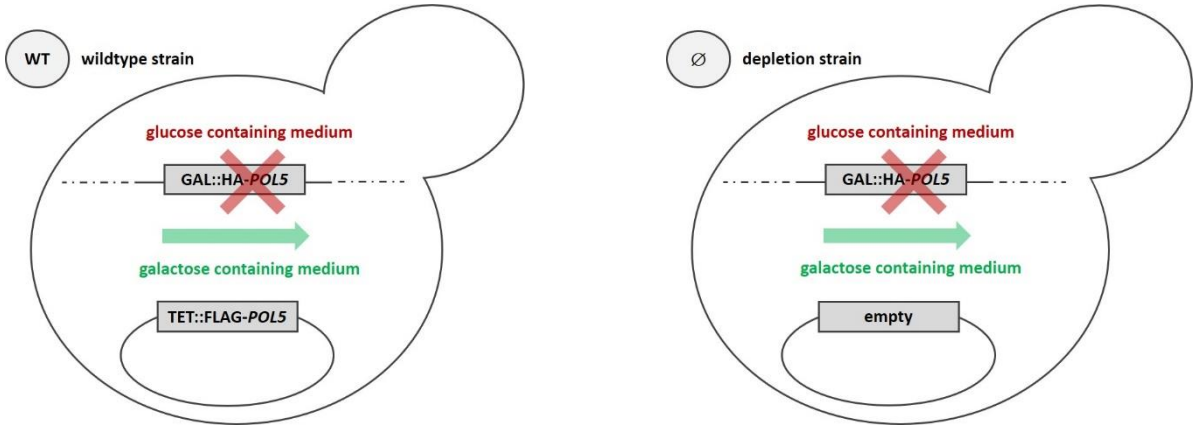

Figure 35: Scheme of the used inducible depletion system.
Both strains express *POL5* gene from the genome under control of a galactose inducible promoter combined with a HA encoding tag fused to the 5' end. "wildtype strain" is transformed with a yeast plasmid harboring *POL5* wildtype gene under control of a promoter, which can be "switched off" in the presence of tetracycline, combined with a FLAG encoding tag fused to the 5' end. "depletion strain" is transformed with the equivalent empty vector. Red X represents inhibition of transcription and green arrow stands for unhindered transcription of the respective gene in the given media conditions.

Accordingly, the genomic *POL5* gene was set under control of a galactose inducible and glucose repressed promoter and expressed with a HA encoding tag fused to the 5' end (as described in detail in section 4.2.2.5). Cells containing this construct transcribe *POL5* when cultivated in galactose containing medium. When exponentially growing cells are shifted to glucose containing medium, the *GAL*-promoter is repressed and transcription of *POL5* from genome is blocked. Therefore, due to the turnover of Pol5 previously expressed from the galactose inducible promoter and the absence of another source of Pol5, the amount of Pol5 present in the cells drops with prolonged growth in glucose containing medium. Within the described approach, the comparative analysis of cells

expressing Pol5 or not implies the comparison of cells cultivated in the presence of galactose and glucose. However, the different effects on the metabolism of the yeast cells in both carbon sources (Carlson, 1987) might cause a misleading interpretation of the obtained results.

To compare expression and depletion of Pol5 on identical metabolic conditions, we use a two-plasmid system, one plasmid contains wildtype *POL5* while the other is an empty vector (as described in detail in section 4.2.2.6). Therefore, "wildtype" situation is obtained by transformation of the described yeast strain with a yeast plasmid containing a FLAG-tagged *POL5* gene under control of a promoter repressed in the presence of tetracycline. Pol5 "depletion" situation is achieved by transformation of the described yeast strain with an empty backbone plasmid. Upon growth in glucose containing medium, transcription of genomic *POL5* is inhibited in both transformed strains. The "wildtype" strain compensates the lack of Pol5 expressed from the genome by the transcription of *POL5* on the plasmid. In contrast, the "depletion" strain carrying an empty vector cannot compensate the absence of Pol5. For the analysis of Pol5 mutants, we cloned mutant versions of *POL5* under the control of a tetracycline repressed promoter, which were transformed in yeast strains containing a chromosomally encoded Pol5 under the control of a *GAL*-promoter.

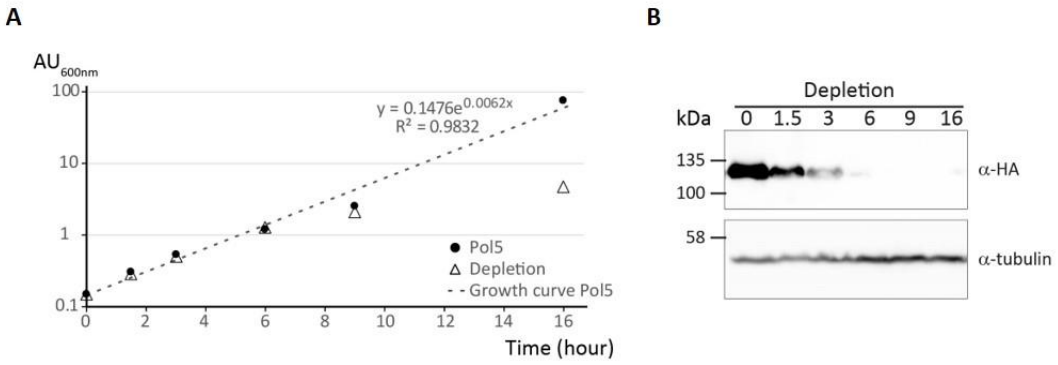

Figure 36: Growth and protein expression analyses comparing Pol5 wildtype and depletion.
(**A**) Growth development of Pol5 wildtype (black dots) and depletion (white triangle) with estimated growth curve for Pol5 wildtype (dashed line). Measured absorption units at 600 nm (AU_{600nm}) were plotted in common logarithmic scale versus depletion time in hours. Depletion was performed in rich medium containing glucose (YPD). During the whole experiment, cells were kept in exponential phase by regularly dilution. (**B**) 5 AUs of cells were harvested at each indicated time point (above) from *GAL::HA-POL5* strain cultivated under depletion conditions. Cells were subjected to denaturing protein extraction. 20% of extracts were resolved in 8% SDS-PAGE followed by western blotting. Detection was performed with an antibody against HA for visualization of chromosomally expressed HA-Pol5 and with an antibody against tubulin as loading control.

To analyze the phenotype caused by the absence of Pol5, we performed growth curves in glucose containing medium using the strain containing the construct *GAL::HA-POL5* transformed with either a *POL5* containing plasmid ("Pol5") or an empty vector ("Depletion") (Figure 36A). The cell cultures were always kept under exponential growth phase conditions at **o**ptical **d**ensities measured at **600** nm (OD_{600}) between 0.2 and 0.8 by regular dilution in fresh medium. At several timepoints, OD_{600} was measured and 5

absorbance **u**nits (AUs) were harvested to check protein expression by western blotting (see 4.2.2.8 and 4.2.2.10) (Figure 36B).
Our results showed the first growth defects induced by depletion of Pol5 at nine hours, with an almost complete discontinued growth around 16 hours. Regarding protein expression of chromosomally encoded Pol5, the signal detected with anti-HA antibody was only faintly detected after depletion for six hours.
Since we did not know the basal level of endogenously expressed Pol5, and the first growth defect was observed at nine hours of depletion, we preliminary estimated an optimal depletion time of seven hours.

2.2.2.2 Analysis of pre-rRNA synthesis influenced by Pol5 depletion

To analyze the consequences caused by the absence of Pol5 in the synthesis of mature rRNAs, we performed experiments of metabolic labeling of RNA.

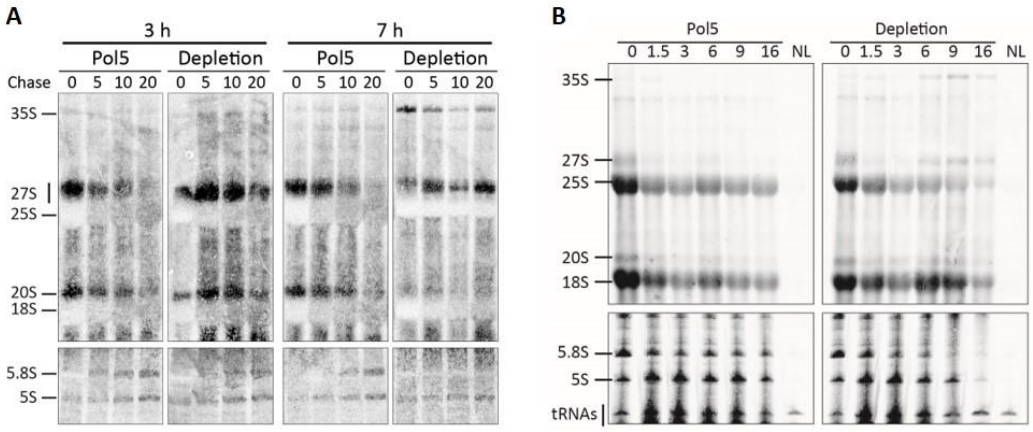

Figure 37: [^{3}H]-Uracil-pulse-chase and 4tU-pulse labeling comparing Pol5 wildtype and depletion. Northern blot analyses of [^{3}H]-Uracil-pulse-chase labeling (A) and 4tU-pulse labeling (B) of *GAL::HA-POL5* cells harboring either a Pol5-WT ("Pol5") or an empty vector ("Depletion"). RNAs were separated on denaturing agarose (above) and acrylamide (below) gels. Names of detected RNA species are indicated on the left side. (**A**) "3 h" and "7 h" refer to cell growth under depletion conditions in hours. Indicated time points for "Chase" give incubation periods with non-labeled uracil in minutes after radioactive labeling. (**B**) Indicated time points give cell growth under depletion conditions in hours. "NL" refers to non-labeled background control kept free of additional 4tU.

First, pulse-chase labeling with [^{3}H] Uracil was done. After depletion periods of three and seven hours, cells containing either the empty or the Pol5-WT plasmids were treated with radioactively labeled uracil and chased with non-labeled uracil for different time periods (see 4.2.2.12) (Figure 37A). Cells were collected and processed for purification of RNA. RNA was resolved either in 1.2% Formaldehyde Agarose Gel (for long RNAs) or in 8% Urea Polyacrylamide Gel (for short RNAs) and transferred to positive charged nylon membranes. Signals were detected using a [^{3}H]-suitable ultra-sensitive phosphor-imager screen (see 4.2.4).
After growth for three hours under depletion conditions, we did not observe significant differences in rRNA production comparing cells expressing or lacking Pol5. In contrast, clear changes between both yeast strains were detected after seven hours of growth

under depletion conditions. When compared to cells expressing Pol5-WT, production of 25S and 5.8S rRNAs in cells lacking Pol5, was strongly impaired and at the same time, 35S pre-rRNA was strongly accumulated. Furthermore, during the chase in the absence of Pol5, global level of 27S pre-rRNAs increased while the level of 20S pre-rRNA heavily decreased. These results would suggest an impaired production of 20S pre-rRNA and a defective processing of 27S pre-rRNAs.
Since working with tritium is subjected to stringent policies for working with long-life radioisotopes, we applied an alternative method for metabolic labeling using 4-thio Uracil (4tU), which is more suitable for extensive use. Therefore, cells were labeled with 4tU after different depletion periods in glucose containing medium (see 4.2.2.11) (Figure 37B). Afterward, cells were collected and processed for purification of RNA. 50 to 100 µg of labeled and extracted RNA were coupled to biotin, which was once more used for RNA extraction (see 4.2.4.2). RNAs were resolved in denaturing agarose or acrylamide gels, transferred to positive charged nylon membranes, and treated with fluorophore-labeled streptavidin for detection in the LI-COR Odyssey IR Imaging System (see 4.2.4.7).
For yeast cells harboring Pol5-WT plasmid, no major changes occurred in the levels of mature rRNAs during the depletion time course. In contrast, yeast cells transformed with empty plasmid showed a strong decrease of 25S and 5.8S rRNAs between six and nine hours of growth under depletion conditions. Moreover, precursor species like 35S and 27S pre-rRNAs accumulated in these cells after six hours of Pol5 depletion. After a longer depletion period of 16 hours, also 18S and 5S rRNA levels strongly decreased in the absence of Pol5.
Altogether, the metabolic labeling results indicate the engagement of Pol5 in the correct processing of 27S pre-rRNAs.

2.2.2.3 Determination of the pre-rRNA processing phenotype induced by Pol5 depletion

To better characterize how Pol5 influences the pre-rRNA processing, we analyzed the steady state levels of rRNA in the presence and absence of Pol5 (Figure 38A to 38C). Cells expressing or not a plasmid encoded Pol5 were cultivated in glucose containing medium. At different time points, cells were collected and processed for purification of RNA. After resolving the RNAs in two different gel types, RNAs were transferred to positively charged nylon membranes and detected with radioactive probes (see 4.2.4).
Between 1.5 and nine hours of depletion, A2A3 and A3B probes detected an increasing accumulation of 35S pre-rRNA, which was not observed in the presence of Pol5. In addition, the probe A2A3 also showed increasing amounts of 23S pre-rRNAs. At 16 hours, we observed a strong decrease of these species, most possibly due to secondary effects caused by the prolonged depletion time. Together with the pulse-chase (see Figure 37A), these results would indicate a delay in the cleavage sites A0, A1, and A2 upon depletion of Pol5.
On the other hand, A2A3 and A3B probes showed increased levels of 27SA2 and 27SA2+27SA3 pre-rRNA species at 1.5 hours depletion time. Since the increase in these pre-rRNAs seems to be independent of Pol5 depletion, it might result from the shift from

galactose to glucose containing medium, which led to a switch from preferred usage of A3 to A2 processing site (Kos-Braun et al., 2017).

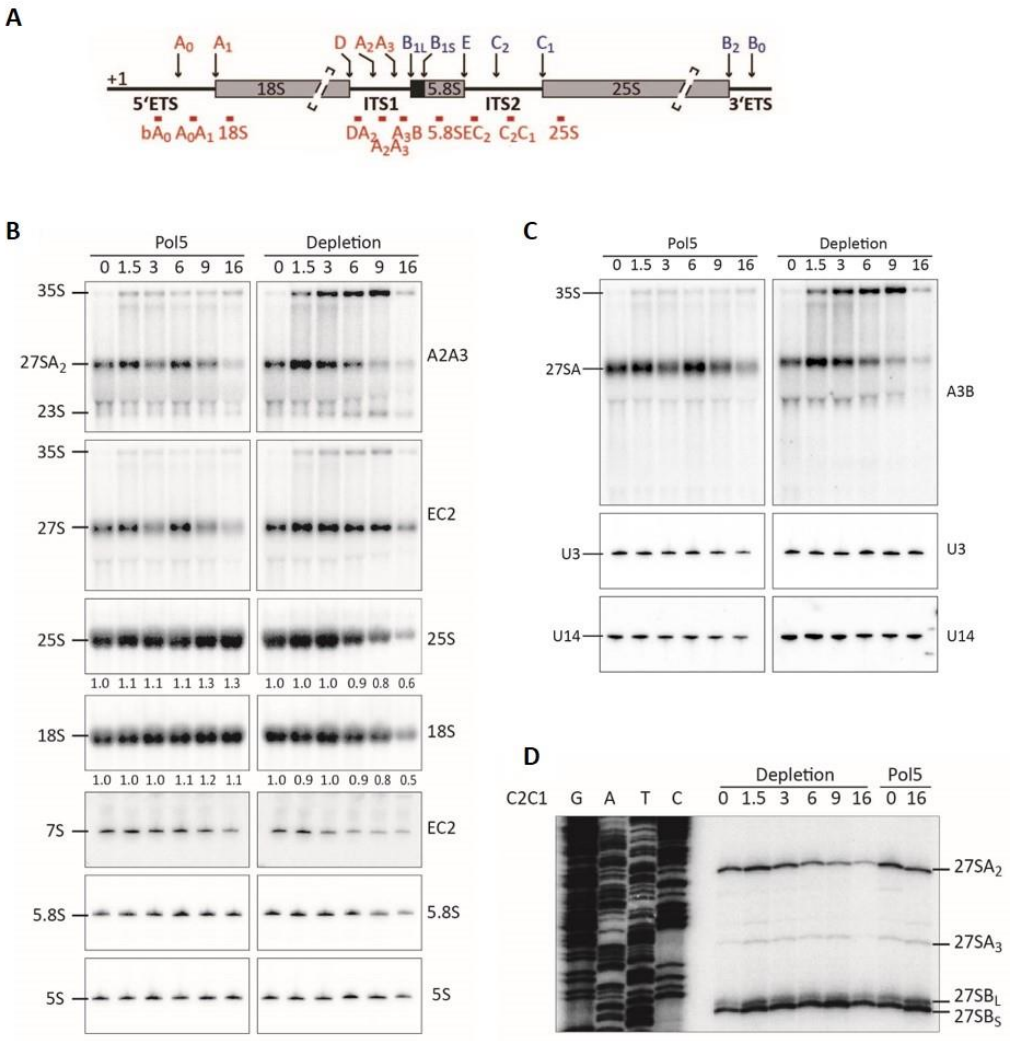

Figure 38: Effects of Pol5 depletion on steady state rRNA levels.
(**A**) Scheme of 35S pre-rRNA locus from yeast. Above, SSU and LSU processing sites are indicated in red and blue, respectively. Below, hybridization sites of probes used for northern blotting (B, C) and primer extension (D) are charted in red. (**B, C**) Northern blot analyses of steady state rRNA processing phenotypes of *GAL::HA-POL5* cells harboring a Pol5-containing plasmid ("Pol5") or an empty vector ("Depletion"). RNAs were separated on denaturing agarose and acrylamide gels. Above, indicated time points of glucose culturing are represented in hours. On the left, names of detected RNA species are assigned. On the right, names of used probes depicted in panel A are given. (**D**) Detail of denaturing primer extension gel showing pre-rRNA species of *GAL::HA-POL5* cells harboring a Pol5-containing plasmid ("Pol5") or an empty vector ("Depletion"). Above, letters indicate the nucleotide at which primer extension stops and numbers indicate time points of glucose culturing in hours. "C2C1" on the left indicates used probe for primer extension. On the right, names of detected RNA species are assigned.

In contrast, both probes showed declining amounts of 27SA2 and 27SA2+27SA3 pre-rRNA species upon Pol5 depletion between three and 16 hours. Nevertheless, overall amounts of 27S pre-rRNAs, comprised of 27SA2, 27SA3, and 27SB species, detected by EC2 probe, decreased only mildly. These results indicate an impaired production of 27SA2 pre-rRNA, but the stabilization of 27SB pre-rRNA upon depletion of Pol5. In agreement with the stabilization of 27SB pre-rRNA upon Pol5 depletion, the amount of 7S pre-rRNA

(also detected with EC2 probe) was reduced in Pol5 depleted cells in comparison to wildtype situation. This result would indicate a defect at C2 cleavage site in the absence of Pol5 and it is consistent with the CRAC data revealing a contact site of Pol5 close to the C2 cleavage site within the ITS2 region (see Figure 34A). Consequently, with the observed defects in pre-rRNA processing, between nine and 16 hours of Pol5 depletion also the levels of the mature rRNAs 25S, 18S, and 5.8S decreased remarkably. Nevertheless, we did not observe any influence of Pol5 depletion on other RNA species like, the 5S rRNA or the snoRNAs U3 and U14.

To get a complete overview of all 27S pre-rRNA species, we performed primer extension experiments with the probe C2C1 (see 4.2.4.9) over total RNA extracts obtained from cells cultivated in glucose containing medium as previously (Figure 38D).

The results showed a clear decrease of 27SA2 and 27SA3 pre-rRNA species between six and 16 hours of Pol5 depletion. In contrast, the levels of these pre-rRNAs in the presence of Pol5 remained unaffected during the time course. As explained in the introduction (see 1.4.2), 5' processing of 27S pre-rRNA can be achieved by two different pathways to produce the long and short versions of 27SB pre-rRNA, named $27SB_L$ and $27SB_S$. Neither the absolute amounts of 27SB nor the ratio between $27SB_L$ and $27SB_S$ was influenced by Pol5 depletion. These results confirm that the absence of Pol5 causes a processing defect at the C2 site but not at 5' end of 27S pre-rRNAs.

Altogether, the results obtained under depletion of Pol5 support an optimal depletion time of seven hours to further analyze Pol5 function. Moreover, the observed effects induced by the absence of Pol5 on pre-rRNA synthesis and processing combined with the CRAC data suggest a dual role of Pol5 in SSU and LSU biogenesis.

2.2.3 Polysome profiles recorded in the presence and absence of Pol5

Polysome profiles obtained by ultracentrifugation of cell extracts in sucrose gradients allow to determine problems in ribosome biogenesis. The most common method uses low salt conditions in the presence of cycloheximide to obtain profiles of translating ribosomes (Baim et al., 1985). In contrast, low magnesium conditions in the absence of cycloheximide lead to a complete separation of small and large subunits, since the interaction between both ribosomal subunits during translation requires the presence of magnesium ions (Chao, 1957; Foiani et al., 1991). Using these two methods (see 4.2.2.18), we compared the effects on ribosome synthesis caused by the presence and absence of Pol5. The profiles obtained in the presence of cycloheximide for cells expressing Pol5 and Pol5 depleted cells differed strongly (Figure 39A). In the presence of Pol5-WT, we observed distinct peaks corresponding to 40S and 60S subunits, as well as to mature 80S ribosomes and ribosomes engaged in translation (or polysomes). In contrast, upon Pol5 depletion, we observed a higher 40S-peak but no defined 60S-peak, suggesting a defective production of LSU. In addition, together with mature 80S ribosomes and polysomes, we observed an associated double maximum. The associated maximum or "half-mer" appears when an additional 40S subunit sits on the mRNA together with mature translating ribosomes (Helser et al., 1981; Rotenberg et al., 1988). Thus, "half-mers" are produced by

a deficient joining of both ribosomal subunits caused by any problem during initiation, including an insufficient production of 60S subunits.

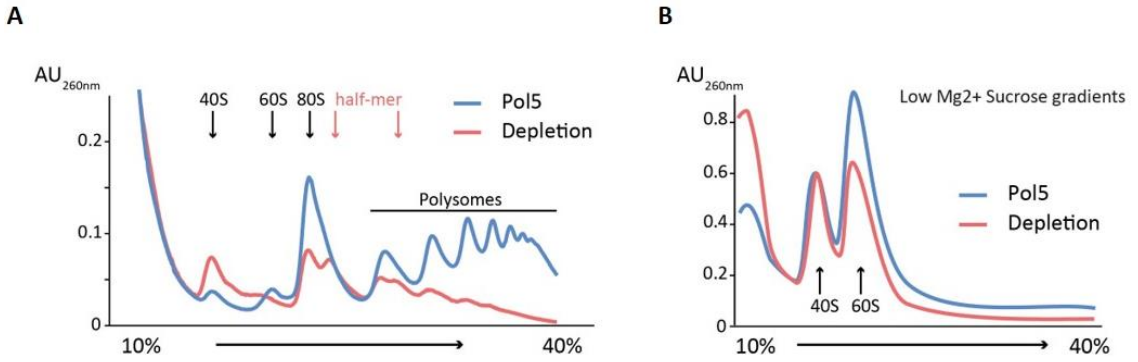

Figure 39: Low salt and low magnesium sucrose gradients of Pol5 wildtype and depletion.
Polysome profiles of *GAL::HA-POL5* cells harboring a Pol5-containing plasmid ("Pol5"; blue) or an empty vector ("Depletion"; red). Cells were cultivated for eight hours under depletion conditions. Gradients between 10% and 40% of sucrose were set up under low salt conditions in the presence of cycloheximide (**A**) and low magnesium conditions in the absence of cycloheximide (**B**). To follow the presence of ribosomal subunits, absorption was measured at 260 nm (AU_{260nm}) during fractionation and plotted versus sucrose concentration.

The imbalance of ribosomal subunits might be more evident in the analysis of gradients obtained in low magnesium conditions (Figure 39B), because only two distinct peaks, for 40S and 60S subunits, are observed during fractionation of these gradients. The Pol5-WT profile contained a 60S-peak that was considerably higher than the 40S-peak. In contrast, in the profile of cells upon Pol5 depletion, the peaks for both subunits had approximately the same size.
The reduced production of 60S ribosomal subunit observed in both experimental setups points to a predominant role of Pol5 in the synthesis of the large ribosomal subunit.

2.2.4 The role of Pol5 in LSU assembly

2.2.4.1 Influence of Pol5 depletion on the protein composition of pre-60S particles

To further characterize the role of Pol5 in the assembly of the large subunit, we decided to analyze the proteome of purified pre-60S particles in the presence and absence of Pol5 (see 4.2.2.13, 4.2.2.15, and 4.2.6). We chose the AFs Noc2 and Rlp7 as bait proteins for the purification, since they associate with most of the nuclear pre-60S particles. As explained in 2.2.1.1, Noc2 is bound to 27S-containing particles until C2 cleavage, whereas Rlp7 is part of complexes containing either 27SB or 7S pre-rRNAs. For cell cultivation, we depleted Pol5 for seven hours as previously determined (see 2.2.2).
Analysis of purified samples by western blotting revealed that Rlp7 co-purified high amounts of Pol5 indicating the existence of particles containing both proteins at the same time. In contrast, Pol5 was not found in Noc2-associated particles (Figure 40A). These results provided novel information about the conformation of pre-60S particles before the C2 cleavage, which will be later discussed. However, for a more detailed

characterization, we performed proteomic analysis of the purified eluates by **q**uantitative **m**ass **s**pectrometry (qMS).

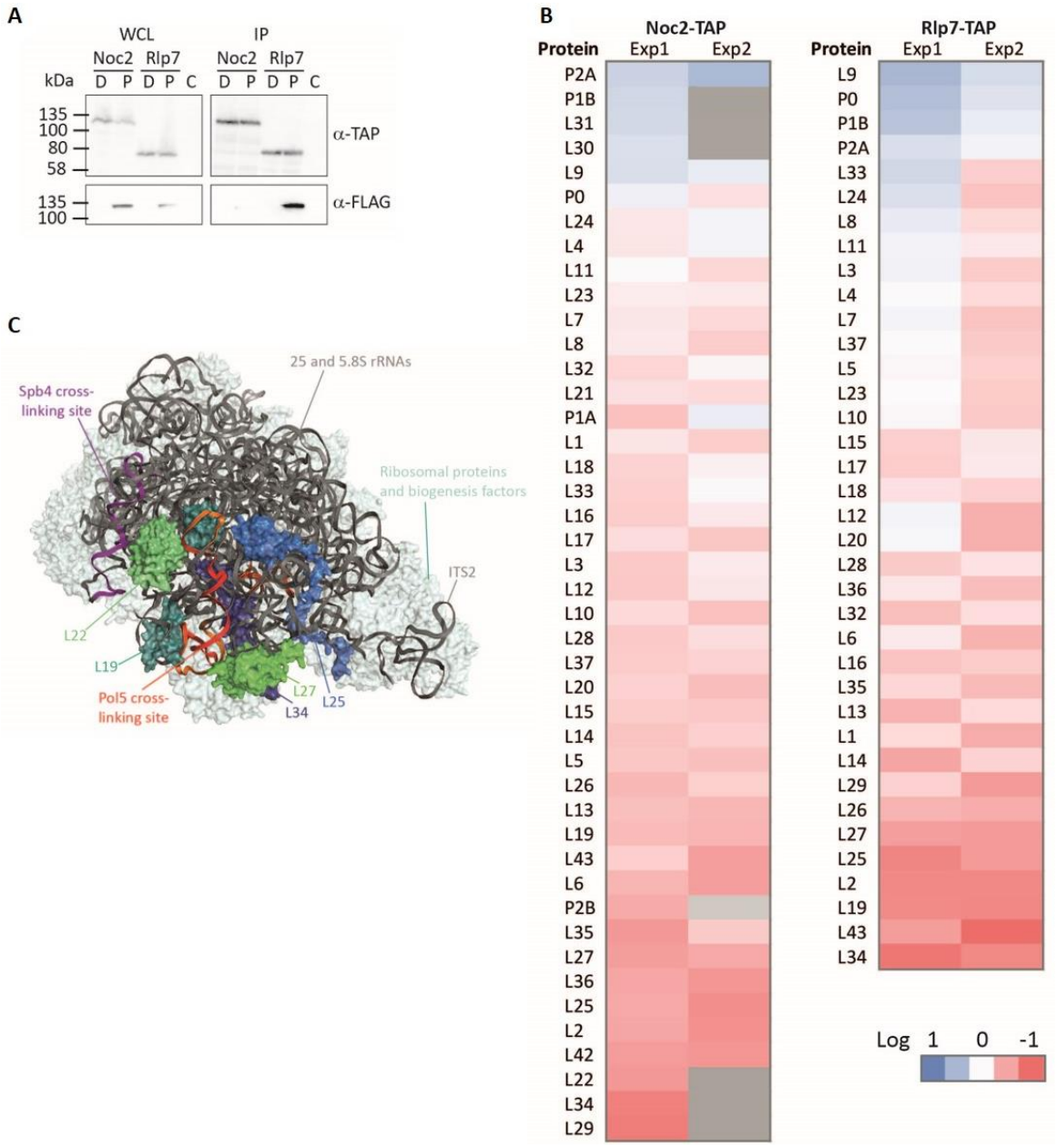

Figure 40: Influence of Pol5 depletion on association of pre-60S RPs.
(**A**) Non-tagged BY4741 strain as control C, and the TAP-tagged Noc2 and Rlp7 containing strains were used for IgG-affinity purification in the absence of Pol5 (D) and in the presence of Pol5 wildtype (P). 0.18% of whole cell lysates (WCL) and 10% of eluates (IP) were resolved in 8% SDS-PAGE followed by western blotting. Bait proteins were detected with an antibody against protein A present in the TAP tag. FLAG-tagged Pol5 was detected with an antibody against FLAG as indicated. (**B**) Heatmap of LSU RPs identified in the qMS analysis of Noc2- and Rlp7-associated particles. Only proteins identified in two independent experiments are considered. Proteins not observed in the individual experiment are depicted in gray. iTRAQ ratios (Pol5 expression versus Pol5 depletion) were calculated and depicted in log2 scale (indicated by color-code) to determine the relative abundance of proteins in the two samples. (**C**) Structure of a pre-60S complex purified via Ytm1 (PDB: 6ELZ) with the putative binding site for Pol5 and the RPs affected by Pol5 depletion highlighted. The rRNA is shown in cartoon view in dark gray and the crosslinking sites of Pol5 and Spb4 are marked in red and purple, respectively. RPs and AFs are depicted in surface view, generally in pale cyan except of RPs depleted in pre-60S particles isolated from cells lacking Pol5, which are shown in colors and labeled.

Regarding the RPs (Figure 40B), the absence of Pol5 led to increased amounts of phospho-stalk components (P0, P1B, P2A) in particles enriched with either Noc2 or Rlp7. In contrast, the levels of several RPs, which associate with domain III of the 25S rRNA (Rpl2, Rpl19, Rpl22, Rpl25, Rpl27, Rpl34, and Rpl43), were decreased in all purified particles upon Pol5 depletion. Interestingly, this set of RPs surrounds the contact sites of Pol5 with the 25S rRNA at helix H58 (Figure 40C).

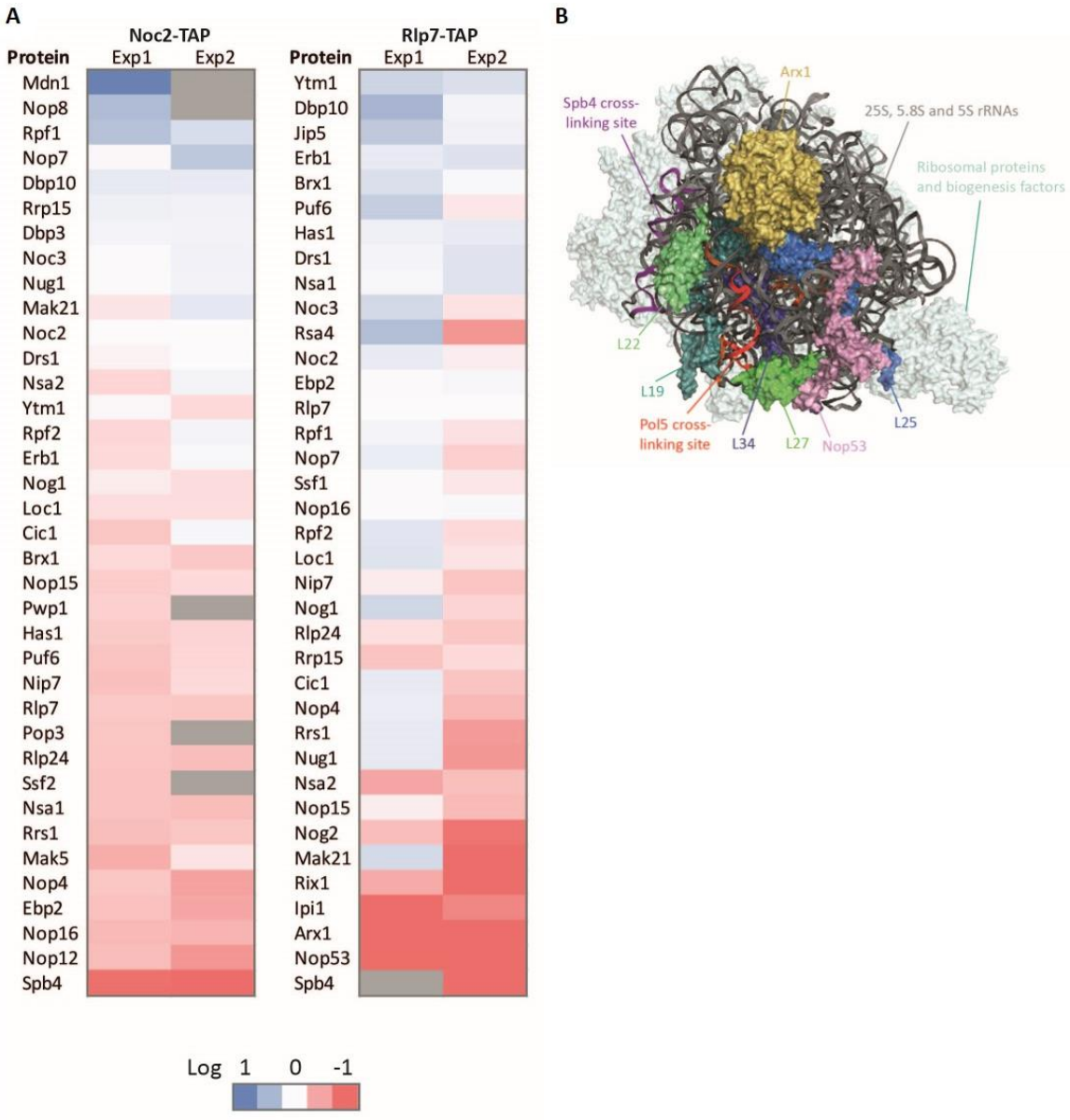

Figure 41: Influence of Pol5 depletion on association of pre-60S AFs.
(**A**) Heatmap of LSU AFs identified in the qMS analysis of Noc2- and Rlp7-associated particles. Only proteins identified in two independent experiments are considered. Proteins not observed in the individual experiment are depicted in gray. iTRAQ ratios (Pol5 expression versus Pol5 depletion) were calculated and depicted in log2 scale (indicated by color-code) to determine the relative abundance of proteins in the two samples. Data were normalized by the ratio of the bait proteins. (**B**) Structure of a pre-60S particle purified via Nog2 (PDB: 3JCT) with the binding sites of Pol5 (red), Spb4 (purple), and selected AFs highlighted and labeled. The rRNA is shown in cartoon view in dark gray. RPs and AFs are depicted in surface view, generally in pale cyan except of RPs depleted in pre-60S particles isolated from cells lacking Pol5, which are shown in colors and labeled.

Altogether, our results suggest that the absence of Pol5 impairs the formation of the polypeptide exit tunnel (Wu et al., 2016). Since the assembly of domain III is required for subsequent C2 cleavage (van Beekvelt et al., 2000; Pöll et al., 2009), the impaired association of the afore mentioned RPs in the absence of Pol5 is consistent with the processing phenotype described upon Pol5 depletion.

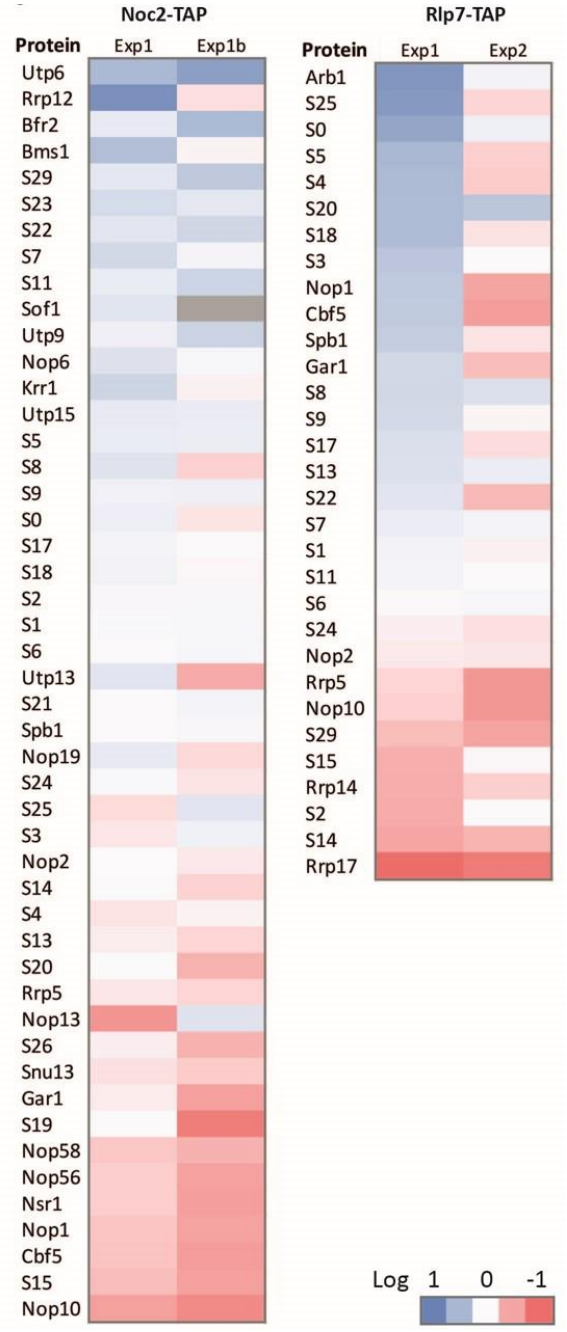

Figure 42: Influence of Pol5 depletion on association of pre-40S RPs and AFs with Noc2 and Rlp7. Heatmap of SSU RPs and AFs identified in the qMS analysis of Noc2- and Rlp7-associated particles. Only proteins identified in two independent experiments with at least two peptides are considered. Proteins not observed in the individual experiment are depicted in gray. iTRAQ ratios (Pol5 expression versus Pol5 depletion) were calculated and depicted in log2 scale (indicated by color-code) to determine the relative abundance of proteins in the two samples. Data were normalized by the ratio of the bait proteins.

Besides RPs, the association of several AFs with pre-60S particles was also influenced by Pol5 depletion (Figure 41A). The AFs Nop4, Nop12, Nop16, and Ebp2 were depleted from Noc2-purified particles, but not significantly influenced in Rlp7 purifications. In contrast, the RNA helicase Spb4 was depleted in both purifications in the absence of Pol5 (Figure 41A and 41B). Since the association site of Sbp4 is not close to the contact sites of Pol5 (Brüning et al., 2018), this result will be further discussed. Moreover, we observed decreased association of the pre-60S export factor Arx1 with Rlp7-containing particles. Since, the presence of Spb4 is required for the stable binding of Arx1 to the pre-60S particles (Brüning et al., 2018), this last result is consistent with the misincorporation of Spb4. In addition, also Nop53 was strongly depleted from Rlp7-purified particles. Altogether, the results provide important clues to characterize the role of Pol5 in the synthesis of 60S but give also relevant information about the assembly events during early steps in the biogenesis of 60S subunits, which will be discussed.
Surprisingly, regarding RPs and AFs involved in the assembly of the small subunit, many of them were enriched up to two-fold in Noc2- and Rlp7-purified particles upon Pol5 depletion (Figure 42). This result suggests that both factors were associated with 90S particles, what will be analyzed at the RNA level and it will be later discussed.

2.2.4.2 Influence of Pol5 depletion on pre-rRNA processing and composition of pre-60S particles

In order to confirm the influence of Pol5 depletion on the association of Spb4 and Nop53 with pre-60S particles, both AFs and Noc2 and Rlp7 were used as baits for affinity purification. Each AF was affinity purified from cells depleted of genome encoded Pol5 but containing either a plasmid encoding Pol5 or an empty vector (see 4.2.2.13 and 4.2.2.14). Analysis of purified bait proteins was performed by western blotting, while enriched RNAs were analyzed by northern blotting with radioactive detection (see 4.2.4). First, western blotting proved that the AFs were efficiently expressed and purified independently of the presence or absence of Pol5 (Figure 43A). Northern blot analyses (Figure 43B), upon Pol5 depletion, showed in the RNAs present in whole cell lysates a decrease in the levels of 27SA2 and 7S pre-rRNAs but an increase in the levels of the pre-rRNAs 35S and 27SB, and of the U3 snoRNA.
In the affinity purified fractions of Noc2 (Figure 43B), the co-purification of 27S precursor species but the absence of 7S pre-rRNA indicates the early association of Noc2 with pre-60S particles and its release prior to C2 cleavage. Rlp7 co-purified only 27SB pre-rRNA species but also 7S pre-rRNA, which points to a later assembly of Rlp7 with pre-60S particles compared to Noc2 and a later release since it remains associated even after C2 cleavage. Since the absence of Pol5 led to reduced amounts of 27SA pre-rRNA species, Noc2 and Rlp7 were mostly bound to 27SB pre-rRNA upon depletion of Pol5. Moreover, 35S and 33S pre-rRNA plus U3 snoRNA levels were enriched in the associated particles to both purified factors. This result points to an association of Noc2 and Rlp7 to 90S particles corroborating the previous observations at the protein level in Figure 42.

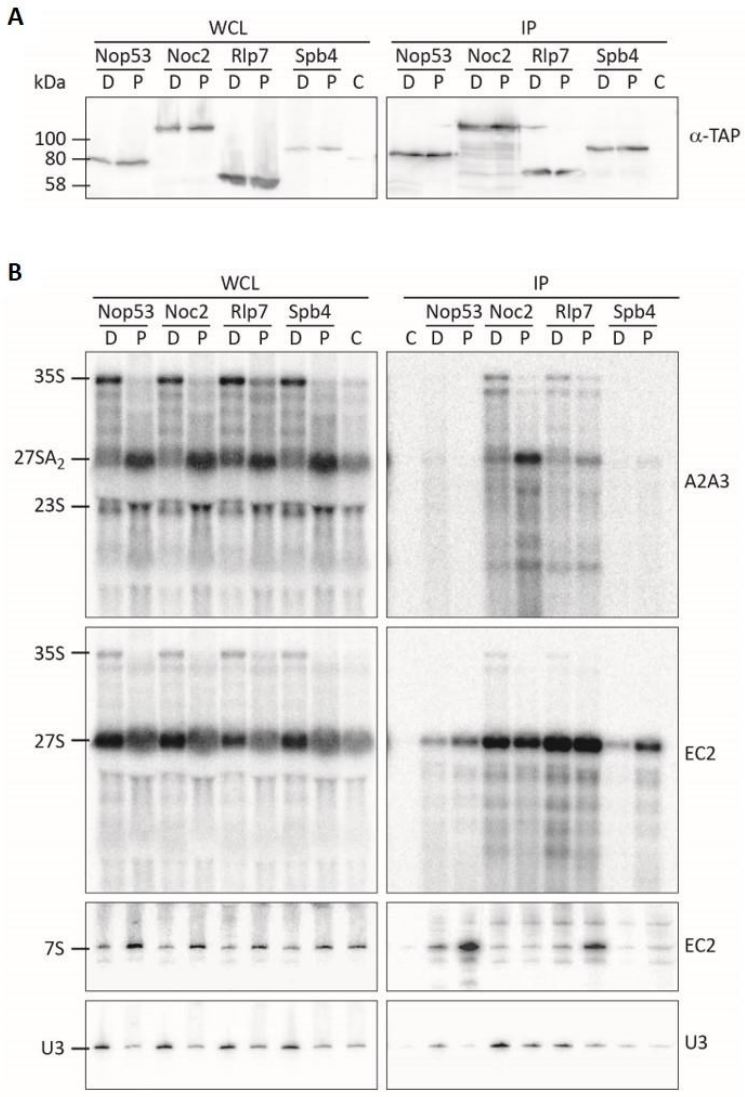

Figure 43: Influence of Pol5 depletion on processing and association of pre-rRNAs to pre-60S particles.
(**A**) Non-tagged BY4741 strain as control C and strains containing TAP tag fused to Nop53, Noc2, Rlp7, and Spb4 were used for IgG-affinity purification in the absence of Pol5 (D) and in the presence of Pol5 wildtype (P). 0.18% of whole cell lysates (WCL) and 6% of eluates (IP) were resolved in 8% SDS-PAGE followed by western blotting. Bait proteins were detected with an antibody against protein A present in the TAP tag. (**B**) Northern blot analyses of RNA samples obtained from whole cell lysates (WCL) and eluates (IP) were resolved on denaturing agarose or acrylamide gels and detected with radioactively labeled probes specified on the right side. Identified RNA species are indicated on the left side.

For Rlp7 and Nop53 (Figure 43B), the association of both factors with 7S pre-rRNA was decreased in the absence of Pol5, most likely due to the reduced amounts of 7S in the absence of Pol5. Nevertheless, the lower amounts of 27SB pre-rRNA co-purified with Nop53 upon Pol5 depletion might indicate the unstable association of Nop53 to pre-60S particles in the absence of Pol5. Alternatively, the levels of 27SB and 7S pre-rRNAs associated with Nop53 (Granato et al., 2005) might be reminiscent of a non-complete depletion of Pol5.
Regarding Spb4 (Figure 43B), as expected in the presence of Pol5, the helicase co-purified 27SB pre-rRNA but not 27SA2 and 7S pre-rRNAs (de la Cruz et al., 1998b; Garcia-Gomez

et al., 2011). In contrast, the amounts of 27SB pre-rRNAs associated with Spb4 were strongly decreased when Pol5 was depleted. This result confirms our previous observation by qMS and supports a hierarchical model, in which the association of Pol5 must take place prior to the association of Spb4.
Altogether, the presented results based on proteome and RNA analyses indicate that the function of Pol5 is required for the efficient recruitment of the AFs Spb4, Arx1, and Nop53, whereas Noc2, Rlp7, and several other AFs manage to associate independently of Pol5.

2.2.5 The role of Pol5 in SSU assembly

Consistent with the description of Pol5 as component of the UTP-A complex together with other tUTP proteins (Krogan et al., 2004), we identified contact sites of Pol5 within the 5'ETS region of the 35S pre-rRNA, around the binding site of the tUTP complex (see Figure 34A and 34B). The association of the tUtps at the 5'ETS is an essential step for the formation of the SSU processome and therefore for the early pre-rRNA processing steps at A0, A1, and A2 (Barandun et al., 2017; Cheng et al., 2017; Gallagher et al., 2004; Pérez-Fernández et al., 2007, 2011; Sun et al., 2017).
In order to examine a putative role of Pol5 in the synthesis of the small ribosomal subunit, we performed affinity purifications with the TAP-tagged tUtps Utp4, Utp5, Utp8, and Utp10 (see 4.2.2.13, 4.2.2.14, and 4.2.4). Once more, we cultured yeast strains containing the TAP-tagged AFs for seven hours in glucose to deplete the chromosomally encoded Pol5 either in the presence or absence of a plasmid encoded Pol5.
Western blot analysis showed that Pol5 depletion did neither hinder the stability of the four bait proteins, nor the association of the tUtps with the UTP-B component Utp18 (Figure 44A). Both findings suggest that formation of the SSU processome might not be affected by the absence of Pol5.
As already observed upon Pol5 depletion, northern blot analyses of RNAs present in whole cell lysates showed decreased levels of 27SA2 and 7S pre-rRNAs but increased levels of 35S and 27SB pre-rRNAs (Figure 44B and 44C). When comparing RNAs detected with DA2 and A2A3 probes in whole cell lysates, upon Pol5 depletion, we observed rising amounts of 22.5S and 21.5S pre-rRNAs but reduced levels of 20S pre-rRNA (Figure 44B). This result denotes the requirement of Pol5 for correct processing at A0, A1, and A2 sites, as previously described. Besides the known processing intermediates, we also recognized the aberrant 22S' pre-rRNA by hybridization of RNA with bA0 probe but not with DA2 or A2A3 probes (Figure 44B). Possible explanations would be the processing of pre-rRNA either at an unknown cleavage site upstream of A2 site or at the D site. This result will be discussed in further detail.
Regarding the affinity purified RNAs, tUtps still associate with the 35S and 23/22.5S pre-rRNAs in the absence of Pol5, but the association levels are lower than expected from the increased levels detected in the whole cell lysates. This would suggest that the depletion of Pol5 leads to decreasing amounts of tUtps, which can associate with 35S and 23/22.5S pre-rRNAs. However, the presence of 35S lacking tUtps is intriguing and it will be further discussed. The 33S and 21.5S precursors were co-purified in higher amounts with the

tUtps in the absence of Pol5 (Figure 44B). This result is outstanding because these pre-rRNAs have been processed at the A0 site and they lack the 5'ETS, which is the binding site of the tUtps. In addition, the 5'ETS fragment, corresponding to the counterpart of 33S and 21.5S pre-rRNAs, was also enriched with the bait proteins upon Pol5 depletion (Figure 44C).

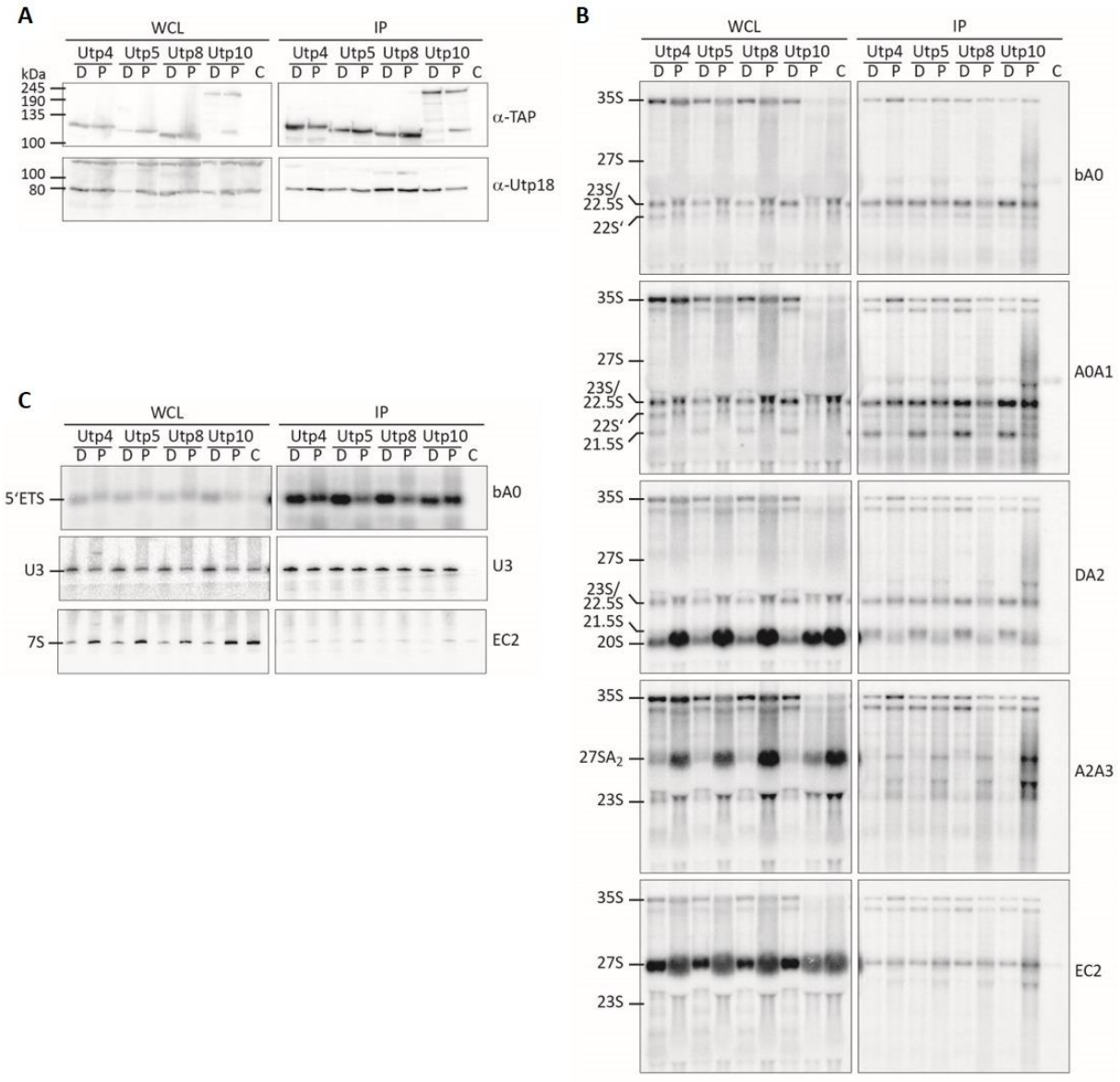

Figure 44: Effects of Pol5 depletion on dissociation of pre-rRNAs from the SSU processome.
(**A**) Non-tagged BY4741 strain as control C and strains containing TAP tag fused to Utp4, Utp5, Utp8, and Utp10 were used for IgG-affinity purification in the absence of Pol5 (D) and the presence of Pol5 wildtype (P). 0.5% of whole cell lysates (WCL) and 6% of eluates (IP) were resolved in 8% SDS-PAGE followed by western blotting. Bait proteins were detected with an antibody against protein A present in TAP tag. The UTP-B component Utp18 was detected with an antibody against Utp18 as indicated. (**B, C**) Northern blot analyses of RNA samples obtained from whole cell lysates (WCL) and eluates (IP) were resolved on denaturing agarose (B) or acrylamide (C) gels and detected with radioactively labeled probes specified on the right side. Identified RNA species are indicated on the left side and schematically represented in Figure 8.

These findings would suggest that A0 and A2 cleavages can be performed without Pol5, but the resulting pre-rRNA fragments are kept within the same particle by protein-protein interactions. Altogether, these results indicate that tUtps remain associated with 5'ETS-containing particles and, therefore, Pol5 might be required for the release of tUtps.

2.3 Pol5 in rDNA transcription

Pol5 has been described to influence transcription of the rDNA by RNA Pol I in *S. cerevisiae* (Gallagher et al., 2004). In addition, the human ortholog of Pol5, MybBP1A, might have a negative effect on RNA Pol I in human cells (Hochstatter et al., 2012). For these reasons, we decided to investigate this putative function of Pol5 in more detail.
First, we analyzed the presence of Pol5 in the rDNA and it was compared with the rDNA occupancy of RNA Pol I and two tUtps (see 2.3.1). Second, we investigated whether the absence of Pol5 would change the rDNA occupancy of RNA Pol I (see 2.3.2).

2.3.1 rDNA occupancy of Utp4, Utp5, and Pol5 compared to RNA Pol I

To analyze the presence of proteins Utp4, Utp5, Pol5, and the RNA Pol I subunit Rpa135 in the rDNA, we used yeast strains, which express these proteins fused to the TAP tag. Each strain was cultivated in three independent cultures in rich medium containing glucose (YPD). During exponential growth phase, cells were treated with formaldehyde to crosslink proteins and DNA (see 4.2.2.17). Afterward, cells were lysed, the DNA was fragmented by sonication, and TAP-tagged proteins were affinity purified using IgG-coupled magnetic beads (see 4.2.2.17). This method allows purification of DNA fragments crosslinked to the bait protein. DNA fragments were released by treatment of the bead fraction with proteinase K and subsequently decrosslinked at 65°C. Finally, obtained DNA fragments were purified by phenol-chloroform extraction, precipitated (see 4.2.2.17), and analyzed by qPCR (see 4.2.3.2) to obtain the ratio of affinity purified DNA versus total DNA in the cell extracts (Figure 45).
The second largest subunit of RNA Pol I (Rpa135) was used as a positive control since a high rDNA occupancy was expected within the transcription unit (Promoter to 3'ETS). Occupancy at the 5S locus provides a measurement for the internal background of the experiment, since its transcription is carried out by RNA Pol III. The rDNA occupancy levels throughout the analyzed loci were similar for both tUtps Utp4 and Utp5 with a two- to three-fold enrichment at the rDNA region between 18S and the 3'ETS region when compared to the non-transcribed spacers (NTS) or the 5S locus. From 18S to ITS1 region, the maximum rDNA occupancy of Utp4, Utp5, and RNA Pol I was reached. Regarding Pol5, the rDNA occupancy at all tested loci was two to three times lower than for the tUtps, but compared with the internal 5S control, the region between 18S and 3'ETS region showed at least a two-fold enrichment. However, we could not detect a maximum rDNA occupancy for Pol5 at any specific region. In addition, Pol5 and the tUtps displayed the strongest differences to RNA Pol I at the promoter region. While RNA Pol I nearly reached its

maximum, the rDNA occupancy of the other factors at this locus did not differ substantially to their occupancy at the 5S rRNA or the NTS2.

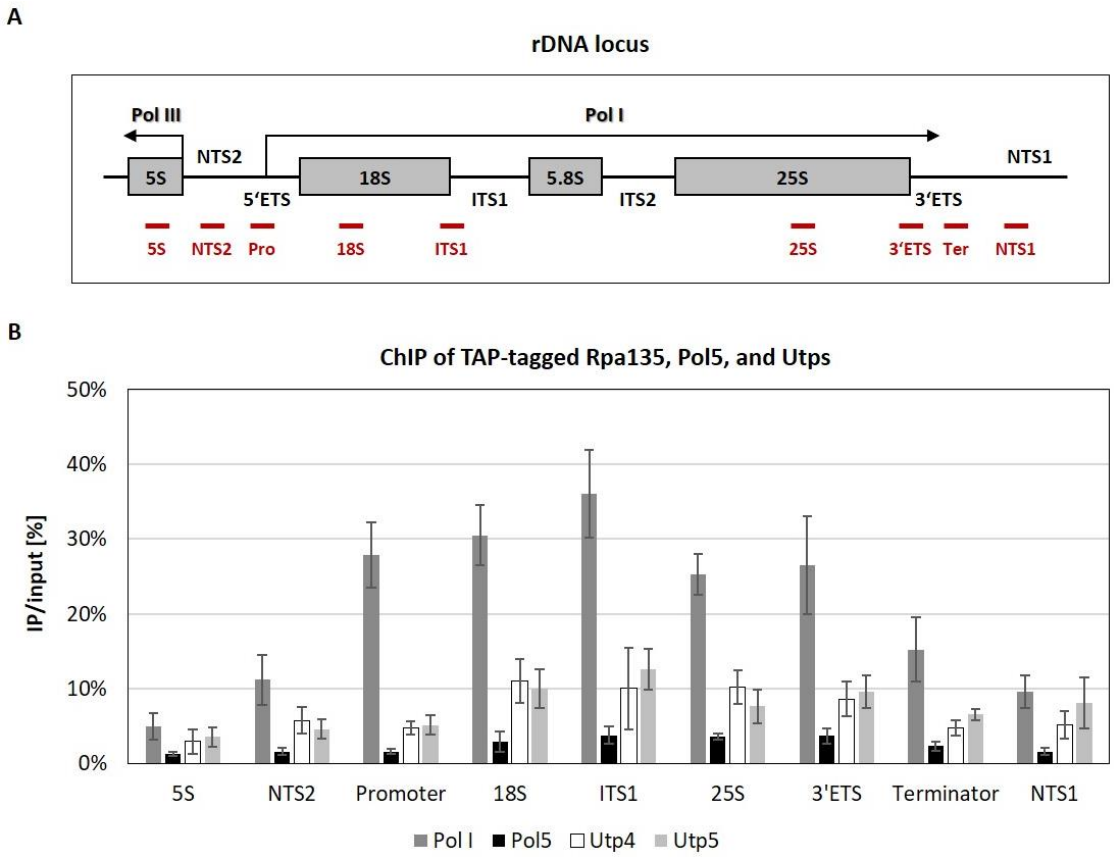

Figure 45: qPCR analysis of IP over input fractions obtained from affinity purifications of TAP-tagged Rpa135, Pol5, Utp4, and Utp5 bait proteins.
(**A**) Scheme of the yeast rDNA locus. Red bars represent positions of the amplicons analyzed by qPCR. Indicated names for the amplicons are referred in panel B and oligonucleotides used are described in Table 4. (**B**) DNA amounts obtained in affinity purified samples of (RNA) Pol I/Rpa135 (gray), Pol5 (black), Utp4 (white), and Utp5 (light gray) were normalized by the DNA amounts obtained in the respective input samples and plotted as percentage. Standard deviations were calculated from three biological replicates of each purification. Names of the analyzed rDNA regions refer to the scheme in panel A.

When compared to published results, our results showed a higher occupancy of Utp4 and Utp5 between 18S and 3'ETS regions (Gallagher et al., 2004; Wery et al., 2009). In addition, we noticed a lower occupancy of Pol5 in the rDNA and the tendency of Pol5 to be more associated with regions located toward the 3'ETS than toward the 5'ETS.

2.3.2 Influence of Pol5 on the rDNA occupancy of RNA Pol I

Based on the obtained results for the rDNA occupancy of Pol5, a direct association of Pol5 with the rDNA locus was unclear. However, Pol5 could be indirectly associated with the rDNA by protein-protein interactions, which were not fixed by formaldehyde crosslinking and, therefore still be able to influence transcription of RNA Pol I. In order to analyze this possibility, we compared the rDNA occupancy of RNA Pol I upon expression and depletion of Pol5 using the depletion system described in section 2.2.2.1.

Thus, we affinity purified Rpa135-TAP from cells containing either a plasmid encoding Pol5 (Pol5-wildtype) or an empty plasmid (Pol5-depletion). Three independent cultures for each strain were cultivated in glucose containing minimal medium (SCD-Leu) for 14 hours in order to deplete the genome encoded Pol5. Following ChIP and qPCR analysis were performed as described in section 2.3.1 (Figure 46).

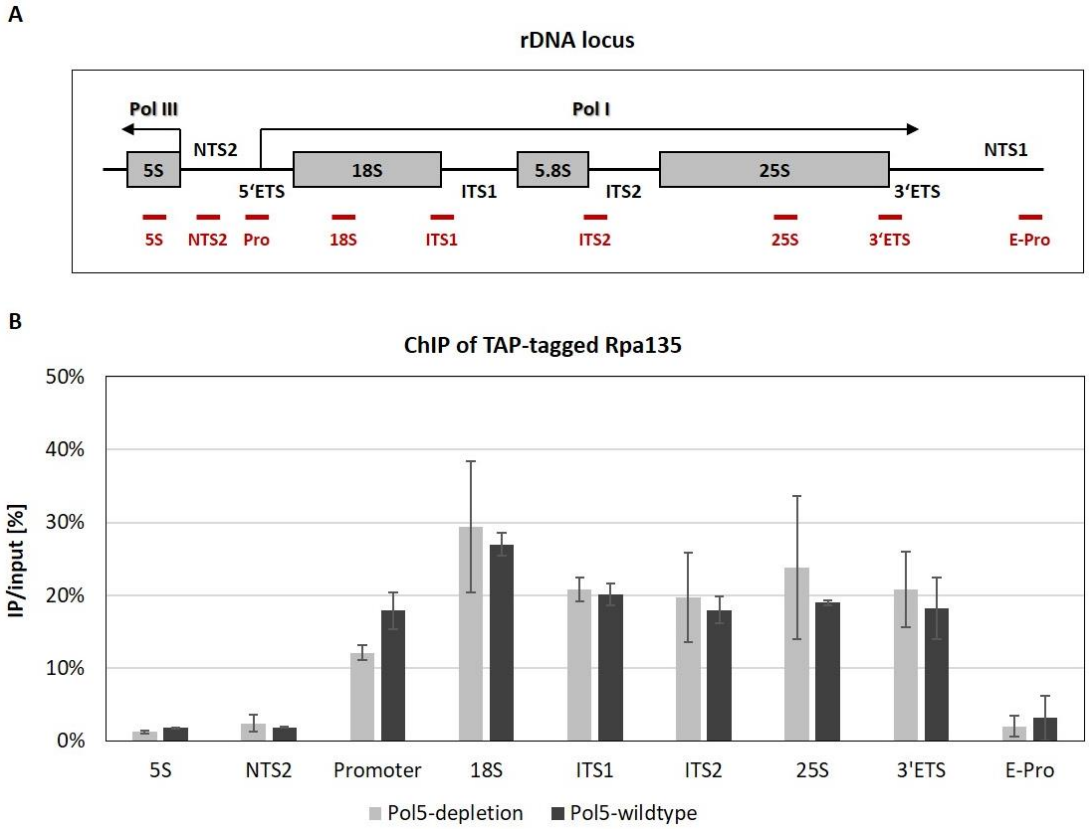

Figure 46: qPCR analysis of IP over input fractions obtained from affinity purification of TAP-tagged Rpa135 upon expression and depletion of Pol5.
(**A**) Scheme of the yeast rDNA locus. Red bars represent positions of the amplicons analyzed by qPCR. Indicated names for the amplicons are referred in panel B and oligonucleotides used are described in Table 4. (**B**) DNA amounts obtained in affinity purified samples of (RNA) Pol I/Rpa135 upon "Pol5-depletion" (light gray) and "Pol5-wildtype" (dark gray) were normalized by the DNA amounts obtained in the respective input samples and plotted as percentage. Standard deviations were calculated from three biological replicates of each purification. names of the analyzed rDNA regions refer to the scheme in panel A.

The observed rDNA occupancy pattern for TAP-tagged Rpa135 in the presence of Pol5 (Pol5-wildtype) was comparable to results depicted for Rpa135 in Figure 45B showing highest values between promoter and terminator regions. The 5S locus served again as internal control for background levels of the assay. The absence of Pol5 (Pol5-depletion) correlated with a 25% decrease of RNA Pol I-occupancy at the promoter region. In contrast, the absence of Pol5 did not cause apparent differences in the rDNA occupancy of RNA Pol I in other regions.
Therefore, our results suggest the participation of Pol5 either in transcription initiation by RNA Pol I or during elongation in the 5'ETS. Nevertheless, further experiments would be required to better characterize this effect and they will be discussed together with our experimental setup.

2.4 Domain characterization of Pol5 by mutant analyses

2.4.1 Prediction of the Pol5 tertiary structure

Since no crystal or electron microscopy structure of Pol5 is available, we rely on a tertiary structure prediction of Pol5 for the rational design of truncation mutants. The structure prediction has been calculated using Rosetta by Dr. Antonio J. Díaz-Quintana and Dr. Jesús de la Cruz (Universidad de Sevilla, Spain), and it is based on the individual folding of possible globular domains and disorganized regions (unpublished).

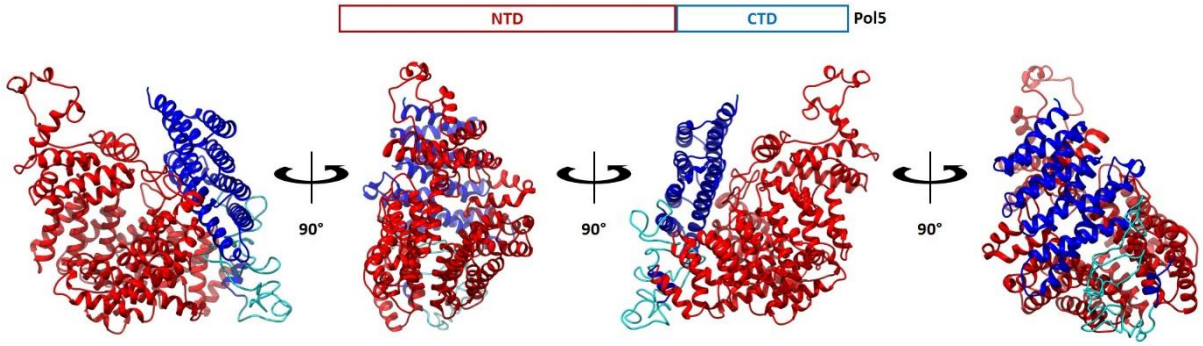

Figure 47: Predicted tertiary structure of Pol5.
360°-view of tertiary structure of Pol5 (unpublished; provided by Dr. Antonio J. Díaz-Quintana and Dr. Jesús de la Cruz). Putative NTD is indicated in red and putative CTD in blue. Disorganized region at the N-terminus of the CTD is indicated in turquois. Above, colored bar schematically represents proportions of both domains referred to complete amino acid sequence of the Pol5 wildtype protein.

The structure prediction of Pol5 shows a folding based on the repetition of α-helical domains interrupted by three loop extensions (Figure 47). This arrangement of α-helix pairs is defined as "armadillo repeat", which was first described in a protein related to segment polarity in *D. melanogaster* (Riggleman et al., 1989).
The organization of the helices suggested the existence of two main folding domains separated by a disorganized region. The whole protein consists of 1022 amino acids and we assume the separation of the domains between the amino acids L679 and D680. Thus, the NTD would enclose about 30 α-helices and two unstructured loop regions, whereas the CTD comprises 8 α-helices and the disorganized region.

2.4.2 Functional analysis of NTD and CTD

2.4.2.1 Growth analysis of Pol5 mutants

Based on the tertiary structure prediction of the Pol5 protein and the assignment of NTD and CTD, we produced several truncations and point mutations of the *POL5* gene. These mutants were transformed in the yeast strain, which conditionally expresses the chromosomally encoded Pol5 (presented in section 2.2.2.1). In order to screen for growth defects of the yeast strains expressing the modified Pol5 proteins, the mutant strains were

analyzed by drop assays on galactose and glucose containing minimal media at different temperatures (see 4.2.2.7).

a) N-terminal truncation mutants of Pol5

First, six N-terminal truncation mutants of Pol5 were produced by consecutive deletions of the coding sequence from the 5' end (Figure 48A).

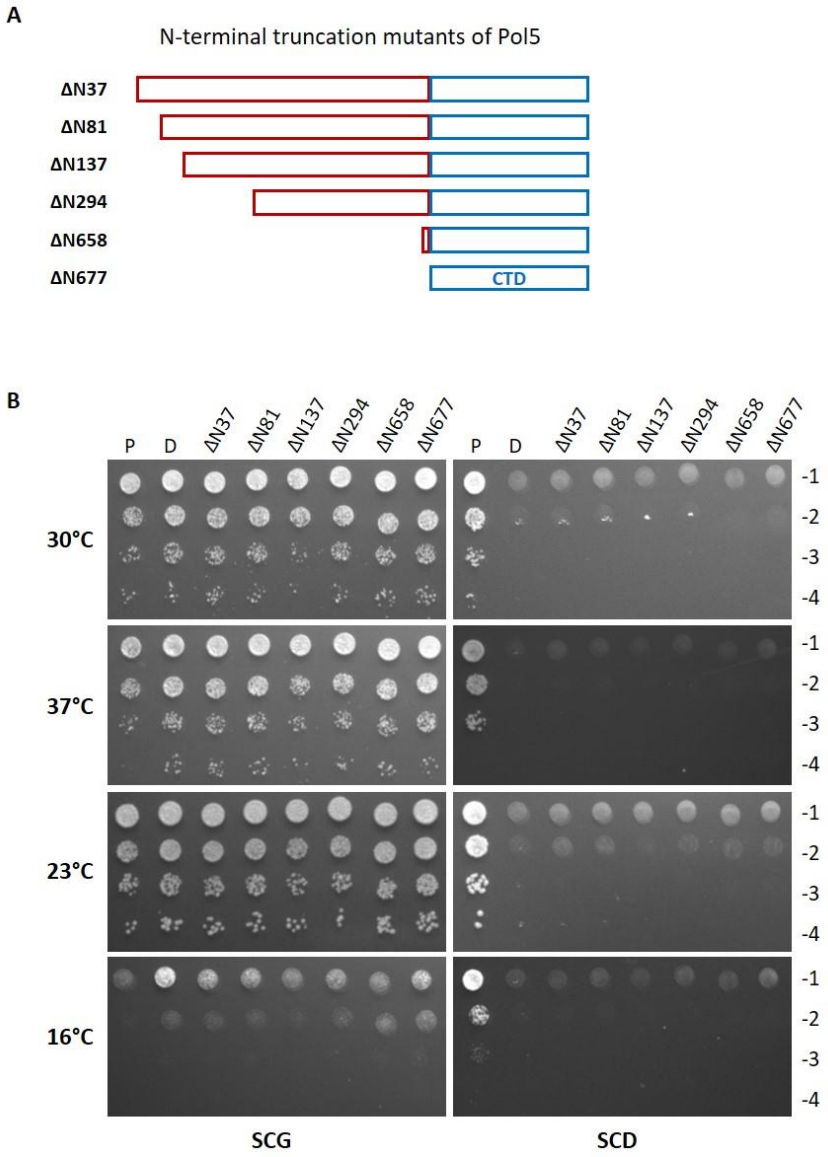

Figure 48: Schematic overview and growth test of N-terminal truncation mutants of Pol5.
(**A**) Schematic representation of N-terminal truncation mutants of Pol5. Names on the left contain number of truncated amino acids from the N-terminus. Red bars depict truncated NTD and blue bars show CTD with color-code as introduced in Figure 47. (**B**) *In vivo* growth test by drop assay comparing growth of yeast strains depleted from Pol5 (D), expressing Pol5-WT (P) or one of the six different N-terminal truncation mutants of Pol5 as introduced in panel A. Growth was tested on galactose and glucose containing minimal media (SCG and SCD) at different temperatures (30, 37, 23, and 16°C) by spotting cell concentrations from $OD_{600} = 10^{-1}$ (-1) to 10^{-4} (-4).

Therefore, we obtained truncation mutants of Pol5 lacking the first 37, 81, 137, and 294 amino acids, corresponding to Pol5 mutants lacking 1, 3, 5, or 11 α-helices from NTD accordingly. In addition, we created the longest truncation lacking the first 677 amino acids, equivalent to a complete removal of the NTD, and the second longest truncation lacking the first 658 amino acids, producing a CTD with an additional 19 amino acids overhang from NTD corresponding to α-helix 30.
Cell growth of the N-terminal mutants was analyzed in comparison to cells depleted from Pol5 or expressing Pol5-WT (Figure 48B). Since all strains expressed Pol5-WT from the genome when cultivated on galactose containing medium (SCG), these spots served as growth control. Our results showed a similar growth for all strains, demonstrating a similar number of cells analyzed for each strain. In addition, we could discard a possible dominant negative effect on cell growth caused by the co-expression of Pol5-WT from the genome and the truncated versions of Pol5 from the plasmid.
The growth on glucose containing medium (SCD) led to the exclusive expression of the Pol5 mutants expressed from plasmids. In comparison with expression of Pol5-WT or the absence of Pol5, the growth assay showed that expression of the N-terminal truncation mutants did not produce viable yeast cells. This result indicates that even truncation of the first α-helix (mutant ΔN37) is enough to impair the function of Pol5 *in vivo*.

b) C-terminal truncation mutants of Pol5

We created five C-terminal truncation mutants of Pol5 by deleting the corresponding coding sequence from the 3' end of the gene (Figure 49A). Therefore, we obtained truncation mutants of Pol5 lacking the last 29, 70, 120, or 252 amino acids, equivalent to Pol5 mutants lacking 1, 3, 5, or 8 α-helices from CTD accordingly. In addition, we created the longest truncation lacking the last 343 amino acids, corresponding to a complete removal of the CTD. Finally, we also created a mutant lacking the disorganized loop region comprising 67 amino acids within the C-terminal domain of Pol5 (Figure 49B).
To analyze the growth phenotype of cells expressing the C-terminal truncation mutants, we performed a drop assay of these strains together with cells depleted from Pol5 or expressing Pol5-WT (Figure 49C).
Growth of the yeast strains on galactose containing medium (SCG) revealed a smaller number of cells applied for the Δ993W-mutant. As for the analysis of the NTD, the similar size of colonies indicates the absence of dominant negative phenotypes due to the co-expression of Pol5-WT from the genome and Pol5 mutants from the plasmid.
Growth of the mutants on glucose containing medium (SCD) demonstrated that only expression of the Pol5 variant lacking the last α-helix (mutant Δ993W) or the disorganized loop region (mutant ΔLoop) led to the production of viable yeast cells growing comparably to Pol5-WT. This result suggests that the last α-helix of Pol5, contrary to the first α-helix (as described in section a)), is not essential to produce a functional protein. Moreover, under the conditions examined, the disorganized loop region seems to be dispensable for protein function *in vivo*.

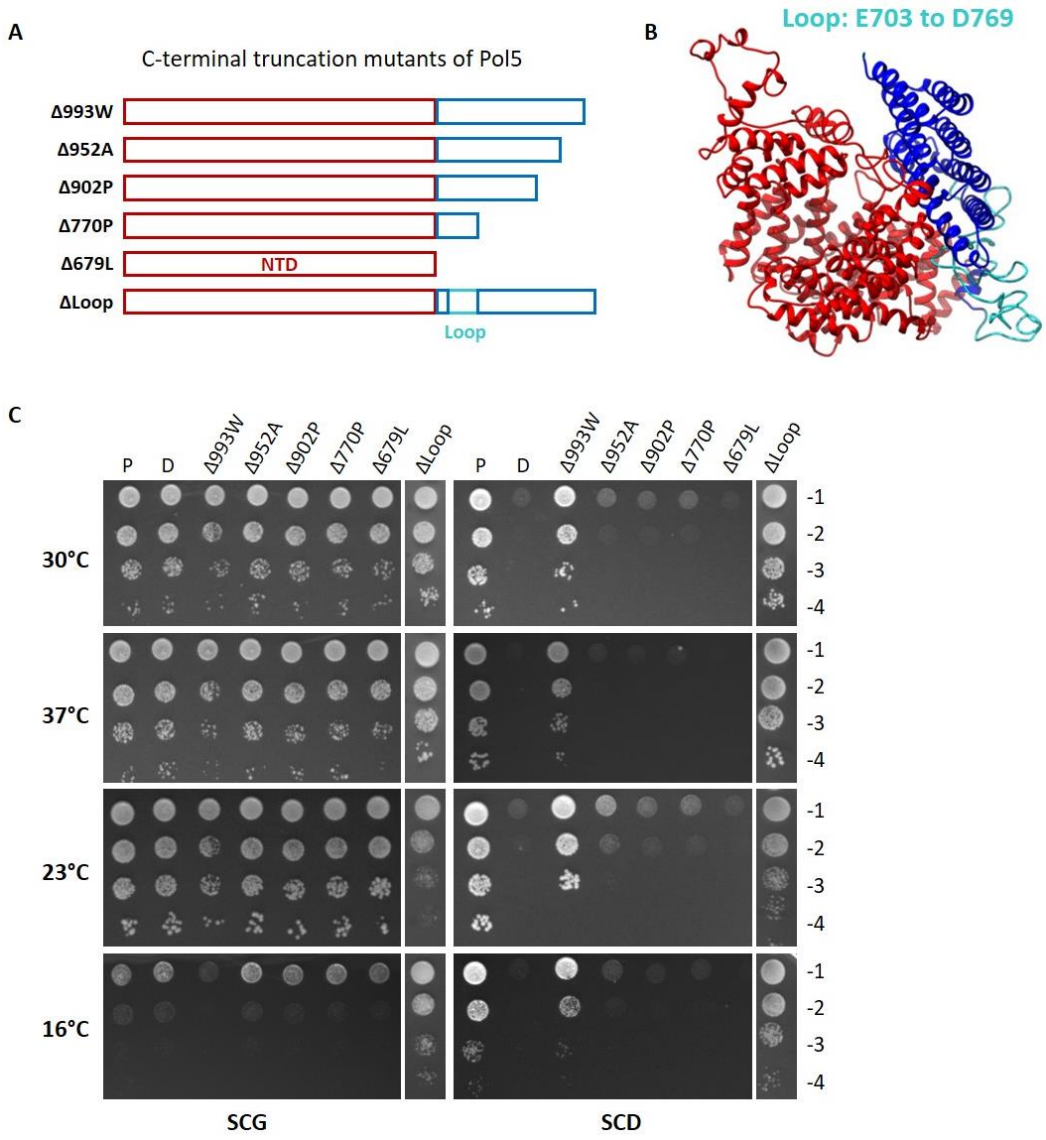

Figure 49: Schematic overview and growth test of C-terminal truncation mutants of Pol5.
(**A**) Schematic representation of C-terminal truncation mutants of Pol5. Names on the left contain number and name of the last amino acid present at the "new" C-terminus of the mutant. "ΔLoop" refers to Loop-deletion mutant lacking the disorganized loop region within the CTD. Red bars depict NTD, blue bars show truncated CTD, and turquois bar indicates the disorganized loop region with color-code as introduced in Figure 47. (**B**) Tertiary structure prediction of Pol5 with NTD, CTD, and disorganized loop region color-coded as in panel A. Disorganized loop region comprises 67 amino acids and reaches from position E703 to D769. (**C**) *In vivo* growth test by drop assay comparing growth of yeast strains depleted from Pol5 (D), expressing Pol5-WT (P) or one of the six different C-terminal truncation mutants of Pol5 as introduced in panel A. Growth was tested on galactose and glucose containing minimal media (SCG and SCD) at different temperatures (30, 37, 23, and 16°C) by spotting cell concentrations from OD_{600} = 10^{-1} (-1) to 10^{-4} (-4) . The details of the *in vivo* growth test of the ΔLoop-mutant is obtained from the drop assay depicted in supplemental Figure 59.

c) AIM domain mutants of Pol5

Analysis of the primary sequence of Pol5 revealed the existence of a putative AIM domain (arch-interaction motif) characterized by the conserved amino acid sequence LFxφD (being x any amino acid and φ an hydrophobic amino acid). The AIM domain, initially found in the proteins Nop53 (LFHVD) and Utp18 (LFFVD) in *S. cerevisiae* (Thoms et al.,

2015), was reported to bind the "arch" domain in Mtr4 to recruit the exosome. In Pol5, the AIM domain has the sequence LFALD between amino acids 477 to 481 within the NTD (Figure 50A and 50B). To investigate the possible role of the AIM domain in the function of Pol5, we created two mutants, in which the amino acid sequence of the AIM domain was altered.

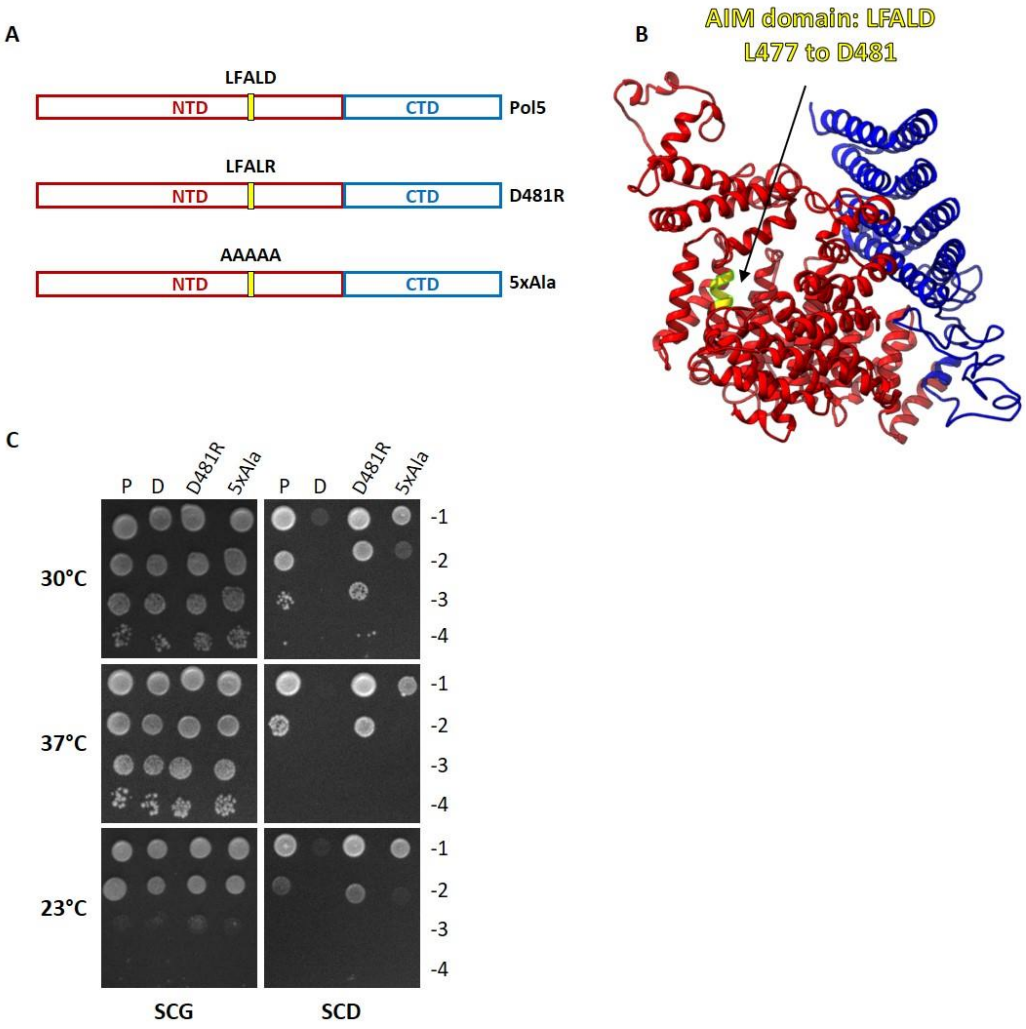

Figure 50: Schematic overview and growth test of AIM domain mutants of Pol5.
(**A, B**) Schematic representation of the position of the AIM domain (yellow) within the primary (A) and tertiary (B) structures of Pol5 with NTDs depicted in red and CTDs depicted in blue as introduced in Figure 47. Amino acid sequence LFALD of the Pol5-AIM domain, reaching from position 477 to 481 (B), was changed to LFALR in the point mutant named D481R (A), or to AAAAA in the mutant named 5xAla (A). (**C**) *In vivo* growth test by drop assay comparing growth of yeast strains depleted from Pol5 (D), expressing Pol5-WT (P) or expressing two different AIM domain mutants of Pol5 as introduced in panel A. Growth was tested on galactose and glucose containing minimal media (SCG and SCD) at different temperatures (30, 37, and 23°C) by spotting cell concentrations from OD_{600} = 10^{-1} (-1) to 10^{-4} (-4).

In one mutant, the codon for Aspartate at position 481 was replaced by an Arginine codon resulting in the mutant "D481R". In the second mutant, codons for the five amino acids within the AIM domain were replaced by Alanine codons, resulting in the mutant "5xAla". The effect of these mutants on cell growth was analyzed by drop assay together with cells depleted from Pol5 or expressing Pol5-WT (Figure 50C). The growth of the strains on

galactose containing medium (SCG) revealed similar number of spotted cells and the absence of a dominant negative phenotype resulting from the simultaneous expression of Pol5-WT from the genome and the AIM mutants from the plasmids.
Regarding the growth phenotypes of these strains on glucose containing medium (SCD), the growth of the D481R mutant did not differ at any temperature from cells expressing the Pol5 wildtype allele. In contrast, the 5xAla mutant did not allow cell growth. This result indicates that at least the first two conserved amino acids of the AIM domain, Leucine and Phenylalanine, are essential to produce a fully functional Pol5.
Altogether, the analysis of growth behavior of the different truncation and point mutants indicates that even small alterations in the Pol5 amino acid sequence have a strong impact on the function of the protein *in vivo*. Moreover, the AIM domain of Pol5 might have an essential function, although as for Utp18 the D481R mutant does not show any growth defect (Thoms et al., 2015).

2.4.2.2 The expression of Pol5 NTD and CTD *in trans*

We wanted to assay if the NTD and CTD correspond to different functional domains (*trans*-complementation assay). To do so, we used plasmids containing *POL5*, or the three longest truncation mutants of Pol5 (ΔN677 or CTD; ΔN658 or CTD+19 aa; Δ679L or NTD; Figure 51A and 51B), C-terminal truncation of 40 amino acids of the NTD (Δ639H, lacking α-helices 29 and 30) (Figure 51B), or N-terminal truncation of 50 amino acids of the CTD (ΔN727, lacking α-helix 31 at the boundary to the NTD and about one third of the disorganized loop) (see Figure 49 and Figure 51B). *POL5* genes were fused either to FLAG or GFP tags, as indicated, for further expression analysis by western blotting (Figure 51C). Plasmids were co-transformed in yeast cells in all possible combinations, which produced the presence of at least one NTD and one CTD. In addition, we used an empty vector in combination with the six plasmids as the negative control of the assay (see 4.2.2.7) (Figure 51C).
As in previous assays, growth on galactose containing medium (SCG) indicated equal number of cells spotted for each strain. In addition, it showed the absence of any dominant negative effect induced by the expression of any variant of Pol5 together with the genomic Pol5-WT. As expected, the co-transformation of an empty vector together with a plasmid expressing a functional Pol5-WT protein did not affect yeast growth on glucose containing medium (SCD). Moreover, consistent with the results presented in section 2.4.2.1, none of the yeast strains co-transformed with Pol5 mutants and empty vectors were able to grow upon depletion conditions. Interestingly, both combinations of plasmids co-expressing NTD (Δ679L) and CTD (ΔN677) produced viable yeast cells growing like wildtype cells. Nevertheless, extension of 19 amino acids in the CTD (ΔN658) had a negative effect and it did not rescue cell growth when expressed in combination with the NTD (Δ679L). Accordingly, shortening of the NTD by 40 amino acids from the C-terminal side (Δ639H) did not rescue growth independently of its expression with the extended CTD (ΔN658) or the CTD alone (ΔN677). Even the N-terminal truncation of the CTD by one α-helix and part of the disorganized loop region (ΔN727), which is not essential, did not rescue growth when expressed in combination with the NTD (Δ679L) (Figure 51B).

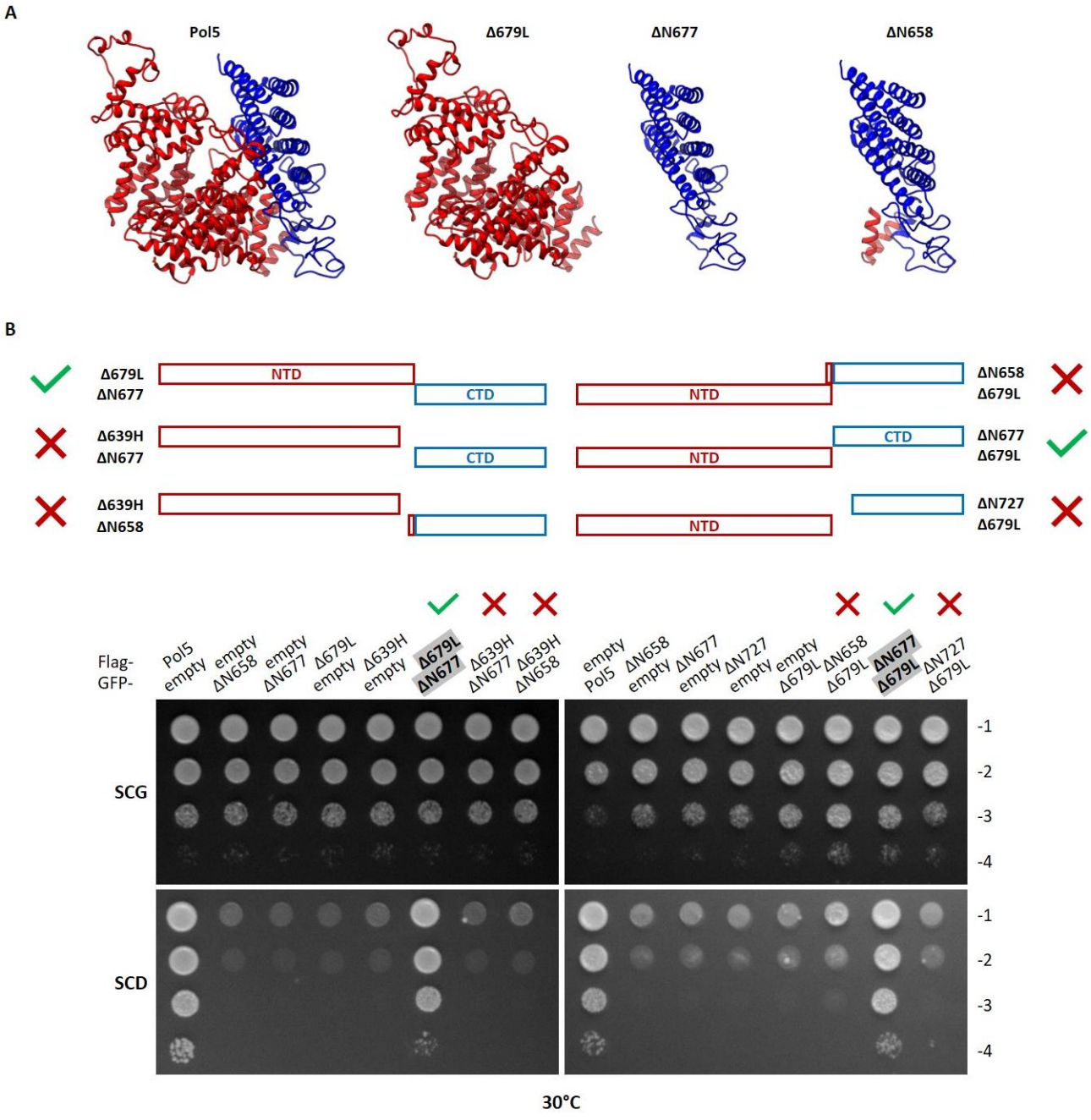
A
Pol5
Δ679L
ΔN677
ΔN658
B
Δ679L ΔN677
Δ639H ΔN677
Δ639H ΔN658
ΔN658 Δ679L
ΔN677 Δ679L
ΔN727 Δ679L
NTD
CTD
Flag-
GFP-
Pol5 empty
empty ΔN658
empty ΔN677
Δ679L empty
Δ639H empty
Δ679L ΔN677
Δ639H ΔN677
Δ639H ΔN658
empty Pol5
ΔN658 empty
ΔN677 empty
ΔN727 empty
empty Δ679L
ΔN658 Δ679L
ΔN677 Δ679L
ΔN727 Δ679L
SCG
SCD
-1
-2
-3
-4
30°C
C
kDa
FLAG-ΔN727
FLAG-Δ639H
FLAG-Pol5
GFP-Pol5
empty
FLAG-ΔN658
GFP-ΔN658
FLAG-ΔN677
GFP-ΔN677
FLAG-Δ679L
GFP-Δ679L
GFP-Pol5
FLAG-Δ679L + GFP-ΔN677
FLAG-ΔN677 + GFP-Δ679L
135
100
80
58
46
32
25
α-FLAG
α-GFP

Figure 51 (previous page): Analysis of *trans*-complementation and expression levels of selected Pol5 truncation mutants.
(**A**) Schematic representation of the tertiary structures of Pol5-WT and N- and C-terminal truncation mutants expressed in the *trans*-complementation assay (B) or analyzed by western blotting (C). NTD or parts of it are depicted in red and CTD is depicted in blue according to the color-code introduced in Figure 47. Names are indicated. (**B**) Above, schematic representation of primary structures of Pol5 mutant combinations analyzed by *trans*-complementation assay. Below, *trans*-complementation test by drop assay to investigate growth of yeast strains co-transformed with plasmids containing the indicated *POL5* allele. The tags of the plasmids are given on the left. Growth was tested on galactose and glucose containing minimal media (SCG and SCD) at 30°C by spotting cell concentrations from OD_{600} = 10^{-1} (-1) to 10^{-4} (-4). Plasmid combinations that rescue growth are written in bold with gray background and are marked with a green hook. Red cross symbolizes inhibited growth. (**C**) 5 AUs of cells expressing the different Pol5 mutants fused to FLAG or GFP tag (indicated above) were subjected to denaturing protein extraction. 20% of extracts were resolved in 10% SDS-PAGE followed by western blotting. Detection was performed with antibodies against FLAG and GFP for visualization of the respectively tagged Pol5 mutants. The image of the complete western blot analysis is depicted in supplemental Figure 60.

These results suggest that expression of NTD and CTD as independent polypeptides complements all essential functions of Pol5. Moreover, the absence of *trans*-complementation when the CTD was extended by one α-helix or shortening of the NTD or the CTD at not essential elements might indicate the structural reconstitution of Pol5.
The cell extracts of the yeast strains analyzed in *trans*-complementation were obtained by denaturing protein extraction (see 4.2.2.10) and analyzed by western blotting (see 4.2.5.4). Since Pol5 or its mutant versions were either fused to FLAG or GFP tag, immunodetection was performed with antibodies against FLAG and GFP (see Table 7 and 4.2.5.6) (Figure 51C).
Compared to the protein expression levels of FLAG-Pol5, even higher levels were detected for FLAG-ΔN677 (CTD) independent of the additional expression of GFP-Δ679L (NTD). Expression levels of FLAG-Δ639H and FLAG-ΔN727 were comparable to FLAG-Pol5 levels, whereas expression levels of FLAG-ΔN658 (CTD+19 aa) were strongly reduced in comparison to FLAG-ΔN677 (CTD) levels and they were also significantly lower than FLAG-Pol5 levels. The protein levels detected for FLAG-Δ679L (NTD) were reduced compared to FLAG-ΔN658 but also compared to FLAG-Δ639H (containing its further truncation at the C-terminal region). Furthermore, the levels did not change upon co-expression of GFP-ΔN677 (CTD). Regarding the GFP-tagged proteins, the tendencies of the expression levels comparing the different versions of Pol5 were similar as observed for the FLAG-tagged proteins. The highest expression levels were observed for GFP-ΔN677 (CTD), next for GFP-Pol5 and GFP-ΔN658, and the lowest levels were observed for GFP-Δ679L.
The sizes of the protein bands prove that the co-transformation of both mutant plasmids into one yeast strain did not lead to a recombination event reproducing the wildtype sequence and thus the wildtype Pol5 on one polypeptide chain. Moreover, the stability of NTDs and CTDs of Pol5 did not increase when co-expressed in the same yeast strain.

2.4.2.3 The role of NTD and CTD in release of tUtps

As explained in section 2.2.5, the depletion of Pol5 hindered the release of the tUtps from the 5'ETS. In order to define, which part of Pol5 might be responsible for this task, all Pol5

mutants, presented in section 2.4.2.1, were investigated. Therefore, Utp5-TAP strains depleted from Pol5 or expressing Pol5-WT or Pol5 mutants were cultivated for seven hours in double selective medium containing glucose (2xSCD; see Table 8). Whole cell lysates were used for affinity purification with IgG-coated beads, RNAs from whole cell lysates and affinity purified fractions were extracted, resolved either in agarose or acrylamide gels, and analyzed by northern blotting (see 4.2.2.13, 4.2.2.14, and 4.2.4). Protein samples from whole cell lysates and affinity purified samples were resolved in 10% SDS-PAGE and analyzed by western blotting.

a) Affinity purification of Utp5 upon expression of NTD mutants

As observed in the western blot analysis (Figure 52A), we confirmed that all *POL5* alleles were expressed even though ΔN294 was present in lowest amounts. This result shows that growth phenotype under expression of these mutants does not correspond to the low expression of the respective mutant (except of ΔN294). Moreover, the expression of Utp5-TAP did not depend on the allele of *POL5* expressed. Regarding the affinity purified fractions, similar levels of Utp5-TAP were observed in all cases except under expression of ΔN658 and ΔN677, where less Utp5 was detected. Interestingly, the three shortest truncation mutants ΔN37, ΔN81, and ΔN137 but not the full length Pol5 were enriched in the affinity purification of Utp5.

Concerning the processing phenotypes of the N-terminal truncation mutants observed in the northern blot analysis of RNAs present in whole cell lysate samples (Figure 52B and 52C), no differences could be detected compared with the depletion of Pol5 (as described in detail in section 2.2.5). This result indicates that correct processing at A0, A1, A2, and C2 sites requires the complete NTD of Pol5.

Based on the analysis of RNAs obtained in the Utp5 affinity purification (Figure 52B), we found that Pol5 depletion and the expression of the Pol5 mutants correlated with a higher enrichment of 35S, 33S, 23S/22.5S, and 21.5S pre-rRNAs in comparison to the wildtype. As described in section 2.2.5, the co-purification of the 21.5S pre-rRNA with Utp5 was striking because the 5'ETS, where Utp5 associates, has already been removed from this precursor by cleavage at the A0 site. Moreover, the 5'ETS, which is detected with probe bA0 (Figure 52C) and their complementary pre-rRNAs, 33S and 21.5S, were also co-purified in high amounts with Utp5 upon Pol5 depletion and upon expression of several N-terminal truncation mutants. Nevertheless, we observed a reduced association of Utp5 with the 5'ETS and the pre-rRNAs 35S, 23S, and 21.5S when mutants ΔN137 and ΔN294 were expressed. This result suggests that both mutant proteins were able to release Utp5 from mentioned precursors, at least partially.

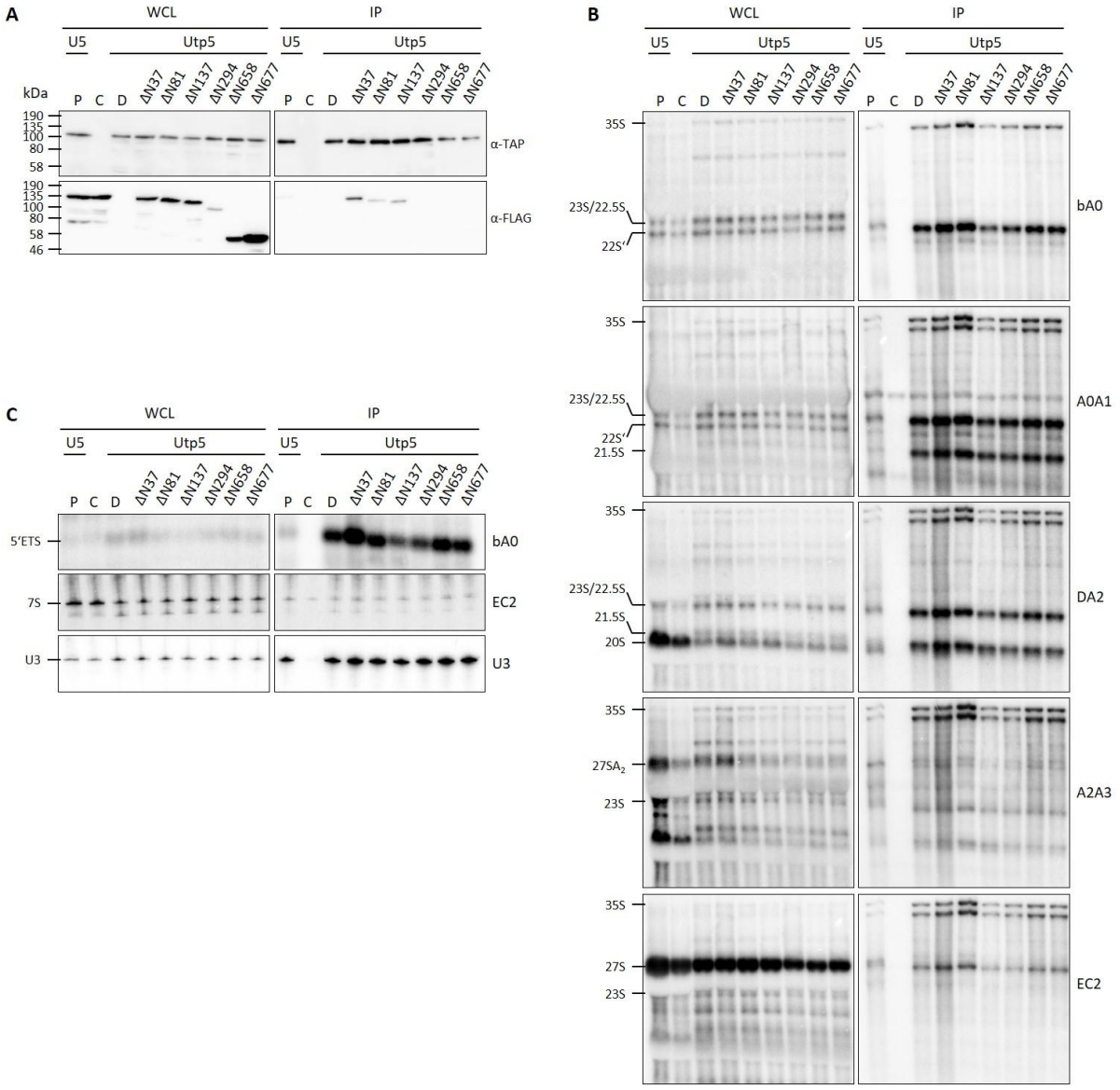

Figure 52: Effects of N-terminal truncation mutants of Pol5 on dissociation of pre-rRNAs from the SSU processome.
(**A**) Non-tagged BY4741 strain as control C and TAP-tagged Utp5 (U5 or Utp5) containing strain were used for IgG-affinity purification in the absence of Pol5 (D), in the presence of Pol5 wildtype (P), and in the presence of the N-terminal truncation mutants of Pol5 (ΔN37-ΔN677) (see Figure 48). 0.15% of whole cell lysates (WCL) and 10% of eluates (IP) were resolved on 10% SDS-PAGE followed by western blotting. Bait proteins were detected with an antibody against protein A present in the TAP tag. FLAG-tagged Pol5 in the wildtype and in the N-terminal truncation mutants was detected with an antibody against FLAG as indicated. (**B, C**) Northern blot analyses of RNA samples obtained from whole cell lysates (WCL) and eluates (IP) were resolved on denaturing agarose (B) or acrylamide (C) gels and detected with radioactively labeled probes specified on the right side. Identified RNA species are indicated on the left side and schematically represented in Figure 8.

b) Affinity purification of Utp5 upon expression of CTD and AIM mutants

As observed for the N-terminal truncation mutants in western blot, neither the expression of the C-terminal truncation nor expression of the AIM mutants influenced the expression of Utp5-TAP (Figure 53A). Concerning the expression of the Pol5 mutants, 5xAla was present in lower amounts than other mutants and expression of Δ952A and Δ902P

mutants were not detected at all. The other mutants were detected in similar levels like Pol5-WT. Western blot analysis of the affinity purified samples showed comparable amounts of Utp5-TAP, although in cells containing the non-detected mutants (Δ952A and Δ902P) less of the bait protein was purified. The detection with an antibody against FLAG revealed that Pol5-WT, 5xAla, and Δ679L were associated with Utp5. Reasons for the observed varying association of Pol5 with Utp5 will be discussed later.

The processing phenotypes of the C-terminal truncation and the AIM mutants were observed by northern blotting of RNAs obtained from the whole cell lysate samples (Figure 53B and 53C). The mutants expressing the *POL5* alleles Δ993W and D481R, which grew like wildtype cells in drop assay (see Figure 49 and Figure 50), did show processing of the pre-rRNA as in the presence of Pol5-WT. The expression of the remaining mutants led to a similar processing phenotype as in the absence of Pol5 (as described in detail in section 2.2.5). This indicates that processing at cleavage sites A0, A1, A2, and C2 does not require the complete CTD.

Regarding the affinity purified samples from strains expressing the C-terminal truncation mutants, Utp5 co-purified similar amounts of precursors in all mutants showing growth defect (see 2.4.2.1). Association with 35S and 23S/22.5S was not influenced and increased levels of 33S, 21.5S pre-rRNAs, and 5'ETS fragment were detected (Figure 53B and 53C). This result would indicate a defective release of Utp5 from the pre-rRNAs in these strains (as described in 2.2.5).

With respect to the AIM domain mutants, Utp5 co-purified the same precursors upon expression of the D481R point mutant (growing like wildtype; see 2.4.2.1) compared to Pol5-WT. In contrast, the affinity purified RNAs obtained from cells expressing the 5xAla mutant indicated an increased association of Utp5 with the 23S/22.5S and 21.5S pre-rRNAs and the 5'ETS fragment compared to Pol5-WT (Figure 53B and 53C). This result suggests a predominant role of the AIM domain in the release of the tUtps.

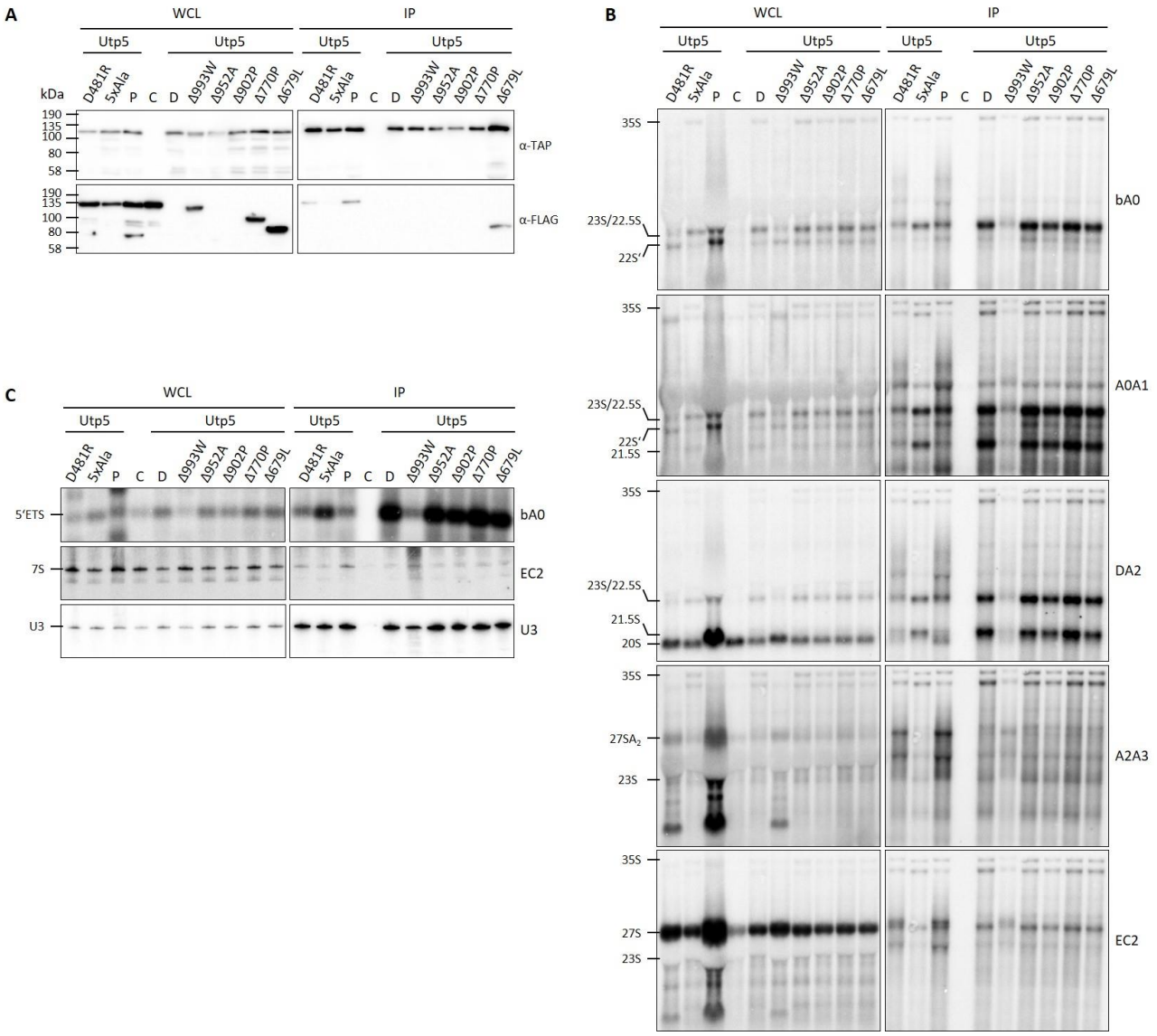

Figure 53: Effects of C-terminal truncation mutants and AIM mutants of Pol5 on dissociation of pre-rRNAs from the SSU processome.
(**A**) Non-tagged BY4741 strain as control C and TAP-tagged Utp5 containing strain were used for IgG-affinity purification in the absence of Pol5 (D), in the presence of Pol5 wildtype (P), and in the presence of the C-terminal truncation mutants of Pol5 (Δ993W-Δ679L) (see Figure 49) and the AIM mutants of Pol5 (D481R, 5xAla) (see Figure 50). 0.15% of whole cell lysates (WCL) and 10% of eluates (IP) were resolved on 10% SDS-PAGE followed by western blotting. Bait proteins were detected with an antibody against protein A present in the TAP tag. FLAG-tagged Pol5 in the wildtype, in the C-terminal truncation mutants, and in the AIM mutants was detected with an antibody against FLAG as indicated. (**B, C**) Northern blot analyses of RNA samples obtained from whole cell lysates (WCL) and eluates (IP) were resolved on denaturing agarose (B) or acrylamide (C) gels and detected with radioactively labeled probes specified on the right side. Identified RNA species are indicated on the left side and schematically represented in Figure 8.

2.4.2.4 The role of the AIM domain in pre-60S particles

To additionally analyze the role of the Pol5-AIM domain in assembly of pre-60S particles, we TAP-tagged the 60S AFs Rlp7 and Spb4 in strains, which conditionally expressed Pol5 *(GAL::HA-POL5)*. Rlp7 and Spb4 were affinity purified from cells depleted of chromosomally encoded Pol5, which expressed either Pol5-WT or the Pol5-AIM mutant

5xAla. Therefore, cells were cultivated for seven hours in double selective medium containing glucose (2xSCD; see Table 8), and RNAs were extracted from whole cell lysates and affinity purified fractions and analyzed by northern blotting (see 4.2.2.13, 4.2.2.14, and 4.2.4).

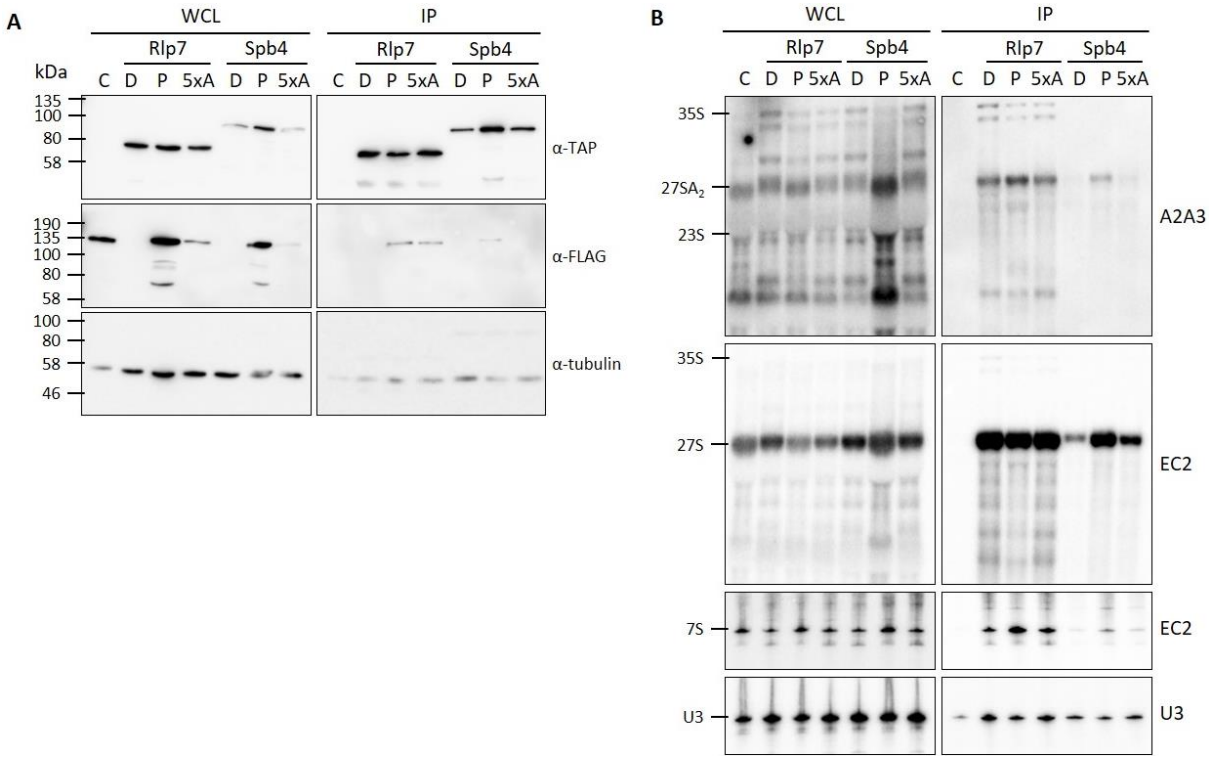

Figure 54: Influence of mutation of the Pol5-AIM domain on processing and association of pre-rRNAs to pre-60S particles.
(**A**) Non-tagged BY4741 strain as control C and strains containing TAP tag fused to Rlp7 and Spb4 were used for IgG-affinity purification in the absence of Pol5 (D), in the presence of Pol5 wildtype (P), and in the presence of the Pol5-AIM-5xAla mutant (5xA) (see Figure 50). 0.15% of whole cell lysates (WCL) and 10% of eluates (IP) were resolved in 10% SDS-PAGE followed by western blotting. Bait proteins were detected with an antibody against protein A present in the TAP tag. FLAG-tagged Pol5 in the wildtype and in the 5xAla mutant was detected with an antibody against FLAG as indicated. An antibody against tubulin was used as loading control. (**B**) Northern blot analyses of RNA samples obtained from whole cell lysates (WCL) and eluates (IP) were resolved on denaturing agarose or acrylamide gels and detected with radioactively labeled probes specified on the right side. Identified RNA species are indicated on the left side.

Western blotting showed similar levels of Rlp7 independently of Pol5, indicating its stable expression. In contrast, Spb4 was apparently destabilized in the absence of Pol5 and under expression of AIM-5xAla mutants. Since Pol5-AIM-5xAla mutant is present in lower amounts, this result might suggest that the absence of the AIM domain destabilizes Pol5, which in turn might cause the destabilization of Spb4 (Figure 54A). Interestingly, Rlp7 co-purified similar amounts of Pol5 wildtype and AIM-5xAla, while Spb4 co-purified with lower amounts of Pol5 wildtype and its association with AIM-5xAla was not detected (Figure 54A). These results suggest that the expression levels of AIM-5xAla mutant are enough to associate with Rlp7-containing particles as the wildtype Pol5. Nevertheless, the putative effect on the stability of Spb4 might be caused by alterations in the synthesis of

60S subunits, and therefore we cannot rule out other possibilities, which will be discussed later.
Northern blot analyses (Figure 54B) of RNAs present in whole cell lysates showed a decrease of 7S pre-rRNA levels upon depletion of Pol5 or expression of the AIM-5xAla mutant. In addition, the band corresponding to 27SB pre-rRNA was less diffuse upon depletion of Pol5 or expression of the AIM-5xAla mutant when compared to the wildtype situation. Altogether, the results suggest an impaired production of 60S and the stabilization of 27SB pre-rRNA.
Northern blot analysis of affinity purified samples (Figure 54B) showed that Rlp7 was associated with 27SB and 7S pre-rRNAs in the presence of Pol5 wildtype. The absence of Pol5 or expression of the AIM-5xAla mutant did not affect the association of Rlp7 with 27SB pre-rRNA but led to reduced amounts of co-purified 7S pre-rRNA. The latter was probably due to reduced production of 7S pre-rRNA, which was decreased in the absence of Pol5. In agreement with our previous observations (see Figure 43), affinity purification of Rlp7 enriched 35S pre-rRNA and U3 snoRNA amounts either after Pol5 depletion or expression of the AIM-5xAla mutant.
In the case of Spb4, it exclusively co-purified 27SB pre-rRNA and it did not interact with 7S pre-rRNA (Figure 54B). As expected, we observed a high amount of 27SB pre-rRNA in the presence of the Pol5 wildtype, comparable to the one in the Rlp7 purification. In contrast, very low amounts were enriched in the absence of Pol5. Despite the reduced levels of 27S pre-rRNA enriched with Spb4 in the presence of the AIM-5xAla mutant, they should not be neglected because the Spb4 purification was not as efficient as in the presence of Pol5 wildtype.
Altogether, the results suggest that mutation of the AIM domain might trigger instability of Pol5. Although mutations in the AIM domain might cause impaired synthesis of the 25S rRNA, it does not seem to be related to the recruitment of Spb4.

2.4.3 Heterologous expression of NTD and CTD in *E. coli*

To investigate in more detail the potential association between NTD and CTD of Pol5 revealed by our *trans*-complementation assay *in vivo*, we performed the heterologous expression and purification of Pol5 and both protein domains from *E. coli* cells. In the future, efficient purification of the domains from *E. coli* cells might also allow high-resolution structural analysis.
Sequences encoding the fragment genes *pol5-ΔN677* (CTD) and *pol5-Δ679L* (NTD) were cloned in IPTG-inducible expression vectors and flanked at N- and C-termini by FLAG and HIS-tag coding sequences, respectively. C-terminally fused HIS tag was used for affinity purification with Ni-NTA agarose beads (see 4.2.1.7). To characterize the purification process, several fractions collected during the experiment were analyzed by western blotting and Coomassie staining (see 4.2.5) (Figure 55A to 55D).
To achieve efficient expression and purification of Pol5 domains as presented below, several conditions were tested at critical steps of the process. To optimize the expression process, several IPTG concentrations (between 0.05 and 0.5 M) for induction, different

time periods (between two and 18 hours), and temperatures (between 16°C and 37°C) for overexpression were tested. The most efficient expression was obtained by inducing the cells with 0.1 M IPTG and culturing for six hours at 24°C (see 4.2.1.6). To lyse the cells, sonication, as well as Precellys and vortexer in the presence of Zirconia-Silicate beads were tested. Best results with highest protein concentrations in the soluble fraction were obtained with vortexer and Zirconia-Silicate beads as described in detail in section 4.2.1.7. Moreover, different buffers were tried for cell lysis, purification, washing, and elution. The presented results were obtained using 20 mM sodium phosphate buffer (pH 7.8), 500 mM NaCl, and 20 mM imidazole for cell lysis and binding on Ni-NTA beads. Washing steps were performed with the same buffer containing 60 mM imidazole, and elution was more efficient with the same buffer but containing 250 mM imidazole (see also Table 9).

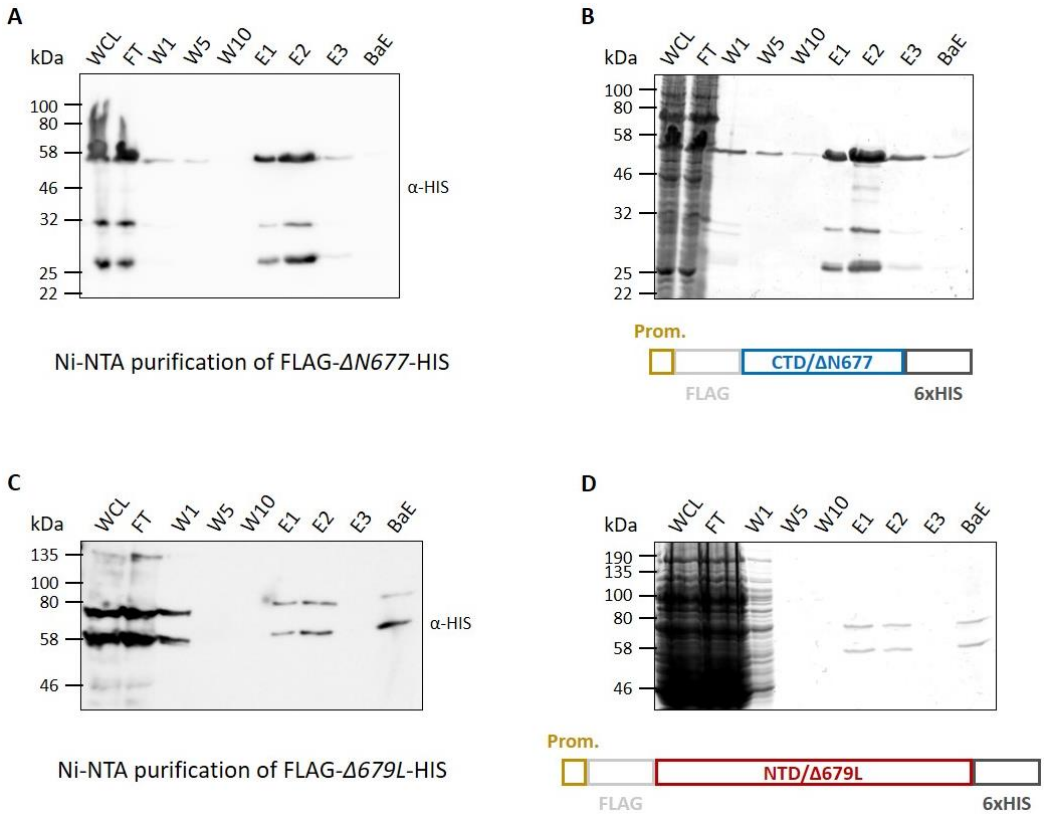

Figure 55: Recombinant purification of the CTD and NTD of Pol5 from *E. coli*.
(**A, B**) As indicated below on the left, the FLAG- and HIS-tagged CTD of Pol5 (referred to as ΔN677 or CTD) expressed in *E. coli* was purified with Ni-NTA coated agarose beads. Below on the right, blue bar depicts CTD with color-coded promoter (Prom.), FLAG tag, and HIS tag. 0.05% of whole cell lysates (WCL) and flow-through fractions (FT), 0.2% of wash steps (W1, W5, W10), and 2% (panel A) or 3% (panel B) of eluates and bead fractions (E1, E2, E3, BaE) were resolved on 10% SDS-PAGEs. Protein detection was performed using western blotting and an antibody against HIS (A) or Coomassie staining (B). (**C, D**) As indicated below on the left, the FLAG- and HIS-tagged NTD of Pol5 (referred to as Δ679L or NTD) expressed in *E. coli* was purified with Ni-NTA coated agarose beads. Below on the right, red bar depicts NTD with color-coded promoter (Prom.), FLAG tag, and HIS tag. For western blotting and detection with antibody against HIS (panel C), 0.1% of whole cell lysates (WCL) and flow-through fraction (FT), 0.2% of wash steps (W1, W5, W10), and 2% of eluates and bead fractions (E1, E2, E3, BaE) were resolved on 8% SDS-PAGE. For Coomassie staining (panel D), 0.2% of whole cell lysates (WCL), flow-through fraction (FT), and wash steps (W1, W5, W10), 6% of eluates 1 (E1), and 3% of remaining eluates and bead fractions (E2, E3, BaE) were resolved on 8% SDS-PAGE.

Regarding the purification of ΔN677, both western blot analysis with an antibody against HIS (Figure 55A) and Coomassie staining (Figure 55B) showed that very high amounts of the protein migrating at 55 kDa were expressed (see WCL) and purified (see E1 and E2). The smaller bands between 22 and 32 kDa likely resulted from C-terminal degradation during expression.
In contrast, the expression of the Δ679L polypeptide, with a molecular weight around 78 kDa, was less efficient in *E. coli* (see WCL). Moreover, the NTD was less stably bound to the beads than the CTD because high amounts of protein were detected in the first wash fraction (see W1). Unexpectedly, elution of this polypeptide was consistently less efficient compared to the CTD since comparatively high amounts of protein were retained on the beads (see E1, E2, and BaE). In addition, we observed a smaller band in all relevant fractions, which might correspond to a stable degradation product of Pol5-NTD from its N-terminus.

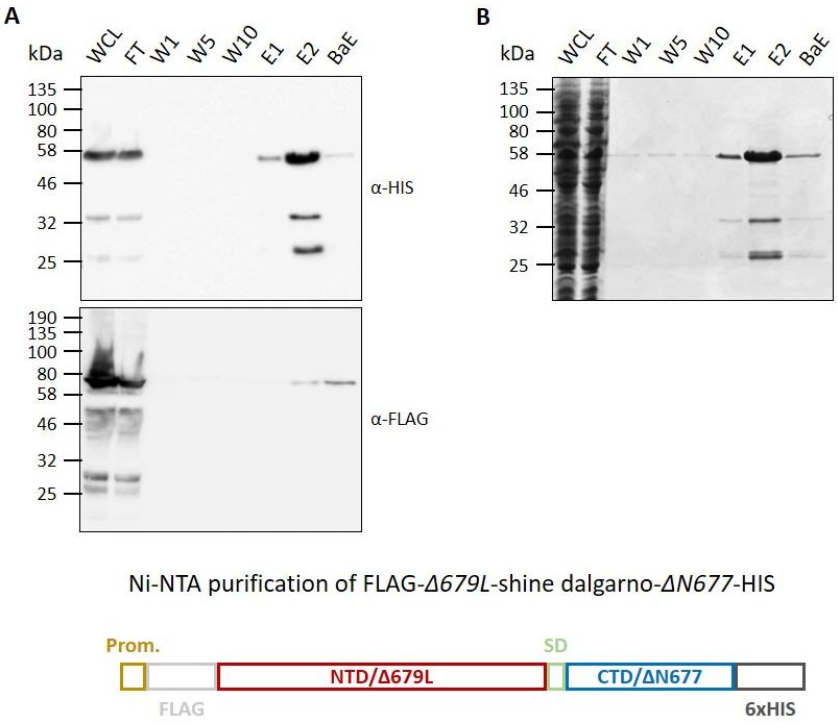

Figure 56: Recombinant co-purification of the NTD with the CTD of Pol5 from *E. coli*.
Below, colored bar depicts NTD of Pol5 (referred to as Δ679L or NTD; red) fused to FLAG tag at N-terminus and CTD of Pol5 (referred to as ΔN677 or CTD; blue) fused to HIS tag at C-terminus. Domains are separated by shine-dalgarno sequence (SD; mint) and under control of the same promoter (Prom.; ocher). After expression in *E. coli*, domains were co-purified with Ni-NTA coated agarose beads. (**A**) For western blotting, 0.08% of whole cell lysate (WCL) and flow-through fraction (FT), 0.2% of wash steps (W1, W5, W10), and 2% of eluates and bead fractions (E1, E2, BaE) were resolved on 10% SDS-PAGE. The bait CTD-HIS (above) was detected with antibody against HIS and the co-purified FLAG-NTD (below) with antibody against FLAG. (**B**) For Coomassie staining, 0.08% of whole cell lysate (WCL) and flow-through fraction (FT), 0.2% of wash steps (W1, W5, W10), and 3% of eluates and bead fractions (E1, E2, BaE) were resolved on 10% SDS-PAGE.

Since NTD and CTD of Pol5 expressed *in trans* restored wildtype growth of yeast cells (see Figure 51B), we cannot exclude that both domains interact with each other. To investigate this possible interaction, we cloned the sequences encoding both domains containing

their own stop codons in a single IPTG-inducible vector but separated by a shine-dalgarno sequence.
In addition, the NTD was fused to a FLAG tag at its N-terminus and the CTD fused to a HIS tag at its C-terminus (Figure 56). We affinity purified the Pol5-ΔN677 (or CTD) with Ni-NTA agarose beads and the fractions collected during the purification process were analyzed by western blotting (Figure 56A) and Coomassie staining (Figure 56B) (see 4.2.1.7 and 4.2.5). For purifications of single Pol5 domains from *E. coli*, we used a buffer with high sodium chloride concentration and without magnesium as indicated above. In order to do not disturb the association of both domains, we used buffer conditions based on the yeast affinity purification protocols (see also Table 9).
Western blot analysis with both antibodies (Figure 56A) revealed high amounts of co-expressed NTD and CTD (see WCL). The purification and elution of the CTD worked as efficiently (see E1, E2, and BaE with anti-HIS) as previously observed for the purification of the single domains (Figure 55). This result indicates that the new buffer conditions had no negative influence on the purification process. In addition, we could detect the NTD with anti-FLAG, in the elution fractions (see E2) and a few of it was retained in the bead fraction (see BaE). This result indicates a possible association of both domains, which might explain the rescue of cell growth in yeast depleted of Pol5 when expressed *in trans*. Since the antibodies against FLAG and HIS do not display the same sensitivity in western blot detection, no conclusion about a stoichiometric co-purification of the two domains is feasible. To have an idea about the stoichiometry of the interaction, the different fractions obtained from the purification process were also analyzed by Coomassie staining (Figure 56B). Unfortunately, we could not observe any band around 80 kDa, which may correspond to the NTD in the eluates or bead fraction (see E1, E2, and BaE). This result indicates the existence of a very small population of CTD associated with the NTD at least *in vitro*. In addition, the result reflects a much higher sensitivity of the anti-FLAG antibody, which could magnify the expression level of the NTD.

3. Discussion

3.1 Method achievement: 4tU-pulse labeling in *S. cerevisiae*

The prototrophy or auxotrophy of yeast cells regarding uracil is not only used in cloning procedures but constitutes also the background for metabolic labeling of RNA. Yeast cells, prototrophic for uracil can synthesize uridine-mono-phosphate (UMP) from carbamoyl phosphoric acid and aspartic acid (Lacroute, 1968). The existence of a salvage pathway allows yeast cells also to reuse pyrimidines, which are produced during nucleotide turnover (Kern et al., 1990, 1991). Moreover, all cells possess two different permeases enabling the uptake of extracellular uracil, uridine (Grenson, 1969), and their derivatives. The possibility to use the uracil/uridine uptake system for metabolic labeling of newly synthesized RNA in yeast cells was discovered early by providing radioactively marked uracil or uridine molecules in the culture medium (Trapman and Planta, 1975). This approach is still used as the gold standard method for pulse and pulse-chase labeling of RNA. For pulse labeling, we provide a labeled compound, e. g. radioactively marked uracil, for a defined time span in the medium, which is ingested by the yeast cells and incorporated in newly synthesized RNA molecules. Thus, the subsequent RNA analysis allows to differentiate between newly synthesized and previously present RNAs (see Figure 37B). For pulse-chase labeling, after the labeling step (pulse), cells are chased by cultivation in cold medium, which does not contain the radioactive compound but an excess of non-radioactive homolog. The incorporation of the non-labeled compound into the newly synthesized RNA enables to specifically track the processing events occurring at previously labeled RNA. Therefore, these analyses allow to differentiate, for instance, between accumulation, degradation or processing of the labeled RNA (see Figure 37A). Interestingly, the potential of non-radioactive uracil- and uridine-derivatives for metabolic labeling was also established early (Melvin et al., 1978), but their application did not become attractive before the development of high-resolution techniques for the visualization of labeled RNA (Duffy et al., 2015, 2019; Herzog et al., 2017; Muthmann et al., 2020).

Based on a protocol established in our institute for the metabolic RNA labeling in Archaea (Knüppel et al., 2017), we adapted a method for pulse labeling of yeast cells using 4-thio Uracil (4tU) (as described in detail in sections 4.2.2.11, 4.2.4.2, and 4.2.4.7). The described method has high potential to be developed further to 4tU pulse-chase labeling in yeast cells. Nevertheless, in our experimental conditions we could not reduce the intracellular pool of 4tU in order to perform the chase step (data not shown). In yeast cells, high amounts of free uracil/uridine obtained either from the salvage pathway or from an exogenous source lead to inhibition of the uracil/uridine permease required for the uptake of the molecules from the cell culture. This negative feedback should preclude the excess accumulation of free uracil/uridine in the cells (Grenson, 1969; Séron et al., 1999). Transferred to the experiment, high amounts of extracellular 4tU provided for a long time can easily accumulate within the cells and lead to the inhibition of the respective

permeases. Thus, inhibition of permeases might counteract the uptake of non-labeled uracil and delay or even inhibit the chase. Based on literature, we suggest a reduction of the pulse time (20 minutes) and of the 4tU concentration (200 µM) to achieve efficient chase with non-labeled uracil. Moreover, preliminary experiments indicated that pulse experiments might also be performed at much lower concentrations of 4tU.

3.2 The role of Pol5 in ribosome biogenesis

3.2.1 Depletion analysis

Pol5 was first described as a **fifth** essential **pol**ymerase in *S. cerevisiae*, corresponding to the B-type DNA polymerases (Shimizu et al., 2002). Nevertheless, the eponymous B-type like DNA polymerase domain turned out to be not essential for the function of Pol5 *in vivo* (Shimizu et al., 2002). In contrast, Pol5 and its human functional ortholog, MybBP1A, localize in the nucleolus and they are supposed to influence the synthesis of ribosomes (Hochstatter et al., 2012; Shimizu et al., 2002). Even though Pol5 was identified as part of the UTP-A complex (Krogan et al., 2004), the role of Pol5 in ribosome biogenesis was only poorly understood so far.

Based on the previous description, we aimed to characterize the role of Pol5 in ribosome biogenesis in the eukaryotic model organism *S. cerevisiae*. Since *POL5* is an essential gene, we constructed a yeast strain allowing the conditional depletion of Pol5 (as described in section 2.2.2.1). Although depletion analyses are very helpful to study the function of proteins encoded by essential genes, removing an essential component of a fundamental process in living organisms, like ribosome biogenesis, can produce unspecific side effects. Moreover, yeast physiology and, therefore, ribosome synthesis is highly dependent on the carbon source present in the culture medium (Kos-Braun et al., 2017).

In order to minimize the differences in cell growth due to different carbon sources, we first created a depletion system based on two plasmids. This system enabled us to compare depletion and expression of a wildtype allele using the same media (see 2.2.2.1). To avoid analyzing the side effects instead of the direct consequences caused by depletion of Pol5, we first determined the depletion time for Pol5 causing the primary effects in ribosome biogenesis. According to our data, we were not able to detect Pol5 after six hours of depletion, but cells were able to grow comparably to the wildtype during the first nine hours of Pol5 depletion (see Figure 36). Accordingly, we did not observe any effect on ribosome synthesis at six hours of Pol5 depletion (see Figure 38). In contrast, depletion of Pol5 for 16 hours was already long enough to cause accumulative defects in ribosome biogenesis, which very likely led to a stop of protein synthesis and cell growth (see Figure 38).

The earlier occurring primary effects of Pol5 depletion, determined by radioactive pulse-chase and non-radioactive pulse labeling as well as steady state rRNA analysis, suggested cleavage defects at the A0, A1, A2, and C2 pre-rRNA processing sites. Cleavages at A0, A1, and A2 sites are likely delayed, because 35S pre-rRNA levels were increased during the

metabolic labeling (see Figure 37B) but not accumulated during the chase (see Figure 37A). Even though no 20S pre-rRNA could be detected at short depletion times, the levels of 18S rRNA were affected later (see Figure 37 and Figure 38). Our observations indicate preference of the A3 site as the initial processing step to produce 23S and 27SA3 pre-rRNAs, both representing processable intermediates (Boissier et al., 2017; Talkish et al., 2016; Woolford and Baserga, 2013). Since cleavage at the A3 site occurs after processing of the 3'ETS (Allmang and Tollervey, 1998), the absence of Pol5 forces the post-transcriptional processing of pre-rRNA. A clear landmark for the absence of SSU-processome AFs (Barandun et al., 2018; Fernández-Pevida et al., 2015; Klinge and Woolford, 2019), which will be discussed in detail later (see 3.5).
Concomitant with the loss of A2 cleavage, we observed a clear processing defect at the C2 site, which abrogated the synthesis of 7S pre-rRNA, caused the accumulation of 27SB pre-rRNA species and the strong depletion of mature 5.8S and 25S rRNAs (see Figure 38). Accordingly, our polysome profiles also indicated a higher impact on the synthesis of the large subunit (see Figure 39) in good agreement with a recent publication (Ramos-Sáenz et al., 2019). Although the contact sites of Pol5 at the pre-rRNA (see Figure 34) are comparable with the contacts established by several "A3 factors" (Granneman et al., 2011), the phenotypes observed under Pol5 depletion suggest a later function of Pol5. In addition, Pol5 associates primary with 27SB pre-rRNA (see Figure 33) and therefore, we suggest that Pol5 belongs to the family of "B factors" (Talkish et al., 2012).

3.2.2 Domain characterization

Based on our data, we assume that Pol5 might fulfill a dual role in the assembly of both ribosomal subunits. So far, only three AFs are known to be involved in the assembly of both ribosomal subunits: the helicases Has1 (Dembowski et al., 2013a; Liang and Fournier, 2006) and Prp43 (Bohnsack et al., 2009; Combs et al., 2006; Pertschy et al., 2009) and the AF Rrp5 (Venema and Tollervey, 1996). Regarding Rrp5, different functions have been assigned for the NTD and the CTD in the assembly of the large and the small subunit, respectively. Moreover, expression of both domains *in trans* restores the function of a *RRP5* functional allele (Eppens et al., 1999; Lebaron et al., 2013).
We could show that expression of the NTD and CTD of Pol5 *in trans* also supported cell growth in yeast cells (see Figure 51). Nevertheless, the presence of an overlapping region of 19 amino acids was enough to disrupt the complementation (see Figure 51). We consider it very likely, that both domains of Pol5 interact physically to rebuild a Pol5 wildtype protein. In agreement with this result, N-terminal shortening of the CTD does not further complement *in trans*, even though this region is not required for the essential function of Pol5 (see Figure 49 and Figure 51). A similar physical interaction was observed in the case of the UTP-B component Utp1 (Boissier et al., 2017). The separate expression of the tWD domain and the CTD of Utp1 allowed the reconstruction of the wildtype protein and its incorporation into a functional UTP-B complex and formation of the SSU processome (Boissier et al., 2017). Thus, the physical reconstitution of proteins from the individual expression of their domains might be a common feature in the *trans*-

complementation assays. This intriguing hypothesis would allow the separation of protein domains without loss-of-function, thereby indicating an evolutive origin of protein complex formations. Nevertheless, the separation of Pol5 functions and domains using the example of Rrp5 is challenging (Eppens et al., 1999). *In vitro* and *in vivo* data on the expression of both domains suggest a high stability and solubility of the CTD, whereas the NTD alone might be prone to precipitate *in vitro* and to be degraded *in vivo* (see Figure 51 and Figure 55). It is likely that the CTD is required to stabilize the full-length Pol5. In this context, further *in vivo* studies on the domains of Pol5 suggested a tendency of Pol5 to dimerize via the CTD in conditions of decelerated ribosome biogenesis induced by nutrient deficiency (data not shown), an aspect that should be further addressed in future works. Thus, drugs like rapamycin could be used to impair growth of the yeast cells (Loewith and Hall, 2011; Powers and Walter, 1999) and to analyze if the dimerization tendency of Pol5 increases upon treatment with these drugs. This experimental setup might also help to clarify if Pol5 dimerization is a cause or an effect of the reduced synthesis of ribosomes. Moreover, since the last α-helix of Pol5 does not fulfill an essential role for yeast growth (see Figure 49), it might be interesting to further analyze if this region is involved in dimerization.

Interestingly, inhibition of ribosome synthesis in human cells impacts the human ortholog of Pol5, MybBP1A, by inducing the truncation of the C-terminus of MybBP1A by proteolytic cleavage (Yamauchi et al., 2008). The truncated versions are transported to the nucleoplasm because the removed C-terminal part includes the nucleolar localization signal (Yamauchi et al., 2008). In yeast cells, Pol5 dimerization might block the activity of Pol5, inhibiting formation of both ribosomal subunits without impairing RNA Pol I occupancy. It would be intriguing to know if Pol5 dimerization also induces delocalization of the protein and to decipher the mechanisms inducing Pol5 dimerization. Interestingly, this kind of mechanism would be highly reversible, allowing a fast resume of growth in case growth conditions ameliorate.

3.2.3 Looking for UTP-A

Our experimental approaches did not allow us to purify the Pol5-containing UTP-A complex as identified once by the Greenblatt-group (Krogan et al., 2004). Since the experimental conditions were not clearly described, the discrepancies might be due to unknown technical differences in the experimental setup.

Two main differences caught our attention:

First, in our experiments, only a minor portion of the 5'ETS is observed in the affinity purifications of tUTP components under active ribosome synthesis (see Figure 44). A result that might be indicative of a fast recycling process. In contrast, the higher presence of fragments corresponding to 5'ETS in the purifications performed by the group of Greenblatt suggests a higher recovery of disassembling complexes. Accordingly, we mainly detected Utp5-containing tUTP complexes in the soluble fraction, containing traces of some AFs of the SSU processome. We think, the SSU-processome AFs detected because of the high sensitivity of the MS analysis were part of disassembly complexes (see

Figure 29 and Figure 31). Since the slow-down of ribosome synthesis might be responsible for larger amount of disassembly complexes and synthesis of ribosomes is closely related to the environmental conditions (Kos-Braun et al., 2017), the discrepancies between both results might rely on different growth conditions for the cultivation of yeast cells.
Second, the presence of 25S but not 18S rRNA sequences in the UTP-A fractions, performed by Greenblatt's group, might also reflect an rRNA degradation problem during purification, which would raise the amount of free sub-complexes regardless of growth conditions.
In agreement with our results, a recent publication indicates a very mild association of Pol5 with tUTP components (Gallagher, 2019). Nevertheless, the author suggests that UTP-A might be a labile complex participating in the earliest steps of ribosome synthesis (Gallagher, 2019; Gallagher et al., 2004). However, this conclusion is not compatible with the late association of Pol5 with the pre-rRNA (Braun et al., 2020; Wery et al., 2009), unless Pol5 interacts twice with pre-ribosomal particles.
Since the absence of Pol5 does not impair the association of tUtps with the nascent transcript, we suggest that the UTP-A complex might be a labile disassembly product containing the 5'ETS, possibly hold up by the presence of RNA.

3.3 Pol5 participates in folding of 25S rRNA domain III

The qMS analysis of pre-ribosomal particles purified with Noc2 or Rlp7 in the absence of Pol5 showed a clear decrease of the RPs Rpl2, Rpl19, Rpl22, Rpl25, Rpl27, Rpl34 and Rpl43 (see Figure 40B). These RPs associate with the domains I and III of the 25S rRNA, clustering around the contact site of Pol5 in the domain III and building a rim around the PET when mapped onto the Ytm1-particle (Braun et al., 2020; Gamalinda et al., 2014; Kater et al., 2017; Wu et al., 2016). The incorporation of Rpl25 and processing of the ITS2 promotes the incorporation of five additional RPs Rpl2, Rpl19, Rpl31, Rpl39, and Rpl43 (Ohmayer et al., 2013). Thus, Rpl25 might connect formation of domain III with the cleavage at the C2 site in the ITS2 region (van Beekvelt et al., 2000; Biedka et al., 2017; Pöll et al., 2009). The failed recruitment of Rpl19 and Rpl25 might also depend on decreased levels of Ssf1 and Rrp15 in Rlp7-purified particles in the absence of Pol5 (see Figure 41A), since Ssf1-Rrp15 and Rrp14 are required for the association of Rpl19, Rpl25, and Rpl31 with pre-60S particles (Biedka et al., 2018).
Moreover, all results are consistent with the C2 processing phenotype observed in the absence of Pol5 (see Figure 38). In addition, our data indicate that Pol5 might establish contacts with the ITS2 region and two helices of domain III (see Figure 34). Since structure probing data and Cryo-EM structures suggest a spatial proximity between both regions (Kater et al., 2017; Pöll et al., 2017; Sanghai et al., 2018), we think that both contact sites of Pol5 constitute one putative binding site within the flexible domain III in pre-60S particles. Altogether, we suggest that Pol5 might play an important role for the recruitment of Rpl25 and for instance of other RPs involved in PET formation as major

constituents. In agreement, recent work from the group of Jesús de la Cruz indicates that the overexpression of Rpl25 and Rpl27 suppresses the thermo-sensitive phenotype of a *pol5* mutant (Ramos-Sáenz et al., 2019). We considered likely that both RPs are recruited during the compaction of domain III in the course of the maturation of intermediate pre-60S particles (intermediate particle in Sanghai et al. (2018) or transition from state C to state D in Kater et al. (2017)). In fact, the accumulation of Rpf1 and Rrp15 in the Noc2-purified particles might indicate the unfolding state of the PET in the absence of Pol5 and, therefore, the absence of the RPs at the rim around the PET (Biedka et al., 2018).
Furthermore, several AFs were depleted from pre-60S particles in the absence of Pol5. Among them, we identified Spb4, Arx1, and Nop53 (see Figure 41A).
In the late nuclear particle, Arx1 and Nop53 are bound close to Rpl25 and it is likely that their association is also hindered due to the failed recruitment of Rpl25 (Gamalinda et al., 2014; Ohmayer et al., 2013; Wu et al., 2016). In agreement with this hypothesis, the export factor Arx1 is bound by Rpl19, Rpl25, and Rpl31 prior to the export of the pre-60S particle from the nucleus and it is very likely that its binding assures the correct maturation of the PET before the particle can enter the cytoplasm (Bradatsch et al., 2012; Kater et al., 2017; Wu et al., 2016).
Pre-rRNA analysis on particles purified with Nop53 demonstrated that its association with 27SB and 7S pre-rRNAs is reduced in the absence of Pol5, corroborating our qMS data. The association of Nop53 at the ITS2 region requires the action of the ATPase Mdn1 to trigger the dissociation of Erb1 and Ytm1 (Bassler et al., 2010; Kater et al., 2017; Sanghai et al., 2018). Since Erb1 and Ytm1 are found to be enriched in the pre-60S particles purified with Rlp7 (see Figure 41A), the failed release of Ytm1 and Erb1 might also inhibit the rotation of Rlp7 toward the foot in the pre-ribosomal particles, which is a prerequisite for the association of Nop53. Since Nop53 might target the exosome to the ITS2 region (Cepeda et al., 2019; Falk et al., 2017; Thoms et al., 2015), coupling cleavage competence at the C2 site with recruitment of Nop53, might be an efficient mechanism for the use of limited resources.
Regarding Spb4, it contacts the ES27 in domain IV and H101 of domain VI of the 25S rRNA in middle and late pre-60S particles. These contact sites are “far away” from the putative binding site of Pol5 domain III (see Figure 41B) (Biedka et al., 2018; Brüning et al., 2018; Sanghai et al., 2018). Nevertheless, formation of the binding site of Spb4 might require compaction of domains IV and VI. Since the maturation of domain III occurs before domains IV and VI are compacted, it is likely that correct folding of domain III is strictly required to consolidate domains IV and VI, forming the interaction surface for Spb4.
Altogether, our data indicate that Pol5 participates in the early assembly of domain III, required for the recruitment of Rpl25 and Rpl27, which is the crucial step explaining all discussed effects of LSU assembly in the absence of Pol5.

3.4 Release of Noc2 from pre-60S particles might depend on Pol5

Our data indicate that Noc2 and Rlp7 associate independently of Pol5 with pre-ribosomes. However, Noc2 assembles prior to Pol5 with 27SA2 pre-rRNA and it is released, like Pol5, prior to C2 cleavage. In contrast, Rlp7 associates stronger with 27SB pre-rRNA, like Pol5, but it remains bound after C2 cleavage with 7S-containing particles (Babiano et al., 2013; Dunbar et al., 2000; Gadal et al., 2002; Hierlmeier et al., 2013; Milkereit et al., 2001). Previous studies reported that Noc2 associates together with Noc1/Mak21 to Rrp5-containing particles in nascent transcripts prior to A2 cleavage (Hierlmeier et al., 2013; Khoshnevis et al., 2019; Milkereit et al., 2001). In accordance, we observed co-purification of Noc2 with 35S and 33/32S pre-rRNAs, U3 snoRNA, and SSU-processome AFs (see Figure 33 and Figure 42). In addition, Noc2 also participates in the synthesis of 60S ribosomes by association with Noc3. However, it is unknown if association of Noc2 and Noc3 requires the release of Noc2-Noc1 from pre-ribosomal particles or if Noc2 remains on the particle and Noc1 is substituted by Noc3 (Milkereit et al., 2001).
Our data also support earlier assembly for Noc2 when compared to Pol5. In addition, since the effects in LSU synthesis caused by the absence of Pol5 are also observed in Noc2-containing particles, we would expect the presence of Pol5 in these particles. Surprisingly, Pol5 co-purifies with Rlp7 but not with Noc2 (see Figure 40A). This controverted result might be explained by the dissociation of the Noc2-Noc1-Rrp5 module after A3 cleavage (Hierlmeier et al., 2013). In this scenario, Pol5 might associate to support the assembly of domain III in pre-60S maturation before Noc2 regains association of pre-60S particles by binding to Noc3. A more likely situation, which does not exclude the previous one, might involve a Pol5 dependent release of Noc2 from Noc3-containing particles. In this regard, the absence of Pol5 might lead to the retention observed for Noc2 and Noc3 within the pre-60S particles purified with Rlp7 (see Figure 41A). The C2 cleavage within the ITS2 is supposed to be triggered by an active secondary structure rearrangement of the ITS2 (Côté et al., 2002; Peculis and Greer, 1998) from a “ring” (Joseph et al., 1999) to a “hairpin” (Yeh and Lee, 1990) structure or to a long helical conformation (Coleman, 2015; Pöll et al., 2017). This structure transition requires specific base pairing within the ITS2 and several “A3 factors” (at least Nop4, Nop15, and Cic1) (Côté et al., 2002; Granneman et al., 2011). As previously described, the absence of Pol5 might impair, directly or not, the structural change in the ITS2 required for efficient C2 cleavage. Therefore, we assume the inhibition of this structural rearrangement being the main cause for Noc2 retention.

3.5 Pol5 is required for the recycling of SSU-processome components

Several known AFs engaged in the “middle” steps of LSU maturation and required for C2 cleavage are supposed to have an additional effect in cleavages at A0, A1, and A2 (Gregory et al., 2019; Hong et al., 1997; Saveanu et al., 2003; Talkish et al., 2012; Zanchin et al., 1997). Regarding Pol5, our data provide evidence for its role as “B factor” and for an

additional role in SSU biogenesis. Besides the contact sites of Pol5 within the ITS2 and the domain III of 25S rRNA, an additional crosslinking region within the 5'ETS was observed (see Figure 34A). Mapping these crosslinks in available SSU-processome structures shows that the contact sites of Pol5 are surrounded by the tUTP components (see Figure 34B) (Braun et al., 2020; Chaker-Margot et al., 2017). This observation is also supported by the description of the Pol5-containing UTP-A complex done by the Greenblatt-group, which mostly co-purified 5'ETS fragments (Krogan et al., 2004). A recent publication, comparing the co-purification of Utp8 and Pol5 on short 5'ETS transcripts showed much higher levels of 5'ETS co-purified with Pol5 than with Utp8 (Gallagher, 2019). Nevertheless, we did not look for such interaction in our analyses, since our probes for the 5'ETS were located at the 3' end.

In the absence of Pol5, our data showed accumulation of purified tUtps with the 5'ETS fragment and several pre-rRNAs, either containing or not the 5'ETS (see Figure 44). This result is consistent with the accumulation of 5'ETS in the absence of Pol5 observed in the data of the Greenblatt-group (Krogan et al., 2004). Altogether, these findings indicate a role of Pol5 in the release of the tUtps from the 5'ETS during disassembly of the 5'ETS particle. Trapping the tUtps and other SSU factors within the 5'ETS particle and the SSU processome would lead to the strong reduction of available SSU AFs, which would induce a defect in the assembly of the SSU. In agreement, our data show an increase of 35S transcripts not associated with tUtps (see Figure 44). Interestingly, the association of tUtps with 5'ETS fragments is not detected when pre-rRNA is synthesized by RNA Pol II (Gallagher, 2019). We think it can be due to a slower production of pre-rRNAs, which are more efficiently processed and, therefore, the transcribed spacers will be more efficiently degraded.

The AIM domain in Pol5 seems to be required for the recycling of the tUtps. Since the exosome activity is involved in the degradation of the 5'ETS (Delan-Forino et al., 2017) and the AIM domain participates in the recruitment of the exosome (Thoms et al., 2015), it is very likely that release of tUtps from 5'ETS requires the action of the nuclear exosome. Consistent with this hypothesis, the truncated NTD, still containing the intact AIM domain, and the complete CTD still support recycling of tUtps although not cell growth (see Figure 52). In contrast, the only presence of the CTD is not enough to support recycling (see Figure 53). The higher stability of the CTD indicates formation of a stable folding, which might be required together with the AIM domain to induce the release of the AFs from the 5'ETS. Therefore, it is now important to determine the function of these Pol5 mutants in the assembly of the LSU. In summary, our model would support the existence of a transient Pol5-containing UTP-A complex associated to the 5'ETS. In this model, formation of UTP-A might be required for Pol5 to recruit the exosome in proximity of the 5'ETS, and most possibly the efficient degradation of the 5'ETS by the exosome recycles the tUtps. Therefore, it will be interesting to investigate if Pol5 is involved in the recruitment of exosome to 5'ETS-containing particles. Moreover, the same approach might be also relevant to look if Pol5 participates in the recruitment of the exosome to degrade the ITS2 region. As an alternative, other proteins as Utp18 and Nop53 might target the exosome to pre-ribosomal particles (Thoms et al., 2015).

tUtps, the primary binders of the pre-rRNA transcripts, stabilize the nascent transcripts by blocking the accessibility of exonucleases (Gallagher et al., 2004; Jakob et al., 2012; Pérez-Fernández et al., 2007; Wery et al., 2009). The depletion of Pol5 led to an accumulation of the 35S pre-rRNA, but the relative 35S levels associated with tUtps were lower (see Figure 44). It is likely that several 35S transcripts are stabilized even if they are not associated with tUtps. This striking result contrasts with the protective role suggested for tUtps (Wery et al., 2009) and it might indicate toward a functional role during RNA Pol I driven transcription. Interestingly, upon prolonged depletion of Pol5, we observed a decrease of RNA Pol I occupancy at the rDNA promoter region (see Figure 46). This effect might be caused by the absence of Pol5 or the reduced pool of tUtps, which are required for efficient rDNA transcription by RNA Pol I (Gallagher, 2019; Gallagher et al., 2004; Schmid, Master thesis, 2019).

Moreover, the absence of Pol5 at the 5'ETS might also influence the cleavage at site D, since a processing intermediate (22S') could be detected reaching from 5'ETS to site D or an alternative site close to D (see Figure 44). Usually, cleavage at site D is performed by Nob1 in the cytoplasm as one of the last steps of SSU maturation (Fatica et al., 2003, 2004; Turowski et al., 2014). On one hand, this could mean that an immature pre-rRNA has been exported to the cytoplasm, but it involves the bypassing of several quality control steps rendering this scenario very unlikely (Lebaron et al., 2012; Parker et al., 2019; Strunk et al., 2012). On the other hand, the pre-rRNA might have been cleaved in the nucleus by the already associated endonuclease Nob1. Although Nob1 should be kept inactive until required in the cytoplasm (Lamanna and Karbstein, 2009, 2011; Lebaron et al., 2012; Strunk et al., 2012), studies on the endonuclease Utp24 indicated alternative cleavage events when pre-ribosomal particles are accumulated (Choque et al., 2018). This scenario would imply a leaky inhibition of Nob1 in the nucleolus when the 5'ETS particle and maybe also other SSU-processome components are not released from the pre-40S particle. In agreement with our results, the absence of Rps27 also correlates with an anomalous cleavage around D site when A2 cleavage is delayed (Ferreira-Cerca et al., 2005).

Altogether, our data suggest a dual role of Pol5 in ribosome assembly. Pol5 is required for the assembly of domain III and the PET within the large ribosomal subunit and for the recycling of the tUtps from the SSU processome. Moreover, the AIM domain of Pol5 might play a role in recruiting the exosome to the 5'ETS region. We propose that Pol5 might act as a sensor for the communication between both assembly processes. Since 18S rRNA will be synthesized independently of 25S rRNA, processivity of RNA Pol I below 100% efficiency might cause an overaccumulation of 40S subunits, which would disrupt protein homeostasis. Therefore, this control mechanism might be raised to fine tune processivity defects of RNA Pol I to assure the stoichiometric production of both ribosomal subunits.

4. Material & Methods

4.1 Material

4.1.1 Host bacteria

The electro-competent *E. coli* strain "XL1BlueMRF" (Stratagene) was used for cloning.
Genotype: *endA1 gyrA96(nalR) thi-1 recA1 relA1 lac glnV44 F' [::Tn10 proAB+ lacIq Δ(lacZ)M15] hsdR17(rK- mK+)*
The chemo-competent *E. coli* strain "Rosetta Star" was used for heterologous expression.
Genotype: *F- ompT hsdSB(RB- mB-) gal dcm λ(DE3 [lacI lacUV5-T7 gene 1 ind1 sam7 nin5]) pLysSRARE (CamR)*

4.1.2 Yeast strains

#	Name	Genotype	Origin
#206	BY4741	MATa; *his3-1*; *leu2-0*; *met15-0*; *ura3-0*	Biochemistry III
#1879	BY4742 NOC2-TAP	MATalpha; *his3-1*; *leu2-0*; *ura3-0*; *lys2-0*; *YOR206W*-TAP-*URA3*	Biochemistry III
#1907	BY4742 UTP4-TAP	MATalpha; *his3-1*; *leu2-0*; *ura3-0*; *lys2-0*; *UTP4*-TAP-*URA3*	Biochemistry III
#2423	BY4741 A135-TEV-ProtA	MATa; *his3-1*; *leu2-0*; *met15-0*; *ura3-0*; *RPA135*-TEV-ProtA::kanMX6	Biochemistry III
#3197	YJPF195-1a	MATa; *his3-1*; *leu2-0*; *met15-0*; *ura3-0*; *POL5*-TAP-*URA3*	Biochemistry III
#3236	YMH1-1a	MATalpha; *his3-1*; *leu2-0*; *ura3-0*; *lys2-0*; *NAN1*-TAP-*URA3*	Biochemistry III
Y281	YMH5-1a	MATa; *his3-1*; *leu2-0*; *met15-0*; *ura3-0*; KANMX::*GAL*::HA-*POL5*	Biochemistry III
Y283	YMH6-1a	MATa; *his3-1*; *leu2-0*; *met15-0*; *ura3-0*; KANMX::*GAL*::HA-*POL5*; *UTP4*-TAP::*URA3*	Biochemistry III
Y356	YCMS6-1a	MATa; *his3-1*; *leu2-0*; *met15-0*; *ura3-0*; KANMX::*GAL*::HA-*POL5; RPA135*-TAP::*URA3*	This study
Y357	YCMS7-1a	MATa; *his3-1*; *leu2-0*; *met15-0*; *ura3-0*; KANMX::*GAL*::HA-*POL5*; *UTP5*-TAP::*URA3*	This study
Y360	YCMS10-1a	MATa; *his3-1*; *leu2-0*; *met15-0*; *ura3-0*; *UTP5*-TAP::*URA3*	This study
Y372	YCMS15-1a	MATa; *his3-1*; *leu2-0*; *met15-0*; *ura3-0*; KANMX::*GAL*::HA-*POL5*; *NOP53*-TAP::*URA3*	This study
Y373	YCMS16-1a	MATa; *his3-1*; *leu2-0*; *met15-0*; *ura3-0*; KANMX::*GAL*::HA-*POL5*; *NOC2*-TAP::*URA3*	This study
Y377	YCMS20-1a	MATa; *his3-1*; *leu2-0*; *met15-0*; *ura3-0*; KANMX::*GAL*::HA-*POL5*; *UTP8*-TAP::*URA3*	This study
Y379	YCMS22-1a	MATa; *his3-1*; *leu2-0*; *met15-0*; *ura3-0*; *UTP10*-TAP::*URA3*	This study
Y380	YCMS23-1a	MATa; *his3-1*; *leu2-0*; *met15-0*; *ura3-0*; KANMX::*GAL*::HA-*POL5*; *UTP10*-TAP::*URA3*	This study
Y383	YCMS24-1a	MATa; *his3-1*; *leu2-0*; *met15-0*; *ura3-0*; *RLP7*-TAP::*URA3*	This study
Y384	YCMS25-1a	MATa; *his3-1*; *leu2-0*; *met15-0*; *ura3-0*; KANMX::*GAL*::HA-*POL5*; *RLP7*-TAP::*URA3*	This study

#	Name	Genotype	Origin
Y390	YCMS27-1a	MATa; *his3-1*; *leu2-0*; *met15-0*; *ura3-0*; KANMX::*GAL*::HA-*POL5*; *SPB4*-TAP::*URA3*	This study

Table 1: Yeast strains used in this study.
Yeast strains marked with "#" belong to the department of Biochemistry III at the University of Regensburg. Yeast strains marked with "Y" belong to the collection of the UTP lab.

4.1.3 Plasmids

#	Name	Gene	Marker	Origin	Cloning procedure
K1	pBS	empty backbone plasmid	Amp	Biochemistry III	
K97	pBS1539	TAP::URA3	Amp/URA3	CellZome	Puig et al. (2001)
K375	pT11	rDNA	Amp	Biochemistry III	
K1224	pYM15	TAP::KANMX	Amp	Biochemistry III	Janke et al. (2004)
K1837	pCM182-LEU2	empty backbone plasmid	Amp/LEU2	Biochemistry III	LEU2 marker replaces TRP1 in pCM182 (Bellí et al., 1998; Garí et al., 1997)
p96	pYM15-TAP-URA	TAP::URA3 with S2-S3 primer	Amp	This study	TAP cassette from pBS1539 was inserted in pYM15 using oligonucleotides #3883 and #3884
p199	ptCMS1	*POL5*, tetOFF	Amp/LEU2	This study	PCR product obtained with oligonucleotides o86-o87 ligated into pCM182-LEU2 digested with BamHI-NotI
p201	pCMS16	*POL5*	Amp	This study	[BamHI-NotI]-fragment from ptCMS1 subcloned in pBS
p202	ptDLS5	FLAG-*RPA12DE*, tetOFF	Amp/LEU2	Dominik Strobel	pCM182-LEU2 plasmid containing FLAG epitope
p203	ptCMS2	FLAG-*POL5*, tetOFF	Amp/LEU2	This study	[BamHI-NotI]-fragment from ptCMS1 subcloned in ptDLS5
p229	pCMS19	*pol5-DCt120*; new name: *pol5-D902P*	Amp	This study	PCR product obtained with oligonucleotides o131-o132 cloned in pCMS16 using AQUA cloning protocol
p230	pCMS20	*pol5-DCt252*; new name: *pol5-D770P*	Amp	This study	PCR product obtained with oligonucleotides o131-o133 cloned in pCMS16 using AQUA cloning protocol
p231	pCMS21	*pol5-DCt343*; new name: *pol5-D679L*	Amp	This study	PCR product obtained with oligonucleotides o131-o134 cloned in pCMS16 using AQUA cloning protocol

#	Name	Gene	Marker	Origin	Cloning procedure
p232	pCMS22	*pol5-DNt137*; new name: *pol5-DN137*	Amp	This study	PCR product obtained with oligonucleotides o135-o138 cloned in pCMS16 using AQUA cloning protocol
p233	pCMS23	*pol5-DNt296;* new name: *pol5-DN296*	Amp	This study	PCR product obtained with oligonucleotides o136-o138 cloned in pCMS16 using AQUA cloning protocol
p234	pCMS24	*pol5-DNt658*; new name: *pol5-DN658*	Amp	This study	PCR product obtained with oligonucleotides o137-o138 cloned in pCMS16 using AQUA cloning protocol
p239	ptCMS7	FLAG-*pol5-DCt120*, tetOFF; new name: FLAG-*pol5-D902P*	Amp/LEU2	This study	[BamHI-NotI]-fragment from pCMS19 subcloned in ptCMS2
p240	ptCMS8	FLAG-*pol5-DCt252*, tetOFF; new name: FLAG-*pol5-D770P*	Amp/LEU2	This study	[BamHI-NotI]-fragment from pCMS20 subcloned in ptCMS2
p241	ptCMS9	FLAG-*pol5-DCt343*, tetOFF; new name: FLAG-*pol5-D679L*	Amp/LEU2	This study	[BamHI-NotI]-fragment from pCMS21 subcloned in ptCMS2
p242	ptCMS10	FLAG-*pol5-DNt137*, tetOFF; new name: FLAG-*pol5-DN137*	Amp/LEU2	This study	[BamHI-NotI]-fragment from pCMS22 subcloned in ptCMS2
p243	ptCMS11	FLAG-*pol5-DNt296*, tetOFF; new name: FLAG-*pol5-DN296*	Amp/LEU2	This study	[BamHI-NotI]-fragment from pCMS23 subcloned in ptCMS2
p244	ptCMS12	FLAG-*pol5-DNt658*, tetOFF; new name: FLAG-*pol5-DN658*	Amp/LEU2	This study	[BamHI-NotI]-fragment from pCMS24 subcloned in ptCMS2
p262	ptAMW3	FLAG-*pol5-DCt30*, tetOFF; new name: FLAG-*pol5-D993W*	Amp/LEU2	Anna Weigert	
p266	pgCMS1	*POL5*	Amp/URA3	Jorge Perez-Fernandez	
p267	pgCMS2	GFP-*pol5-DCt343*; new name: GFP-*pol5-D679L*	Amp/URA3	Jorge Perez-Fernandez	

#	Name	Gene	Marker	Origin	Cloning procedure
p268	pgCMS3	GFP-*pol5-DNt658*; new name: GFP-*pol5-DN658*	Amp/URA3	Jorge Perez-Fernandez	
p269	pgCMS4	GFP-*pol5-DNt678*; new name: GFP-*pol5-DN677*	Amp/URA3	Jorge Perez-Fernandez	
p274	pExJPF4	FLAG-*POL5-shine*-HIS	Kan	Jorge Perez-Fernandez	
p279	pExJPF4-CTD	FLAG-*pol5-CTD*-HIS	Kan	This study	[NdeI]-fragment from pExJPF4 ligated to pExJPF4-CTD
p282	pExJPF4-NTD	FLAG-*pol5-NTD*-HIS	Kan	This study	[Xho]-fragment from pExJPF4 ligated to pExJPF4-NTD
p283	ptCMS15	FLAG-*pol5-DNt678*, tetOFF; new name: FLAG-*pol5-DN677*	Amp/LEU2	This study	[BamHI-NotI]-fragment from pgCMS4 subcloned in ptCMS2
p286	ptJPF3	FLAG-*pol5-DCt70*, tetOFF; new name: FLAG-*pol5-D952A*	Amp/LEU2	Jorge Perez-Fernandez	
p287	ptAMW4	FLAG-*pol5-DNt37*, tetOFF; new name: FLAG-*pol5-DN37*	Amp/LEU2	Anna Weigert	
p288	ptAMW5	FLAG-*pol5-DNt81*, tetOFF; new name: FLAG-*pol5-DN81*	Amp/LEU2	Anna Weigert	
p300	ptCMS17	FLAG-*pol5-DN38Int*, tetOFF; new name: FLAG-*pol5-D639H*	Amp/LEU2	This study	[BamHI-NotI]-fragment from pCMS25 subcloned in ptCMS2
p313	pCMS25	*pol5-DN38Int*; new name: *pol5-D639H*	Amp	This study	PCR product obtained with oligonucleotides o131-o249 cloned in pCMS16 using AQUA cloning protocol
p314	pCMS26	*pol5-DN75Int*; new name: *pol5-D602T*	Amp	This study	PCR product obtained with oligonucleotides o131-o250 cloned in pCMS16 using AQUA cloning protocol
p315	pCMS27	*pol5-DC50Int*; new name: *pol5-DN727*	Amp	This study	PCR product obtained with oligonucleotides o138-o251 cloned in pCMS16 using AQUA cloning protocol

#	Name	Gene	Marker	Origin	Cloning procedure
p316	pCMS28	*pol5-DC92Int*; new name: *pol5-DN769*	Amp	This study	PCR product obtained with oligonucleotides o138-o252 cloned in pCMS16 using AQUA cloning protocol
p317	ptCMS19	FLAG-*pol5-DN75Int*, tetOFF; new name: FLAG-*pol5-D602T*	Amp/LEU	This study	[BamHI-NotI]-fragment from pCMS26 subcloned in ptCMS2
p318	ptCMS20	FLAG-*pol5-DC50Int*, tetOFF; new name: FLAG-*pol5-DN727*	Amp/LEU2	This study	[BamHI-NotI]-fragment from pCMS27 subcloned in ptCMS2
p319	ptCMS21	FLAG-*pol5-DC92Int*, tetOFF; new name: FLAG-*pol5-DN769*	Amp/LEU2	This study	[BamHI-NotI]-fragment from pCMS28 subcloned in ptCMS2
p324	ptJPF4	FLAG-*pol5-D481R*, tetOFF	Amp/LEU2	Jorge Perez-Fernandez	
p325	ptJPF5	FLAG-*pol5-5xAla*, tetOFF	Amp/LEU2	Jorge Perez-Fernandez	
p327	pgJPF2	GFP_woFlag	Amp/URA3	Jorge Perez-Fernandez	
p344	ptJPF8	FLAG-*pol5-nls3*, tetOFF	Amp/LEU2	Jorge Perez-Fernandez	
p345	ptJPF9	FLAG-*pol5-Dnls*, tetOFF	Amp/LEU2	Jorge Perez-Fernandez	
p346	ptJPF10	FLAG-*pol5-DLoop*, tetOFF	Amp/LEU2	Jorge Perez-Fernandez	

Table 2: Plasmids used in this study.
Plasmids marked with "K" belong to the department of Biochemistry III at the University of Regensburg. Plasmids marked with "p" belong to the collection of the UTP lab.

4.1.4 Oligonucleotides

4.1.4.1 Primer for PCR amplification and sequencing

#	Name	5'-3'-sequence	Purpose
	M13-21/M13	TGTAAAACGACGGCCAG	forward primer provided for sequencing by Thermo Fisher GENEART and Microsynth SEQLAB
	M13-R/M13r	CAGGAAACAGCTATGAC	reverse primer provided for sequencing by Thermo Fisher GENEART and Microsynth SEQLAB
#621	Noc2-TAP FP	AAGTGATGATGACAACGAAGATG TTGAAATGTCAGACGCTTCCATGG AAAAGAGAAG	forward primer used to amplify TAP tag from pBS1539 for yeast homologous recombination at the C-terminus of *NOC2*

#	Name	5'-3'-sequence	Purpose
#622	Noc2-TAP RP	CTATTGAATTCAAGACAAAAAATC AAATCTTGCTGAGTTGTACGACTC ACTATAGGG	reverse primer used to amplify TAP tag from pBS1539 for yeast homologous recombination at the C-terminus of *NOC2*
#1203	RPA135-pYM-for	CTATCCGCAATGGGTATAAGATTG CGTTATAATGTAGAGCCCAAACGT ACGCTGCAGGTCGAC	forward primer used to amplify TAP tag from pYM15-TAP-URA for yeast homologous recombination at the C-terminus of *RPA135*
#1204	RPA135-pYM-rev	CCTTCATTTACCATTCTATATCAA TTTGGAAAGAAGGGTATTTCTATC GATGAATTCGAGCTC	reverse primer used to amplify TAP tag from pYM15-TAP-URA for yeast homologous recombination at the C-terminus of *RPA135*
#1813	Utp4-TAP-F	ACTTTTCACTCCAAACAAAAGGCG TTTATTCAACCAAAGTTAGTGTTT TCCATGGAAAAGAGAAG	forward primer used to amplify TAP tag from pBS1539 for yeast homologous recombination at the C-terminus of *UTP4*
#1814	Utp4-TAP-R	GCCTTTTAATAGCATCTCTCTATT CTTCGGTATGTTGACTTAAATTAA TACGACTCACTATAGGG	reverse primer used to amplify TAP tag from pBS1539 for yeast homologous recombination at the C-terminus of *UTP4*
#2934	NOP53-TAP_fw	AGTGCCCGTTAGGAAAGGTAGAA AGTATAAGCAGAAAATCACTGAA AAGTGGACACATAAGGACTTCAA ATCCATGGAAAAGAGAAG	forward primer used to amplify TAP tag from pBS1539 for yeast homologous recombination at the C-terminus of *NOP53*
#2935	NOP53-TAP_rev	ATCTCACTTGATGAATCCACGTAT CAAGGACAACCTTTTCATGGAAAC ATATACTGTAAAACAAAAAACTT ACGACTCACTATAGGG	reverse primer used to amplify TAP tag from pBS1539 for yeast homologous recombination at the C-terminus of *NOP53*
#3696	UTP5-S3-fw	AGCGACGGCGAGGAGGAAGCCGGA TATAGTGACGTTGAGATGGAACG TACGCTGCAGGTCGAC	forward primer used to amplify TAP tag from pYM15-TAP-URA for yeast homologous recombination at the C-terminus of *UTP5*
#3697	UTP5-S2-rev	ATTTTTGTATTCTGATGCGTGAAA GCATTTTATGCATGATATCCTATC GATGAATTCGAGCTCG	reverse primer used to amplify TAP tag from pYM15-TAP-URA for yeast homologous recombination at the C-terminus of *UTP5*
#3698	UTP8-S3-fw	CAGAAGCGAGCCTTACCCACTTAC ACCATGGAATACTTGGACATTCGT ACGCTGCAGGTCGAC	forward primer used to amplify TAP tag from pYM15-TAP-URA for yeast homologous recombination at the C-terminus of *UTP8*
#3699	UTP8-S2-rev	TTTTCTATATAGGTATTATACAAT ACAATCAAATTCATTGCATACATC GATGAATTCGAGCTCG	reverse primer used to amplify TAP tag from pYM15-TAP-URA for yeast homologous recombination at the C-terminus of *UTP8*
#3702	UTP10-S3-fw	GTTGTTGAAAACGTTTTAGGGGA ACCTTTTGATAGGTATTTAGATCG TACGCTGCAGGTCGAC	forward primer used to amplify TAP tag from pYM15-TAP-URA for yeast homologous recombination at the C-terminus of *UTP10*
#3703	UTP10-S2-rev	GTGTTTTACTTTACAAAAATTTAC ATAATACTTCACCTTTTTTTTATC GATGAATTCGAGCTCG	reverse primer used to amplify TAP tag from pYM15-TAP-URA for yeast homologous recombination at the C-terminus of *UTP10*
#3883	S3_TAP	CAGCTGAAGCTTCGTACGCTGCAG GTCGACATGGAAAAGAGAAGATG GAAAAAG	forward primer used to amplify TAP tag from pBS1539
#3884	S2_TAP	GGATCTGATATCATCGATGAATTC GAGCTCGATACGACTCACTATAGG GCG	reverse primer used to amplify TAP tag from pBS1539

#	Name	5'-3'-sequence	Purpose
#3890	Pol5(2529)_fo	CGTTATCTCGTTCAAGCATAGAG	forward primer for sequencing of mutated *pol5* on pCMS16 and ptCMS2
#3891	Pol5(3380)_re	ACAAACACCTGATGACGCGG	reverse primer for sequencing of mutated *pol5* on pCMS16 and ptCMS2
#3912	Pol5(572)_fo	TATGGATGAAAGTTCCGCTG	forward primer for sequencing of mutated *pol5* on pCMS16 and ptCMS2
#3913	Pol5(2634)_re	ACGAGCTTGCTTAATGAGCC	reverse primer for sequencing of mutated *pol5* on pCMS16 and ptCMS2
#4072	RLP7_For_Int	CCAGTTATCGAAGTTGACATTGAC TCTTTATTAGCCAAGTTGAATTCC ATGGAAAAGAGAAG	forward primer used to amplify TAP tag from pBS1539 for yeast homologous recombination at the C-terminus of *RLP7*
#4073	RLP7_Rev_Int	TAACTAACAACCTATGTACTATAC AATTTTAAAATACTCTCTTAATAC GACTCACTATAGGG	reverse primer used to amplify TAP tag from pBS1539 for yeast homologous recombination at the C-terminus of *RLP7*
o86	FLAG_POL5_F	ATGGATTACAAGGATGACGACGA TAAGGGTACCGGATCCATGACAGG GAAAGTCAACAGAG	forward primer used to amplify *POL5* from genomic DNA of BY4741 for cloning into pCM182-LEU2
o87	NotI_POL5_Re	GGAAACAGCTATGACCATGATTAC GCCAAGCTTGCATGCGCGGCCGCA GGTATGGACTCGTATGTTTATC	reverse primer used to amplify *POL5* from genomic DNA of BY4741 for cloning into pCM182-LEU2
o99	Pol5_713_rev	TTCAAATCCAACACCGAGGG	reverse primer for sequencing of mutated *pol5* on pCMS16 and ptCMS2
o127	Spb4_S3_fw	CGGAAGAAAGTTTCCAGCAAAGCT ATCCAAGGCAATTTTGACGACTTA CGTACGCTGCAGGTCGAC	forward primer used to amplify TAP tag from pYM15-TAP-URA for yeast homologous recombination at the C-terminus of *SPB4*
o128	Spb4_S2_rev	CCATTGGTTAAGAATGTTGAGTGA TTCTACGAACAAGGTAACTTTTTT TCCATAAATCGATGAATTCGAGCT CG	reverse primer used to amplify TAP tag from pYM15-TAP-URA for yeast homologous recombination at the C-terminus of *SPB4*
o131	Pol5_DCt_PmeI_fw	GTTTAAACCTAAGTATATTTTATC ACTCCTCAAAATCGG	forward primer used to amplify *POL5* from pCMS16 for C-terminal truncation of *POL5*
o132	Pol5_DCt120_rev	GAGGAGTGATAAAATATACTTAG GTTTAAACTGGCCTATCAAGAGTT TCATTGAC	reverse primer used to amplify *POL5* from pCMS16 for C-terminal truncation of last 120 amino acids of *POL5*
o133	Pol5_DCt252_rev	GAGGAGTGATAAAATATACTTAG GTTTAAACGGGTAAATTTAACGCC TTCACTAAGGC	reverse primer used to amplify *POL5* from pCMS16 for C-terminal truncation of last 252 amino acids of *POL5*
o134	Pol5_DCt343_rev	GAGGAGTGATAAAATATACTTAG GTTTAAACCAAACCAACTTCTTCA ATAAACTGC	reverse primer used to amplify *POL5* from pCMS16 for C-terminal truncation of last 343 amino acids of *POL5*
o135	Pol5_DNt137_fw	CCTGCAGCCCGGGGGATCCATGCC TTTATTCTCAGAAATATTTGTTAA AGATTTGG	forward primer used to amplify *POL5* from pCMS16 for N-terminal truncation of first 137 amino acids of *POL5*

#	Name	5'-3'-sequence	Purpose
o136	Pol5_DNt293_fw	CCTGCAGCCCGGGGGATCCATGCT GCTACCGTTGTTTGGTAATGG	forward primer used to amplify *POL5* from pCMS16 for N-terminal truncation of first 293 amino acids of *POL5*
o137	Pol5_DNt658_fw	CCTGCAGCCCGGGGGATCCATGAA GGCCTTACTCAGGAAATTGAG	forward primer used to amplify *POL5* from pCMS16 for N-terminal truncation of first 658 amino acids of *POL5*
o138	Pol5_DNt_rev	CATGGATCCCCCGGGCTGCAGGAA TTCG	reverse primer used to amplify *POL5* from pCMS16 for N-terminal truncation of *POL5*
o152	Seq_ptets	CAAAGTCGAGTTTCTCGATCG	forward primer for sequencing of plasmids containing tet-promoter
o249	Pol5_DN38_rev	GAGGAGTGATAAAATATACTTAG GTTTAAACGTGTTTGGAAAATTCG CAAAGTTC	reverse primer used to amplify *POL5* from pCMS16 for C-terminal truncation of *pol5-D679L*
o250	Pol5_DN75_rev	GAGGAGTGATAAAATATACTTAG GTTTAAACAGTTCTTGATCTGCAA ACTTTACT	reverse primer used to amplify *POL5* from pCMS16 for C-terminal truncation of *pol5-D679L*
o251	Pol5_DC50_fw	CCTGCAGCCCGGGGGATCCATGAG TGAAAGTGAAAGTGAGAGTGATA GCGATGAT	forward primer used to amplify *POL5* from pCMS16 for N-terminal truncation of *pol5-DN677*
o252	Pol5_DC92_fw	CCTGCAGCCCGGGGGATCCATGCC CGATAACATAGTTAATGATAAAG GGGAAGTT	forward primer used to amplify *POL5* from pCMS16 for N-terminal truncation of *pol5-DN677*

Table 3: Primer for PCR amplification and sequencing used in this study.
Oligonucleotides marked with "#" belong to the department of Biochemistry III at the University of Regensburg. Oligonucleotides marked with "o" belong to the collection of the UTP lab.

4.1.4.2 Primer for qPCR amplification

#	Name	5'-3'-sequence	Purpose
#710 ("25S")	M1	TGGAGCAAAGAAATCACCGC	reverse primer for amplification within 25S rDNA locus; position +6414 from ATG
#711 ("25S")	M2	CCGCTGGATTATGGCTGAAC	forward primer for amplification within 25S rDNA locus; position +6366 from ATG
#712 ("18S")	M3	GAGTCCTTGTGGCTCTTGGC	forward primer for amplification within 18S rDNA locus; position +1431 from ATG
#713 ("18S")	M4	AATACTGATGCCCCCGACC	reverse primer for amplification within 18S rDNA locus; position +1589 from ATG
#920 ("5S")	5S ChIP-F1	GCCATATCTACCAGAAAGCACC	forward primer for amplification within 5S rDNA locus; position -1357 from ATG
#921 ("5S")	5S ChIP-R1	GATTGCAGCACCTGAGTTTCG	reverse primer for amplification within 5S rDNA locus; position -1265 from ATG
#969 ("Pro-moter")	Prom ChIP-F2	TCATGGAGTACAAGTGTGAGGA	forward primer for amplification within rDNA promoter; position -43 from ATG
#970 ("Pro-moter")	Prom ChIP-R1	TAACGAACGACAAGCCTACTC	reverse primer for amplification within rDNA promoter; position +70 from ATG

#	Name	5'-3'-sequence	Purpose
#1049 ("ITS1")	R25	GCTTAGAGAAGGGGGCAACT	forward primer for amplification at the end of 18S rDNA locus; position +2404 from ATG
#2421 ("E-Pro")	E-Pro_2_fwd	CAGAGAGGCAGCGTAAAAGG	forward primer for amplification within E-Pro downstream of rDNA terminator; +7245 from ATG
#2422 ("E-Pro")	E-Pro_2_rev	CTTATTCCTTCCCGCTTTCC	reverse primer for amplification within E-Pro downstream of rDNA terminator; +7457 from ATG
#2863 ("ITS1")	R25-rev-q	CGGCTGGACTCTCCATCTCT	reverse primer for amplification at the end of 18S rDNA locus; position +2596 from ATG
#2864 ("ITS2")	ITS2-up-q	GCATGCCTGTTTGAGCGTC	forward primer for amplification at the end of 5.8S locus; position +3015 from ATG
#2865 ("ITS2")	ITS2-do-q	CGACCGTACTTGCATTATACC	reverse primer for amplification at the end of 5.8S locus; position +3153 from ATG
#2882 ("3'ETS")	25S-Jo-up	ATCATTTGTATACGACTTAGATGTACAACG	forward primer for amplification at the end of 25S rDNA locus; position +6576 from ATG
#2883 ("3'ETS")	25S-Jo-do	AACAAATCAGACAACAAAGGCTTAATC	reverse primer for amplification at the end of 25S rDNA locus; position +6648 from ATG
#2884 ("Terminator")	3'-REB-Jo-up	TACGATGAGGATGATAGTGTGTAAGAGTG	forward primer for amplification within rDNA terminator; position +6821 from ATG
#2885 ("Terminator")	3'-REB-Jo-do	TCTCTTTCAACCCATCTTTGCAA	reverse primer for amplification within rDNA terminator; position +6917 from ATG
#2886 ("NTS1")	Fob-bs-Jo-up	GAGAAAAGCTCATTTCCTATAGTTAACAG	forward primer for amplification within NTS1 downstream of rDNA terminator; position +7066 from ATG
#2887 ("NTS1")	Fob-bs-Jo-do	TTCACTTGTCTCTTACATCTTTCTTGG	reverse primer for amplification within NTS1 downstream of rDNA terminator; position +7138 from ATG
#3249 ("NTS2")	rARS1_fwd	TGACGGAAATACGCTTCAGA	reverse primer for amplification within NTS2 upstream of rDNA promoter; position -473 from ATG
#3250 ("NTS2")	rARS1_rev	GTCAGATGAAAGATGAATAGACA	forward primer for amplification within NTS2 upstream of rDNA promoter; position -609 from ATG

Table 4: Primer for qPCR amplification used in this study.
Oligonucleotides marked with "#" belong to the department of Biochemistry III at the University of Regensburg. Names in brackets correspond to denomination in qPCR diagrams.

4.1.4.3 Probes for northern blot detection and primer extension

#	Name	5'-3'-sequence	Hybridization site
#205 ("18S")	o2-18S	CATGGCTTAATCTTTGAGAC	rDNA, 18S
#207 ("A2A3")	o4-A2/A3	TGTTACCTCTGGGCCC	rDNA, ITS1

#	Name	5'-3'-sequence	Hybridization site
#208 ("A3B")	o5-A3/B1	AATTTCCAGTTACGAAAATTCTTG	rDNA, ITS1
#210 ("EC2")	o7-E/C2	GGCCAGCAATTTCAAGTTA	rDNA, ITS2
#211 ("C2C1")	o8-C1/C2	GAACATTGTTCGCCTAGA	rDNA, ITS2
#212 ("25S")	o9-25S	CTCCGCTTATTGATATGC	rDNA, 25S
#2474 ("5S")	5S-rDNA	CAGCGGGTACTCCTACCTGATT	rDNA, 5S
#2921 ("A0A1")	A0A1-Sonde	CCCACCTATTCCCTCTTGCTAG	rDNA, 5'ETS
#2959 ("5.8S")	5.8S rRNA 3'	AAATGACGCTCAAACAGGCAT	rDNA, 5.8S
#3468 ("U3")	U3-SnR17A	CCGCTAAGGATTGCGGACCAAGC	U3
#3470 ("U14")	SnR128-U14	TCACTCAGACATCCTAGGAAGG	U14
#3839 ("DA2")	ITS1 D-A2 mid	AAGCCTAGCAAGACCGCGCA	rDNA, ITS1
o67 ("bA0")	vA0	CGCTGCTCACCAATGG	rDNA, 5'ETS

Table 5: Probes for northern blot detection and primer extension used in this study.
Oligonucleotides marked with "#" belong to the department of Biochemistry III at the University of Regensburg. Oligonucleotides marked with "o" belong to the collection of the UTP lab.

4.1.5 Enzymes

All enzymes were used with the provided buffers.

Enzyme	Manufacturer
Antarctic Phosphatase	New England Biolabs
Herculase II Fusion DNA Polymerase	Agilent
HotStarTaq DNA Polymerase	Qiagen
Proteinase K	Sigma Aldrich
Restriction Endonucleases	New England Biolabs
RNase A (20 mg/ml)	Invitrogen
RNasin® Plus RNase Inhibitor	Promega
SuperScript III Reverse Transcriptase	Thermo Fisher Scientific
T4 DNA Ligase	New England Biolabs
T4 Polynucleotide Kinase (T4 PNK)	New England Biolabs
TEV Protease (2.6 mg/ml)	Biochemistry III
Thermo Sequenase DNA Polymerase	Thermo Fisher Scientific
Trypsin Sequencing Grade	Roche
Zymolyase 100T (100,000 U/g)	Seikagagu Biobusiness Corporation

Table 6: Enzymes used in this study.

4.1.6 Antibodies

Antibody	Origin	Dilution	Manufacturer
Anti-FLAG	rat	1:1,000	Agilent (200473)
Anti-HA	rat	1:5,000	Roche (11867431001)
Anti-HIS (peroxidase conjugated)	-	1:5,000	Pierce Protein Biology (INDIA-His-HRP)

Antibody	Origin	Dilution	Manufacturer
Anti-PAP (peroxidase conjugated)	rabbit	1:5,000	GenScript (A01435-100)
Anti-Tubulin	rat	1:2,000	Abcam
Anti-Utp18	rabbit	1:1,000	Agro-Bio
Anti-rabbit (peroxidase conjugated)	goat	1:5,000	Dianova (111-035-003)
Anti-rat (peroxidase conjugated)	goat	1:5,000	Dianova (112-035-068)

Table 7: Antibodies used in this study.

4.1.7 Media and buffers

Unless stated otherwise, all solutions have been prepared in water, which has a resistivity of 18.2 MΩ-cm and total organic content of less than five parts per billion. The pH values were measured and adjusted at room temperature. Percentage is mass per volume (m/v) and pH was adjusted with HCl or NaOH if not indicated otherwise.
All media were autoclaved for 20 minutes at 121°C and stored at room temperature. Plates were stored at 4°C in the dark after hardening.

Medium	Ingredients	Concentration
LB	Bacto Yeast Extract Bacto Tryptone NaCl	0.5% 1% 1%
LB+AMP	Ampicillin (in H_2O) LB medium Agar (plates)	100 µg/ml 2%
LB+KAN+CHL	Kanamycin (in H_2O) Chloramphenicol (in ethanol) LB medium Agar (plates)	50 µg/ml 30 µg/ml 2%
SCD/SCG	YNB+Nitrogen CSM-His-Leu-Ura Glucose/Galactose Histidine Leucine Uracil NaOH (plates) Agar (plates)	0.67% 0.062% 2% 0.1 g/l 0.1 g/l 0.1 g/l 1.375 mM 2%
2xSCD	YNB+Nitrogen CSM-His-Leu-Ura Glucose Histidine Leucine Uracil	1.34% 0.124% 2% 0.1 g/l 0.1 g/l 0.1 g/l
YPD/YPG	Bacto Yeast Extract Bacto Peptone Glucose/Galactose Agar (plates)	1% 2% 2% 2%

Table 8: Media used in this study.

Buffer/Solution	Ingredients	Concentration
1% Agarose Gel	Agarose TBE (solvent) SYBR Safe	1% 1x 1:10,000

Buffer/Solution	Ingredients	Concentration
100x Protease Inhibitors	Benzamidine PMSF ethanol (solvent) store at -20°C	200 mM 100 mM
10x Biotinylation Buffer	Tris-HCl, pH 7.4 EDTA, pH 8.0	100 mM 10 mM
10x PBS, pH 7.4	NaCl KCl Na_2HPO_4 KH_2PO_4	1.37 M 27 mM 100 mM 18 mM
10x SDS Running Buffer	Tris Glycine SDS	250 mM 1.92 M 1%
10x TBS, pH 7.0	Tris NaCl adjust to pH 7.0	1 M 9%
1x TBS-T	TBS, pH 7.0 Tween20	1x 0.05%
20x SSC	NaCl Sodium Citrate Dihydrate	3 M 300 mM
20x Taurine Buffer	Tris Taurine Na_2EDTA	1.78 M 575 mM 11 mM
5% SDS Stacking Gel	Acrylamide Mix (AA:Bis-AA 37.5:1) Tris-HCl, pH 6.8 SDS TEMED APS	5% 125 mM 0.1% 0.001% (v/v) 0.1%
5x TBE	Tris Boric Acid EDTA, pH 8.0	445 mM 445 mM 10 mM
6x Laemmli Buffer	Tris-HCl, pH 6.8 Glycerin SDS β-Mercaptoethanol Bromophenol Blue	375 mM 60% 12.6% 855 mM
8%/10% SDS Resolving Gel	Acrylamide Mix (AA:Bis-AA 37.5:1) Tris-HCl, pH 8.8 SDS TEMED APS	8%/10% 375 mM 0.1% 0.06 % (v/v) 0.1%
Biotin Blocking Buffer	PBS, pH 7.4 EDTA, pH 8.0 SDS	1x 1 mM 10%
Biotin Staining Buffer	PBS, pH 7.4 EDTA, pH 8.0 SDS IR-dye conjugated Streptavidin	1x 1 mM 10% 0.1 µg/ml
Biotin Wash Buffer 1	PBS, pH 7.4 EDTA, pH 8.0 SDS	1x 1 mM 1%
Biotin Wash Buffer 2	PBS, pH 7.4 EDTA, pH 8.0 SDS	1x 1 mM 0.1%

Buffer/Solution	Ingredients	Concentration
ChIP IRN Buffer	Tris-HCl, pH 8.0 EDTA, pH 8.0 NaCl	50 mM 20 mM 500 mM
ChIP Lysis Buffer	HEPES-KOH NaCl EDTA, pH 8.0 Triton Na-Deoxycholate Protease Inhibitors	50 mM 140 mM 5 mM 1% 0.1% 1x
ChIP Na-Deoxycholate Buffer	Tris-HCl, pH 8.0 EDTA, pH 8.0 LiCl NP-40 Na-Deoxycholate	10 mM 2 mM 250 mM 0.5% 0.5% (v/v)
ChIP Quenching Buffer	Tris-HCl, pH 8.0 Glycine	10 mM 2.5 M
ChIP TE Buffer, pH 8.0	Tris-HCl, pH 8.0 EDTA, pH 8.0	10 mM 1 mM
ChIP Wash Buffer	HEPES-KOH NaCl EDTA, pH 8.0 Triton Na-Deoxycholate SDS	50 mM 500 mM 1 mM 1% 0.1% (v/v) 0.1% (v/v)
Coomassie Destaining Solution	Methanol Acetic Acid	40% (v/v) 10% (v/v)
Coomassie Staining Solution	Methanol Acetic Acid Coomassie Brilliant Blue	40% (v/v) 10% (v/v) 1%
EC Elution Buffer	Sodium Phosphate Buffer, pH 7.8 NaCl Imidazole	20 mM 500 mM 250 mM
EC Extraction Buffer	Sodium Phosphate Buffer, pH 7.8 NaCl Imidazole Protease Inhibitors	20 mM 500 mM 20 mM 1x
EC P1 Elution Buffer	KAc Tris-HCl, pH 8.0 $MgCl_2$ β-Mercaptoethanol Imidazole	150 mM 20 mM 5 mM 5 mM 250 mM
EC P1 Wash Buffer	KAc Tris-HCl, pH 8.0 $MgCl_2$ β-Mercaptoethanol Imidazole	150 mM 20 mM 5 mM 5 mM 60 mM
EC P1P Extraction Buffer	KAc Tris-HCl, pH 8.0 $MgCl_2$ β-Mercaptoethanol Imidazole Protease Inhibitors	150 mM 20 mM 5 mM 5 mM 20 mM 1x
EC Wash Buffer	Sodium Phosphate Buffer, pH 7.8 NaCl Imidazole	20 mM 500 mM 60 mM
gDNA Extraction Lysis Buffer	Sorbitol EDTA, pH 8.0 Zymolyase 100T	1 M 100 mM 2.5 mg/ml

Buffer/Solution	Ingredients	Concentration
HU Buffer	SDS Tris-HCl, pH 6.8 EDTA, pH 8.0 β-Mercaptoethanol Urea Bromophenol blue	5% 200 mM 1 mM 2.13 mM 8 M
IP P1 Buffer	KAc Tris-HCl, pH 8.0 $MgCl_2$ DTT Triton	150 mM 20 mM 5 mM 1 mM 0.2%
IP P1P Buffer	P1 Buffer Protease Inhibitors	 1x
IP P1PR Buffer	P1 Buffer Protease Inhibitors RNasin	 1x 40 U/ml
LitAc-TE, pH 8.0	Tris-HCl, pH 8.0 LiOAc EDTA, pH 8.0	10 mM 100 mM 1 mM
Lit-PEG	LitAc-TE, pH 8.0 (solvent) Polyethylene Glycol (PEG3350) sterile filtration	 40%
Lit-SORB	LitAc-TE, pH 8.0 (solvent) Sorbitol sterile filtration	 1 M
Low-Mg^{2+} Lysis Buffer	KAc Tris-HCl, pH 8.0 $MgCl_2$ DTT Triton Protease Inhibitors	150 mM 20 mM 5 mM 1 mM 0.2% 1x
Low-Mg^{2+} Sucrose Gradient Buffer	Tris-HCl, pH 7.4 NaCl DTT Sucrose Bromophenol Blue (only 60%)	50 mM 50 mM 1 mM 10%/40%/60%
Low-Salt Lysis Buffer	Tris-HCl, pH 7.5 NaCl $MgCl_2$ Cycloheximide Heparin Protease Inhibitors	10 mM 100 mM 30 mM 100 µg/ml 200 µg/ml 1x
Low-Salt Sucrose Gradient Buffer	Tris-Ac, pH 7.5 NH_4Cl $MgCl_2$ DTT Sucrose Bromophenol Blue (only 60%)	50 mM 50 mM 12 mM 1 mM 10%/40%/60%
MS AC Buffer	NH_4Ac, pH 7.4 $MgCl_2$	100 mM 0.1 mM
MS Acetonitrile-TFA	Acetonitrile TFA	70% (v/v) 0.1% (v/v)
MS AH Buffer	NH_4OH	500 mM
MS Matrix	α-Cyano-4-hydroxycinnamicacid MS Acetonitrile-TFA (solvent)	4 mg/ml

Buffer/Solution	Ingredients	Concentration
NB 10x Formaldehyde Running Buffer	Sodium Acetate Trihydrate MOPS EDTA, pH 8.0 adjust to pH 7.0 store in the dark	80 mM 200 mM 10 mM
NB AE Buffer	NaAc, pH 5.3 EDTA, pH 8.0	50 mM 10 mM
NB Church Buffer	BSA Fraction V EDTA, pH 8.0 Sodium Phosphate Buffer, pH 6.3 SDS	1% 1 mM 500 mM 7%
NB Formaldehyde Agarose Gel	Agarose solubilize in H_2O by heating Formaldehyde Running Buffer Formaldehyde	1.2% 1x 2% (v/v)
NB Formaldehyde Agarose Gel Electrophoresis Buffer	Formaldehyde Running Buffer Formaldehyde	1x 2% (v/v)
NB Formaldehyde Agarose Gel Staining Solution	Ethidium Bromide TBE (solvent)	0.5 µg/ml 0.5x
NB Formaldehyde RNA Loading Buffer	Glycerin EDTA, pH 8.0 Bromophenol Blue Xylene Cyanol	50% 10 mM
NB Formaldehyde RNA Preparation Buffer	Formamide (not deionized) Formaldehyde Formaldehyde Running Buffer	50% (v/v) 6.475% (v/v) 0.5x
NB Urea Polyacrylamide Gel	Urea TBE Acrylamide Mix (AA:Bis-AA 37.5:1) TEMED APS	7 M 0.5x 8% 0.075% (v/v) 0.075%
NB Urea Polyacrylamide RNA Loading Buffer	Formamide (deionized) TBE Bromophenol Blue Xylene Cyanol	95% (v/v) 0.125x 0.025% 0.025%
NB Wash Buffer 1	SSC SDS	2x 0.5%
NB Wash Buffer 2	SSC SDS	0.5x 0.05%
PEX RNA Loading Buffer	Formamide (deionized) EDTA, pH 8.0 Bromophenol Blue Xylene Cyanol	95% 20 mM
PEX Sequencing Gel	Urea Taurine Buffer Acryl Solution A (30%) Bis-Acryl Solution B (2%) TEMED APS	7 M 1x 5.7% 0.3% 0.11% (v/v) 0.11%
Ponceau S Solution	Ponceau S Acetic acid	0.5% 1% (v/v)
Pretreatment Solution	β-Mercaptoethanol NaOH	7.5% (v/v) 1.85 M
Sodium Phosphate Buffer, pH 6.3	Na_2HPO_4 NaH_2PO_4	77.4% 22.6%
Sodium Phosphate Buffer, pH 7.8	Na_2HPO_4 NaH_2PO_4	89.6% 10.4%

Buffer/Solution	Ingredients	Concentration
TE Buffer, pH 7.5	Tris-HCl, pH 7.5 EDTA, pH 8.0	50 mM 20 mM
WB Transfer Buffer	Methanol Glycine Tris	20% (v/v) 192 mM 24 mM

Table 9: Buffers and solutions used in this study.

4.1.8 Kits

Kit	Manufacturer
Herculase II Fusion DNA Polymerase Kit (with dNTP combo)	Agilent
Invitrogen™ SuperScript™ III Reverse Transcriptase Kit	Thermo Fisher Scientific
iTRAQ® Reagent Multi-Plex Kit	AB Sciex
peqGOLD Plasmid Miniprep Kit II	Peqlab
QIAEX II Gel Extraction Kit	Qiagen
QIAquick Gel Extraction Kit	Qiagen
Roche BM Chemiluminescence Western Blotting Substrate (POD)	Merck
Thermo Sequenase Cycle Sequencing Kit	Thermo Fisher Scientific

Table 10: Kits used in this study.

4.1.9 Chemicals and consumables

The ingredients for growth media were purchased from BD Biosciences (Bacto Agar, Bacto Peptone, Bacto Tryptone and Bacto Yeast Extract), Q-Biogene, Bio101, Inc. or Sunrise Science Products (Complete supplement mixtures (CSM), Yeast nitrogen base (YNB), amino acids, and adenine), Sigma-Aldrich (D(+)-glucose, amino acids, and uracil), and Serva (D(+)-galactose). Deionized water was obtained with an Elga Purelab Ultra device prior to use.
Unless stated otherwise, all chemicals and solvents used in this work were purchased at the highest available purity from Sigma Aldrich, Merck, Fluka, Roth or J.T.Baker.

Chemical/consumable	Manufacturer
[5-6-^{3}H] Uracil	American Radiolabeled Chemicals, Inc.
1 kb DNA Ladder	New England Biolabs
2-Log DNA Ladder	New England Biolabs
4-thio-Uracil	Merck
6 Peptide Mixture (P/N 4368762) for Calibration	AB Sciex
6x DNA Loading Dye	New England Biolabs
Acclaim 3µm PepMap100 C18 Nano LC Columns with nanoViper Fittings (75µm x 150 mm) (P/N 164568)	Thermo Scientific
Agarose Electrophoresis Grade	Invitrogen
ANTI-FLAG® M2 Affinity Gel	Merck
BcMag Epoxy-Activated Magnetic Beads	Bioclone Inc.
BSA Solution (10 mg/ml stock)	New England Biolabs
Color Prestained Protein Standard, Broad Range (10-250 kDa)	New England Biolabs
Coomassie Brilliant Blue	Bio-Rad
dNTPs Mix (25 mM each)	Agilent Technologies
Extra Thick Blot Paper	Bio-Rad
Filter Paper 3 mm	Whatman

Chemical/consumable	Manufacturer
Filter Paper Type 601	Rotilab
Gene Pulser Cuvettes	Bio-Rad
Glass Beads (0.75-1 mm)	Roth
Glycogen (5 mg/ml)	Ambion
Heparin	Serva
IgG Sepharose TM 6 Fast Flow	GE Healthcare
Immobilon-P Transfer Membrane PVDF 0.45 µm	Millipore
IRDye 800CW Streptavidin	Pierce
Low Binding Micro Tubes 1.5 ml	Sarstedt
Luminescent Marker	Marabu fun & fancy Window Color
Membrane PositiveTM	MP Biomedicals
Micro Bio-Spin 6 Columns	Bio-Rad
Milk Powder	Sukofin
MTSEA-Biotin-XX	Biotium (90066)
Ni-NTA Agarose	Qiagen
NuPAGE™ 4-12% Bis-Tris Gel	Invitrogen
Polamét (metal care)	Anti-black
Polyallomer Tubes for SW40 Ti (14x95 mm)	Beckman
Polycarbonate Tubes for TFT 70.13 (10.4 ml)	Beckman
PolyPrep Chromatography Columns	Bio-Rad
Precision Wipes (11x21cm)	Kimberly-Clark
Protein Assay "Dye Reagent Concentrate"	Bio-Rad
Quartz QS Micro Cell	Hellma
Salmon Sperm DNA (10 mg/ml)	Invitrogen
SimplyBlue™ SafeStain	Invitrogen
SYBR Green	Roche
SYBR Safe DNA Gel Stain	Invitrogen
Ultima Gold Liquid Scintillation Cocktail	Perkin Elmer
Zirconia-Silicate Beads (0.1-0.15 mm)	BioSpec
α-Cyano-4-hydroxycinnamicacid (matrix)	Sigma Aldrich
γ-[^{32}P]-ATP	Hartmann Analytic
µ-Precolumn (300µm x 5mm) C18PepMap100, 5µm, 100Å (P/N 160454)	Thermo Scientific

Table 11: Chemicals and material consumed in this study.

4.1.10 Equipment

Device	Manufacturer
1600TR Liquid Scintillation Analyzer	Packard
4800 Proteomics Analyzer MALDI-TOF/TOF	AB Sciex
Avanti J-26 XP Centrifuge	Beckman Coulter
Avanti J-26S XP Centrifuge	Beckman Coulter
BAS Cassette 2040	Fujifilm
BAS-III Imaging Plate (^{32}P)	Fujifilm
BAS-TR2040 Imaging Plate (^{3}H)	Fujifilm
BioLogic LP Fractionator	Bio-Rad
Branson Sonifier S-250A	Branson
Centrikon T-1170 Ultracentrifuge	Kontron
Concentrator Plus	Eppendorf
Eraser	Raytest
Fluo-Link	Vilber Lourmat
Gel Documentation System	Intas
Gradient Master 107 IP	Biocomp
LAS-3000 Chemiluminescence Imager	Fujifilm
MicroPulser Electroporation Apparatus	Bio-Rad

Device	Manufacturer
Nanodrop ND-1000	Thermo Scientific
Odyssey Infrared Imaging System	LI-COR
Optima L-80 XP Ultracentrifuge	Beckman Coulter
PCR Cycler	Bio-Rad
Pierce G2 FastBlotter	Thermo Scientific
PowerPac HV Power Supply	Bio-Rad
Precellys Evolution with Cryolys	Bertin Instruments
Probot	LC Packings (Dionex)
Research Plus 8 Channel Pipettes	Eppendorf
Rotor Gene RG-3000	Corbett Research
Rotor SW40 Ti	Beckman Coulter
Rotor TFT 70.13	Kontron
Sequi-Gen GT	Bio-Rad
Sub-Cell GT	Bio-Rad
Trans-Blot Cell	Bio-Rad
Typhoon FLA-9500	GE Healthcare
UltiMate 3000 NanoHPLC	LC Packings (Dionex)
Ultraspec 3100pro	Amersham Biosciences
Vertical Double Gel System	Peqlab
Water System PureLab	ELGA
XCell SureLock Mini-/Midi-Cell Electrophoresis	Invitrogen

Table 12: Equipment used in this study.

4.1.11 Software

Software	Producer
µcarrier V.2.0	LC Packings (Dionex)
4000 Series Explorer v.3.6	Applied Biosystems
Acrobat Reader Pro	Adobe
BioLogic LP Data View Software	Bio-Rad
Chromeleon V.6.80	LC Packings (Dionex)
Data Explorer v.4.5 C	Applied Biosystems
Fiji	Java
Gel Documentation Software	Intas
GPS Explorer v.3.5	Applied Biosystems
Image Reader LAS-3000 Control Software	Fujifilm
SWISS-PROT	UniProtKB
Microsoft Office 365	Microsoft
MultiGauge v.3.0	Fujifilm
NanoDrop ND-1000 Operating Software	Peqlab Biotechnologies GmbH
Odyssey Infrared Imaging System Application Software	LI-COR
Protein Pilot	Applied Biosystems
Rotor Gene 6000	Corbett Research
SnapGene® Viewer	SnapGene
Typhoon FLA 9500 Control Software	GE Healthcare
Zotero	George Mason University, USA

Table 13: Software used in this study.

4.2 Methods

4.2.1 Work with *E. coli*

4.2.1.1 Cultivation of bacterial cells

Bacterial strains were cultivated at 37°C in liquid LB medium containing antibiotic(s) (see Table 8) for plasmid selection. Culture growth was monitored by measuring the absorbance at **600** nm to determine the **o**ptical **d**ensity of cell cultures (OD_{600}).
Cultivation on solid agar plates was performed in plates containing LB medium and the required antibiotic(s) for plasmid selection. Individual colonies or aliquots of glycerol stocks were streaked out using sterile disposable inoculation loops. Plates were incubated upside down at 37°C for not longer than 24 hours. Short-term storage of the bacterial clones was possible at 4°C.

4.2.1.2 Transformation of electro-competent bacterial cells by electroporation

A 75 µl-aliquot of electro competent *E. coli* cells XL1 blue MRF was thawed on ice and 3 µl of a ligated plasmid sample (see 4.2.3.6 or 4.2.3.10) or 0.5 µl of a plasmid was added and mixed. The mixture was transferred to cold 0.2 cm cuvettes for electroporation and the pulse was performed in a Bio-Rad MicroPulser Electroporation apparatus using program EC2. After the electroporation, 1 ml of LB medium was added and the sample was incubated for 45 minutes at 37°C. The suspension was then transferred to a 1.5 ml-tube and centrifuged at 4,000 rpm for 4 minutes at RT. 900 µl of the supernatant was discarded. The pellet was resuspended in the remaining volume, plated on LB supplemented with antibiotic(s), and incubated overnight at 37°C. For re-transformed plasmids, centrifugation step was skipped and 100 µl of regenerated cells was directly plated and incubated overnight at 37°C.

4.2.1.3 Transformation of chemo-competent bacterial "Rosetta Star" cells by heat shock

A 75 µl-aliquot of chemo competent *E. coli* cells Rosetta Star was thawed on ice and 0.5 µl of an *E. coli* expression plasmid pExJPF (see Table 2) was added and mixed. The mixture was transferred to 1.5 ml-tube and incubated for 5 minutes on ice. The heat shock was performed for 45 seconds at 42°C. After a second incubation step for 5 minutes on ice, the cells were supplemented with 1 ml LB medium and incubated for 2 hours at 37°C. 100 µl of regenerated cells was plated on LB supplemented with antibiotics Kanamycin and Chloramphenicol and incubated overnight at 37°C.

4.2.1.4 Long-term storage of plasmid DNA in *E. coli*

Plasmids to be stored were transformed into electro-competent *E. coli* cells (see 4.2.1.2). Single colonies were streaked out as dense patches in the appropriate medium and

incubated overnight at 37°C. Cells were recovered with inoculation loops and suspended in 1 ml sterile 20% (v/v) glycerol. Glycerol stocks were stored at -80°C.

4.2.1.5 Purification of plasmid DNA from *E. coli* ("mini-preparation")

Plasmid DNA was isolated from *E. coli* using the peqGOLD Plasmid Miniprep Kit II from Peqlab according to manufacturer's instructions. Bacterial cells used for mini preparation were streaked out as dense patches on LB supplemented with antibiotic(s) and cultivated overnight at 37°C. Cells were collected by a sterile disposable inoculation loop and suspended in 250 µl "Solution I" (second step in manufacturer's manual). Elution of DNA was performed with 100 µl H_2O.

4.2.1.6 Heterologous expression of HIS-tagged yeast proteins in *E. coli*

For heterologous expression of yeast protein Pol5 or Pol5 domains in *E. coli*, one single colony of "Rosetta Star" cells containing the respective *E. coli* expression plasmid (see 4.2.1.3) was used to inoculate 100 ml LB+KAN+CHL liquid medium (see Table 8). The culture was incubated overnight at 37°C and the next day, it was used to inoculate 1 L LB+KAN+CHL liquid culture to an OD_{600} of 0.1. After growth at 37°C to an OD_{600} of about 0.8, the protein expression was induced by a concentration of 0.1 mM IPTG in the liquid culture and cells were incubated for 6 h at 24°C. Subsequently, cells were harvested by centrifugation at 5,000 rpm for 10 minutes at RT. Resulting cell pellet was resuspended in 40 ml of supernatant medium, transferred to 50 ml-falcon tube, and centrifuged again at 4,500 rpm for 3 minutes at 4°C. Pellets were frozen in liquid nitrogen and stored at -20°C.

4.2.1.7 Affinity purification of HIS-tagged yeast proteins expressed in *E. coli*

Cell pellet corresponding to 1 L *E. coli* culture, which was obtained as described in section 4.2.1.6, was thawed completely on ice and resuspended in 10 ml EC (P1P) Extraction Buffer (see Table 9) using a syringe and a cannula. After addition of 1.5 g Zirconia-Silicate beads, cell lysis was performed on a vortexer by 10 steps consisting 30 seconds vortex and 30 seconds cooling on ice. The lysate was centrifuged at 15,000x g for 15 minutes at 4°C and transferred to new 50 ml-falcon tube to separate the Zirconia-Silicate beads. The resuspension step with syringe and canula as well as the cell lysis with Zirconia-Silicate beads and vortex was repeated once more. Next, the lysate was centrifuged at 15,000x g for 5 minutes and 4°C and transferred to new 15 ml-falcon tube. Volume of the lysate was adjusted to 12 ml with EC (P1P) Extraction Buffer, supplemented with 1% Triton X-100 and 5 µg/ml RNase A, and incubated for 10 minutes at 4°C under gentle rotation. After that, the lysate was clarified by centrifugation at 15,000x g for 30 minutes at 4°C.
The clarified whole cell lysate (WCL) was transferred to a new 15 ml-falcon tube and 1% of the WCL was collected, mixed with 6x Laemmli Buffer, and stored at -20°C for subsequent SDS-PAGE analysis (see 4.2.5.2) by Coomassie staining (see 4.2.5.3) and western blotting (see 4.2.5.4). Protein concentration was determined using Bradford

Assay (Protein Assay "Dye Reagent Concentrate", Bio-Rad) according to manufacturer's indications (see 4.2.5.1). Rest of the WCL was added to a new 15 ml-falcon tube containing 200 µl slurry of Ni-NTA agarose beads. The beads had been previously equilibrated with EC (P1P) Extraction Buffer containing 1% Triton X-100. The WCL was incubated with beads for 2 hours at 4°C under gentle rotation.
Afterward, lysate suspension was centrifuged at 800 rpm for 3 minutes at 4°C and 1% of supernatant was collected, mixed with 6x Laemmli Buffer, boiled at 95°C, and stored at -20°C as flow-through (FT) for subsequent SDS-PAGE analyses. Remaining supernatant was discarded and first washing step was performed by adding 10 ml EC (P1P) Extraction Buffer, resuspending the beads, and centrifuging at 800 rpm for 1 minute at 4°C. Supernatant was discarded and beads were resuspended again in 10 ml EC (P1P) Extraction Buffer. Suspension was completely transferred to PolyPrep Chromatography Column. Beads were washed ten times with 10 ml EC (P1) Wash Buffer (see Table 9) each time. 1% of flow-through from the first, fifth, and last washing step (W1, W5, W10) was collected, mixed with 6x Laemmli Buffer, boiled at 95°C, and stored at -20°C for analyses. For protein elution, the first elution step was performed by adding 500 µl EC (P1) Elution Buffer (see Table 9) to column and eluate 1 was collected. For the second elution step, beads were resuspended in 1 ml EC (P1) Elution Buffer, the suspension was transferred to 1.5 ml-tube of low protein binding, which was incubated under rotation for 30 minutes at 4°C. Afterward, the elution fraction was collected from the supernatant after centrifugation at 800 rpm for 1 minute at 4°C and it was saved as eluate 2. Last elution step was performed in 1 ml EC (P1) Elution Buffer by incubating the bead suspension under rotation overnight at 4°C. Eluate 3 was obtained as described for eluate 2. 100 µl of each eluate was mixed with 6x Laemmli Buffer, boiled at 95°C, and stored at -20°C for subsequent SDS-PAGE analyses. Finally, beads were resuspended with 1 ml EC (P1) Elution Buffer and one 100 µl-aliquot of suspension was mixed with 6x Laemmli Buffer (Beads after Elution, BaE). Samples BaE were boiled for 10 minutes at 95°C and stored at -20°C for analysis. Rest of eluates and remaining beads were stored at 4°C.

4.2.2 Work with *S. cerevisiae*

4.2.2.1 Cultivation and harvest of yeast strains

Yeast strains were cultivated in the appropriate liquid or solid medium (see Table 8) at 30°C, unless indicated otherwise.
For cultivation on solid agar plates, single colonies or small aliquots of glycerol stocks were streaked out using sterile disposable inoculation loops in order to obtain individual colonies. Plates were incubated upside down at the respective temperatures for 2-4 days. Short-term storage of the yeast cells was possible at 4°C, for long-term storage see section 4.2.2.2.
For cultivation in liquid medium, the appropriate media indicated in Table 8 were used as specified in the result section. Liquid cultures never exceeded one third of the flask volume. Culture growth was monitored by measuring the absorbance at **600** nm to determine the **o**ptical **d**ensity of cell cultures (OD_{600}). Incubation periods, desired OD_{600},

and other details were specific for each experiment. Harvest of cells from liquid culture was performed by centrifugation at 6,000 rpm for 8 minutes at RT. Resulting cell pellets were resuspended in cold H_2O, transferred to 50 ml-falcon tubes, and centrifuged at 4,000 rpm for 3 minutes at 4°C. Cell pellets were directly used or frozen in liquid nitrogen and stored at -20°C.

4.2.2.2 Long-term storage of yeast strains

Yeast strains to be stored were streaked out as dense patches in the appropriate medium and incubated for 1-2 days at 30°C. Cells were recovered with inoculation loops and suspended in 1 ml sterile 20% (v/v) glycerol. Glycerol stocks were stored at -80°C.

4.2.2.3 Preparation of competent yeast cells

50 ml of an exponentially growing yeast culture (OD_{600} = 0.5-0.7) was centrifuged at 4,000 rpm for 5 minutes at RT to harvest the yeast cells. Subsequent washing steps included suspension of cell pellets and centrifugation at 4,000 rpm for 5 minutes at RT to collect cells. Therefore, the resulting pellet was resuspended first in 25 ml sterile H_2O, then in 5 ml LitAc-TE, pH 8.0 (see Table 9), and finally in 5 ml Lit-SORB (see Table 9). Cells were suspended in 500 µl Lit-SORB, transferred to a sterile 1.5 ml-tube, and centrifuged again. Supernatant was completely removed, and the pellet was suspended in 360 µl Lit-SORB and mixed with 40 µl of Salmon Sperm DNA (previously denatured by boiling for 5 minutes at 95°C and chilled on ice). Finally, 50 µl-aliquots were transferred to sterilized 1.5 ml-tubes and stored at -80°C.

4.2.2.4 Transformation of competent yeast cells

A single 50 µl-aliquot of competent yeast cells (see 4.2.2.3) was thawed on ice. For the transformation with plasmids, 10-15 µl of competent cells and 0.1-0.55 µg of plasmid DNA (obtained by "mini-preparation", see 4.2.1.5) were mixed. For transformation with precipitated PCR products (see 4.2.3.1 and 4.2.3.3) for homologous recombination, 50 µl aliquots of competent cells were mixed with different amounts of precipitated PCR product (0.2-2 µg was used). Afterward, 185 µl Lit-PEG was added (see Table 9), and the suspension was mixed and incubated for at least 30 minutes at 30°C. 20 µl of sterile DMSO was added, samples were mixed again, and incubated for 15 minutes at 42°C. 450 µl of 9‰ NaCl was added to the cell suspension, which was harvested by centrifugation at 2,000 rpm for 3 minutes at RT. Cells were resuspended in 100-150 µl 9‰ NaCl, plated on the respective agar medium, and incubated for 3-4 days at 30°C.

4.2.2.5 Generation of yeast strains for this study

Proteins of interest were C-terminally tagged with the tandem affinity purification (TAP) tag fusion protein using a PCR based tagging cassette and homologous recombination as described (Janke et al., 2004).

Individual primer pairs for the DNA encoding the respective proteins to be TAP-tagged (see Table 3) were used to amplify TAP tag from plasmid p96 (see Table 2). PCR products were precipitated (see 4.2.3.3), resuspended in 20 µl H_2O, and used to transform competent cells of yeast strains (see Table 1) as indicated in section 4.2.2.4. Selection of transformants was done by growing the yeast cells on appropriate medium (see Table 8). Several clones were analyzed by western blotting to check protein tagging. To do that proteins were extracted using the denaturing protein extraction protocol (see 4.2.2.10). Samples were resolved by SDS-PAGE (see 4.2.5.2) and analyzed by western blotting (see 4.2.5.4) using antibodies against protein A (see Table 7 and 4.2.5.6) to detect the expression of TAP-tagged proteins of interest. For each strain, two positive clones were stored at -80°C (see 4.2.2.2 and Table 1).

4.2.2.6 Generation of yeast plasmids for this study

POL5 locus containing 5' and 3' regulatory sequences was amplified from genomic DNA by PCR using oligonucleotides o86-o87 (see Table 3 and 4.2.3.1). The obtained PCR product was ligated into plasmid K1837 (see Table 2) after digestion with BamHI-NotI restriction endonucleases (see 4.2.3.7 and 4.2.3.10). The resulting plasmid ptCMS1 containing *POL5* coding sequence was digested with BamHI-NotI and the fragment was subcloned in plasmid p202 (see Table 2) to obtain plasmid ptCMS2 and in plasmid K1 (see Table 2) to obtain plasmid pCMS16. Plasmid ptCMS1 and ptCMS2 express respectively Pol5 or Pol5 fused to a FLAG tag at the N-terminus. Plasmid pCMS16 was used to construct all site directed and truncation mutants of *POL5* by AQUA cloning (Beyer et al., 2015; Jacobus and Gross, 2015) of PCR products obtained with the respective oligonucleotides (see Table 2, Table 3, 4.2.3.1, and 4.2.3.6). The mutant sequences of *POL5* were subcloned into ptCMS2 by BamHI-NotI restriction sites to obtain the desired yeast plasmids (see Table 2).
All constructs were verified by sequencing with different oligonucleotides (see Table 3) at Thermo Fisher GENEART or Microsynth SEQLAB (see 4.2.3.11). Correct plasmids were stored at -80°C (see 4.2.1.4 and Table 2).

4.2.2.7 *In vivo* growth test of yeast strains by drop assay

Yeast strains transformed with different mutant plasmids (see 4.2.2.4) were inoculated in 4 ml of the appropriate selective medium containing galactose and cultured overnight at 30°C. Overnight cultures were diluted 1:10 in 4 ml of the appropriate selective medium containing glucose and cultured for additional 5 hours at 30°C. Each yeast strain to be analyzed was diluted to OD_{600} of 10^{-1} in 200 µl H_2O. Based on this start concentration, a serial dilution of OD_{600} from 10^{-2} to 10^{-4} was prepared in H_2O. Finally, 5 µl of each strain and each dilution was spot on the appropriate selective plates, which were incubated at different temperatures (16°C, 23°C, 30°C, and 37°C) for at least 48 hours. Images were obtained using the Intas Gel Documentation System.

4.2.2.8 Cell culture to determine the depletion phenotype of yeast strains

Yeast strain Y281 (YMH5-1a; GAL::HA-*POL5*) (see Table 1) was transformed with empty backbone plasmid K1837 to obtain a null mutant phenotype or with plasmid p203 (ptCMS2; FLAG-*POL5*) for the wildtype phenotype (see Table 2 and 4.2.2.4).
To avoid loss of plasmids, strains were cultivated in galactose containing minimal medium lacking leucine (SCG-Leu) (see Table 8). Cultures to characterize the phenotype of Pol5 depletion in cell growth, Pol5 expression, and rRNA production were inoculated in SCD-Leu at OD_{600} of 0.15 from exponentially growing (OD_{600} = 0.6-0.8) SCG-Leu cultures. For each strain, the OD_{600} was measured after growth for 0, 1.5, 3, 6, 9, and 16 hours in glucose containing medium. Cultures were kept during the experiment at OD_{600} between 0.2 and 0.8 by dilution in fresh SCD-Leu medium. First point t0 was obtained immediately after inoculation in SCD-Leu medium.
Collected optical density values and dilution factors were plotted in Microsoft Excel to calculate the generation time of each strain. Furthermore, 5 AUs of cell cultures were collected at each indicated time point for comparative analysis of depletion and wildtype phenotypes at RNA (see 4.2.4) and protein levels (see 4.2.2.10 and 4.2.5).

4.2.2.9 Purification of genomic DNA from yeast

To obtain yeast genomic DNA (gDNA), 5 ml of an overnight culture was centrifuged at 2,000 rpm for 5 minutes at RT and the supernatant was discarded. The cell pellet was resuspended in 500 µl of gDNA Extraction Lysis Buffer (see Table 9) and transferred to 1.5 ml-tube. Sample was incubated for 60 minutes at 37°C in the presence of Zymolyase 100T (250 U/ml) to digest the cell wall. Cell suspension was centrifuged at 10,000x g for 1 minute at RT and the supernatant was discarded. Obtained spheroplasts in the pellet fraction were resuspended in 500 µl TE Buffer, pH 7.5 (see Table 9), 50 µl of 10% SDS was added, and sample was mixed. Subsequently, sample was incubated for 30 minutes at 65°C. 200 µl of 5 M KAc was added and the sample was incubated for 60 minutes on ice, and finally centrifuged at 10,000x g for 5 minutes at RT.
The obtained supernatant was transferred to a fresh tube, 1 volume of Isopropanol was added, and the mixture was incubated for 5 minutes at RT and afterward centrifuged at 10,000x g for 10 seconds at RT. The supernatant was discarded, the pellet air-dried, and suspended in 300 µl TE Buffer, pH 7.5. In order to get rid of RNAs, the gDNA sample was treated with 1.5 µl RNase A (20 mg/ml stock) and incubated for 30 minutes at 37°C. The gDNA was again precipitated by addition of 20 µl of 3 M NaAc, pH 5.3, 1 volume of 100% Isopropanol, and centrifugation at 10,000x g for 10 seconds at RT. The supernatant was discarded, and the pellet was air-dried, suspended in 100 µl TE Buffer, pH 7.5, and stored at 4°C.

4.2.2.10 Denaturing protein extraction from yeast

Yeast cell pellet corresponding to 5 AUs was suspended in 1 ml H_2O and 150 µl of freshly prepared Pretreatment Solution (see Table 9). After vortex, the mixture was incubated for

15 minutes on ice. Sample was treated with 150 µl of 55% (w/v) TCA for 10 minutes on ice and centrifuged at 13,000 rpm for 10 minutes at 4°C. The supernatant was discarded, and the pellet was suspended in 200 µl HU Buffer (see Table 9). The pH of the sample (indicated by Bromophenol Blue present in HU Buffer) was neutralized (blue color indicates basic pH) using NH_3 gas, if necessary (yellow color indicates acidic pH). The precipitated proteins were solubilized by incubating the sample for 10 minutes at 65°C. Cell debris and insoluble molecules were precipitated by centrifugation at 13,000 rpm for 5 minutes and RT. Supernatant was collected, resolved by SDS-PAGE (see 4.2.5.2), and analyzed by western blotting (see 4.2.5.4).

4.2.2.11 4-thio Uracil-pulse labeling of yeast cells

Cell cultures were performed as described in section 4.2.2.8 using SCD-Leu-Ura medium, since the lack of uracil in the medium facilitates the uptake of uracil-derivatives by the yeast cells.
At the time points given in section 4.2.2.8, 200 µM 4-thio Uracil (4tU; in DMSO) were added to 20 AUs of liquid cultures for pulse labeling and cultures were incubated for additional 20 minutes in the same growth conditions. After 3 hours (t3), additional 20 AUs cells were collected and treated identic but without addition of 4tU as non-labeled control. After pulse labeling, cells were harvested, frozen in liquid nitrogen, and stored at -20°C until RNA extraction (see 4.2.4.1) was performed.

4.2.2.12 [5-6-^{3}H]-Uracil-pulse-chase labeling of yeast cells

Cell cultures were performed as described in section 4.2.2.8 using SCD-Leu-Ura medium, since the lack of uracil in the medium facilitates the uptake of uracil-derivatives by the yeast cells.
After 3 and 7 hours of growth in glucose containing medium, 30 AUs of cells of each strain were collected and resuspended in 1.2 ml of SCD-Ura medium (see Table 8). Then, cells were treated for 5 minutes with 75 µCi of [5-6-^{3}H] Uracil and chased with 7.5 mM non-radioactive uracil for 0, 5, 10, and 20 minutes. Aliquots of 5 AUs of cells were collected at each chase-time point, immediately frozen in liquid nitrogen, and stored at -20°C until RNA extraction (see 4.2.4.1) was performed.

4.2.2.13 Preparation of yeast cell extracts for affinity purifications

Cell pellet (see 4.2.2.1) corresponding to 500 ml yeast culture (containing TAP or FLAG tag) with OD_{600} between 0.6 and 0.8 was resuspended in 10 ml IP P1P Buffer (see Table 9) and centrifuged at 3,000 rpm for 3 minutes at 4°C. Pellet was thawed on ice when required. Cell pellets were weighed and diluted in 1.5 volumes of IP P1PR Buffer (see Table 9) per gram of cell pellet. For mechanic cell lysis, 1.4 g ice cold glass beads (diameter 0.75-1.0 mm) was added to 800 µl aliquots of cell suspension. Cell disruption was performed in Precellys Evolution coupled to Cryolys cooling unit at 4°C with 6 cycles of 30 seconds shaking at 6,000 rpm alternated with 30 seconds pausing. After separation of

glass beads, cell lysates were clarified by two centrifugation steps, each at 13,000 rpm for 15 minutes at 4°C. The protein concentration was determined using Bradford Assay (Protein Assay "Dye Reagent Concentrate", Bio-Rad) according to manufacturer's indications (see 4.2.5.1).

4.2.2.14 Yeast affinity purification using IgG-coupled sepharose beads or ANTI-FLAG M2 affinity gel for downstream western and northern blot analysis

Two 100 µl-aliquots of whole cell lysate (WCL), obtained as described in section 4.2.2.13, were kept for subsequent analysis by northern and western blotting (input fractions). Input fractions for northern blot were supplemented with 400 µl NB AE Buffer (see Table 9) and frozen at -20°C for RNA extraction (see 4.2.4.1). Input fractions for western blot were mixed with 20 µl 6x Laemmli Buffer, boiled for 10 minutes at 95°C, and stored at -20°C for SDS-PAGE (see 4.2.5.2).
The rest of the WCL was added to PolyPrep Chromatography Columns containing IgG-coupled sepharose beads (TAP tag) or ANTI-FLAG M2 affinity gel (FLAG tag). 150 µl slurry (IgG) or 100 µl slurry (ANTI-FLAG) of affinity matrix was previously equilibrated by washing once in 10 ml H_2O and twice in 10 ml IP P1 Buffer (see Table 9). Binding of the bait protein to the affinity matrix was performed for 2 hours at 4°C under gentle rotation. Subsequently, 100 µl of flow-through fraction (FT) was collected and prepared for SDS-PAGE as described for WCL. Remaining flow-through was discarded and beads were washed twice with 1 ml IP P1PR Buffer (see Table 9), 5 times with 2 ml IP P1P Buffer (see Table 9), and finally once more with 10 ml IP P1 Buffer. 100 µl of the last washing step (W) was collected and prepared for SDS-PAGE as described for WCL.
After washing, two thirds of beads were recovered from column in 1 ml IP P1 Buffer for subsequent analysis by northern blotting (IP fraction). The remaining one third of beads was recovered from column in 500 µl IP P1 Buffer for subsequent analysis by SDS-PAGE and western blotting (eluate). Therefore, beads were centrifuged at 2,000 rpm for 1 minute at 4°C and supernatant was discarded. Northern blot IP fraction was supplemented with 500 µl NB AE Buffer and sample was stored at -20°C for RNA extraction (see 4.2.4.1). Eluate for SDS-PAGE analysis was mixed with 100 µl IP P1 Buffer and 20 µl 6x Laemmli Buffer, boiled for 10 minutes at 95°C, and stored at -20°C (see 4.2.5.2).

4.2.2.15 Yeast affinity purification using IgG-coupled magnetic beads for downstream western blot and semi-quantitative mass spectrometry analysis

A 100 µl-aliquot of whole cell lysate (WCL), obtained as described in section 4.2.2.13, was kept for subsequent analysis by SDS-PAGE (input fraction) (see 4.2.5.2). Therefore, the aliquot was first supplemented with 20 µl 6x Laemmli Buffer, boiled for 10 minutes at 95°C, and stored at -20°C.
The rest of the clarified WCL was incubated for 2 hours at 4°C under gentle rotation with 100 µl slurry of IgG-coupled magnetic beads previously equilibrated 3 times in 1 ml IP P1 Buffer (see Table 9).

Subsequently, 100 µl of the fraction not associated with the beads (flow-through, FT) was collected and prepared for SDS-PAGE as described for WCL. Remaining flow-through was discarded and beads were washed 3 times with 1 ml IP P1P Buffer (see Table 9) and once with 1 ml IP P1 Buffer. For each wash step beads were resuspended in the corresponding buffer and incubated for 5 minutes at 4°C under gentle rotation. Then buffer and beads were split using a magnet. 100 µl of last washing step (W) was collected and prepared for SDS-PAGE as described for WCL. In order to remove remaining salt, beads were washed twice with 1 ml MS AC Buffer (see Table 9).
Elution of the affinity purified sample was performed in four steps (2x 5 minutes, 2x 20 minutes) at RT under gentle rotation using 4 times 500 µl freshly prepared MS AH Buffer (see Table 9). All fractions were pooled, frozen in liquid nitrogen, and lyophilized overnight at RT using Eppendorf Concentrator Plus. Lyophilized samples were used for semi-quantitative mass spectrometry analyses (see 4.2.6). After elution, beads (Beads after Elution, BaE) were resuspended in 100 µl IP P1 Buffer and 20 µl 6x Laemmli Buffer, boiled for 10 minutes at 95°C, and stored at -20°C until required for subsequent SDS-PAGE analysis (see 4.2.5.2).

4.2.2.16 Yeast affinity purification for downstream in-gel-trypsin digest and mass spectrometry analysis (according to Krogan et al., 2004)

A 100 µl-aliquot of whole cell lysate (WCL), obtained as described in section 4.2.2.13, was kept for subsequent analysis by SDS-PAGE (input fraction) (see 4.2.5.2). Therefore, the aliquot was supplemented with 20 µl 6x Laemmli Buffer, boiled for 10 minutes at 95°C, and stored at -20°C.
The rest of the clarified WCL was transferred to 10.4 ml-Polycarbonate Tube for TFT 70.13 rotor (see Table 11) and tared exactly by filling up with IP P1P Buffer (see Table 9). Ultracentrifugation was performed in TFT 70.13 rotor with Kontron Centrikon Ultracentrifuge T-1170 at 110,000x g for 1 hour at 4°C. After centrifugation, the supernatant (WCL-LF; light fraction) was transferred to 15 ml-falcon tube. The pellet (WCL-HF; heavy fraction) was resuspended in 3 ml IP P1P Buffer and the suspension was transferred to a 15 ml-falcon tube as well. 100 µl of WCL-LF and WCL-HF were saved and prepared for SDS-PAGE as described for WCL. The rests of supernatant and pellet suspensions were incubated for 2 hours at 4°C under gentle rotation with 100 µl slurry of IgG-coupled magnetic beads previously equilibrated for 3 times with 1 ml IP P1 Buffer (see Table 9).
Subsequently, 100 µl of the fractions not associated with the beads (flow-through; FT-LF, FT-HF) were collected and prepared for SDS-PAGE as described for WCL. Remaining flow-through was discarded and beads were washed 3 times with 1 ml IP P1P Buffer and 3 times more with 1 ml IP P1 Buffer. For each wash step beads were resuspended in the corresponding buffer and incubated for 5 minutes at 4°C under gentle rotation. Then, buffer and beads were split using a magnet. 100 µl of last washing step (W-LF, W-HF) was collected and prepared for SDS-PAGE as described for WCL.
For first elution, 50 µl of IP P1 Buffer and 20 µg of TEV Protease (2.6 mg/ml stock) were added to the beads and incubated overnight at 1,400 rpm and 4°C. The elution fraction

was collected by splitting beads and soluble fraction with a magnet. A second elution step was performed by adding 100 µl IP P1 Buffer to the beads and rotating for 2 hours at 16°C. Both elution fractions (E1 and E2) were combined, mixed with 30 µl 6x Laemmli Buffer, boiled for 10 minutes at 95°C, and stored at -20°C. After elution, beads (Beads after Elution, BaE) were resuspended in 100 µl IP P1 Buffer and 20 µl 6x Laemmli Buffer, boiled for 10 minutes at 95°C, and stored at -20°C until required for subsequent SDS-PAGE analysis.
Elution samples were resolved in normal SDS-PAGE for western blot analysis (see 4.2.5.2 and 4.2.5.4), or in commercially available SDS-PAGE using Invitrogen NuPAGE 4-12% Bis-Tris Gel system (see 4.2.5.2) for protein staining with SimplyBlue SafeStain according to manufacturer's instructions (see 4.2.5.3).
Band excision, digestion with trypsin in gel, mass spectrometry analyses on MaXis Mass Spectrometer (Bruker Corporation), and data collection were performed by Dr. Astrid Bruckmann and colleagues at the department of Biochemistry I at the University of Regensburg.

4.2.2.17 Yeast chromatin immunoprecipitation (ChIP)

Three independent cultures of yeast cells in exponential growth phase were used for each strain and treated as described by Bruckmann et al. (2016).
Cultures were performed in 50 ml of appropriate medium till an OD_{600} between 0.5 and 0.8. Afterward, cultures were mixed with 1.4 ml of 37% formaldehyde stock solution (1% formaldehyde final concentration) and incubated for additional 15 minutes in the same growth conditions to crosslink proteins and DNA. The excess of formaldehyde was quenched by addition of 2.7 ml ChIP Quenching Buffer (see Table 9) and cells were incubated for another 5 minutes. Subsequently, cells were harvested by centrifugation at 3,000 rpm for 3 minutes at 4°C.
Cell pellets were washed twice with 20 ml cold 1x PBS (see Table 9) and once with 1 ml cold 1x PBS in order to transfer cells to 1.5 ml-tubes. After centrifugation at 3,000 rpm for 3 minutes at 4°C, supernatant was discarded, and each pellet was resuspended in 400 µl cold ChIP Lysis Buffer (see Table 9). 500 µl ice cold glass beads was added to each sample and cell disruption was performed in Precellys Evolution coupled to Cryolys cooling unit at 4°C with 6 cycles of 30 seconds shaking at 6,000 rpm alternated with 30 seconds pausing. After separation of the glass beads, cell lysates were transferred to 15 ml-falcon tubes and centrifuged at 3,500 rpm for 5 minutes at 4°C. Pellet samples were resuspended in 400 µl ChIP Lysis Buffer and lysate samples were sonicated using Branson Sonifier S-250A. Sonifier was set to output control 3, timer hold, and duty cycle nearly constant. The sonication was done in five rounds consisting of 10 pulses followed by 30 seconds resting in ethanol-ice bath.
Sonicated extracts were transferred to 1.5 ml-tubes and centrifuged at 13,000 rpm (strain having Rpa135 fused to protein A tag; see Table 1) or at 4,000 rpm (all other TAP-tagged strains; see Table 1) for 5 minutes at 4°C. Supernatants containing soluble extracts were put into new 1.5 ml-tubes and RNA concentration was determined. Therefore, absorption at 260 nm using 10 µl of extracts diluted in 1 ml H_2O was measured in Hellma Quartz QS

Micro Cell. Cell extracts were adjusted to a concentration of 4.5 AU_{260} (for Rpa135-ProtA strain) or 9 AU_{260} (for all other strains) in 300 µl ChIP Lysis Buffer.
For each sample 3 aliquots of 20 µl each were saved as "smear", "ChIP input", and "WCL". All samples were stored at -20°C until further use. 200 µl of the lysate was incubated with 50 µl slurry of IgG-coupled magnetic beads overnight at 4°C under gentle rotation. Beads were previously equilibrated by 3 wash steps with 1 ml ChIP Lysis Buffer.

The next day, after split beads and soluble fractions in a magnet, 20 µl of the soluble fractions (flow-through; FT) were collected. WCL and FT samples were subsequently processed for SDS-PAGE (see 4.2.5.2) and western blot analysis (see 4.2.5.4). Therefore, samples were mixed with 4 µl 6x Laemmli Buffer and boiled for 10 minutes at 95°C.
Remaining FT was discarded and beads were washed 3 times with 1 ml ChIP Lysis Buffer, twice with 1 ml ChIP Wash Buffer, twice with 1 ml ChIP Na-Deoxycholate Buffer, and once with 1 ml ChIP TE Buffer, pH 8.0 (see Table 9). For each wash step beads were resuspended in the corresponding buffer and incubated for 5 minutes at 4°C under gentle rotation. Then buffer and beads were split using a magnet. 20 µl of the last washing step (W) for each sample was collected and prepared for SDS-PAGE as described above.
Beads were resuspended in 75 µl ChIP IRN Buffer (see Table 9). 25 µl of bead suspensions were supplemented with 5 µl 6x Laemmli Buffer, boiled for 10 minutes at 95°C, and supernatants were stored at -20°C as eluates (E) for SDS-PAGE.
The remaining 50 µl of "ChIP" suspensions were supplemented with 200 µl ChIP IRN Buffer and 2 µl RNase A (20 mg/ml stock). Samples "smear" and "ChIP input" were thawed and supplemented with 230 µl ChIP IRN Buffer and 2 µl RNase A (20 mg/ml stock). All samples were incubated at 700 rpm for 1 hour at 37°C prior to addition of 10 µl 10% SDS and 2 µl Proteinase K (20 mg/ml stock in 20 mM Tris-HCl, pH 7.4). Samples were first incubated at 700 rpm for 1 hour at 56°C and then overnight at 65°C for reverse crosslinking between amino acids and DNA.

Samples incubated overnight were centrifuged shortly and mixed with 48 µl ChIP IRN Buffer and 4 µl Glycogen (5 mg/ml stock). DNA extraction of these samples was performed by addition of 300 µl Phenol:Chloroform:Isoamylalcohol. Samples were mixed in vortexer for 30 seconds and centrifuged at 13,000 rpm for 5 minutes at RT. 220 µl of the aqueous phases was extracted, transferred to new 1.5 ml-tubes, and precipitated in 600 µl ethanol at -20°C for at least 2 hours.
DNA was finally recovered by centrifugation at 13,000 rpm for 30 minutes at 4°C, supernatants were discarded completely, and DNA pellets were air-dried. "ChIP" and "ChIP input" samples were resuspended in 200 µl ChIP TE Buffer, pH 8.0 and they were analyzed by qPCR (see 4.2.3.2). "Smear" samples were resuspended in 20 µl ChIP TE Buffer, pH 8.0 and resolved by native agarose gel electrophoresis (see 4.2.3.4) to check the length of DNA fragments after sonication.

4.2.2.18 Yeast polysome fractionation with low salt or low Mg^{2+} concentrations

For polysome fractionation with low salt, 200 ml exponentially growing yeast cells (OD_{600} between 0.5 and 0.8) was mixed with 25 mg Cycloheximide and incubated for 5 minutes

on ice with gentle shaking. Cells were harvested by centrifugation at 3,000 rpm for 5 minutes at 4°C and pellets were washed in 20 ml of cold 1x PBS (see Table 9) supplemented with 2 mg Cycloheximide. Afterward, cells were transferred to 50 ml-falcon tubes and centrifuged at 3,000 rpm for 5 minutes at 4°C. Pellets were frozen in liquid nitrogen and stored at -20°C until further use.
For polysome fractionation with low Mg^{2+}, cells were treated as described for low salt conditions but in the absence of Cycloheximide.
Cell pellets were thawed on ice, resuspended in 20 ml Low-Salt or Low-Mg^{2+} Lysis Buffer (see Table 9), respectively, and centrifuged at 3,000 rpm for 3 minutes at 4°C. Cell pellets were resuspended in 500 µl of the respective buffer and mixed with 500 µl ice cold glass beads (diameter 0.75-1.0 mm) for cell lysis. Cell disruption was performed in Precellys Evolution coupled to Cryolys cooling unit at 4°C with 6 cycles of 30 seconds shaking at 6,000 rpm alternated with 30 seconds pausing. After separation of the glass beads, cell lysates were clarified by centrifugation at 13,000 rpm for 10 minutes at 4°C.
Next, concentration of the clarified cell extract was estimated at 260 nm in Hellma Quartz QS Micro Cell using 2 µl and 5 µl of cell extracts in 1 ml of water. Aliquots containing 15 AUs of cell extract were prepared in 150 µl of the respective buffer containing 10% glycerol.
10% and 40% sucrose solutions were prepared freshly in Low-Salt or Low-Mg^{2+} Sucrose Gradient Buffer (see Table 9), respectively. Sucrose gradients were created between 10% and 40% in Beckman Polyallomer Tubes (see Table 11) using the program "SW40 LONG SUCR 10 40" of the Biocomp Gradient Master 107 IP.
150 µl-aliquot of cell extract, corresponding to 15 AU, was added to prepared gradients, which were centrifuged in Beckman Coulter SW40 Ti-rotor at 39,000 rpm for 3 hours at 4°C. Acceleration of Beckman Coulter Optima L-80 X Ultracentrifuge was set to maximum and brake to 5.
After centrifugation, polysome fractionation was conducted in Bio-Rad BioLogic LP Fractionator. Collected absorption data were plotted in Microsoft Excel.

4.2.3 Work with DNA

4.2.3.1 Polymerase chain reaction (PCR)

The proofreading enzyme Herculase II Fusion Polymerase was used for PCR. 50 µl-reactions containing template DNA (30 ng of plasmid DNA obtained as described in section 4.2.1.5 or 100-400 ng of genomic DNA obtained as described in section 4.2.2.9), 1 µl of the Herculase II Fusion DNA Polymerase, 10 µl of 5x Herculase II Reaction Buffer, 0.25 µM of forward and reverse primer, and 250 µM of each dNTP were prepared. Settings of the PCR program were chosen according to manufacturer's instructions and depending on the used oligonucleotides. PCR products were stored at 4°C when required.

4.2.3.2 Quantitative real-time PCR (qPCR)

qPCR was used to determine absolute or relative amounts of specific DNA fragments via fluorescence intensity measurement after each PCR cycle. Therefore, the dye SYBR Green (Roche), which is excited at 509 nm and emits light at 526 nm, was added to qPCR reactions. Since fluorescence emission of SYBR Green is increased 1,000-fold when bound to DNA double helices (Botes et al., 2013), the detected fluorescence intensity correlates with the amount of PCR product present after each cycle.
For qPCR reactions, "ChIP" samples were diluted 10^{-1} in H_2O and "ChIP input" samples were diluted 10^{-2} and 10^{-3} in H_2O. Both sample types were obtained by chromatin immunoprecipitation (ChIP) described in section 4.2.2.17. Furthermore, a serial dilution of genomic DNA, extracted (see 4.2.2.9) from yeast wildtype strain BY4741 (#206; see Table 1), was prepared in H_2O from 10^{-2} to 10^{-5}. This gDNA provides a standard measure to compare amplified products using different primers without a major influence on the individual amplification efficiencies. To improve the statistical analysis, all dilutions obtained for each sample were analyzed by triplicate.
20 µl-reactions, prepared in 100 µl-tubes, contained 4 µl diluted DNA and 16 µl master mix. The master mix consisted of 4 pmol of forward and reverse primers (see Table 4), 0.05 mM of each dNTP, 1 mM of Qiagen Mg^{2+}, 0.25 µl of 1:400,000-diluted Roche SYBR Green (in DMSO and thawed in the dark), 1x Qiagen DNA HotStarTaq DNA Polymerase Buffer, and 0.4 U of Qiagen HotStarTaq DNA Polymerase. qPCR was performed in Corbett Research Rotor Gene RG-3000 device. PCR programs included an initially denaturing step of 10 minutes at 95°C and 40 amplification cycles, consisting of 10 seconds at 95°C, 20 seconds at 56°C, and 30 seconds at 72°C. Furthermore, a DNA melting curve of each sample was recorded by the emission of SYBR Green under the following conditions: an initial step of 90 seconds at pre-melt conditions and a ramp from 72°C to 95°C consisting of individual steps of 5 seconds increasing each time by 0.5°C.
The obtained data were evaluated using the Corbett Research Rotor Gene 6000 Software and further processed in Microsoft Excel considering the dilutions of the different samples.

4.2.3.3 Ethanol precipitation of DNA

To precipitate DNA from PCR reactions (see 4.2.3.1) or digested plasmids (see 4.2.3.7), 0.1 volumes of 3 M NaAc, pH 5.3 were added and mixed before addition of 2.5 volumes of 100% ethanol. Samples were mixed and precipitation was induced by incubation for at least 20 minutes at -20°C. DNA was pelleted by centrifugation at 13,000 rpm for 20 minutes at 4°C. Supernatant was discarded and DNA containing pellet was air-dried for 10 minutes at RT and dissolved in 20 µl H_2O unless stated otherwise.

4.2.3.4 Native agarose gel electrophoresis

Native agarose gel electrophoresis was used to separate DNA fragments of different length.

The electrophoresis was performed with gels composed of 1% (w/v) agarose dissolved in 1x TBE and containing SYBRsafe in a 1:10,000 dilution (see also Table 9). Samples were supplemented with 6x DNA Loading Dye prior to loading on the agarose gel. 1x TBE was used as electrophoresis buffer and gels were run at 180 V and 400 mA. To determine the length of the separated fragments, 1 µg of a DNA standard (1 kb or 2-Log DNA Ladder) was loaded. DNA fragments were visualized by exposing the gel to blue light of 470 nm in Intas Gel Documentation System.

4.2.3.5 Quantitation of DNA

DNA separated by native agarose gel electrophoresis (see 4.2.3.4) and visualized by the Intas Gel Documentation System was quantified with the software MultiGauge v.3.0. Therefore, band intensities of the samples were compared to marker bands of similar size of known concentration. Molar concentrations were calculated, when required, using the molecular weight of random 1 kb dsDNA (0.66 µg kb^{-1} $pmol^{-1}$).

4.2.3.6 AQUA cloning

Advanced quick assembly (AQUA) cloning was performed as described (Beyer et al., 2015; Jacobus and Gross, 2015) in order to re-circularize plasmids mutagenized by PCR (see 4.2.3.1).
In summary, 1 µg of precipitated PCR product (see 4.2.3.3) was digested with 20 U of DpnI in a 20 µl-reaction and incubated for 30 minutes at 37°C. DpnI was inactivated by incubation for 20 minutes at 80°C. 3 µl of DpnI-digested PCR product was diluted in 7 µl H_2O and incubated for 1 hour at RT. Afterward, 3 µl of digested and diluted PCR product was used for transformation of electro-competent *E. coli* cells (see 4.2.1.2).

4.2.3.7 Digestion of DNA with restriction endonucleases

Digestion of DNA (from plasmids obtained as described in section 4.2.1.5 or from PCR obtained as described in section 4.2.3.1) with a variety of restriction endonucleases was performed in buffer and temperature conditions as indicated by NEB. Analytic digestions to screen for clones containing the correct mutations were performed in 10 µl reaction volume, whereas preparative digestions were performed in 100 µl reaction volume. After digestion, the DNA fragments were always resolved by native agarose gel electrophoresis (see 4.2.3.4).

4.2.3.8 Dephosphorylation of vector DNA

To inhibit re-ligation of vector DNA during the ligation reaction (see 4.2.3.10), the vector was dephosphorylated with Antarctic Phosphatase after preparative restriction enzyme digestion (see 4.2.3.7). Therefore, 6 µl of 10x Phosphatase Buffer and 1 µl of Antarctic Phosphatase were added to 100 µl of digestion reaction. Reaction was carried out during 30 minutes at 37°C. Restriction enzymes and phosphatase were heat inactivated by

incubation for 5 minutes at 70°C. Vector DNA was precipitated (see 4.2.3.3) and applied for ligation.

4.2.3.9 Gel extraction of DNA fragments

DNA fragments obtained by preparative digestion (see 4.2.3.7) were resolved on native agarose gels (see 4.2.3.4) and bands of interest were excised from the agarose gel. DNA was purified from the agarose using QIAEX II or QIAquick Gel Extraction Kit and the instructions provided by the manufacturer. The elution of DNA was performed with 20 µl H_2O.

4.2.3.10 DNA Ligation

DNA ligation was used for subcloning of DNA fragments. Therefore, a 10 µl-reaction was prepared containing 0.01 pmol of digested and dephosphorylated vector DNA (see 4.2.3.7 and 4.2.3.8), 0.03 pmol of digested insert DNA (see 4.2.3.7), 1 µl of T4 DNA Ligase Buffer, and 1 µl of T4 DNA Ligase. Reaction was performed for at least 30 minutes at RT and 3 µl of the ligated plasmid DNA was used for transformation of electro-competent *E. coli* cells (see 4.2.1.2).

4.2.3.11 Order of oligonucleotides and sequencing of DNA

The oligonucleotides listed in section 4.1.4 were ordered from Eurofins MWG Operon.
DNA sequencing was performed by the Thermo Fisher GENEART or Microsynth SEQLAB companies with the required oligonucleotides (listed in Table 3) and the conditions demanded from the service providers. Obtained sequences were compared with *in silico* constructs using SnapGene Viewer.

4.2.4 Work with RNA

4.2.4.1 RNA extraction

RNA extractions from cell pellets (obtained as described in sections 4.2.2.8, 4.2.2.11, and 4.2.2.12), whole cell extracts, or affinity purified material (obtained as described in section 4.2.2.14) were performed as described previously (Schmitt et al., 1990).
Briefly, cell pellets were thawed on ice and resuspended in 500 µl NB AE Buffer (see Table 9). Whole cell extracts and affinity purified material were already supplemented with NB AE Buffer (see 4.2.2.14) and thawed on ice. Afterward, samples were mixed with 50 µl 10% SDS and 500 µl phenol equilibrated in NB AE Buffer. Samples were incubated at 1,400 rpm for 4 minutes at 65°C in a thermomixer and subsequently chilled on ice for 2 minutes. After centrifugation at 13,000 rpm for 2 minutes at 4°C, 450 µl of the aqueous phase was collected and mixed with 500 µl of phenol equilibrated in NB AE Buffer in vortexer. Next, the samples were centrifuged at 13,000 rpm for 30 seconds at 4°C and 390 µl of the aqueous phase was mixed with 500 µl of chloroform in new tubes with vortexer.

Afterward, samples were centrifuged, as before, 300 µl of the aqueous phase was collected and mixed with 30 µl 3 M NaAc, pH 5.3 and 800 µl 100% ice cold ethanol. Affinity purified samples were additionally supplemented with 2 µl Glycogen (stock concentration 5 mg/ml) to favor precipitation of low concentrated RNA samples. Precipitation was also favored by incubation for at least 1 hour at -20°C, although samples could also be stored for a long time at this step.
RNA was precipitated by centrifugation at 13,000 rpm for 30 minutes at 4°C and the supernatant was discarded. RNA containing pellets obtained from cells or whole cell extract samples were resuspended in 20 µl H_2O, and RNA concentration was determined in Nanodrop, and adjusted to 1.4 µg/µl (except of 4tU- and [^{3}H]-labeled samples). RNA containing pellets from affinity purified samples were resuspended in 15 µl H_2O and RNA concentration was determined in Nanodrop.

4.2.4.2 Biotinylation of 4tU-labeled samples

Biotin labeling was performed with 50-100 µg of total RNA (see 4.2.4.1), obtained from 4tU-treated cells, and 5 µg MTSEA-Biotin-XX in 1x Biotinylation Buffer (see Table 9) in a total volume of 250 µl by incubation in the dark for 30 minutes (Duffy et al., 2015; Knüppel et al., 2017). Biotinylated RNAs were supplemented with 250 µl NB AE Buffer (see Table 9), extracted once in phenol and once in chloroform, and precipitated (see 4.2.4.1).
After precipitation, pellets were resuspended in 20 µl H_2O and RNA concentration was measured in Nanodrop again.

4.2.4.3 Analysis of RNA with high molecular weight by formaldehyde agarose gel electrophoresis

Denaturing formaldehyde agarose gel electrophoresis was used to separate RNA species longer than 1,000 bases, meaning 25S, 18S rRNAs, and their respective precursor molecules.
Gel contained of 1.2% (w/v) agarose, 2% (v/v) formaldehyde, and 1x NB Formaldehyde Running Buffer (see also Table 9). For sample preparation, 5 µl of the extracted RNA samples (see 4.2.4.1) was mixed with 17 µl of NB Formaldehyde RNA Preparation Buffer (see Table 9), spun down, and incubated for 10 minutes at 65°C. After incubation, samples were cooled down on ice and spun down again. After addition of 2 µl of NB Formaldehyde RNA Loading Buffer (see Table 9), samples were mixed in vortexer, spun down and either half or total volumes of prepared RNA samples were loaded on the gel. Electrophoresis was performed in NB Formaldehyde Agarose Gel Electrophoresis Buffer (see Table 9) for 16 hours at 35 V.
To analyze the conservation of mature rRNA species (25S and 18S), gel was stained for 10 minutes in 200 ml NB Formaldehyde Agarose Gel Staining Solution (see Table 9), washed 2x 20 minutes in 200 ml 0.5x TBE, and RNA containing bands were observed by exposing the gel to UV light of 254 nm.
It is very important to not perform staining of gels when (4tU-labeled) biotinylated RNAs were analyzed.

4.2.4.4 Analysis of RNA with low molecular weight by urea polyacrylamide gel electrophoresis

Denaturing urea polyacrylamide gel electrophoresis was used to separate RNA species between 100 and 500 bases length (meaning tRNAs, snoRNAs, 5S rRNAs, 5.8S rRNAs, and 7S pre-rRNAs).
Gel consisted of 8% (w/v) acrylamide-mix (AA:Bis-AA 37.5:1), 7 M urea, and 0.5x TBE (see also Table 9). 0.5x TBE was used to flush the pockets of the acrylamide gel before loading the RNA samples. For sample preparation, 5 µl of the RNA extracted samples (see 4.2.4.1) was mixed with 10 µl of NB Urea Polyacrylamide RNA Loading Buffer (see Table 9), spun down, and incubated for 15 minutes at 65°C. Afterward, the samples were cooled down on ice, spun down, and either half or total volumes of prepared RNA samples were loaded on the gel. Electrophoresis was performed in 0.5x TBE for 1.5 hours at 150 V.

4.2.4.5 Northern blotting of formaldehyde agarose gel via passive capillary transfer

RNAs separated on formaldehyde agarose gel were transferred and immobilized on positively charged membranes (Positive MP Biomedicals) using passive capillary transfer. Prior to transfer, the agarose gel was washed twice for 5 minutes in H_2O and twice for at least 20 minutes in 10x SSC. Transfer of the RNAs from the agarose gel to the membrane was done during three days by drawing 1 L of transfer buffer (10x SSC) from a downward reservoir through the gel into a stack of paper towels. The RNAs were carried by the buffer stream from the gel to the positively charged membrane.
After the transfer, membranes were dried and RNAs were crosslinked by exposing the membranes to UV light (0.3 J/cm^2) twice in the Fluo-Link device.

4.2.4.6 Northern blotting of urea polyacrylamide gel via electro transfer

RNAs separated on urea polyacrylamide gel were transferred and immobilized on positively charged membranes (Positive MP Biomedicals) by electro transfer. The transfer was performed in 0.5x TBE using a wet tank blotting apparatus and applying 50 V and 400 mA for 80 minutes.
After the transfer, membranes were dried and RNAs were crosslinked by exposing the membranes to UV light (0.3 J/cm^2) twice in the Fluo-Link device.

4.2.4.7 IR-dye conjugated Streptavidin labeling and detection of biotinylated RNA

After blotting and crosslinking (see sections 4.2.4.3 to 4.2.4.6), membranes carrying biotinylated samples (see 4.2.4.2) were blocked for 30 minutes under gentle shaking in Biotin Blocking Buffer (see Table 9). Membranes were incubated for 20 minutes under gentle shaking in the dark at RT with Biotin Staining Buffer (containing IR-dye conjugated Streptavidin from Pierce; see Table 9). Membranes were washed for 10 minutes, twice with Biotin Blocking Buffer, twice with Biotin Wash Buffer 1, and twice with Biotin Wash

Buffer 2 (see Table 9). Wet membranes carrying labeled RNAs were detected using LI-COR Odyssey IR Imaging System.

4.2.4.8 Radioactive probe labeling and detection of RNA

Different (non-labeled) RNA species immobilized on the membranes (see 4.2.4.5 and 4.2.4.6) were detected using specific DNA oligonucleotides listed in Table 5.
The 5' ends of all probes were labeled with [^{32}P]. Therefore, 15 µl-reactions containing 10 pmol of oligonucleotide, 50 µCi of γ-[^{32}P]-ATP, and 10 U T4 PNK were incubated for 45 minutes at 37°C. Reaction was stopped by addition of 30 µl (probes for radioactive primer extension; see 4.2.4.9) or 50 µl TE Buffer, pH 7.5 (probes for northern blot detection). The radioactively labeled probes were purified from non-incorporated nucleotides by centrifugation through a size exclusion column (Bio-Rad Micro Bio-Spin 6 Columns) at 1,000x g for 2 minutes at RT. The incorporated radioactivity was estimated by counting 1 µl of purified labeled probes together with 1.3 ml scintillation solution in a scintillation counter.
Membranes carrying the RNAs were pre-hybridized for at least 20 minutes at 52°C in 20 ml NB Church Buffer (see Table 9) under gentle rotation. Then, total volume of radioactively labeled probe was added and membranes were incubated overnight at 52°C under gentle rotation. Blots were washed twice in 50 ml NB Wash Buffer 1 (see Table 9) for 20 minutes at 52°C. Third wash step was performed in 50 ml NB Wash Buffer 2 (see Table 9) for 20 minutes at 30°C.
Radioactive detection of [^{32}P]-labeled RNAs was acquired by exposing the membranes for different periods to Phosphor Imager Screens (BAS-III Imaging Plate; see Table 12), which were read out by Phosphor Imager (Typhoon FLA-9500). The obtained data were analyzed and further processed using the software MultiGauge v.3.0. After readout, blots detected with [^{32}P]-labeled probes were stripped by incubation with 0.1% SDS solution for 10 minutes at 80°C. Stripping was done to allow detection with different probes or for the save storage of the used membranes.
Radioactive detection of [^{3}H]-labeled RNAs was achieved by exposing the dried and crosslinked membranes for different periods to ultra-sensitive Phosphor Imager Screens (BAS-TR2040 Imaging Plate; see Table 12), which were also read out by Phosphor Imager (Typhoon FLA-9500).

4.2.4.9 Radioactive primer extension with total RNA extracts

Concentration of RNA extracts (obtained as described in section 4.2.4.1) was adjusted with H_2O to 100 ng/µl in 50 µl sample volume.
13 µl-reactions were prepared containing 300 ng RNA extract (3 µl), 2 µl of respective [^{32}P]-labeled probe (see 4.2.4.8), 1 µl of 10 mM dNTP mix, and 7 µl H_2O. Samples were put for 5 minutes at 65°C and for at least 2 minutes on ice. Subsequently, samples were completed to a total volume of 20 µl by addition of 5x First Strand Buffer (Invitrogen), 5 mM DTT (Invitrogen), 40 U RNasin (Promega), and 200 U Superskript III (Invitrogen). Afterward, 20 µl-reactions were incubated for 90 minutes at 46°C to perform the primer

extension. RNAs were hydrolyzed for 30 minutes at 56°C in a total volume of 23 µl containing 110 mM NaOH and 11 mM EDTA, pH 8.0. Samples were completed to a total volume of 140 µl for RNA precipitation by addition of 18 mM HCl, 4 µg Glycogen (stock concentration 5 mg/ml), 660 mM NH_4Ac, and 70% ethanol.
RNAs were incubated overnight at -20°C and precipitated by centrifugation at 13,000 rpm for 15 minutes at 4°C. Pellets were washed in 100 µl ice cold 70% ethanol and dried for 3 minutes at 80°C. PEX RNA Loading Buffer (see Table 9) was diluted 1:2 in H_2O and 10 µl was used to resuspend dried RNA pellets. After shaking for 3 minutes at 75°C, samples were put on ice and 5 µl was used to load PEX sequencing gel.
For preparation of sequencing standard, Thermo Sequenase Cycle Sequencing Kit and plasmid K375 (encoding rDNA locus of *S. cerevisiae*; see Table 2) were used according to manufacturer's instructions in the presence of the corresponding labeled primer. 2.5 µl of sequencing reaction was used to load PEX sequencing gel.
In order to obtain 55 ml of a 5.7% denaturing taurine gel solution, 23.1 g urea, 2.75 ml 20x taurine buffer, 10.45 ml 30% Acryl Solution A, 8.32 ml 2% Bis-Acryl Solution B, 15.4 ml H_2O, 600 µl 10% APS, and 60 µl TEMED were mixed (see also Table 9). PEX sequencing gel was prepared in BioRad Sequi-Gen GT apparatus. Prior to sample loading, pockets were flushed with running buffer (1x Taurine Buffer). Gel was run at 50°C and 70 W for 1.5 to 3 hours. After running, gel was put on Rotilab filter paper type 601 and vacuum dried for 1-2 hours at 80°C.
The corresponding signals were acquired by exposing the membranes for different periods to Phosphor Imager Screens (BAS-III Imaging Plate; see Table 12) that were read out by Phosphor Imager (Typhoon FLA-9500). The obtained data were analyzed and further processed using the software MultiGauge v.3.0.

4.2.5 Work with protein

4.2.5.1 Determination of protein concentration by Bradford Assay

Protein concentrations of cell lysates (see 4.2.1.7 and 4.2.2.13) were determined using the Bio-Rad Protein Assay ("Dye Reagent Concentrate"), which is based on Bradford's method (Bradford, 1976).
In order to create a standard curve to determine the protein concentration, a serial dilution of BSA (stock 10 mg/ml; NEB) was prepared by mixing 0, 2, 4, 6, 8, and 10 µg of BSA in 10 µl of the buffer used for cell lysis. Then, 1:2 and 1:5 dilutions of the cell lysate to be tested were prepared in 10 µl of the buffer used for cell lysis. Finally, the arranged samples were filled to 200 µl with H_2O and 800 µl of 1:4 diluted Bio-Rad Protein Assay was added. After incubation for 5 minutes at RT, the samples were transferred to disposable Semi-Micro cuvettes, and the absorbance was measured at 595 nm.
Absorption data were plotted in Microsoft Excel and protein concentration of the cell lysates was calculated by the BSA standard curve.

4.2.5.2 SDS-polyacrylamide gel electrophoresis (SDS-PAGE)

Proteins were resolved according to their molecular weight using the vertical discontinuous SDS-polyacrylamide gel electrophoresis method introduced by Laemmli (Laemmli, 1970).
The discontinuous system used in this work consisted of a lower resolving gel composed of 8% or 10% acrylamide and an upper stacking gel composed of 5% acrylamide (see Table 9). Gels were run for about 1.5 hours at 180 V and 50 mA in 1x SDS Running Buffer.
Protein eluates used for mass spectrometry analyses were resolved according to their molecular weight in NuPAGE NOVEX 4-12% Mini or Midi gradient gels (Invitrogen). Gels were run for 2 hours at 180 V and 50 mA in 1x MOPS SDS Running Buffer (20x stock; Invitrogen).
Molecular weights of the identified protein bands were estimated using protein markers of known molecular weight (see Table 11).

4.2.5.3 Coomassie staining of SDS-polyacrylamide gels

After running, self-prepared 8% or 10% SDS-polyacrylamide gels (see 4.2.5.2) were stained by incubation in Coomassie Staining Solution (see Table 9) for 2 hours at RT. Then, destaining was performed in Coomassie Destaining Solution (see Table 9) by 3 washes for 30 minutes each at RT. Finally, gels were washed twice in H_2O for 1 hour at RT.
NuPAGE NOVEX 4-12% Mini or Midi gradient gels were stained by SimplyBlue SafeStain (Invitrogen) and decolorized in H_2O according to manufacturer's instructions.
Images were obtained using the Intas Gel Documentation System.

4.2.5.4 Western blotting of SDS-polyacrylamide gels

Proteins resolved by SDS-PAGE (see 4.2.5.2), not stained with Coomassie or SimplyBlue SafeStain (see 4.2.5.3), were transferred to a PVDF membrane using a Thermo Scientific Pierce G2 FastBlotter. The gel and the subjacent PVDF membrane, pre-treated with methanol, were equilibrated in WB Transfer Buffer (see Table 9) and placed in the blotting apparatus between two piles of three Whatman filter papers soaked in WB Transfer Buffer. The transfer was performed during 40 minutes at 25 V (limit) and 500 mA (constant).

4.2.5.5 Ponceau S staining after western blotting

After western blotting (see 4.2.5.4), membranes were stained in Ponceau S Solution (see Table 9) for 3 minutes at RT under gentle shaking. Destaining was performed in H_2O at RT under permanent shaking as required.
Ponceau S staining was used to check protein loading, transfer quality, and to mark the lanes for easier assignment of the lanes during immunodetection (see 4.2.5.6).

4.2.5.6 Immunodetection of transferred proteins

The membrane was blocked, after Ponceau S staining (see 4.2.5.5) and prior to specific immunodetection, with non-related proteins from bovine milk or bovine serum albumin by incubation with 5% (w/v) milk powder or 1.5% (w/v) BSA (only anti-HIS; see Table 7) in 1x TBS-T (see Table 9) under shaking for 1 hour at RT or overnight at 4°C (avoided for detection with anti-HIS). This step avoids unspecific binding of antibodies to the membrane. Antibodies were diluted to their optimal concentration (see Table 7) in 1x TBS-T containing 2% (w/v) milk powder or 1% (w/v) BSA (only anti-HIS). Incubations were performed in sealed foils on a stirring wheel for 1 hour (primary antibodies) or 30 minutes (secondary antibodies) at RT. After the incubation steps with each antibody, the membrane was washed 3 times with 1x TBS-T for 5 minutes under gentle shaking.
In order to detect the specifically bound antibodies, membranes were incubated for about 1 minute at RT with 2 ml BM Chemiluminescence Western Blotting Substrate (Roche), which was prepared according to manufacturer's instructions. This reagent contains hydrogen peroxide and luminal, which is a substrate for the horseradish peroxidase conjugated to the secondary antibodies (or primary antibody in case of anti-PAP and anti-HIS). The light emitted during this reaction at the corresponding specific positions on the membrane was detected with a LAS-3000 Chemiluminescence Imager. A luminescent marker was used to identify the positions of the protein marker bands and the corresponding lanes on the membrane.

4.2.6 Semi quantitative mass spectrometry analysis (according to Jakob et al., 2012 and Ohmayer, PhD thesis, 2014)

4.2.6.1 iTRAQ® labeling of protein samples

Lyophilized samples obtained from the affinity purification using IgG-coupled magnetic beads (see 4.2.2.15) were resuspended in 60 µl Dissolution Buffer (iTRAQ® Reagent Multi-Plex Kit). 20 µl was mixed with 4 µl 6x Laemmli Buffer, boiled for 10 minutes at 95°C, and resolved in SDS-PAGE (eluate fraction; see 4.2.5.2).
The remaining 40 µl was prepared for MS analysis by incubation with 2 µl Reducing Reagent (5 mM Tris-(2-carboxyethyl)phosphine) at 5,000 rpm for 2 hours at 60°C. Free cysteine residues were blocked by incubation with 1 µl Cysteine Blocking Reagent (10 mM methyl-methanethiosulfonate or MMTS) for 10 minutes at RT. Proteins were digested with trypsin by an overnight incubation with 5.5 µg trypsin at 37°C. The tryptic peptides of each individual purification were labeled with one of the four iTRAQ reagents (carrying the reporter groups of 114, 115, 116, and 117 Da) according to manufacturer's instructions. Subsequently, differentially labeled peptides of four purifications were combined, frozen in liquid nitrogen, and lyophilized for about 6 hours. When required samples could be stored at -20°C at this step.
Finally, lyophilized iTRAQ labeled samples were thoroughly resuspended in 30 µl 0.1% (v/v) TFA, mixed, and centrifuged twice at 13,000 rpm for 10 minutes at 4°C to remove

undissolved material. The supernatant was transferred to an appropriate tube, which is compatible with the nano HPLC device.

4.2.6.2 HPLC run

The separation of the iTRAQ labeled tryptic peptides was done on an Ultimate 3000 nano HPLC device from LC Packings (Dionex). Half of the sample (15 µl) was injected with a draw speed of 100 nl/s. Loading occurred with a loading pump flow of 20 µl/min. After loading onto the pre-column (Ø 300 µm x 5 mm; C18 PepMap100, 5 µm particle size, 100 Å pore size (P/N 160454) Thermo Scientific) the sample was eluted from the main column (C18-Pep-Mep column (LC-Packings or Thermo Fischer), Ø 75 µm x 150 mm; 3 µm particle size, 100 Å pore size (P/N 164568)) and a constant micro pump flow of 0.3-0.33 µl/min (depending on the column pressure which should be in a range of 100-130 bar) was started. A gradient of solution A (0.055% (v/v) TFA) and B (80% Acetonitrile (v/v) and 0.05% (v/v) TFA) was run as followed: 0-12 minutes from 5% solution B to 15% solution B; 12-95 minutes from 15% solution B to 37% solution B; 95-143 minutes from 37% solution B to 62% solution B; 143-155 minutes from 62% solution B to 95% solution B; 155-168 minutes constantly 95% solution B; 168-173 minutes from 95% solution B to 5% solution B; 173-180 minutes constantly 5% solution B. In order to control and follow the performance of the nano HPLC device, several parameters were recorded: UV absorbance at 214 nm, loading pump pressure, and micro pump pressure. The signal to start the spotting with the Probot was given between 35 and 45 minutes after loading the sample depending on the UV chromatogram of pre-run standards. The machine was operated with the Chromeleon software.

4.2.6.3 MS plate preparation

To constantly mix the material eluting from the nano HPLC with the MALDI matrix material and to "spot" this mixture on each of the 384 spots of the sample carrier for the mass spectrometer, the "Probot" device (LC packing/Dionex) was used. 5 times the volume eluting from the column of MS Matrix (see Table 9) was added to the elution via a syringe pump. This mixture was spotted for 20 sec on each of the 384 spots resulting in 127 minutes total spotting time.
After the run, 0.6 µl of a peptide calibration mix (a 1:20 dilution of the commercially available 6 Peptide Mixture (AB Sciex; P/N 4368762) in MS Matrix) was spotted manually on each of the 13 calibrations spots distributed over the whole sample plate. When required sample plates could be stored in a dry room at 16°C for up to 4 weeks.

4.2.6.4 Chosen MS and MS/MS settings

All MS analyses were performed on an Applied Biosystems 4800 Proteomics Analyzer MALDI-TOF/TOF mass spectrometer operated in positive ion reflector mode. The m/z range was between 800-4,000 Da (m/z) with a focus mass of 2,000 Da (m/z). In the "MS mode" 50 sub-spectra were recorded for each of the 384 spots with 37 shots per sub-

spectrum. The laser intensity was adapted before each run to achieve an average peak intensity of 10^3-10^4. The sample plate was moved before every sub-spectrum in a "random uniform" manner. Prior to each analysis, an internal calibration using a peptide calibration mix (see 4.2.6.3) was done with the following settings: S/N ratio > 20; Flag mono-isomeric peak; adduct: H; mass tolerance 0.5 m/z; ≥ 5 of the 6 peptides had to match; max. outlier error: 10 ppm; minimum peak width at full width half maximum (FWHM) 2.9 (bins); local noise window width: 250 m/z. Subsequently performed MS and MS/MS modes were based on this calibration.
After the "MS run" (without fragmentation) of each of the 384 spots, all obtained spectra were subjected to an "interpretation" in which the most appropriate ions were selected for fragmentation in the MS/MS mode. All tryptic peptides derived from trypsin itself were excluded for further fragmentation. The "minimum chromatogram peak width" was set to 1 with a fraction to fraction mass tolerance of 200 ppm and a minimum S/N ratio of 10. Precursors of one spot within a resolution of 200 were excluded. For each spot, up to 11 precursors were selected for further fragmentation. The strongest precursor ions were first fragmented.
The MS/MS run was done in an "MS-MS-1kV-positive" operating mode. The fragmentation of the precursor ions occurred via collision induced dissociation (CID). The "metastable suppressor" setting was switched "on". Again, the sample plate was moved before every sub-spectrum. For each selected fragment ion, 50 shots per sub-spectrum added up to a total of 2750 sub-spectra which were added up. The laser intensity for the MS/MS mode was adapted before the run (and was typically 30% higher than the laser intensity chosen for the MS mode).

4.2.6.5 Database search and settings for iTRAQ quantification

The SWISS-PROT protein sequence database implemented in the GPS Explorer software (V.3.6; Applied Biosystems) was used to solve the identity of the peptides and to quantify the respective ratios of the iTRAQ reporter ions. Prior to the database search, the MS/MS spectra had to be filtered with the following settings: mass range: 50-20 Da below precursor mass; minimum S/N filter: 5; mass exclusion tolerance: 3 Da; mass exclusion list: 115.5 Da; peak density filter: 50 peaks per 200 Da; max. Number of peaks: 80.
The search was restricted to proteins from *S. cerevisiae*. Three modifications of the tryptic peptides were set as fixed: the mass of iTRAQ (+145 Da) was added to the N-terminus of each peptide and the ε-amino group of each lysine residue; to cysteine residues the mass of the MMTS was added. Oxidation of methionine residues (methionine-sulfoxid) was set as variable modification (+16 Da). The maximum number of missed trypsin cleavages was set to 1. Further settings: MS/MS fragment tolerance mass: 0.2 Da (monoisotopic); precursor tolerance: 150 ppm; peptide charges: +1; maximum peptide ranks: 2. The total ion score, given as confidence interval (C.I. score) was set at 95%.
For the quantification of the reporter ion peaks a fragment tolerance of 0.1 Da was defined. The correction factors for the iTRAQ reagents, which are given in each kit (iTRAQ® Reagent Multi-Plex Kit; AB Sciex), were considered by the GPS explorer software during the calculation.

4.2.6.6 Analysis of MS raw data

The iTRAQ ratios were obtained by setting one of the four labeled samples (e.g. wildtype sample) as reference for the three remaining samples. In this way, three iTRAQ ratios, each referring to the reference, were obtained for each protein found. The proteins were transformed and expressed in a log2 scale to depict ratios below and above 1 in an equivalent way. For normalization, the ratios of the bait protein were set one, demonstrated as zero in log2 scale. iTRAQ ratios > 1 mean that the respective protein is enriched, whereas a value < 1 means that the respective protein is depleted under the tested conditions referred to the reference.

5. References

Allmang, C., and Tollervey, D. (1998). The role of the 3' external transcribed spacer in yeast pre-rRNA processing. J. Mol. Biol. *278*, 67–78.

Allmang, C., Henry, Y., Wood, H., Morrissey, J.P., Petfalski, E., and Tollervey, D. (1996). Recognition of cleavage site A(2) in the yeast pre-rRNA. RNA N. Y. N *2*, 51–62.

Allmang, C., Mitchell, P., Petfalski, E., and Tollervey, D. (2000). Degradation of ribosomal RNA precursors by the exosome. Nucleic Acids Res. *28*, 1684–1691.

Asano, N., Kato, K., Nakamura, A., Komoda, K., Tanaka, I., and Yao, M. (2015). Structural and functional analysis of the Rpf2-Rrs1 complex in ribosome biogenesis. Nucleic Acids Res. *43*, 4746–4757.

Atzorn, V., Fragapane, P., and Kiss, T. (2004). U17/snR30 is a ubiquitous snoRNA with two conserved sequence motifs essential for 18S rRNA production. Mol. Cell. Biol. *24*, 1769–1778.

Babiano, R., Badis, G., Saveanu, C., Namane, A., Doyen, A., Díaz-Quintana, A., Jacquier, A., Fromont-Racine, M., and de la Cruz, J. (2013). Yeast ribosomal protein L7 and its homologue Rlp7 are simultaneously present at distinct sites on pre-60S ribosomal particles. Nucleic Acids Res. *41*, 9461–9470.

Baim, S.B., Pietras, D.F., Eustice, D.C., and Sherman, F. (1985). A mutation allowing an mRNA secondary structure diminishes translation of Saccharomyces cerevisiae iso-1-cytochrome c. Mol. Cell. Biol. *5*, 1839–1846.

Barandun, J., Chaker-Margot, M., Hunziker, M., Molloy, K.R., Chait, B.T., and Klinge, S. (2017). The complete structure of the small-subunit processome. Nat. Struct. Mol. Biol. *24*, 944–953.

Barandun, J., Hunziker, M., and Klinge, S. (2018). Assembly and structure of the SSU processome — a nucleolar precursor of the small ribosomal subunit. Curr. Opin. Struct. Biol. *49*, 85–93.

Barrio-Garcia, C., Thoms, M., Flemming, D., Kater, L., Berninghausen, O., Baßler, J., Beckmann, R., and Hurt, E. (2016). Architecture of the Rix1–Rea1 checkpoint machinery during pre-60S-ribosome remodeling. Nat. Struct. Mol. Biol. *23*, 37–44.

Baßler, J., Grandi, P., Gadal, O., Leßmann, T., Petfalski, E., Tollervey, D., Lechner, J., and Hurt, E. (2001). Identification of a 60S Preribosomal Particle that Is Closely Linked to Nuclear Export. Mol. Cell *8*, 517–529.

Bassler, J., Kallas, M., Pertschy, B., Ulbrich, C., Thoms, M., and Hurt, E. (2010). The AAA-ATPase Rea1 drives removal of biogenesis factors during multiple stages of 60S ribosome assembly. Mol. Cell *38*, 712–721.

van Beekvelt, C.A., Kooi, E.A., de Graaff-Vincent, M., Riet, J., Venema, J., and Raué, H.A. (2000). Domain III of Saccharomyces cerevisiae 25 S ribosomal RNA: its role in binding of ribosomal protein L25 and 60 S subunit formation. J. Mol. Biol. *296*, 7–17.

Belhabich-Baumas, K., Joret, C., Jády, B.E., Plisson-Chastang, C., Shayan, R., Klopp, C., Henras, A.K., Henry, Y., and Mougin, A. (2017). The Rio1p ATPase hinders premature entry into translation of late pre-40S pre-ribosomal particles. Nucleic Acids Res. *45*, 10824–10836.

Bellí, G., Garí, E., Piedrafita, L., Aldea, M., and Herrero, E. (1998). An activator/repressor dual system allows tight tetracycline-regulated gene expression in budding yeast. Nucleic Acids Res. *26*, 942–947.

Beltrame, M., and Tollervey, D. (1992). Identification and functional analysis of two U3 binding sites on yeast pre-ribosomal RNA. EMBO J. *11*, 1531–1542.

Beltrame, M., and Tollervey, D. (1995). Base pairing between U3 and the pre-ribosomal RNA is required for 18S rRNA synthesis. EMBO J. *14*, 4350–4356.

Beltrame, M., Henry, Y., and Tollervey, D. (1994). Mutational analysis of an essential binding site for the U3 snoRNA in the 5' external transcribed spacer of yeast pre-rRNA. Nucleic Acids Res. *22*, 5139–5147.

Ben-Shem, A., Garreau de Loubresse, N., Melnikov, S., Jenner, L., Yusupova, G., and Yusupov, M. (2011). The structure of the eukaryotic ribosome at 3.0 Å resolution. Science *334*, 1524–1529.

Bernstein, J., Patterson, D.N., Wilson, G.M., and Toth, E.A. (2008). Characterization of the essential activities of Saccharomyces cerevisiae Mtr4p, a 3'->5' helicase partner of the nuclear exosome. J. Biol. Chem. *283*, 4930–4942.

Beyer, H.M., Gonschorek, P., Samodelov, S.L., Meier, M., Weber, W., and Zurbriggen, M.D. (2015). AQUA Cloning: A Versatile and Simple Enzyme-Free Cloning Approach. PloS One *10*, e0137652.

Biedka, S., Wu, S., LaPeruta, A.J., Gao, N., and Woolford, J.L. (2017). Insights into remodeling events during eukaryotic large ribosomal subunit assembly provided by high resolution cryo-EM structures. RNA Biol. *14*, 1306–1313.

Biedka, S., Micic, J., Wilson, D., Brown, H., Diorio-Toth, L., and Woolford, J.L. (2018). Hierarchical recruitment of ribosomal proteins and assembly factors remodels nucleolar pre-60S ribosomes. J. Cell Biol. *217*, 2503–2518.

Billy, E., Wegierski, T., Nasr, F., and Filipowicz, W. (2000). Rcl1p, the yeast protein similar to the RNA 3'-phosphate cyclase, associates with U3 snoRNP and is required for 18S rRNA biogenesis. EMBO J. *19*, 2115–2126.

Bleichert, F., Granneman, S., Osheim, Y.N., Beyer, A.L., and Baserga, S.J. (2006). The PINc domain protein Utp24, a putative nuclease, is required for the early cleavage steps in 18S rRNA maturation. Proc. Natl. Acad. Sci. U. S. A. *103*, 9464–9469.

Bohnsack, M.T., Kos, M., and Tollervey, D. (2008). Quantitative analysis of snoRNA association with pre-ribosomes and release of snR30 by Rok1 helicase. EMBO Rep. *9*, 1230–1236.

Bohnsack, M.T., Martin, R., Granneman, S., Ruprecht, M., Schleiff, E., and Tollervey, D. (2009). Prp43 bound at different sites on the pre-rRNA performs distinct functions in ribosome synthesis. Mol. Cell *36*, 583–592.

Boissier, F., Schmidt, C.M., Linnemann, J., Fribourg, S., and Perez-Fernandez, J. (2017). Pwp2 mediates UTP-B assembly via two structurally independent domains. Sci. Rep. *7*, 3169.

Botes, M., de Kwaadsteniet, M., and Cloete, T.E. (2013). Application of quantitative PCR for the detection of microorganisms in water. Anal. Bioanal. Chem. *405*, 91–108.

Bradatsch, B., Leidig, C., Granneman, S., Gnädig, M., Tollervey, D., Böttcher, B., Beckmann, R., and Hurt, E. (2012). Structure of the pre-60S ribosomal subunit with nuclear export factor Arx1 bound at the exit tunnel. Nat. Struct. Mol. Biol. *19*, 1234–1241.

Bradford, M.M. (1976). A rapid and sensitive method for the quantitation of microgram quantities of protein utilizing the principle of protein-dye binding. Anal. Biochem. *72*, 248–254.

Brandman, O., and Hegde, R.S. (2016). Ribosome-associated protein quality control. Nat. Struct. Mol. Biol. *23*, 7–15.

Brandman, O., Stewart-Ornstein, J., Wong, D., Larson, A., Williams, C.C., Li, G.-W., Zhou, S., King, D., Shen, P.S., Weibezahn, J., et al. (2012). A ribosome-bound quality control complex triggers degradation of nascent peptides and signals translation stress. Cell *151*, 1042–1054.

Braun, C.M., Hackert, P., Schmid, C.E., Bohnsack, M.T., Bohnsack, K.E., and Perez-Fernandez, J. (2020). Pol5 is required for recycling of small subunit biogenesis factors and for formation of the peptide exit tunnel of the large ribosomal subunit. Nucleic Acids Res. *48*, 405–420.

Bruckmann, A., Linnemann, J., and Perez-Fernandez, J. (2016). Purification of RNA Polymerase I-Associated Chromatin from Yeast Cells. In The Nucleolus, A. Németh, ed. (New York, NY: Springer New York), pp. 213–223.

Brüning, L., Hackert, P., Martin, R., Davila Gallesio, J., Aquino, G.R.R., Urlaub, H., Sloan, K.E., and Bohnsack, M.T. (2018). RNA helicases mediate structural transitions and compositional changes in pre-ribosomal complexes. Nat. Commun. *9*, 5383.

Bussiere, C., Hashem, Y., Arora, S., Frank, J., and Johnson, A.W. (2012). Integrity of the P-site is probed during maturation of the 60S ribosomal subunit. J. Cell Biol. *197*, 747–759.

Carlson, M. (1987). Regulation of sugar utilization in Saccharomyces species. J. Bacteriol. *169*, 4873–4877.

Cepeda, L.P.P., Bagatelli, F.F.M., Santos, R.M., Santos, M.D.M., Nogueira, F.C.S., and Oliveira, C.C. (2019). The ribosome assembly factor Nop53 controls association of the RNA exosome with pre-60S particles in yeast. J. Biol. Chem. *294*, 19365–19380.

Chaker-Margot, M. (2018). Assembly of the small ribosomal subunit in yeast: mechanism and regulation. RNA N. Y. N *24*, 881–891.

Chaker-Margot, M., and Klinge, S. (2019). Assembly and early maturation of large subunit precursors. RNA N. Y. N *25*, 465–471.

Chaker-Margot, M., Hunziker, M., Barandun, J., Dill, B.D., and Klinge, S. (2015). Stage-specific assembly events of the 6-MDa small-subunit processome initiate eukaryotic ribosome biogenesis. Nat. Struct. Mol. Biol. *22*, 920–923.

Chaker-Margot, M., Barandun, J., Hunziker, M., and Klinge, S. (2017). Architecture of the yeast small subunit processome. Science *355*.

Chamberlain, J.R., Lee, Y., Lane, W.S., and Engelke, D.R. (1998). Purification and characterization of the nuclear RNase P holoenzyme complex reveals extensive subunit overlap with RNase MRP. Genes Dev. *12*, 1678–1690.

Chao, F.C. (1957). Dissociation of macromolecular ribonucleoprotein of yeast. Arch. Biochem. Biophys. *70*, 426–431.

Chen, W., Xie, Z., Yang, F., and Ye, K. (2017). Stepwise assembly of the earliest precursors of large ribosomal subunits in yeast. Nucleic Acids Res. *45*, 6837–6847.

Cheng, J., Kellner, N., Berninghausen, O., Hurt, E., and Beckmann, R. (2017). 3.2-Å-resolution structure of the 90S preribosome before A1 pre-rRNA cleavage. Nat. Struct. Mol. Biol. *24*, 954–964.

Cheng, Z., Mugler, C.F., Keskin, A., Hodapp, S., Chan, L.Y.-L., Weis, K., Mertins, P., Regev, A., Jovanovic, M., and Brar, G.A. (2019). Small and Large Ribosomal Subunit Deficiencies Lead to Distinct Gene Expression Signatures that Reflect Cellular Growth Rate. Mol. Cell *73*, 36-47.e10.

Choque, E., Schneider, C., Gadal, O., and Dez, C. (2018). Turnover of aberrant pre-40S pre-ribosomal particles is initiated by a novel endonucleolytic decay pathway. Nucleic Acids Res. *46*, 4699–4714.

Chu, S., Archer, R.H., Zengel, J.M., and Lindahl, L. (1994). The RNA of RNase MRP is required for normal processing of ribosomal RNA. Proc. Natl. Acad. Sci. U. S. A. *91*, 659–663.

Coleman, A.W. (2015). Nuclear rRNA transcript processing versus internal transcribed spacer secondary structure. Trends Genet. TIG *31*, 157–163.

Collins, J.C., Ghalei, H., Doherty, J.R., Huang, H., Culver, R.N., and Karbstein, K. (2018). Ribosome biogenesis factor Ltv1 chaperones the assembly of the small subunit head. J. Cell Biol. *217*, 4141–4154.

Combs, D.J., Nagel, R.J., Ares, M., and Stevens, S.W. (2006). Prp43p is a DEAH-box spliceosome disassembly factor essential for ribosome biogenesis. Mol. Cell. Biol. *26*, 523–534.

Costello, J.L., Stead, J.A., Feigenbutz, M., Jones, R.M., and Mitchell, P. (2011). The C-terminal region of the exosome-associated protein Rrp47 is specifically required for box C/D small nucleolar RNA 3'-maturation. J. Biol. Chem. *286*, 4535–4543.

Côté, C.A., Greer, C.L., and Peculis, B.A. (2002). Dynamic conformational model for the role of ITS2 in pre-rRNA processing in yeast. RNA N. Y. N *8*, 786–797.

de la Cruz, J., Kressler, D., Tollervey, D., and Linder, P. (1998a). Dob1p (Mtr4p) is a putative ATP-dependent RNA helicase required for the 3' end formation of 5.8S rRNA in Saccharomyces cerevisiae. EMBO J. *17*, 1128–1140.

de la Cruz, J., Kressler, D., Rojo, M., Tollervey, D., and Linder, P. (1998b). Spb4p, an essential putative RNA helicase, is required for a late step in the assembly of 60S ribosomal subunits in Saccharomyces cerevisiae. RNA N. Y. N *4*, 1268–1281.

de la Cruz, J., Lacombe, T., Deloche, O., Linder, P., and Kressler, D. (2004). The putative RNA helicase Dbp6p functionally interacts with Rpl3p, Nop8p and the novel trans-acting Factor Rsa3p during biogenesis of 60S ribosomal subunits in Saccharomyces cerevisiae. Genetics *166*, 1687–1699.

de la Cruz, J., Karbstein, K., and Woolford, J.L. (2015). Functions of Ribosomal Proteins in Assembly of Eukaryotic Ribosomes In Vivo. Annu. Rev. Biochem. *84*, 93–129.

Delan-Forino, C., Schneider, C., and Tollervey, D. (2017). Transcriptome-wide analysis of alternative routes for RNA substrates into the exosome complex. PLoS Genet. *13*, e1006699.

Deley, J. (1964). SEDIMENTATION COEFFICIENTS OF YEAST RIBOSOMES. J. Gen. Microbiol. *37*, 153–156.

Delprato, A., Al Kadri, Y., Pérébaskine, N., Monfoulet, C., Henry, Y., Henras, A.K., and Fribourg, S. (2014). Crucial role of the Rcl1p-Bms1p interaction for yeast pre-ribosomal RNA processing. Nucleic Acids Res. *42*, 10161–10172.

Dembowski, J.A., Kuo, B., and Woolford, J.L. (2013a). Has1 regulates consecutive maturation and processing steps for assembly of 60S ribosomal subunits. Nucleic Acids Res. *41*, 7889–7904.

Dembowski, J.A., Ramesh, M., McManus, C.J., and Woolford, J.L. (2013b). Identification of the binding site of Rlp7 on assembling 60S ribosomal subunits in Saccharomyces cerevisiae. RNA N. Y. N *19*, 1639–1647.

Dez, C., Houseley, J., and Tollervey, D. (2006). Surveillance of nuclear-restricted pre-ribosomes within a subnucleolar region of Saccharomyces cerevisiae. EMBO J. *25*, 1534–1546.

Dieci, G., Fiorino, G., Castelnuovo, M., Teichmann, M., and Pagano, A. (2007). The expanding RNA polymerase III transcriptome. Trends Genet. TIG *23*, 614–622.

Dinman, J.D. (2005). 5S rRNA: Structure and Function from Head to Toe. Int. J. Biomed. Sci. IJBS *1*, 2–7.

Doma, M.K., and Parker, R. (2006). Endonucleolytic cleavage of eukaryotic mRNAs with stalls in translation elongation. Nature *440*, 561–564.

D'Orazio, K.N., Wu, C.C.-C., Sinha, N., Loll-Krippleber, R., Brown, G.W., and Green, R. (2019). The endonuclease Cue2 cleaves mRNAs at stalled ribosomes during No Go Decay. ELife *8*.

Dosil, M., and Bustelo, X.R. (2004). Functional characterization of Pwp2, a WD family protein essential for the assembly of the 90 S pre-ribosomal particle. J. Biol. Chem. *279*, 37385–37397.

Dragon, F., Gallagher, J.E.G., Compagnone-Post, P.A., Mitchell, B.M., Porwancher, K.A., Wehner, K.A., Wormsley, S., Settlage, R.E., Shabanowitz, J., Osheim, Y., et al. (2002). A large nucleolar U3 ribonucleoprotein required for 18S ribosomal RNA biogenesis. Nature *417*, 967–970.

Duffy, E.E., Rutenberg-Schoenberg, M., Stark, C.D., Kitchen, R.R., Gerstein, M.B., and Simon, M.D. (2015). Tracking Distinct RNA Populations Using Efficient and Reversible Covalent Chemistry. Mol. Cell *59*, 858–866.

Duffy, E.E., Schofield, J.A., and Simon, M.D. (2019). Gaining insight into transcriptome-wide RNA population dynamics through the chemistry of 4-thiouridine. Wiley Interdiscip. Rev. RNA *10*, e1513.

Dunbar, D.A., Dragon, F., Lee, S.J., and Baserga, S.J. (2000). A nucleolar protein related to ribosomal protein L7 is required for an early step in large ribosomal subunit biogenesis. Proc. Natl. Acad. Sci. U. S. A. *97*, 13027–13032.

Dutca, L.M., Gallagher, J.E.G., and Baserga, S.J. (2011). The initial U3 snoRNA:pre-rRNA base pairing interaction required for pre-18S rRNA folding revealed by in vivo chemical probing. Nucleic Acids Res. *39*, 5164–5180.

El Hage, A., Koper, M., Kufel, J., and Tollervey, D. (2008). Efficient termination of transcription by RNA polymerase I requires the 5' exonuclease Rat1 in yeast. Genes Dev. *22*, 1069–1081.

Elela, S.A., Igel, H., and Ares, M. (1996). RNase III cleaves eukaryotic preribosomal RNA at a U3 snoRNP-dependent site. Cell *85*, 115–124.

Engel, C., Neyer, S., and Cramer, P. (2018). Distinct Mechanisms of Transcription Initiation by RNA Polymerases I and II. Annu. Rev. Biophys. *47*, 425–446.

Eppens, N.A., Rensen, S., Granneman, S., Raué, H.A., and Venema, J. (1999). The roles of Rrp5p in the synthesis of yeast 18S and 5.8S rRNA can be functionally and physically separated. RNA N. Y. N *5*, 779–793.

Faber, A.W., Van Dijk, M., Raué, H.A., and Vos, J.C. (2002). Ngl2p is a Ccr4p-like RNA nuclease essential for the final step in 3'-end processing of 5.8S rRNA in Saccharomyces cerevisiae. RNA N. Y. N *8*, 1095–1101.

Faber, A.W., Vos, H.R., Vos, J.C., and Raué, H.A. (2006). 5'-end formation of yeast 5.8SL rRNA is an endonucleolytic event. Biochem. Biophys. Res. Commun. *345*, 796–802.

Falk, S., Tants, J.-N., Basquin, J., Thoms, M., Hurt, E., Sattler, M., and Conti, E. (2017). Structural insights into the interaction of the nuclear exosome helicase Mtr4 with the preribosomal protein Nop53. RNA N. Y. N *23*, 1780–1787.

Fatica, A., Oeffinger, M., Dlakić, M., and Tollervey, D. (2003). Nob1p is required for cleavage of the 3' end of 18S rRNA. Mol. Cell. Biol. *23*, 1798–1807.

Fatica, A., Tollervey, D., and Dlakić, M. (2004). PIN domain of Nob1p is required for D-site cleavage in 20S pre-rRNA. RNA N. Y. N *10*, 1698–1701.

Fayet-Lebaron, E., Atzorn, V., Henry, Y., and Kiss, T. (2009). 18S rRNA processing requires base pairings of snR30 H/ACA snoRNA to eukaryote-specific 18S sequences. EMBO J. *28*, 1260–1270.

Fernández-Pevida, A., Kressler, D., and de la Cruz, J. (2015). Processing of preribosomal RNA in Saccharomyces cerevisiae. Wiley Interdiscip. Rev. RNA *6*, 191–209.

Ferreira-Cerca, S., Pöll, G., Gleizes, P.-E., Tschochner, H., and Milkereit, P. (2005). Roles of eukaryotic ribosomal proteins in maturation and transport of pre-18S rRNA and ribosome function. Mol. Cell *20*, 263–275.

Ferreira-Cerca, S., Sagar, V., Schäfer, T., Diop, M., Wesseling, A.-M., Lu, H., Chai, E., Hurt, E., and LaRonde-LeBlanc, N. (2012). ATPase-dependent role of the atypical kinase Rio2 on the evolving pre-40S ribosomal subunit. Nat. Struct. Mol. Biol. *19*, 1316–1323.

Foiani, M., Cigan, A.M., Paddon, C.J., Harashima, S., and Hinnebusch, A.G. (1991). GCD2, a translational repressor of the GCN4 gene, has a general function in the initiation of protein synthesis in Saccharomyces cerevisiae. Mol. Cell. Biol. *11*, 3203–3216.

Francisco-Velilla, R., Remacha, M., and Ballesta, J.P.G. (2013). Carboxy terminal modifications of the P0 protein reveal alternative mechanisms of nuclear ribosomal stalk assembly. Nucleic Acids Res. *41*, 8628–8636.

French, S.L., Osheim, Y.N., Cioci, F., Nomura, M., and Beyer, A.L. (2003). In exponentially growing Saccharomyces cerevisiae cells, rRNA synthesis is determined by the summed RNA polymerase I loading rate rather than by the number of active genes. Mol. Cell. Biol. *23*, 1558–1568.

Fromm, L., Falk, S., Flemming, D., Schuller, J.M., Thoms, M., Conti, E., and Hurt, E. (2017). Reconstitution of the complete pathway of ITS2 processing at the pre-ribosome. Nat. Commun. *8*, 1787.

Fuentes, J.L., Datta, K., Sullivan, S.M., Walker, A., and Maddock, J.R. (2007). In vivo functional characterization of the Saccharomyces cerevisiae 60S biogenesis GTPase Nog1. Mol. Genet. Genomics MGG *278*, 105–123.

Gadal, O., Strauss, D., Braspenning, J., Hoepfner, D., Petfalski, E., Philippsen, P., Tollervey, D., and Hurt, E. (2001). A nuclear AAA-type ATPase (Rix7p) is required for biogenesis and nuclear export of 60S ribosomal subunits. EMBO J. *20*, 3695–3704.

Gadal, O., Strauss, D., Petfalski, E., Gleizes, P.-E., Gas, N., Tollervey, D., and Hurt, E. (2002). Rlp7p is associated with 60S preribosomes, restricted to the granular component of the nucleolus, and required for pre-rRNA processing. J. Cell Biol. *157*, 941–951.

Gallagher, J.E.G. (2019). Proteins and RNA sequences required for the transition of the t-Utp complex into the SSU processome. FEMS Yeast Res. *19*.

Gallagher, J.E.G., Dunbar, D.A., Granneman, S., Mitchell, B.M., Osheim, Y., Beyer, A.L., and Baserga, S.J. (2004). RNA polymerase I transcription and pre-rRNA processing are linked by specific SSU processome components. Genes Dev. *18*, 2506–2517.

Gamalinda, M., Jakovljevic, J., Babiano, R., Talkish, J., de la Cruz, J., and Woolford, J.L. (2013). Yeast polypeptide exit tunnel ribosomal proteins L17, L35 and L37 are necessary to recruit late-assembling factors required for 27SB pre-rRNA processing. Nucleic Acids Res. *41*, 1965–1983.

Gamalinda, M., Ohmayer, U., Jakovljevic, J., Kumcuoglu, B., Woolford, J., Mbom, B., Lin, L., and Woolford, J.L. (2014). A hierarchical model for assembly of eukaryotic 60S ribosomal subunit domains. Genes Dev. *28*, 198–210.

Garcia-Gomez, J.J., Lebaron, S., Froment, C., Monsarrat, B., Henry, Y., and de la Cruz, J. (2011). Dynamics of the Putative RNA Helicase Spb4 during Ribosome Assembly in Saccharomyces cerevisiae. Mol. Cell. Biol. *31*, 4156–4164.

Garí, E., Piedrafita, L., Aldea, M., and Herrero, E. (1997). A set of vectors with a tetracycline-regulatable promoter system for modulated gene expression in Saccharomyces cerevisiae. Yeast Chichester Engl. *13*, 837–848.

Gartmann, M., Blau, M., Armache, J.-P., Mielke, T., Topf, M., and Beckmann, R. (2010). Mechanism of eIF6-mediated inhibition of ribosomal subunit joining. J. Biol. Chem. *285*, 14848–14851.

Gasse, L., Flemming, D., and Hurt, E. (2015). Coordinated Ribosomal ITS2 RNA Processing by the Las1 Complex Integrating Endonuclease, Polynucleotide Kinase, and Exonuclease Activities. Mol. Cell *60*, 808–815.

Geerlings, T.H., Vos, J.C., and Raué, H.A. (2000). The final step in the formation of 25S rRNA in Saccharomyces cerevisiae is performed by 5'-->3' exonucleases. RNA N. Y. N *6*, 1698–1703.

Gérczei, T., Shah, B.N., Manzo, A.J., Walter, N.G., and Correll, C.C. (2009). RNA Chaperones Stimulate Formation and Yield of the U3 snoRNA–Pre-rRNA Duplexes Needed for Eukaryotic Ribosome Biogenesis. J. Mol. Biol. *390*, 991–1006.

Ghalei, H., Trepreau, J., Collins, J.C., Bhaskaran, H., Strunk, B.S., and Karbstein, K. (2017). The ATPase Fap7 Tests the Ability to Carry Out Translocation-like Conformational Changes and Releases Dim1 during 40S Ribosome Maturation. Mol. Cell *67*, 990-1000.e3.

Gijsbers, A., García-Márquez, A., Luviano, A., and Sánchez-Puig, N. (2013). Guanine nucleotide exchange in the ribosomal GTPase EFL1 is modulated by the protein mutated in the Shwachman-Diamond syndrome. Biochem. Biophys. Res. Commun. *437*, 349–354.

Granato, D.C., Gonzales, F.A., Luz, J.S., Cassiola, F., Machado-Santelli, G.M., and Oliveira, C.C. (2005). Nop53p, an essential nucleolar protein that interacts with Nop17p and Nip7p, is required for pre-rRNA processing in Saccharomyces cerevisiae. FEBS J. *272*, 4450–4463.

Granneman, S., Petfalski, E., and Tollervey, D. (2011). A cluster of ribosome synthesis factors regulate pre-rRNA folding and 5.8S rRNA maturation by the Rat1 exonuclease. EMBO J. *30*, 4006–4019.

Greber, B.J., Gerhardy, S., Leitner, A., Leibundgut, M., Salem, M., Boehringer, D., Leulliot, N., Aebersold, R., Panse, V.G., and Ban, N. (2016). Insertion of the Biogenesis Factor Rei1 Probes the Ribosomal Tunnel during 60S Maturation. Cell *164*, 91–102.

Gregory, B., Rahman, N., Bommakanti, A., Shamsuzzaman, M., Thapa, M., Lescure, A., Zengel, J.M., and Lindahl, L. (2019). The small and large ribosomal subunits depend on each other for stability and accumulation. Life Sci. Alliance *2*, e201800150.

Grenson, M. (1969). The utilization of exogenous pyrimidines and the recycling of uridine-5'-phosphate derivatives in Saccharomyces cerevisiae, as studied by means of mutants affected in pyrimidine uptake and metabolism. Eur. J. Biochem. *11*, 249–260.

Harnpicharnchai, P., Jakovljevic, J., Horsey, E., Miles, T., Roman, J., Rout, M., Meagher, D., Imai, B., Guo, Y., Brame, C.J., et al. (2001). Composition and Functional Characterization of Yeast 66S Ribosome Assembly Intermediates. Mol. Cell *8*, 505–515.

Hector, R.D., Burlacu, E., Aitken, S., Bihan, T.L., Tuijtel, M., Zaplatina, A., Cook, A.G., and Granneman, S. (2014). Snapshots of pre-rRNA structural flexibility reveal eukaryotic 40S assembly dynamics at nucleotide resolution. Nucleic Acids Res. *42*, 12138–12154.

Helser, T.L., Baan, R.A., and Dahlberg, A.E. (1981). Characterization of a 40S ribosomal subunit complex in polyribosomes of Saccharomyces cerevisiae treated with cycloheximide. Mol. Cell. Biol. *1*, 51–57.

Henry, Y., Wood, H., Morrissey, J.P., Petfalski, E., Kearsey, S., and Tollervey, D. (1994). The 5' end of yeast 5.8S rRNA is generated by exonucleases from an upstream cleavage site. EMBO J. *13*, 2452–2463.

Herzog, V.A., Reichholf, B., Neumann, T., Rescheneder, P., Bhat, P., Burkard, T.R., Wlotzka, W., von Haeseler, A., Zuber, J., and Ameres, S.L. (2017). Thiol-linked alkylation of RNA to assess expression dynamics. Nat. Methods *14*, 1198–1204.

Heuer, A., Thomson, E., Schmidt, C., Berninghausen, O., Becker, T., Hurt, E., and Beckmann, R. (2017). Cryo-EM structure of a late pre-40S ribosomal subunit from Saccharomyces cerevisiae. ELife *6*.

Hierlmeier, T., Merl, J., Sauert, M., Perez-Fernandez, J., Schultz, P., Bruckmann, A., Hamperl, S., Ohmayer, U., Rachel, R., Jacob, A., et al. (2013). Rrp5p, Noc1p and Noc2p form a protein module which is part of early large ribosomal subunit precursors in S. cerevisiae. Nucleic Acids Res. *41*, 1191–1210.

Hitchen, J., Ivakine, E., Melekhovets, Y.F., Lalev, A., and Nazar, R.N. (1997). Structural features in the 3' external transcribed spacer affecting intragenic processing of yeast rRNA. J. Mol. Biol. *274*, 481–490.

Hochstatter, J., Hölzel, M., Rohrmoser, M., Schermelleh, L., Leonhardt, H., Keough, R., Gonda, T.J., Imhof, A., Eick, D., Längst, G., et al. (2012). Myb-binding Protein 1a (Mybbp1a) Regulates Levels and Processing of Pre-ribosomal RNA. J. Biol. Chem. *287*, 24365–24377.

Hong, B., Brockenbrough, J.S., Wu, P., and Aris, J.P. (1997). Nop2p is required for pre-rRNA processing and 60S ribosome subunit synthesis in yeast. Mol. Cell. Biol. *17*, 378–388.

van Hoof, A., Lennertz, P., and Parker, R. (2000). Three conserved members of the RNase D family have unique and overlapping functions in the processing of 5S, 5.8S, U4, U5, RNase MRP and RNase P RNAs in yeast. EMBO J. *19*, 1357–1365.

Horn, D.M., Mason, S.L., and Karbstein, K. (2011). Rcl1 protein, a novel nuclease for 18 S ribosomal RNA production. J. Biol. Chem. *286*, 34082–34087.

Houseley, J., and Tollervey, D. (2009). The Many Pathways of RNA Degradation. Cell *136*, 763–776.

Hunziker, M., Barandun, J., Petfalski, E., Tan, D., Delan-Forino, C., Molloy, K.R., Kim, K.H., Dunn-Davies, H., Shi, Y., Chaker-Margot, M., et al. (2016). UtpA and UtpB chaperone nascent pre-ribosomal RNA and U3 snoRNA to initiate eukaryotic ribosome assembly. Nat. Commun. *7*, 12090.

Hunziker, M., Barandun, J., Buzovetsky, O., Steckler, C., Molina, H., and Klinge, S. (2019). Conformational switches control early maturation of the eukaryotic small ribosomal subunit. ELife *8*, e45185.

Jackson, R.N., Klauer, A.A., Hintze, B.J., Robinson, H., van Hoof, A., and Johnson, S.J. (2010). The crystal structure of Mtr4 reveals a novel arch domain required for rRNA processing. EMBO J. *29*, 2205–2216.

Jacobus, A.P., and Gross, J. (2015). Optimal Cloning of PCR Fragments by Homologous Recombination in Escherichia coli. PLOS ONE *10*, e0119221.

Jakob, S., Ohmayer, U., Neueder, A., Hierlmeier, T., Perez-Fernandez, J., Hochmuth, E., Deutzmann, R., Griesenbeck, J., Tschochner, H., and Milkereit, P. (2012). Interrelationships between yeast ribosomal protein assembly events and transient ribosome biogenesis factors interactions in early pre-ribosomes. PloS One *7*, e32552.

Jakovljevic, J., Ohmayer, U., Gamalinda, M., Talkish, J., Alexander, L., Linnemann, J., Milkereit, P., and Woolford, J.L. (2012). Ribosomal proteins L7 and L8 function in concert with six A_3 assembly factors to propagate assembly of domains I and II of 25S rRNA in yeast 60S ribosomal subunits. RNA N. Y. N *18*, 1805–1822.

Janke, C., Magiera, M.M., Rathfelder, N., Taxis, C., Reber, S., Maekawa, H., Moreno-Borchart, A., Doenges, G., Schwob, E., Schiebel, E., et al. (2004). A versatile toolbox for PCR-based tagging of yeast genes: new fluorescent proteins, more markers and promoter substitution cassettes. Yeast Chichester Engl. *21*, 947–962.

Johnson, A.W. (1997). Rat1p and Xrn1p are functionally interchangeable exoribonucleases that are restricted to and required in the nucleus and cytoplasm, respectively. Mol. Cell. Biol. *17*, 6122–6130.

Johnson, M.C., Ghalei, H., Doxtader, K.A., Karbstein, K., and Stroupe, M.E. (2017). Structural Heterogeneity in Pre-40S Ribosomes. Structure *25*, 329–340.

Joseph, N., Krauskopf, E., Vera, M.I., and Michot, B. (1999). Ribosomal internal transcribed spacer 2 (ITS2) exhibits a common core of secondary structure in vertebrates and yeast. Nucleic Acids Res. *27*, 4533–4540.

Kappel, L., Loibl, M., Zisser, G., Klein, I., Fruhmann, G., Gruber, C., Unterweger, S., Rechberger, G., Pertschy, B., and Bergler, H. (2012). Rlp24 activates the AAA-ATPase Drg1 to initiate cytoplasmic pre-60S maturation. J. Cell Biol. *199*, 771–782.

Karbstein, K. (2013). Quality control mechanisms during ribosome maturation. Trends Cell Biol. *23*, 242–250.

Kater, L., Thoms, M., Barrio-Garcia, C., Cheng, J., Ismail, S., Ahmed, Y.L., Bange, G., Kressler, D., Berninghausen, O., Sinning, I., et al. (2017). Visualizing the Assembly Pathway of Nucleolar Pre-60S Ribosomes. Cell *171*, 1599-1610.e14.

Keener, J., Dodd, J.A., Lalo, D., and Nomura, M. (1997). Histones H3 and H4 are components of upstream activation factor required for the high-level transcription of yeast rDNA by RNA polymerase I. Proc. Natl. Acad. Sci. U. S. A. *94*, 13458–13462.

Kemmler, S., Occhipinti, L., Veisu, M., and Panse, V.G. (2009). Yvh1 is required for a late maturation step in the 60S biogenesis pathway. J. Cell Biol. *186*, 863–880.

Kern, L., de Montigny, J., Jund, R., and Lacroute, F. (1990). The FUR1 gene of Saccharomyces cerevisiae: cloning, structure and expression of wild-type and mutant alleles. Gene *88*, 149–157.

Kern, L., de Montigny, J., Lacroute, F., and Jund, R. (1991). Regulation of the pyrimidine salvage pathway by the FUR1 gene product of Saccharomyces cerevisiae. Curr. Genet. *19*, 333–337.

Keys, D.A., Vu, L., Steffan, J.S., Dodd, J.A., Yamamoto, R.T., Nogi, Y., and Nomura, M. (1994). RRN6 and RRN7 encode subunits of a multiprotein complex essential for the initiation of rDNA transcription by RNA polymerase I in Saccharomyces cerevisiae. Genes Dev. *8*, 2349–2362.

Keys, D.A., Lee, B.S., Dodd, J.A., Nguyen, T.T., Vu, L., Fantino, E., Burson, L.M., Nogi, Y., and Nomura, M. (1996). Multiprotein transcription factor UAF interacts with the upstream element of the yeast RNA polymerase I promoter and forms a stable preinitiation complex. Genes Dev. *10*, 887–903.

Khajuria, R.K., Munschauer, M., Ulirsch, J.C., Fiorini, C., Ludwig, L.S., McFarland, S.K., Abdulhay, N.J., Specht, H., Keshishian, H., Mani, D.R., et al. (2018). Ribosome Levels Selectively Regulate Translation and Lineage Commitment in Human Hematopoiesis. Cell *173*, 90-103.e19.

Kharde, S., Calviño, F.R., Gumiero, A., Wild, K., and Sinning, I. (2015). The structure of Rpf2-Rrs1 explains its role in ribosome biogenesis. Nucleic Acids Res. *43*, 7083–7095.

Khoshnevis, S., Askenasy, I., Johnson, M.C., Dattolo, M.D., Young-Erdos, C.L., Stroupe, M.E., and Karbstein, K. (2016). The DEAD-box Protein Rok1 Orchestrates 40S and 60S Ribosome Assembly by Promoting the Release of Rrp5 from Pre-40S Ribosomes to Allow for 60S Maturation. PLoS Biol. *14*, e1002480.

Khoshnevis, S., Liu, X., Dattolo, M.D., and Karbstein, K. (2019). Rrp5 establishes a checkpoint for 60S assembly during 40S maturation. RNA N. Y. N *25*, 1164–1176.

Kimball, S.R. (1999). Eukaryotic initiation factor eIF2. Int. J. Biochem. Cell Biol. *31*, 25–29.

Kiss, T., Fayet-Lebaron, E., and Jády, B.E. (2010). Box H/ACA small ribonucleoproteins. Mol. Cell *37*, 597–606.

Klinge, S., and Woolford, J.L. (2019). Ribosome assembly coming into focus. Nat. Rev. Mol. Cell Biol. *20*, 116–131.

Klinge, S., Voigts-Hoffmann, F., Leibundgut, M., Arpagaus, S., and Ban, N. (2011). Crystal structure of the eukaryotic 60S ribosomal subunit in complex with initiation factor 6. Science *334*, 941–948.

Knüppel, R., Kuttenberger, C., and Ferreira-Cerca, S. (2017). Toward Time-Resolved Analysis of RNA Metabolism in Archaea Using 4-Thiouracil. Front. Microbiol. *8*, 286.

Konikkat, S., and Woolford, J.L. (2017). Principles of 60S ribosomal subunit assembly emerging from recent studies in yeast. Biochem. J. *474*, 195–214.

Kos, M., and Tollervey, D. (2010). Yeast pre-rRNA processing and modification occur cotranscriptionally. Mol. Cell *37*, 809–820.

Kos-Braun, I.C., Jung, I., and Koš, M. (2017). Tor1 and CK2 kinases control a switch between alternative ribosome biogenesis pathways in a growth-dependent manner. PLoS Biol. *15*, e2000245.

Kostova, K.K., Hickey, K.L., Osuna, B.A., Hussmann, J.A., Frost, A., Weinberg, D.E., and Weissman, J.S. (2017). CAT-tailing as a fail-safe mechanism for efficient degradation of stalled nascent polypeptides. Science *357*, 414–417.

Kressler, D., Roser, D., Pertschy, B., and Hurt, E. (2008). The AAA ATPase Rix7 powers progression of ribosome biogenesis by stripping Nsa1 from pre-60S particles. J. Cell Biol. *181*, 935–944.

Kressler, D., Hurt, E., and Baßler, J. (2017). A Puzzle of Life: Crafting Ribosomal Subunits. Trends Biochem. Sci. *42*, 640–654.

Krogan, N.J., Peng, W.-T., Cagney, G., Robinson, M.D., Haw, R., Zhong, G., Guo, X., Zhang, X., Canadien, V., Richards, D.P., et al. (2004). High-definition macromolecular composition of yeast RNA-processing complexes. Mol. Cell *13*, 225–239.

Kufel, J., Dichtl, B., and Tollervey, D. (1999). Yeast Rnt1p is required for cleavage of the pre-ribosomal RNA in the 3' ETS but not the 5' ETS. RNA N. Y. N *5*, 909–917.

LaCava, J., Houseley, J., Saveanu, C., Petfalski, E., Thompson, E., Jacquier, A., and Tollervey, D. (2005). RNA degradation by the exosome is promoted by a nuclear polyadenylation complex. Cell *121*, 713–724.

Lacroute, F. (1968). Regulation of pyrimidine biosynthesis in Saccharomyces cerevisiae. J. Bacteriol. *95*, 824–832.

Laemmli, U.K. (1970). Cleavage of structural proteins during the assembly of the head of bacteriophage T4. Nature *227*, 680–685.

Lafontaine, D.L.J. (2010). A "garbage can" for ribosomes: how eukaryotes degrade their ribosomes. Trends Biochem. Sci. *35*, 267–277.

Lafontaine, D.L., and Tollervey, D. (2000). Synthesis and assembly of the box C+D small nucleolar RNPs. Mol. Cell. Biol. *20*, 2650–2659.

Lalo, D., Steffan, J.S., Dodd, J.A., and Nomura, M. (1996). RRN11 encodes the third subunit of the complex containing Rrn6p and Rrn7p that is essential for the initiation of rDNA transcription by yeast RNA polymerase I. J. Biol. Chem. *271*, 21062–21067.

Lamanna, A.C., and Karbstein, K. (2009). Nob1 binds the single-stranded cleavage site D at the 3'-end of 18S rRNA with its PIN domain. Proc. Natl. Acad. Sci. U. S. A. *106*, 14259–14264.

Lamanna, A.C., and Karbstein, K. (2011). An RNA conformational switch regulates pre-18S rRNA cleavage. J. Mol. Biol. *405*, 3–17.

Lebaron, S., Schneider, C., van Nues, R.W., Swiatkowska, A., Walsh, D., Böttcher, B., Granneman, S., Watkins, N.J., and Tollervey, D. (2012). Proofreading of pre-40S ribosome maturation by a translation initiation factor and 60S subunits. Nat. Struct. Mol. Biol. *19*, 744–753.

Lebaron, S., Segerstolpe, A., French, S.L., Dudnakova, T., de Lima Alves, F., Granneman, S., Rappsilber, J., Beyer, A.L., Wieslander, L., and Tollervey, D. (2013). Rrp5 binding at multiple sites coordinates pre-rRNA processing and assembly. Mol. Cell *52*, 707–719.

Lebreton, A., Saveanu, C., Decourty, L., Jacquier, A., and Fromont-Racine, M. (2006). Nsa2 is an unstable, conserved factor required for the maturation of 27 SB pre-rRNAs. J. Biol. Chem. *281*, 27099–27108.

Lebreton, A., Tomecki, R., Dziembowski, A., and Séraphin, B. (2008a). Endonucleolytic RNA cleavage by a eukaryotic exosome. Nature *456*, 993–996.

Lebreton, A., Rousselle, J.-C., Lenormand, P., Namane, A., Jacquier, A., Fromont-Racine, M., and Saveanu, C. (2008b). 60S ribosomal subunit assembly dynamics defined by semi-quantitative mass spectrometry of purified complexes. Nucleic Acids Res. *36*, 4988–4999.

Léger-Silvestre, I., Milkereit, P., Ferreira-Cerca, S., Saveanu, C., Rousselle, J.-C., Choesmel, V., Guinefoleau, C., Gas, N., and Gleizes, P.-E. (2004). The ribosomal protein Rps15p is required for nuclear exit of the 40S subunit precursors in yeast. EMBO J. *23*, 2336–2347.

Liang, W.Q., and Fournier, M.J. (1995). U14 base-pairs with 18S rRNA: a novel snoRNA interaction required for rRNA processing. Genes Dev. *9*, 2433–2443.

Liang, X.-H., and Fournier, M.J. (2006). The helicase Has1p is required for snoRNA release from pre-rRNA. Mol. Cell. Biol. *26*, 7437–7450.

Lin, J., Lu, J., Feng, Y., Sun, M., and Ye, K. (2013). An RNA-binding complex involved in ribosome biogenesis contains a protein with homology to tRNA CCA-adding enzyme. PLoS Biol. *11*, e1001669.

Liu, Q., Greimann, J.C., and Lima, C.D. (2006). Reconstitution, activities, and structure of the eukaryotic RNA exosome. Cell *127*, 1223–1237.

Lo, K.-Y., Li, Z., Wang, F., Marcotte, E.M., and Johnson, A.W. (2009). Ribosome stalk assembly requires the dual-specificity phosphatase Yvh1 for the exchange of Mrt4 with P0. J. Cell Biol. *186*, 849–862.

Lodish, H.F. (1974). Model for the regulation of mRNA translation applied to haemoglobin synthesis. Nature *251*, 385–388.

Loewith, R., and Hall, M.N. (2011). Target of rapamycin (TOR) in nutrient signaling and growth control. Genetics *189*, 1177–1201.

Ludwig, L.S., Gazda, H.T., Eng, J.C., Eichhorn, S.W., Thiru, P., Ghazvinian, R., George, T.I., Gotlib, J.R., Beggs, A.H., Sieff, C.A., et al. (2014). Altered translation of GATA1 in Diamond-Blackfan anemia. Nat. Med. *20*, 748–753.

Luviano, A., Cruz-Castañeda, R., Sánchez-Puig, N., and García-Hernández, E. (2019). Cooperative energetic effects elicited by the yeast Shwachman-Diamond syndrome protein (Sdo1) and guanine nucleotides modulate the complex conformational landscape of the elongation factor-like 1 (Efl1) GTPase. Biophys. Chem. *247*, 13–24.

Lygerou, Z., Allmang, C., Tollervey, D., and Séraphin, B. (1996). Accurate processing of a eukaryotic precursor ribosomal RNA by ribonuclease MRP in vitro. Science *272*, 268–270.

Ma, C., Wu, S., Li, N., Chen, Y., Yan, K., Li, Z., Zheng, L., Lei, J., Woolford, J.L., and Gao, N. (2017). Structural snapshot of cytoplasmic pre-60S ribosomal particles bound by Nmd3, Lsg1, Tif6 and Reh1. Nat. Struct. Mol. Biol. *24*, 214–220.

Malyutin, A.G., Musalgaonkar, S., Patchett, S., Frank, J., and Johnson, A.W. (2017). Nmd3 is a structural mimic of eIF5A, and activates the cpGTPase Lsg1 during 60S ribosome biogenesis. EMBO J. *36*, 854–868.

Marmier-Gourrier, N., Cléry, A., Schlotter, F., Senty-Ségault, V., and Branlant, C. (2011). A second base pair interaction between U3 small nucleolar RNA and the 5'-ETS region is required for early cleavage of the yeast pre-ribosomal RNA. Nucleic Acids Res. *39*, 9731–9745.

Martin, R., Hackert, P., Ruprecht, M., Simm, S., Brüning, L., Mirus, O., Sloan, K.E., Kudla, G., Schleiff, E., and Bohnsack, M.T. (2014). A pre-ribosomal RNA interaction network involving snoRNAs and the Rok1 helicase. RNA N. Y. N *20*, 1173–1182.

Matsuo, Y., Ikeuchi, K., Saeki, Y., Iwasaki, S., Schmidt, C., Udagawa, T., Sato, F., Tsuchiya, H., Becker, T., Tanaka, K., et al. (2017). Ubiquitination of stalled ribosome triggers ribosome-associated quality control. Nat. Commun. *8*, 159.

McCann, K.L., Charette, J.M., Vincent, N.G., and Baserga, S.J. (2015). A protein interaction map of the LSU processome. Genes Dev. *29*, 862–875.

McCaughan, U.M., Jayachandran, U., Shchepachev, V., Chen, Z.A., Rappsilber, J., Tollervey, D., and Cook, A.G. (2016). Pre-40S ribosome biogenesis factor Tsr1 is an inactive structural mimic of translational GTPases. Nat. Commun. *7*, 11789.

Melvin, W.T., Milne, H.B., Slater, A.A., Allen, H.J., and Keir, H.M. (1978). Incorporation of 6-thioguanosine and 4-thiouridine into RNA. Application to isolation of newly synthesised RNA by affinity chromatography. Eur. J. Biochem. *92*, 373–379.

Milkereit, P., Gadal, O., Podtelejnikov, A., Trumtel, S., Gas, N., Petfalski, E., Tollervey, D., Mann, M., Hurt, E., and Tschochner, H. (2001). Maturation and intranuclear transport of pre-ribosomes requires Noc proteins. Cell *105*, 499–509.

Miller, O.L., and Beatty, B.R. (1969). Visualization of nucleolar genes. Science *164*, 955–957.

Mitchell, P., Petfalski, E., and Tollervey, D. (1996). The 3' end of yeast 5.8S rRNA is generated by an exonuclease processing mechanism. Genes Dev. *10*, 502–513.

Mitchell, P., Petfalski, E., Shevchenko, A., Mann, M., and Tollervey, D. (1997). The exosome: a conserved eukaryotic RNA processing complex containing multiple 3'-->5' exoribonucleases. Cell *91*, 457–466.

Mitterer, V., Murat, G., Réty, S., Blaud, M., Delbos, L., Stanborough, T., Bergler, H., Leulliot, N., Kressler, D., and Pertschy, B. (2016). Sequential domain assembly of ribosomal protein S3 drives 40S subunit maturation. Nat. Commun. *7*, 10336.

Muthmann, N., Hartstock, K., and Rentmeister, A. (2020). Chemo-enzymatic treatment of RNA to facilitate analyses. Wiley Interdiscip. Rev. RNA *11*, e1561.

Oeffinger, M., Zenklusen, D., Ferguson, A., Wei, K.E., El Hage, A., Tollervey, D., Chait, B.T., Singer, R.H., and Rout, M.P. (2009). Rrp17p is a eukaryotic exonuclease required for 5' end processing of Pre-60S ribosomal RNA. Mol. Cell *36*, 768–781.

Ohmayer, U. (2014). Studies on the assembly process of large subunit ribosomal proteins in *S. cerevisiae*. PhD thesis.

Ohmayer, U., Gamalinda, M., Sauert, M., Ossowski, J., Pöll, G., Linnemann, J., Hierlmeier, T., Perez-Fernandez, J., Kumcuoglu, B., Leger-Silvestre, I., et al. (2013). Studies on the assembly characteristics of large subunit ribosomal proteins in S. cerevisae. PloS One *8*, e68412.

Osheim, Y.N., French, S.L., Keck, K.M., Champion, E.A., Spasov, K., Dragon, F., Baserga, S.J., and Beyer, A.L. (2004). Pre-18S ribosomal RNA is structurally compacted into the SSU processome prior to being cleaved from nascent transcripts in Saccharomyces cerevisiae. Mol. Cell *16*, 943–954.

Parker, M.D., Collins, J.C., Korona, B., Ghalei, H., and Karbstein, K. (2019). A kinase-dependent checkpoint prevents escape of immature ribosomes into the translating pool. PLoS Biol. *17*, e3000329.

Patchett, S., Musalgaonkar, S., Malyutin, A.G., and Johnson, A.W. (2017). The T-cell leukemia related rpl10-R98S mutant traps the 60S export adapter Nmd3 in the ribosomal P site in yeast. PLoS Genet. *13*, e1006894.

Peculis, B.A., and Greer, C.L. (1998). The structure of the ITS2-proximal stem is required for pre-rRNA processing in yeast. RNA N. Y. N *4*, 1610–1622.

Peña, C., Hurt, E., and Panse, V.G. (2017). Eukaryotic ribosome assembly, transport and quality control. Nat. Struct. Mol. Biol. *24*, 689–699.

Pérez-Fernández, J., Remacha, M., and Ballesta, J.P.G. (2005). The acidic protein binding site is partially hidden in the free Saccharomyces cerevisiae ribosomal stalk protein P0. Biochemistry *44*, 5532–5540.

Pérez-Fernández, J., Román, A., De Las Rivas, J., Bustelo, X.R., and Dosil, M. (2007). The 90S preribosome is a multimodular structure that is assembled through a hierarchical mechanism. Mol. Cell. Biol. *27*, 5414–5429.

Pérez-Fernández, J., Martín-Marcos, P., and Dosil, M. (2011). Elucidation of the assembly events required for the recruitment of Utp20, Imp4 and Bms1 onto nascent pre-ribosomes. Nucleic Acids Res. *39*, 8105–8121.

Pertschy, B., Schneider, C., Gnädig, M., Schäfer, T., Tollervey, D., and Hurt, E. (2009). RNA helicase Prp43 and its co-factor Pfa1 promote 20 to 18 S rRNA processing catalyzed by the endonuclease Nob1. J. Biol. Chem. *284*, 35079–35091.

Petes, T.D. (1979). Yeast ribosomal DNA genes are located on chromosome XII. Proc. Natl. Acad. Sci. U. S. A. *76*, 410–414.

Petfalski, E., Dandekar, T., Henry, Y., and Tollervey, D. (1998). Processing of the precursors to small nucleolar RNAs and rRNAs requires common components. Mol. Cell. Biol. *18*, 1181–1189.

Philippi, A., Steinbauer, R., Reiter, A., Fath, S., Leger-Silvestre, I., Milkereit, P., Griesenbeck, J., and Tschochner, H. (2010). TOR-dependent reduction in the expression level of Rrn3p lowers the activity of the yeast RNA Pol I machinery, but does not account for the strong inhibition of rRNA production. Nucleic Acids Res. *38*, 5315–5326.

Pöll, G., Braun, T., Jakovljevic, J., Neueder, A., Jakob, S., Woolford, J.L., Tschochner, H., and Milkereit, P. (2009). rRNA maturation in yeast cells depleted of large ribosomal subunit proteins. PloS One *4*, e8249.

Pöll, G., Li, S., Ohmayer, U., Hierlmeier, T., Milkereit, P., and Perez-Fernandez, J. (2014). In vitro reconstitution of yeast tUTP/UTP A and UTP B subcomplexes provides new insights into their modular architecture. PloS One *9*, e114898.

Pöll, G., Müller, C., Bodden, M., Teubl, F., Eichner, N., Lehmann, G., Griesenbeck, J., Tschochner, H., and Milkereit, P. (2017). Structural transitions during large ribosomal subunit maturation analyzed by tethered nuclease structure probing in S. cerevisiae. PLOS ONE *12*, e0179405.

Powers, T., and Walter, P. (1999). Regulation of ribosome biogenesis by the rapamycin-sensitive TOR-signaling pathway in Saccharomyces cerevisiae. Mol. Biol. Cell *10*, 987–1000.

Puig, O., Caspary, F., Rigaut, G., Rutz, B., Bouveret, E., Bragado-Nilsson, E., Wilm, M., and Séraphin, B. (2001). The tandem affinity purification (TAP) method: a general procedure of protein complex purification. Methods San Diego Calif *24*, 218–229.

Ramos-Sáenz, A., González-Álvarez, D., Rodríguez-Galán, O., Rodríguez-Gil, A., Gaspar, S.G., Villalobo, E., Dosil, M., and de la Cruz, J. (2019). Pol5 is an essential ribosome biogenesis factor required for 60S ribosomal subunit maturation in *Saccharomyces cerevisiae*. RNA *25*, 1561–1575.

Riggleman, B., Wieschaus, E., and Schedl, P. (1989). Molecular analysis of the armadillo locus: uniformly distributed transcripts and a protein with novel internal repeats are associated with a Drosophila segment polarity gene. Genes Dev. *3*, 96–113.

Ripmaster, T.L., Vaughn, G.P., and Woolford, J.L. (1992). A putative ATP-dependent RNA helicase involved in Saccharomyces cerevisiae ribosome assembly. Proc. Natl. Acad. Sci. *89*, 11131–11135.

Rodríguez-Mateos, M., García-Gómez, J.J., Francisco-Velilla, R., Remacha, M., de la Cruz, J., and Ballesta, J.P.G. (2009a). Role and dynamics of the ribosomal protein P0 and its related trans-acting factor Mrt4 during ribosome assembly in Saccharomyces cerevisiae. Nucleic Acids Res. *37*, 7519–7532.

Rodríguez-Mateos, M., Abia, D., García-Gómez, J.J., Morreale, A., de la Cruz, J., Santos, C., Remacha, M., and Ballesta, J.P.G. (2009b). The amino terminal domain from Mrt4 protein can functionally replace the RNA binding domain of the ribosomal P0 protein. Nucleic Acids Res. *37*, 3514–3521.

Rosado, I.V., Kressler, D., and de la Cruz, J. (2007a). Functional analysis of Saccharomyces cerevisiae ribosomal protein Rpl3p in ribosome synthesis. Nucleic Acids Res. *35*, 4203–4213.

Rosado, I.V., Dez, C., Lebaron, S., Caizergues-Ferrer, M., Henry, Y., and de la Cruz, J. (2007b). Characterization of Saccharomyces cerevisiae Npa2p (Urb2p) reveals a low-molecular-mass complex containing Dbp6p, Npa1p (Urb1p), Nop8p, and Rsa3p involved in early steps of 60S ribosomal subunit biogenesis. Mol. Cell. Biol. *27*, 1207–1221.

Rotenberg, M.O., Moritz, M., and Woolford, J.L. (1988). Depletion of Saccharomyces cerevisiae ribosomal protein L16 causes a decrease in 60S ribosomal subunits and formation of half-mer polyribosomes. Genes Dev. *2*, 160–172.

Sahasranaman, A., Dembowski, J., Strahler, J., Andrews, P., Maddock, J., and Woolford, J.L. (2011). Assembly of Saccharomyces cerevisiae 60S ribosomal subunits: role of factors required for 27S pre-rRNA processing. EMBO J. *30*, 4020–4032.

Sá-Moura, B., Kornprobst, M., Kharde, S., Ahmed, Y.L., Stier, G., Kunze, R., Sinning, I., and Hurt, E. (2017). Mpp10 represents a platform for the interaction of multiple factors within the 90S pre-ribosome. PloS One *12*, e0183272.

Sandmeier, J.J., Celic, I., Boeke, J.D., and Smith, J.S. (2002). Telomeric and rDNA silencing in Saccharomyces cerevisiae are dependent on a nuclear NAD(+) salvage pathway. Genetics *160*, 877–889.

Sanghai, Z.A., Miller, L., Molloy, K.R., Barandun, J., Hunziker, M., Chaker-Margot, M., Wang, J., Chait, B.T., and Klinge, S. (2018). Modular assembly of the nucleolar pre-60S ribosomal subunit. Nature *556*, 126–129.

Santos, C., and Ballesta, J.P.G. (2005). Characterization of the 26S rRNA-binding domain in Saccharomyces cerevisiae ribosomal stalk phosphoprotein P0. Mol. Microbiol. *58*, 217–226.

Sardana, R., Liu, X., Granneman, S., Zhu, J., Gill, M., Papoulas, O., Marcotte, E.M., Tollervey, D., Correll, C.C., and Johnson, A.W. (2015). The DEAH-box helicase Dhr1 dissociates U3 from the pre-rRNA to promote formation of the central pseudoknot. PLoS Biol. *13*, e1002083.

Sarkar, A., Thoms, M., Barrio-Garcia, C., Thomson, E., Flemming, D., Beckmann, R., and Hurt, E. (2017). Preribosomes escaping from the nucleus are caught during translation by cytoplasmic quality control. Nat. Struct. Mol. Biol. *24*, 1107–1115.

Saveanu, C., Bienvenu, D., Namane, A., Gleizes, P.E., Gas, N., Jacquier, A., and Fromont-Racine, M. (2001). Nog2p, a putative GTPase associated with pre-60S subunits and required for late 60S maturation steps. EMBO J. *20*, 6475–6484.

Saveanu, C., Namane, A., Gleizes, P.-E., Lebreton, A., Rousselle, J.-C., Noaillac-Depeyre, J., Gas, N., Jacquier, A., and Fromont-Racine, M. (2003). Sequential protein association with nascent 60S ribosomal particles. Mol. Cell. Biol. *23*, 4449–4460.

Scaiola, A., Peña, C., Weisser, M., Böhringer, D., Leibundgut, M., Klingauf-Nerurkar, P., Gerhardy, S., Panse, V.G., and Ban, N. (2018). Structure of a eukaryotic cytoplasmic pre-40S ribosomal subunit. EMBO J. *37*.

Schäfer, T., Strauss, D., Petfalski, E., Tollervey, D., and Hurt, E. (2003). The path from nucleolar 90S to cytoplasmic 40S pre-ribosomes. EMBO J. *22*, 1370–1380.

Schäfer, T., Maco, B., Petfalski, E., Tollervey, D., Böttcher, B., Aebi, U., and Hurt, E. (2006). Hrr25-dependent phosphorylation state regulates organization of the pre-40S subunit. Nature *441*, 651–655.

Schillewaert, S., Wacheul, L., Lhomme, F., and Lafontaine, D.L.J. (2012). The evolutionarily conserved protein Las1 is required for pre-rRNA processing at both ends of ITS2. Mol. Cell. Biol. *32*, 430–444.

Schmid, C. (2019). Assembly of the t-UTP complex *in vivo* and the role of t-UTP components in ribosome biogenesis. Master thesis.

Schmitt, M.E., and Clayton, D.A. (1993). Nuclear RNase MRP is required for correct processing of pre-5.8S rRNA in Saccharomyces cerevisiae. Mol. Cell. Biol. *13*, 7935–7941.

Schmitt, M.E., Brown, T.A., and Trumpower, B.L. (1990). A rapid and simple method for preparation of RNA from Saccharomyces cerevisiae. Nucleic Acids Res. *18*, 3091–3092.

Schweizer, E., MacKechnie, C., and Halvorson, H.O. (1969). The redundancy of ribosomal and transfer RNA genes in Saccharomyces cerevisiae. J. Mol. Biol. *40*, 261–277.

Sengupta, J., Bussiere, C., Pallesen, J., West, M., Johnson, A.W., and Frank, J. (2010). Characterization of the nuclear export adaptor protein Nmd3 in association with the 60S ribosomal subunit. J. Cell Biol. *189*, 1079–1086.

Séron, K., Blondel, M.O., Haguenauer-Tsapis, R., and Volland, C. (1999). Uracil-induced down-regulation of the yeast uracil permease. J. Bacteriol. *181*, 1793–1800.

Shah, B.N., Liu, X., and Correll, C.C. (2013). Imp3 unfolds stem structures in pre-rRNA and U3 snoRNA to form a duplex essential for small subunit processing. RNA *19*, 1372–1383.

Shao, S., Brown, A., Santhanam, B., and Hegde, R.S. (2015). Structure and assembly pathway of the ribosome quality control complex. Mol. Cell *57*, 433–444.

Sharma, K., Venema, J., and Tollervey, D. (1999). The 5' end of the 18S rRNA can be positioned from within the mature rRNA. RNA N. Y. N *5*, 678–686.

Shimizu, K., Kawasaki, Y., Hiraga, S.-I., Tawaramoto, M., Nakashima, N., and Sugino, A. (2002). The fifth essential DNA polymerase phi in Saccharomyces cerevisiae is localized to the nucleolus and plays an important role in synthesis of rRNA. Proc. Natl. Acad. Sci. U. S. A. *99*, 9133–9138.

Shoemaker, C.J., Eyler, D.E., and Green, R. (2010). Dom34:Hbs1 promotes subunit dissociation and peptidyl-tRNA drop-off to initiate no-go decay. Science *330*, 369–372.

Siddiqi, I.N. (2001). Transcription of chromosomal rRNA genes by both RNA polymerase I and II in yeast uaf30 mutants lacking the 30 kDa subunit of transcription factor UAF. EMBO J. *20*, 4512–4521.

Simms, C.L., Kim, K.Q., Yan, L.L., Qiu, J., and Zaher, H.S. (2018). Interactions between the mRNA and Rps3/uS3 at the entry tunnel of the ribosomal small subunit are important for no-go decay. PLoS Genet. *14*, e1007818.

Smith, M.W., Meskauskas, A., Wang, P., Sergiev, P.V., and Dinman, J.D. (2001). Saturation mutagenesis of 5S rRNA in Saccharomyces cerevisiae. Mol. Cell. Biol. *21*, 8264–8275.

Soltanieh, S., Lapensée, M., and Dragon, F. (2014). Nucleolar proteins Bfr2 and Enp2 interact with DEAD-box RNA helicase Dbp4 in two different complexes. Nucleic Acids Res. *42*, 3194–3206.

Soudet, J., Gélugne, J.-P., Belhabich-Baumas, K., Caizergues-Ferrer, M., and Mougin, A. (2010). Immature small ribosomal subunits can engage in translation initiation in Saccharomyces cerevisiae. EMBO J. *29*, 80–92.

Steffan, J.S., Keys, D.A., Dodd, J.A., and Nomura, M. (1996). The role of TBP in rDNA transcription by RNA polymerase I in Saccharomyces cerevisiae: TBP is required for upstream activation factor-dependent recruitment of core factor. Genes Dev. *10*, 2551–2563.

Stevens, A., Hsu, C.L., Isham, K.R., and Larimer, F.W. (1991). Fragments of the internal transcribed spacer 1 of pre-rRNA accumulate in Saccharomyces cerevisiae lacking 5'----3' exoribonuclease 1. J. Bacteriol. *173*, 7024–7028.

Strunk, B.S., Loucks, C.R., Su, M., Vashisth, H., Cheng, S., Schilling, J., Brooks, C.L., Karbstein, K., and Skiniotis, G. (2011). Ribosome assembly factors prevent premature translation initiation by 40S assembly intermediates. Science *333*, 1449–1453.

Strunk, B.S., Novak, M.N., Young, C.L., and Karbstein, K. (2012). A translation-like cycle is a quality control checkpoint for maturing 40S ribosome subunits. Cell *150*, 111–121.

Sun, C., and Woolford, J.L. (1994). The yeast NOP4 gene product is an essential nucleolar protein required for pre-rRNA processing and accumulation of 60S ribosomal subunits. EMBO J. *13*, 3127–3135.

Sun, Q., Zhu, X., Qi, J., An, W., Lan, P., Tan, D., Chen, R., Wang, B., Zheng, S., Zhang, C., et al. (2017). Molecular architecture of the 90S small subunit pre-ribosome. ELife *6*.

Suzuki, N., Noguchi, E., Nakashima, N., Oki, M., Ohba, T., Tartakoff, A., Ohishi, M., and Nishimoto, T. (2001). The Saccharomyces cerevisiae small GTPase, Gsp1p/Ran, is involved in 3' processing of 7S-to-5.8S rRNA and in degradation of the excised 5'-A0 fragment of 35S pre-rRNA, both of which are carried out by the exosome. Genetics *158*, 613–625.

Talkish, J., Zhang, J., Jakovljevic, J., Horsey, E.W., and Woolford, J.L. (2012). Hierarchical recruitment into nascent ribosomes of assembly factors required for 27SB pre-rRNA processing in Saccharomyces cerevisiae. Nucleic Acids Res. *40*, 8646–8661.

Talkish, J., Campbell, I.W., Sahasranaman, A., Jakovljevic, J., and Woolford, J.L. (2014). Ribosome assembly factors Pwp1 and Nop12 are important for folding of 5.8S rRNA during ribosome biogenesis in Saccharomyces cerevisiae. Mol. Cell. Biol. *34*, 1863–1877.

Talkish, J., Biedka, S., Jakovljevic, J., Zhang, J., Tang, L., Strahler, J.R., Andrews, P.C., Maddock, J.R., and Woolford, J.L. (2016). Disruption of ribosome assembly in yeast blocks cotranscriptional pre-rRNA processing and affects the global hierarchy of ribosome biogenesis. RNA *22*, 852–866.

Tan, B., Yang, C.-C., Hsieh, C.-L., Chou, Y.-H., Zhong, C.-Z., Yung, B., and Liu, H. (2012). Epigeneitc silencing of ribosomal RNA genes by Mybbp1a. J. Biomed. Sci. *19*, 57.

Thoms, M., Thomson, E., Baßler, J., Gnädig, M., Griesel, S., and Hurt, E. (2015). The Exosome Is Recruited to RNA Substrates through Specific Adaptor Proteins. Cell *162*, 1029–1038.

Thomson, E., and Tollervey, D. (2010). The final step in 5.8S rRNA processing is cytoplasmic in Saccharomyces cerevisiae. Mol. Cell. Biol. *30*, 976–984.

Torchet, C., Jacq, C., and Hermann-Le Denmat, S. (1998). Two mutant forms of the S1/TPR-containing protein Rrp5p affect the 18S rRNA synthesis in Saccharomyces cerevisiae. RNA N. Y. N *4*, 1636–1652.

Trapman, J., and Planta, R.J. (1975). Detailed analysis of the ribosomal RNA synthesis in yeast. Biochim. Biophys. Acta *414*, 115–125.

Turowski, T.W., Lebaron, S., Zhang, E., Peil, L., Dudnakova, T., Petfalski, E., Granneman, S., Rappsilber, J., and Tollervey, D. (2014). Rio1 mediates ATP-dependent final maturation of 40S ribosomal subunits. Nucleic Acids Res. *42*, 12189–12199.

Udem, S.A., and Warner, J.R. (1972). Ribosomal RNA synthesis in Saccharomyces cerevisiae. J. Mol. Biol. *65*, 227–242.

Udem, S.A., and Warner, J.R. (1973). The cytoplasmic maturation of a ribosomal precursor ribonucleic acid in yeast. J. Biol. Chem. *248*, 1412–1416.

Venema, J., and Tollervey, D. (1996). RRP5 is required for formation of both 18S and 5.8S rRNA in yeast. EMBO J. *15*, 5701–5714.

Venema, J., Henry, Y., and Tollervey, D. (1995). Two distinct recognition signals define the site of endonucleolytic cleavage at the 5'-end of yeast 18S rRNA. EMBO J. *14*, 4883–4892.

Voorhees, R.M., Schmeing, T.M., Kelley, A.C., and Ramakrishnan, V. (2010). The mechanism for activation of GTP hydrolysis on the ribosome. Science *330*, 835–838.

Warner, J.R. (1999). The economics of ribosome biosynthesis in yeast. Trends Biochem. Sci. *24*, 437–440.

Watkins, N.J., Ségault, V., Charpentier, B., Nottrott, S., Fabrizio, P., Bachi, A., Wilm, M., Rosbash, M., Branlant, C., and Lührmann, R. (2000). A common core RNP structure shared between the small nucleoar box C/D RNPs and the spliceosomal U4 snRNP. Cell *103*, 457–466.

Weaver, P.L., Sun, C., and Chang, T.H. (1997). Dbp3p, a putative RNA helicase in Saccharomyces cerevisiae, is required for efficient pre-rRNA processing predominantly at site A3. Mol. Cell. Biol. *17*, 1354–1365.

Wells, G.R., Weichmann, F., Colvin, D., Sloan, K.E., Kudla, G., Tollervey, D., Watkins, N.J., and Schneider, C. (2016). The PIN domain endonuclease Utp24 cleaves pre-ribosomal RNA at two coupled sites in yeast and humans. Nucleic Acids Res. *44*, 5399–5409.

Wery, M., Ruidant, S., Schillewaert, S., Leporé, N., and Lafontaine, D.L.J. (2009). The nuclear poly(A) polymerase and Exosome cofactor Trf5 is recruited cotranscriptionally to nucleolar surveillance. RNA N. Y. N *15*, 406–419.

Wiederkehr, T., Prétôt, R.F., and Minvielle-Sebastia, L. (1998). Synthetic lethal interactions with conditional poly(A) polymerase alleles identify LCP5, a gene involved in 18S rRNA maturation. RNA N. Y. N *4*, 1357–1372.

Woolford, J.L., and Baserga, S.J. (2013). Ribosome biogenesis in the yeast Saccharomyces cerevisiae. Genetics *195*, 643–681.

Wu, S., Tutuncuoglu, B., Yan, K., Brown, H., Zhang, Y., Tan, D., Gamalinda, M., Yuan, Y., Li, Z., Jakovljevic, J., et al. (2016). Diverse roles of assembly factors revealed by structures of late nuclear pre-60S ribosomes. Nature *534*, 133–137.

Yamamoto, R.T., Nogi, Y., Dodd, J.A., and Nomura, M. (1996). RRN3 gene of Saccharomyces cerevisiae encodes an essential RNA polymerase I transcription factor which interacts with the polymerase independently of DNA template. EMBO J. *15*, 3964–3973.

Yamauchi, T., Keough, R.A., Gonda, T.J., and Ishii, S. (2008). Ribosomal stress induces processing of Mybbp1a and its translocation from the nucleolus to the nucleoplasm. Genes Cells Devoted Mol. Cell. Mech. *13*, 27–39.

Yan, L.L., and Zaher, H.S. (2019). Ubiquitin-a beacon for all during quality control on the ribosome. EMBO J. *38*.

Yang, W., Rogozin, I.B., and Koonin, E.V. (2003). Yeast POL5 is an evolutionarily conserved regulator of rDNA transcription unrelated to any known DNA polymerases. Cell Cycle Georget. Tex *2*, 120–122.

Yeh, L.C., and Lee, J.C. (1990). Structural analysis of the internal transcribed spacer 2 of the precursor ribosomal RNA from Saccharomyces cerevisiae. J. Mol. Biol. *211*, 699–712.

Zanchin, N.I., and Goldfarb, D.S. (1999). The exosome subunit Rrp43p is required for the efficient maturation of 5.8S, 18S and 25S rRNA. Nucleic Acids Res. *27*, 1283–1288.

Zanchin, N.I., Roberts, P., DeSilva, A., Sherman, F., and Goldfarb, D.S. (1997). Saccharomyces cerevisiae Nip7p is required for efficient 60S ribosome subunit biogenesis. Mol. Cell. Biol. *17*, 5001–5015.

Zhang, C., Sun, Q., Chen, R., Chen, X., Lin, J., and Ye, K. (2016a). Integrative structural analysis of the UTPB complex, an early assembly factor for eukaryotic small ribosomal subunits. Nucleic Acids Res. *44*, 7475–7486.

Zhang, J., Harnpicharnchai, P., Jakovljevic, J., Tang, L., Guo, Y., Oeffinger, M., Rout, M.P., Hiley, S.L., Hughes, T., and Woolford, J.L. (2007). Assembly factors Rpf2 and Rrs1 recruit 5S rRNA and ribosomal proteins rpL5 and rpL11 into nascent ribosomes. Genes Dev. *21*, 2580–2592.

Zhang, L., Wu, C., Cai, G., Chen, S., and Ye, K. (2016b). Stepwise and dynamic assembly of the earliest precursors of small ribosomal subunits in yeast. Genes Dev. *30*, 718–732.

Zhang, Y., Smith, A.D., Renfrow, M.B., and Schneider, D.A. (2010). The RNA polymerase-associated factor 1 complex (Paf1C) directly increases the elongation rate of RNA polymerase I and is required for efficient regulation of rRNA synthesis. J. Biol. Chem. *285*, 14152–14159.

Zhou, D., Zhu, X., Zheng, S., Tan, D., Dong, M.-Q., and Ye, K. (2019a). Cryo-EM structure of an early precursor of large ribosomal subunit reveals a half-assembled intermediate. Protein Cell *10*, 120–130.

Zhou, Y., Musalgaonkar, S., Johnson, A.W., and Taylor, D.W. (2019b). Tightly-orchestrated rearrangements govern catalytic center assembly of the ribosome. Nat. Commun. *10*, 958.

Zurita Rendón, O., Fredrickson, E.K., Howard, C.J., Van Vranken, J., Fogarty, S., Tolley, N.D., Kalia, R., Osuna, B.A., Shen, P.S., Hill, C.P., et al. (2018). Vms1p is a release factor for the ribosome-associated quality control complex. Nat. Commun. *9*, 2197.

6. Supplemental figures

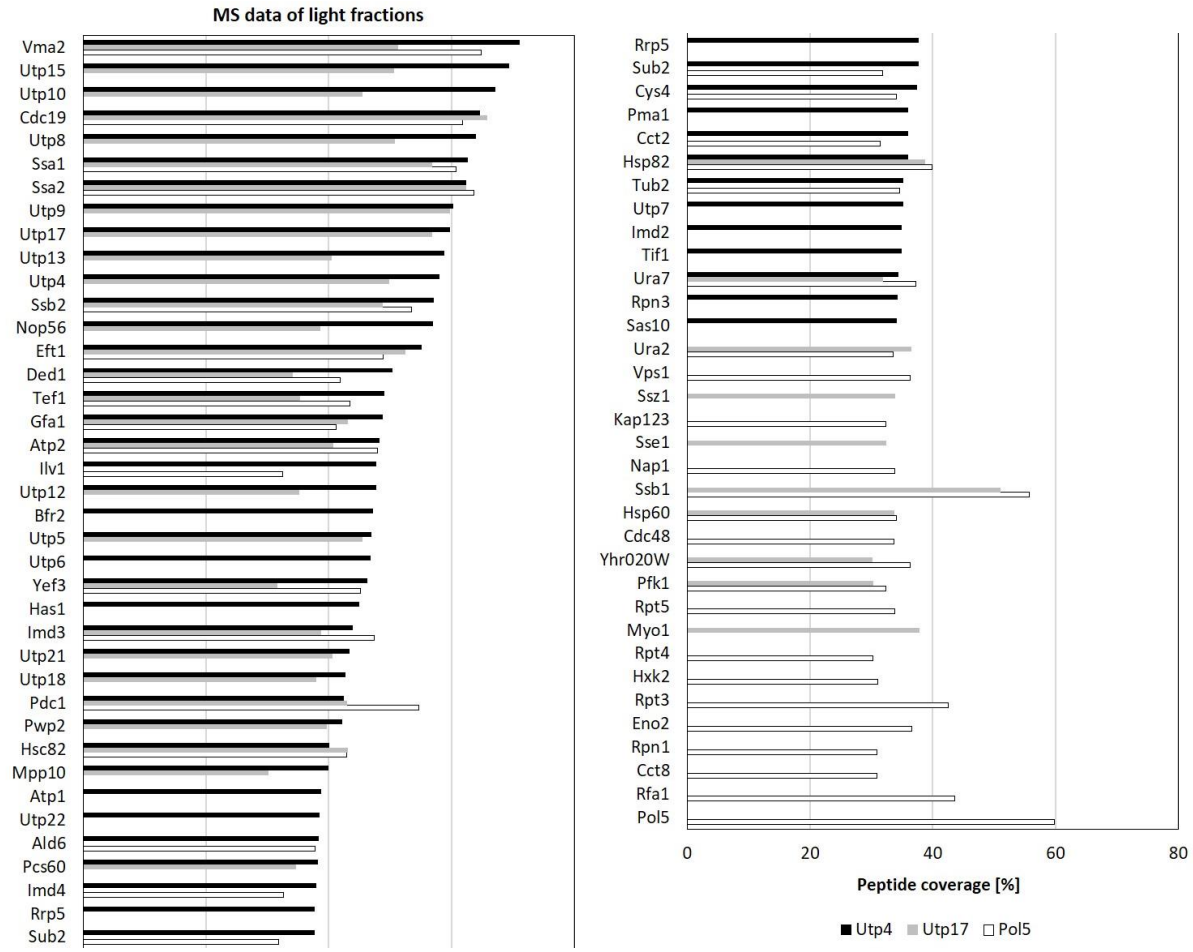

Figure 57: HPLC-ESI-MS datasets of light fractions obtained from TAP-tagged and affinity purified Utp4, Utp17, and Pol5.
Extended MS datasets from the eluates of the affinity purified light fractions of TAP-tagged Utp4 (black), Utp17 (gray), and Pol5 (white) depicted in Figure 29A. All proteins found with a peptide coverage higher than 30% were plotted.

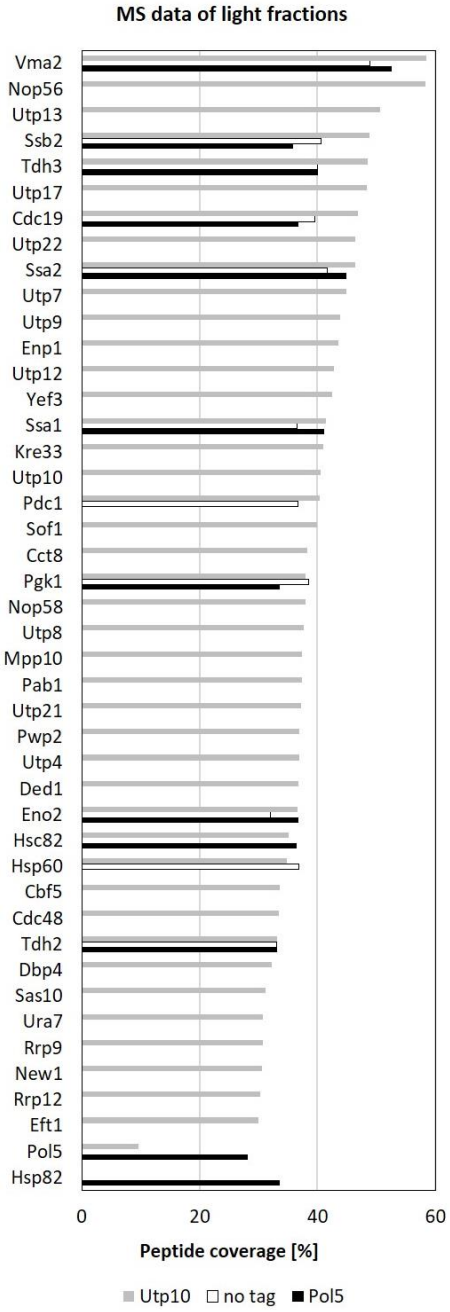

Figure 58: HPLC-ESI-MS datasets of light fractions obtained from non-tagged control and TAP-tagged and affinity purified Utp10 and Pol5.
Extended MS datasets from the bead fractions of the affinity purified light fractions of non-tagged control (white), TAP-tagged Utp10 (gray), and TAP-tagged Pol5 (black) depicted in Figure 31. All proteins found with a peptide coverage higher than 30% were plotted.

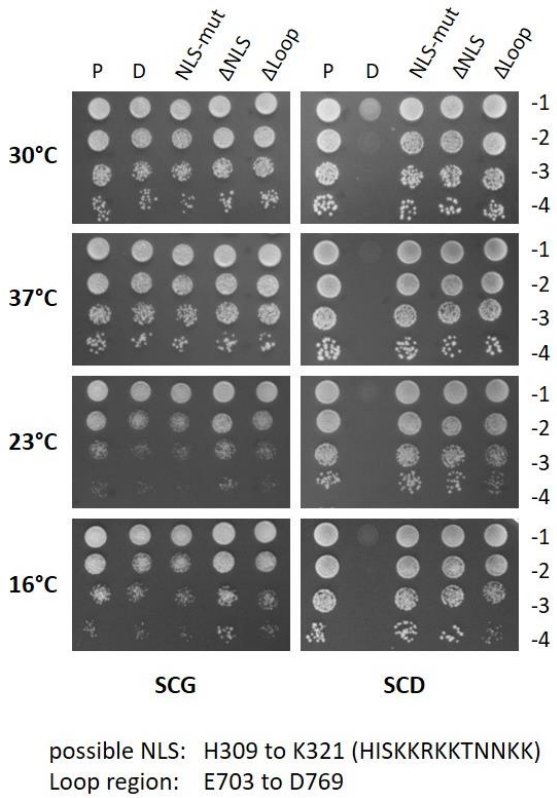

Figure 59: Growth test of NLS-point mutant and of NLS- and Loop-deletion mutants of Pol5.
In vivo growth test by drop assay comparing growth of yeast strains depleted from Pol5 (D), expressing Pol5-WT (P), NLS-point mutant (NLS-mut), NLS-deletion mutant (ΔNLS), or Loop-deletion mutant (ΔLoop). Positions of putative NLS and of disorganized loop region within primary sequence of Pol5 are given. Growth was tested on galactose and glucose containing minimal media (SCG and SCD) at different temperatures (30, 37, 23, and 16°C) by spotting cell concentrations from OD_{600} = 10^{-1} (-1) to 10^{-4} (-4). Growth of loop-deletion mutant is also depicted in Figure 49C together with C-terminal truncation mutants of Pol5.

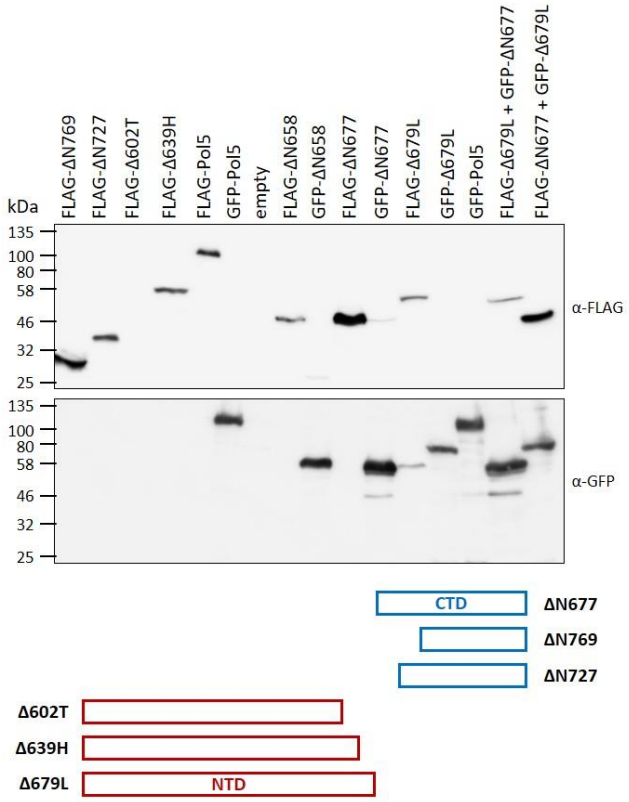

Figure 60: Analysis of expression levels of selected Pol5 truncation mutants.
5 AUs of cells expressing the different Pol5 mutants fused to FLAG or GFP tag (indicated above) were subjected to denaturing protein extraction. 20% of extracts were resolved in 10% SDS-PAGE followed by western blotting. Detection was performed with antibodies against FLAG and GFP for visualization of the respectively tagged Pol5 mutants. Details of the western blot images are depicted in Figure 51C. Below, schematic representation of primary structures of Pol5 CTD (blue) and NTD (red) truncations are depicted.

7. List of figures

8. List of tables

9. Publications & Presentations

2019 Christina M. Braun, Philipp Hackert, Catharina E. Schmid, Markus T. Bohnsack, Katherine E. Bohnsack and Jorge Perez-Fernandez
Pol5 is required for recycling of small subunit biogenesis factors and for formation of the peptide exit tunnel of the large ribosomal subunit.
Nucleic Acids Res. 2020 Jan 10; 48(1):405-420.

2017 Fanny Boissier*, Christina Maria Schmidt*, Jan Linnemann, Sébastien Fribourg and Jorge Perez-Fernandez
Pwp2 mediates UTP-B assembly via two structurally independent domains.
Sci Rep. 2017 Jun 9; 7(1):3169.

*These authors contributed equally to the publication.

2019 Christina Braun
Talk: **Pol5 is required for assembly of the large ribosomal subunit and recycling of the small subunit biogenesis factors.**
1st Munich Yeast Meeting 2019, Germany

2019 Christina Maria Schmidt, Philipp Hackert, Katherine E. Bohnsack, Michael Brummer, Markus T. Bohnsack and Jorge Perez-Fernandez
Poster: **Pol5 is required for assembly of the large ribosomal subunit and recycling of the small subunit biogenesis factors.**
RNA Society 24th Annual Meeting in Krakow, Poland

2018 Christina Schmidt, Katherine E. Sloan, Dietmar Sperling, Michael Brummer, Markus T. Bohnsack and Jorge Perez-Fernandez
Poster: **Functional analysis of Pol5 in the production of the small and large ribosomal subunits.**
The 11th International Conference on Ribosome Synthesis in Orford, Canada

2017 Christina Schmidt, Michael Brummer and Jorge Perez-Fernandez
Poster: **Assembly and disassembly of the SSU processome.**
SFB960 Conference on "The Biology of RNA-Protein Complexes" in Regensburg, Germany

10. Danksagung

Abschließend möchte ich mich bei allen bedanken, die zum Gelingen meiner Doktorarbeit beigetragen haben.

Allen voran bedanke ich mich bei meinem Betreuer PD Dr. Jorge Pérez-Fernández dafür, dass ich nun schon seit über fünf Jahren mit ihm zusammenarbeiten darf.
Danke Jorge, dass du mich schon in meiner Masterarbeit betreut hast und damit einverstanden warst, mich auch als Doktorandin in dein Team aufzunehmen. Danke, dass du dir immer für meine Fragen Zeit genommen hast und alles solange mit mir diskutiert hast, bis ich zufrieden war. Danke, dass du auf den Konferenzen diverse Koryphäen zu meinen Postern gebracht hast und mich immer ermuntert hast, meine Komfortzone zu verlassen. Danke, dass du mir viele wertvolle Tipps zum Verfassen dieses Werkes gegeben hast und dir so viel Zeit für die Korrekturen genommen hast. Und danke natürlich auch für die leckere spanische Salami äh Chorizo natürlich ;-)
¡Gracias por todo, Jorge!

Außerdem möchte ich mich bei Prof. Dr. Herbert Tschochner bedanken, dass ich an seinem Lehrstuhl promovieren durfte und er immer einen Weg gefunden hat, Geld für mich aufzutreiben. Ich bedanke mich auch für sein Mentorat während der Doktorarbeit und dass er den Vorsitz in meinem Prüfungskomitee übernimmt.

Bei Prof. Dr. Gunter Meister bedanke ich mich dafür, dass er sich bereit erklärt hat, meine Arbeit als Zweitgutachter zu bewerten und dementsprechend auch Teil meines Prüfungskomitees zu sein.

Prof. Dr. Wolfgang Seufert möchte ich dafür danken, dass er die Aufgabe des Drittprüfers in meinem Prüfungskomitee übernimmt.

Auch bei Prof. Dr. Dina Grohmann bedanke ich mich, dass sie sofort zugesagt hat, als Ersatzprüferin in meinem Prüfungskomitee zu fungieren.

Im Nachgang möchte ich mich noch herzlich bei Prof. Dr. Ute Kothe von der University of Lethbridge (Kanada) bedanken, dass sie ein Drittgutachten über meine Arbeit angefertigt hat.

Bei Prof. Dr. Markus Bohnsack von der Universität Göttingen möchte ich mich dafür bedanken, dass er das Mentorat meiner Doktorarbeit übernommen hat. Außerdem bedanke ich mich bei ihm und seiner Frau Dr. Katherine Bohnsack für die gute Zusammenarbeit und die Unterstützung bei der Veröffentlichung unserer Publikation über Pol5.

Bei Robert Hrdina möchte ich mich bedanken, dass er einen Weg gefunden hat, dass ich meine Arbeit trotz der wegen des Corona-Virus geltenden Kontaktbeschränkungen abgeben kann.

Ich bedanke mich auch bei Kinga Ay, Carolin Apfel, Kevin Kramm, den übrigen Mitgliedern des RNA Biology Board und bei den PhD Representatives der anderen RIGeL Sections für die gute und erfolgreiche Zusammenarbeit.

Ein besonderer Dank gilt auch den Mitgliedern der Ribonoc-Subgruppe, vor allem den PIs Achim, Philipp und Sébastien für die interessanten und aufschlussreichen Diskussionen.

Dafür, dass sie mir die Arbeit in Labor und Büro während der letzten vier Jahre meiner Doktorarbeit wirklich versüßt haben, bedanke ich mich bei meinen liebsten Kollegen und Mit-Doktoranden.
Bei meinen langjährigen Mitstreitern Robert, Fabian und Christopher bedanke ich mich für alles, was sie in dieser Zeit für mich getan haben. Es war eine schöne Zeit mit Euch, in der wir Freude und Frust geteilt haben und ich hoffe, dass wir noch ein paar gemeinsame Stunden im Labor oder viel lieber privat verbringen werden (z. B. Gaibonfest). Bei Fabian bedanke ich mich auch dafür, dass wir die Schulbesuche am Gymnasium Neutraubling so erfolgreich durchführen konnten. (Fürn Fabili Fabille no drei Sachen: D Ständer stenga da vorn, die könnts Eich holen. Es gibt nix bessers wie a Radler beim Globus. Und nix gega d Muse in Labor 1 sunst schepperts.)
Bei Michi (MJ, staatlich geprüfter Lappentester) und auch bei Robert bedanke ich mich vor allem dafür, dass sie mich zum Espresso bekehrt haben. Ich hätte die letzte Phase meiner Doktorarbeit ohne Koffein sicher nicht überstanden. Außerdem danke ich Euch, dass ihr meine Arbeit zum Schluss noch korrekturgelesen habt und wertvolle Anmerkungen gemacht habt. Und natürlich bin ich Euch und Maresa dankbar für die Boulder-Abende, wobei meine Lappigkeit in den letzten Wochen wieder exponentiell zugenommen hat… Und MJ, bei dir muss ich mich auch noch für das sogenannte AC/DC üben bedanken!
Außerdem bedanke ich mich bei allen, die in Büro 2 für gute Laune sorgen. Dazu gehören vor allem Kristin, MJ, Robert und Kati und neuerdings auch Sebastian, Catha und Nicolas. Ich wünsche mir, dass noch oft Friday und Payday auf den gleichen Tag fallen, weil die musikalische Untermalung einfach so wunderschön ist!

Natürlich bedanke ich mich auch bei unseren TAs Kristin, Tobi (Carl Carsten, CC) und Gisela, die den Laden am Laufen halten und von denen ich viel fürs Leben gelernt habe.

Allen anderen Mitgliedern des Lehrstuhls danke ich für die gute Atmosphäre und für die Ratschläge und Diskussionen, die zum Gelingen meiner Arbeit beigetragen haben.

Außerdem bedanke ich mich bei Dani, Franzi und Cori, die mich schon mein ganzes Studium begleiten und sehr gute Freundinnen geworden sind. Ich hoffe, dass wir noch viele gemeinsame Stunden verbringen werden.

Bei meinen Eltern möchte ich mich ganz besonders für die finanzielle und noch viel wichtigere moralische Unterstützung während meines gesamten Studiums und eigentlich während meines ganzen Lebens bedanken. Danke für alles, was ihr in den letzten 30 Jahren für mich getan habt und noch für mich tun werdet!

Zum Schluss möchte ich mich noch bei meinem Mann Daniel bedanken, der immer für mich da ist und zu mir steht.
Danke, dass du nicht allzu genervt warst, wenn ich während der stressigen Laborphasen wenig Zeit für dich hatte und dich manchmal, vor allem beim Zusammenschreiben, regelrecht vernachlässigt habe. Danke für deine Geduld und dass du mich aufmunterst oder auf den Boden der Tatsachen zurückholst, je nachdem was gerade notwendig ist.
Und natürlich vielen Dank für die Blumen in meinem „Büro“ und übrigens: I gfrei mi scho narrisch af Malle!